INCLUSION COMPOUNDS
OF
MULTIPEDAL HOSTS

by

Katherine Lindsay Gifford Nash

B.Sc (Honours) University of Cape Town

Thesis presented to the

UNIVERSITY OF CAPE TOWN

for the degree of

DOCTOR OF PHILOSOPHY

Department of Chemistry

University of Cape Town

Rondebosch, 7701

South Africa

September 1997

ACKNOWLEDGEMENTS

I would like to thank :

my supervisors, Dr Susan Bourne and Professor Luigi Nassimbeni, for their guidance and enthusiasm.

Dr Anita Coetzee for data collections.

the members of the Crystallography Research Group and Kidney Stone Laboratory for their friendship, and enlightening discussions.

Tracy Bretherton, Diane Brown, Barbara Hibbert, Anthony Radford and my brother, Timothy, for the many laughs and words of encouragement.

my parents for their love and support.

the University of Cape Town, and Foundation for Research Development for financial assistance.

PUBLICATIONS AND CONFERENCES

Parts of this thesis have been published :

1. Susan A. Bourne, Katherine L. Gifford Nash, F. Toda, *J. Chem. Soc., Perkin Trans.* 2, 1996, 2145.
2. Susan A. Bourne, Katherine L. Gifford Nash, F. Toda, *Supramol. Chem.*, 1997, **8**, 137.
3. Susan A. Bourne, Katherine L. Gifford Nash, F. Toda, *J. Incl. Phenom*, submitted.
4. Susan A. Bourne, Katherine L. Gifford Nash, F. Toda, *J. Mol. Struct.*, submitted.

Parts of this thesis have been presented at the following conferences :

1. 33rd Convention of the South African Chemical Institute, Cape Town, South Africa, 29 January - 2 February 1996.
2. XVII International Union of Crystallography Congress and General Assembly, Seattle, Washington, USA, 8-17 August 1996.
3. 10th International Symposium on Organic Crystal Chemistry, Poznan-Rydzyna, Poland, 17-21 August 1997.

ABSTRACT

The inclusion properties of three multipedal host compounds have been investigated.

The host compounds : hexakis(3-hydroxy-3,3-diphenyl-2-propynyl)benzene (host **1**), 1,2,3,5,6,7-hexakis(3-hydroxy-3,3-diphenyl-2-propynyl)naphthalene (host **2**), and tetra(3-hydroxy-3,3-diphenyl-2-propynyl)ethylene (host **3**), are characterised by a planar electron-rich central region with bulky substituent groups attached to it. Each substituent contains a hydroxyl group capable of hydrogen bonding. These features enable the inclusion of small organic solvent molecules, with suitable functional groups, within the host framework.

The crystal structures of selected inclusion compounds and the α-phases of hosts **1** and **3** are presented. The hydrogen bonding patterns and host-guest interactions are analysed. The packing motif of the host compounds and host conformation within each structure is also discussed.

The thermal decomposition behaviour of these compounds was investigated using thermogravimetry and differential scanning calorimetry. The kinetics of desolvation for some of the inclusion compounds was determined using isothermal thermogravimetry. Rate laws describing the desolvation mechanisms are ascribed, and the activation energies determined.

ABBREVIATIONS AND SYMBOLS

The abbreviations and symbols used are widely accepted in the chemical literature.

A	Arrhenius pre-exponential factor
b.p.	normal boiling point
CSD	Cambridge Structural Database
DSC	differential scanning calorimetry
E_a	activation energy
G	guest
H	host
k	rate constant
NMR	nuclear magnetic spectroscopy
TG	thermogravimetry
V	cell volume
XRD	X-ray powder diffraction
Z	number of structural units per cell
α	angle between *b* and *c* unit cell axes, or extent of reaction, or host compound with no included guest molecules.
β	angle between *a* and *c* unit cell axes, or known inclusion compound phase.
γ	angle between *a* and *b* unit cell axes
τ	torsion angle
...	non-bonded contact, such as a hydrogen bond

TABLE OF CONTENTS

CHAPTER 1

INTRODUCTION

Supramolecular chemistry is "chemistry beyond the molecule"[1], involving the investigation of the non-covalent bonds and spatial fit between molecules that form host-guest complexes[2,3]. It has been said that "supermolecules are to molecules and the intermolecular bond what molecules are to atoms and the covalent bond"[4].

Crystalline inclusion compounds may involve a whole range of supramolecular interactions, both attractive and repulsive, which balance out to produce the net stability and selectivity of the supramolecular crystalline system. Therefore, a crystal structure represents a situation where all the bonding and non-bonding forces are at an energetic minimum. It contains all the information regarding the importance of, and balance between, intermolecular forces[5]. Crystal engineering is defined as the understanding of these intermolecular interactions in the context of crystal packing, and the utilisation of such understanding in the design of new solids with desired physical and chemical properties[6].

The three basic aspects of supramolecular chemistry include molecular recognition, supramolecular reactivity and catalysis, and transport processes[7]. The first, molecular recognition, which is of interest here, is a fundamental process, mainly dealing with selective complexation of the host-guest type. A host that forms complexes of different stabilities with two similar guests is said to show molecular recognition. Selective complexation plays an essential role in the various aspects of supramolecular functions[8]. Generally, it has been found that in order to achieve selectivity a host molecule must be rigid so as to allow a preorganised binding site which is complementary in size and polarity to a particular guest. The design of artificial complexing agents provides information about the steric and electronic requirements of molecular recognition[7,8,9].

Intermolecular interactions are the fundamental causes for the formation and crystallisation of supermolecules[6,10]. Crystal structures are defined by the energies of different intermolecular interactions, and the degree to which

these interactions have compatible directional requirements. Stable crystal packings are largely determined by two types of interactions. The first type are medium range, nondirectional forces, which are typically isotropic in character, and define molecular shape, size and close packing. The most significant of these forces are the dispersion and repulsive forces (van der Waals forces). The second type of interaction are long range forces. These are directional and anisotropic in nature, and are responsible for supramolecular construction. The most important directional interaction is hydrogen bonding[11-14].

Hydrogen bonding is generally regarded as the strongest and most directional of the weak intermolecular interactions that cause molecules to form liquids or solids[14,15]. It is primarily the result of electrostatic attraction[16,17,18], and is the motivating cause for the formation of a number of clathrate intercalates and solvates. Interestingly all hydrogen bonds found in crystals may be characterised as belonging to one of only four fundamental hydrogen bond patterns, namely, chain, ring, dimer or intramolecular[13].

The general prerequisites for the formation of a hydrogen bond are the presence of a relatively polarised hydrogen bond donor, for example, O-H, N-H, P-H, S-H, and C-H, and a suitable hydrogen bond acceptor. There are two types of hydrogen bond acceptors, those that possess a lone pair of electrons, for example O, N, P, S, and those that have centres of high electron density, such as alkenes, alkynes and aromatic π-clouds. Certain elements and functional groups have a higher tendency to form hydrogen bonds than others, and as a result form stronger bonds.

The relative abundance of non-linear hydrogen bonds suggest that optimum hydrogen bond angles are not necessarily linear. A number of surveys have correlated the geometry of the hydrogen bond in the solid state with the nature and environment of the donor and acceptor groups, and some important trends have been identified[11,19,20]. In recent years, the importance, and frequency, of weak hydrogen bond interactions, for example, C-H...X (X = O, N, Cl)[21-26], C-H...π-bond[27-31] and X-H...arene (π hydrogen bonds)[32-34], have been recognised. They play a significant role in influencing crystal structures, and should not be ignored or forgotten[14]. Within the fields of supramolecular

chemistry, molecular recognition and crystal engineering, hydrogen bonding has been recognised as an indispensable tool for designing inclusion compounds.

There are two distinct types of inclusion compounds that may be identified, namely molecular complexes and lattice clathrates. A schematic representation is shown in figure 1.1.

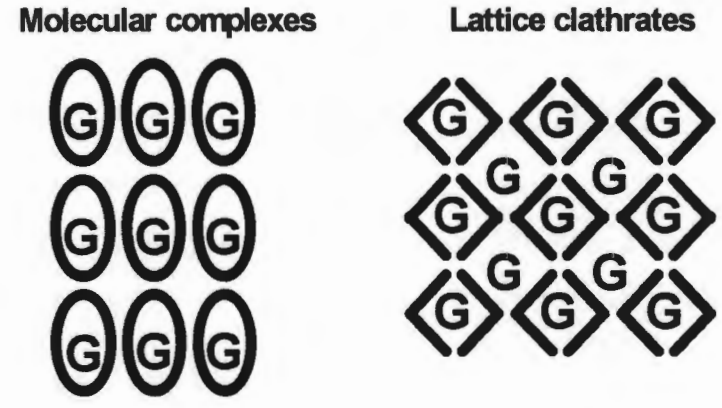

Figure 1.1 : Types of inclusion compounds.

Molecular Complexes :

In molecular complexes, the host compound is a single molecule and the guest molecule or molecules are located within the host. The host molecules can contain cavities that are either rigid or are developed by reorganisation of the hosts during the complexation process[35]. The importance of this type of compound can be gauged by the award of the 1987 Nobel Prize in chemistry to Pedersen[36], Cram[37] and Lehn[4] for their pioneering studies in this field. Their work has provided inspiration for many of the recent studies of molecular recognition in host-guest complexes, which are receiving a lot of attention because of their biometric importance and potential role as enzyme models. Typical examples include cyclodextrins, calixarenes, corands, cryptands and cavitands.

Cyclodextrins are the most studied of the naturally occurring compounds that contain rigid cavities[38]. They are cyclic oligomers of the 1,4-glucopyranoside unit, and are obtained from the renewable resource, starch. Crystalline cyclodextrins have torus-shaped cavities, the internal diameter of which increases with the number of units, while the height remains constant (figure 1.2). Cyclodextrins can serve as organic host molecules since the internal cavity is able to accommodate one or two guest molecules, shown schematically in figure 1.3. Stable complexes with a large variety of organic molecules are known. Cyclodextrins are of interest because they are stable, and can be modified in a regioselective manner[39]. Examples of monosubstituted cyclodextrin derivatives with functional groups have been reported[40,41]. They are of interest for the development of new host-guest systems, since it is expected that the properties of such compounds will be strongly modified by the variation of the spatial relationship between the substituent group and the parent macrocycle, leading to changes in the molecular conformation and intermolecular interactions.

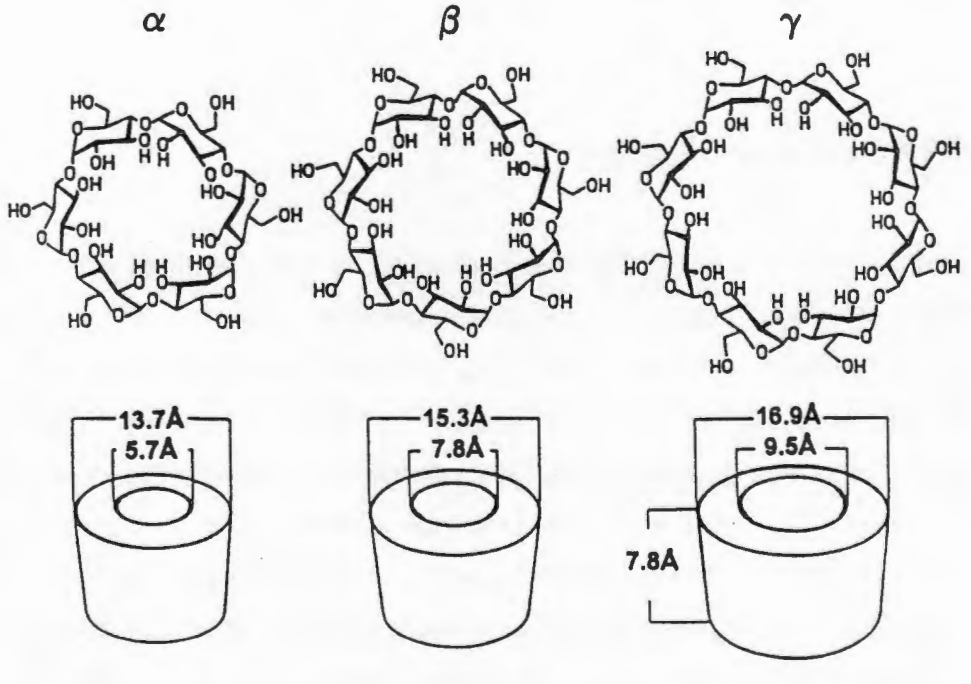

Figure 1.2 : The structure and molecular dimensions of the α, β, and γ-cyclodextrins.

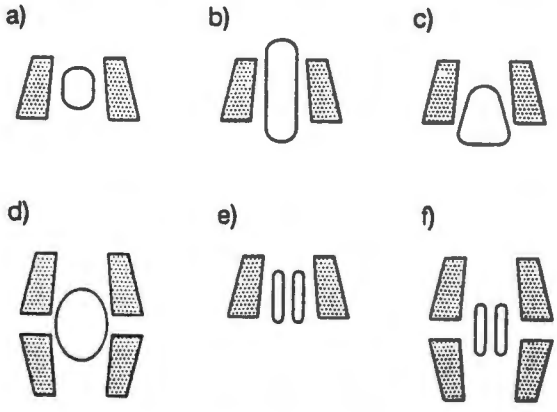

Figure 1.3 : Topology of cyclodextrin inclusion compounds with a) complete, b) axial, c) partial and d) sandwich-type inclusion; e) 1:2 and f) 2:2 host to guest ratios.[39]

Artificial organic hosts are being designed and synthesised which contain enforced cavities large enough to complex and even surround simple inorganic and organic guest compounds. For example cavitands, spherands, cryptands, and cryptapherands, are rigid hosts whose cavities are enforced and exist in the uncomplexed state[35,42]. These cavities are then filled on complexation (figure 1.4).

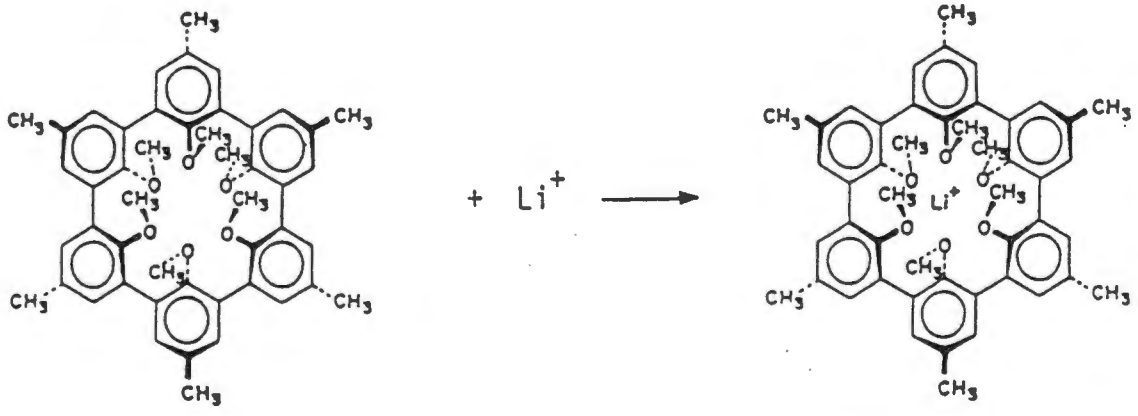

a spherand
(enforced cavity)

a lithiospherium complex
(cavity filled by Li^+)

Figure 1.4 : An example of a spherand. The cavity is filled on complexation.[35]

Calixarenes are cyclic oligomers derived from the condensation of *p*-substituted phenols and formaldehyde. The class name 'calixarene' was chosen due to the characteristic calix- or cone-like conformation[43]. A representative example of a calixarene, along with its calix-conformation, and an example of a typical inclusion compound are shown in figure 1.5. Calixarenes can easily be synthesised on a large scale, and their size and conformational properties offer nearly boundless possibilities for chemical modification[46]. Functionalization of calixarenes at the 'lower rim' (phenolic OH groups) or at the 'upper rim' (aromatic nuclei) often produces derivatives with reduced conformational mobility thus creating new shapes useful for arranging binding or catalytic groups in space. Calixarenes are considered as attractive starting materials for organic hosts which may mimic biological processes; as a result they are a growing facet of host-guest chemistry.

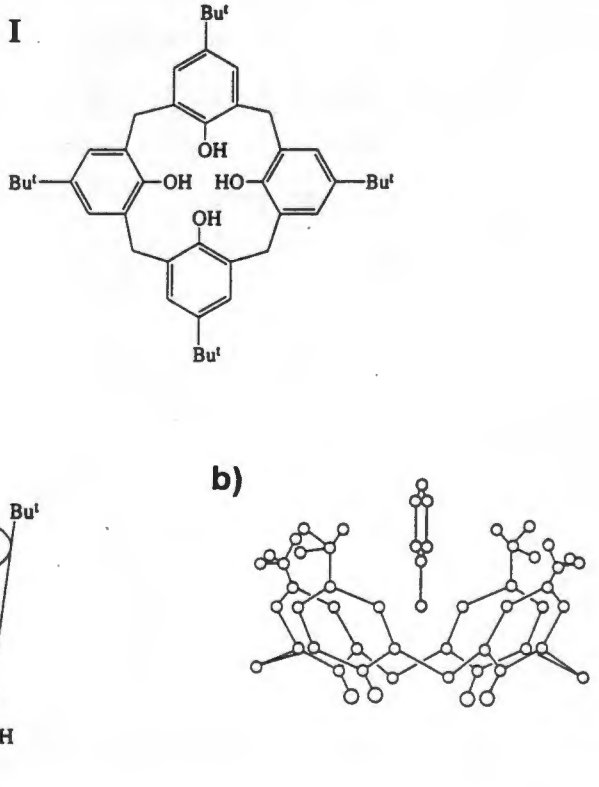

Figure 1.5 : Structural details of p-tert-butylcalix[4]arene (**I**), (a) The calix-conformation, and (b) the inclusion complex of **I** with toluene[45,44].

Corands and cryptands are examples of hosts, which when in the uncomplexed form fill their own cavities. On complexation, they are

reorganised by the guest, and cavities are developed (figure 1.6). Corands, or crown ethers, first studied by Pedersen[47], are macrocyclic polyethers whose oxygens are separated by $(CH_2)_n$ groups or groups of the *ortho*-phenylene type; while cryptands, designed and studied by Lehn[48], are macrobicyclic polyethers, which are characterised by their polycyclic structures and bridgeheads composed of $N(CH_2)_3$ units.

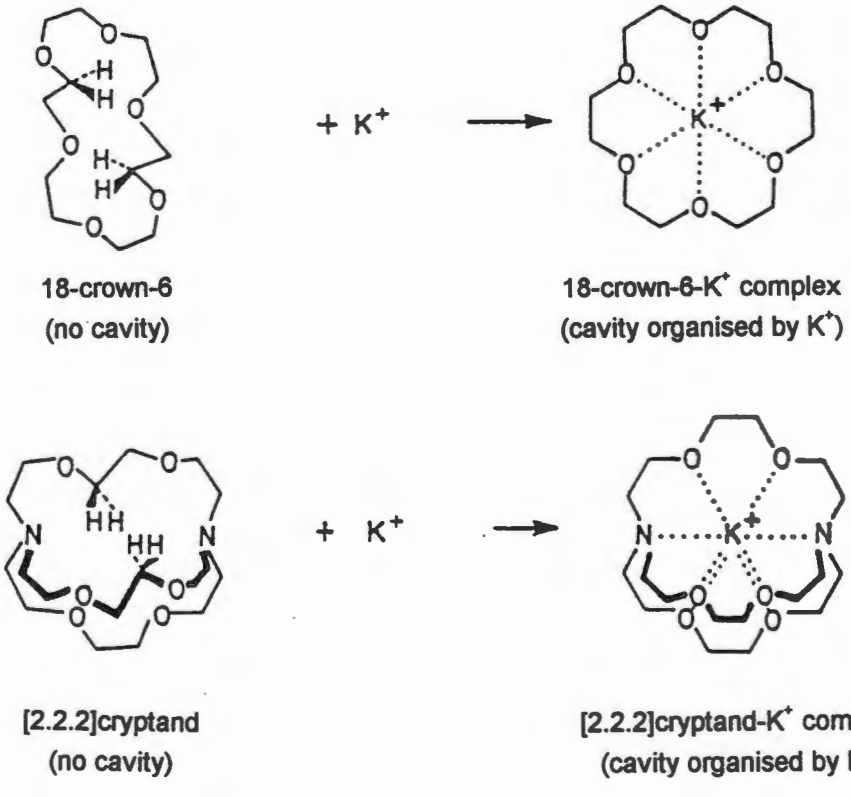

Figure 1.6 : An example of the structural reorganisation of a corand and a cryptand on complexation.[35]

Lattice Clathrates :

The second type of inclusion compounds are lattice clathrates (figure 1.1). Due to combinations of certain factors, that will be discussed shortly, some organic molecules are unable to obey the principles of crystal packing[49] to form close packed structures. A second molecule, the guest, fits into the intermolecular spaces created by the packing of these molecules, improving the packing efficiency. The voids found in the host framework may be cavities

or cages, channels, interconnected cavities, intersecting channels, or two-dimensional layers (figure 1.7)[50]. Inclusion compounds of this type can be further classified into those which include the guest compounds in a stoichiometric ratio as opposed to those for which non-stoichiometric host to guest ratios are found[51].

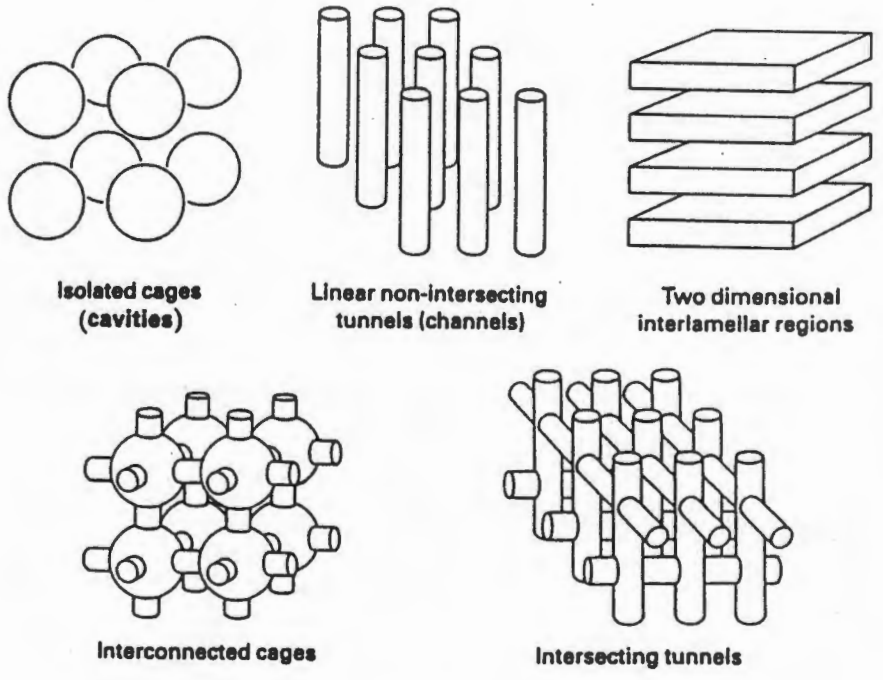

Figure 1.7 : Some of the typical topologies of voids found in crystalline host solids. The smallest dimension of each of these voids is of the order of the molecular dimensions.[50]

A number of different lattice inclusions have been observed[52], and are shown schematically in figure 1.8. They include (a) inclusion formation where there is steric compatibility between the host and guest, (b) additional stabilization of the lattice network due to functional group interaction between the host molecules, (c) interactions between host and guest, or (d) a combination of (b) and (c).

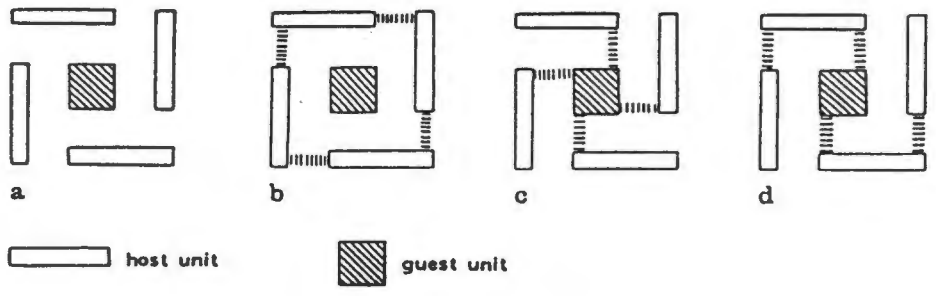

Figure 1.8 : Diagrammatic representation of different lattice inclusions. (a)-(d) show host-host and/or host-guest interactions. Interactions, such as hydrogen bonds, are indicated by broken lines.[52]

Lattice inclusion compounds have been known since the beginning of the last century, when Davy, in 1811, discovered the chlorine hydrate by bubbling chlorine into water[53]. Most of the earlier inclusion compounds were discovered purely by chance[54]. Now however, they are less commonly found by accident, but are more often the products of rational design and synthesis. Some well established host molecules efficient in lattice inclusion are shown in figure 1.9.

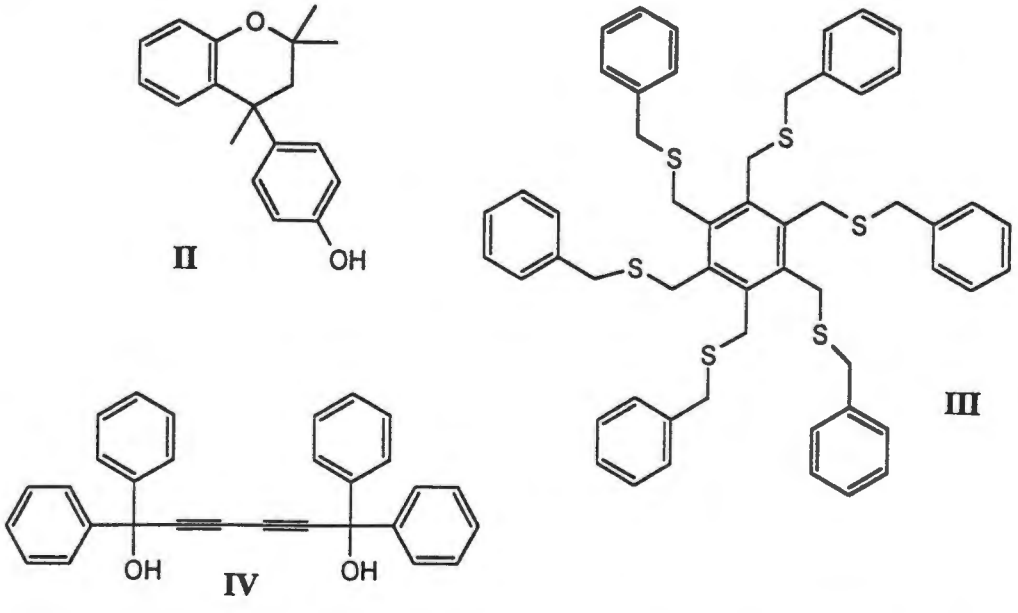

Figure 1.9 : Examples of some well known organic crystalline hosts : (**II**) Dianin's compound, (**III**) an example of a 'hexa-host', (**IV**) an example of a 'wheel-and-axle' host.

Initially new host compounds were created by altering an individual section of a known host. Marked changes in cavity geometry and guest selectivity may be produced by sensible modification of the structure of the host molecules. An example of this is the modification of Dianin's compound.

4-*p*-Hydroxyphenyl-2,2,4-trimethylchroman, **II**, named after the Russian chemist, Dianin, who first synthesised it[55], proved to be a very versatile host[56]. In its lattice the host forms a hexameric system of hydrogen bonding, which encloses a cavity in two directions. The cavity formed has an hour glass shape. Once the potential of this host had been recognised, a number of possible modifications were investigated[56]. By systematically introducing structural changes into Dianin's compound, the influence of heteroatoms and substituents on the formation of clathrates was determined. For example, on substituting the oxygen with sulphur, the resulting thiachroman was also found to be a versatile host, with interesting characteristics[57]. The dimensions of the hour glass shape cavity, which forms on crystallisation, are very similar to those of Dianin's compound. The introduction of only one additional methyl group was, however, found to lead to a dramatic change in the geometry of the cavity (figure 1.10).

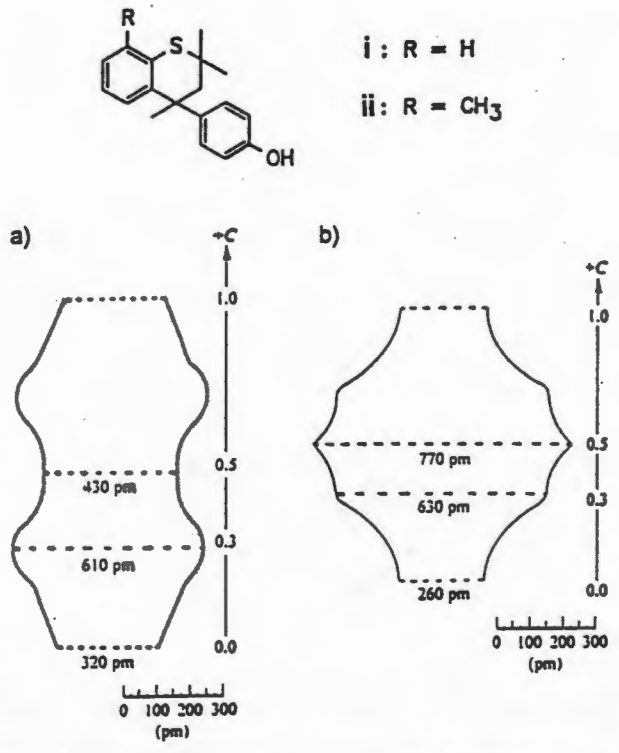

Figure 1.10 : Sections through the van der Waals surface of the cavities of (a) compound (i), and (b) compound (ii).[57]

The challenge of producing a new host without a known host molecule as a starting point is a significant one, since in order to minimise the potential energy of the system, the majority of organic molecules pack together efficiently, leaving no suitable intermolecular voids available for guest accommodation. Systematic chemical approaches have been developed, and the various concepts of molecular design of hosts for the induced formation of inclusion compounds have been evaluated[3,58]. The basic design principles for forming a crystalline host structure include molecular bulkiness, rigidity, co-ordinating groups in suitable positions and a degree of symmetry.

The bulky and rigid parts of the molecular framework are important since they are required not only to construct the cavities, that is, the non-close-packed host lattices, but also to prevent the functional groups of the individual host molecules from interacting with one another. Functional groups are characterised as hydrogen bond donors and/or acceptors of different strengths, and provide insight into the elementary interactions of functional groups on which molecular recognition is generally based. The use of functional group interactions between host and guest molecules allows for planned inclusion properties. Symmetry, particularly rotational symmetry, is a factor of growing importance for the design of new host compounds capable of forming crystalline inclusion compounds.

There are a number of design elements available for making host compounds with the above design principles, shown schematically in figure 1.11. They include : (a) planar structural elements, for example, an aromatic ring, (b) rod-like supports, such as linear bonds to ethyne, (c) bridged building blocks, or other spacious units, for example, a bicyclic system or a tertiary butyl group, (d) branching core molecules, and (e) cohesive or anchor groups, for example, functional groups such as hydroxy, carboxy and amide groups, which are prone to form strong hydrogen bonds. Joining these components together gives rise to a tremendous number of molecular geometries and shapes, which may be expected to have host properties[58].

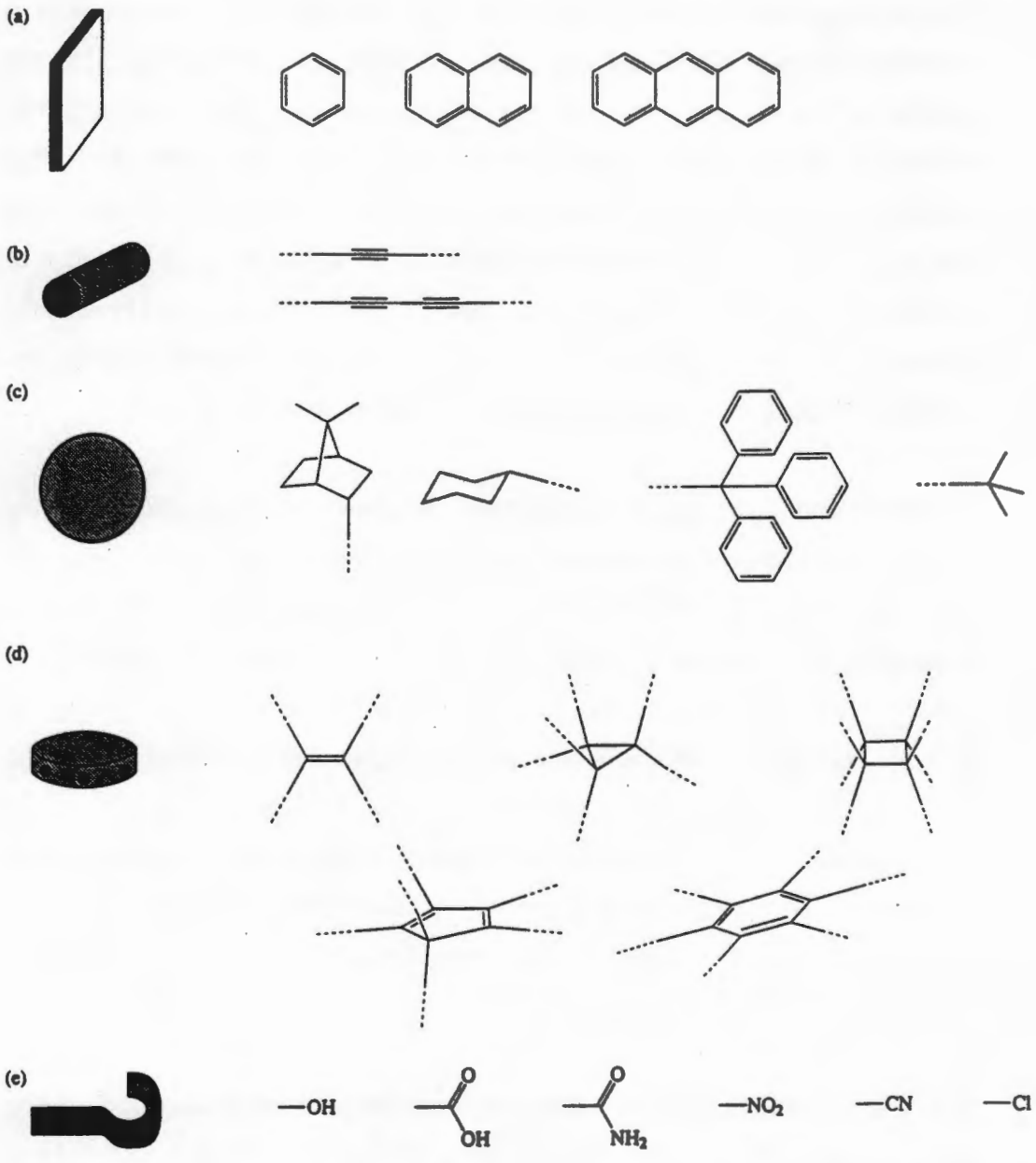

Figure 1.11 : Structural building elements : (a) planes, (b) rods, (c) bridged elements and spacious units, (d) branching core modules and (e) anchor groups.[58]

In the mid-1970's, the first systematic design of a new host with no direct structural relationship to any known host was accomplished. These hosts were called 'hexa-hosts'[59]. The concept of their design was based on the similarity between a hexa-substituted benzene, and the pre-existing hydrogen bonded hexameric unit of a number of important phenolic hosts, namely hydroquinone, phenol, Dianin's compound and related systems, and is shown

in figure 1.12. By choosing suitable substituents on the molecular periphery, non-close packed structures were obtained which resulted in molecular inclusion. **III**, in figure 1.9, is an example of one of the earliest 'hexa-hosts'. A vast range of new inclusion behaviour was immediately uncovered[60]. Not only did many of these 'hexa-hosts' show interesting inclusion behaviour on recrystallisation from single component solvents, but a number also exhibited selective inclusion behaviour from solvent mixtures. The guest molecules are usually accommodated in cages, but channel type 'hexa-host' inclusion compounds are also known[61].

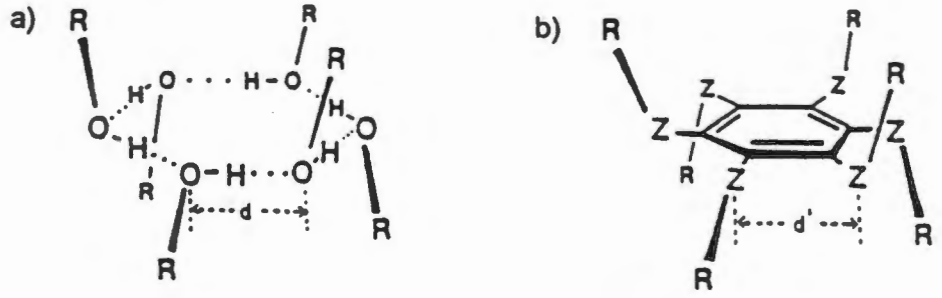

Figure 1.12 : Comparison of (a) hydrogen-bonded hexamer unit with (b) hexasubstituted benzene analogue. Z denotes a general atom or group attached directly to the central benzene ring.[59]

Awkwardness in molecular shape may also be exploited to avoid close packing of the host molecules, for example, the 'wheel-and-axle' hosts. In 1968, Toda *et al.*[62] found 1,1,6,6-tetraphenyl-2,4-hexadiyne-1,6-diol (**IV**) (figure 1.9) and 1,1,4,4-tetraphenyl-2-butyne-1,4-diol formed stoichiometric inclusion compounds with a number of different organic solvent molecules. The alkyne linkage was shown not to be necessary for the formation of inclusion compounds, since 1,1,2,2-tetraphenyl-1,2-ethanediol has similar inclusion ability with various guest molecules. Molecular rigidity, however, is essential for guest inclusion. These 'wheel-and-axle' host molecules contain the essential structural characteristics that favour guest inclusion, that is the ability to form hydrogen bonds, the possibility for π-interactions, and a rigid central portion. The high inclusion ability of these hosts is probably due to the bulky end groups, which cause steric crowding around the hydroxy groups, thereby

preventing host to host hydrogen bonding and favouring the formation of intermolecular cavities in the lattice. The guest molecules are located in the cavities, and form a hydrogen bond network with the host molecules, for example, host-OH...guest...HO-host, thus forming a stable crystalline inclusion compound.

Since the synthesis of the 'wheel-and-axle' hosts, Toda has used 1,1-diphenyl-2-propyn-1-ol (**R**) as a very useful building block, and a number of new host compounds have been designed and synthesised using it (figure 1.13)[63]. Most of these hosts have shown high inclusion ability towards guests, and three of them, namely hexakis(3-hydroxy-3,3-diphenyl-2-propynyl)benzene (**1**), 1,2,3,5,6,7-hexakis(3-hydroxy-3,3-diphenyl-2-propynyl)naphthalene (**2**) and tetra(3-hydroxy-3,3-diphenyl-2-propynyl)ethylene (**3**) were studied in this project.

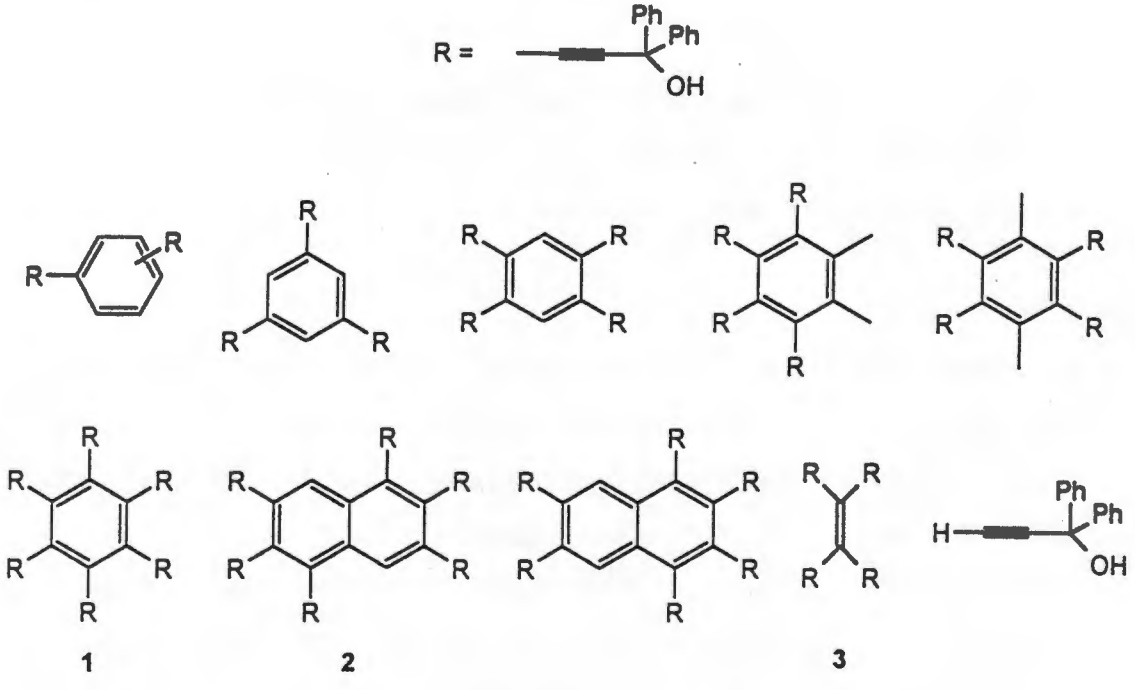

Figure 1.13 : Host compounds designed and prepared using the building block 1,1-diphenyl-2-propyn-1-ol (**R**).

Kinetics of desolvation of organic host-guest systems :

In recent years, the kinetics of desolvation of a number of organic host-guest inclusion compounds have been determined using thermogravimetry. Both rising temperature and isothermal experiments have been used. For rising temperature experiments a number of assumptions need to be made, and a number of different methods can be used to analyse the data. The methods of analysis described by Flynn and Wall[64], and Borchardt and Daniels[65] have been used to determine the kinetics of desolvation of some organic host-guest inclusion compounds, and a few examples are reported in table 1.1. The host compounds are shown in figure 1.14. The treatment of isothermal kinetic data requires fewer assumptions and the kinetic information obtained appears to be more reliable. Some examples of the kinetics of desolvation obtained using isothermal techniques are shown in table 1.2, and the host compounds involved are shown in figure 1.15 (isothermal thermogravimetry was used in this study).

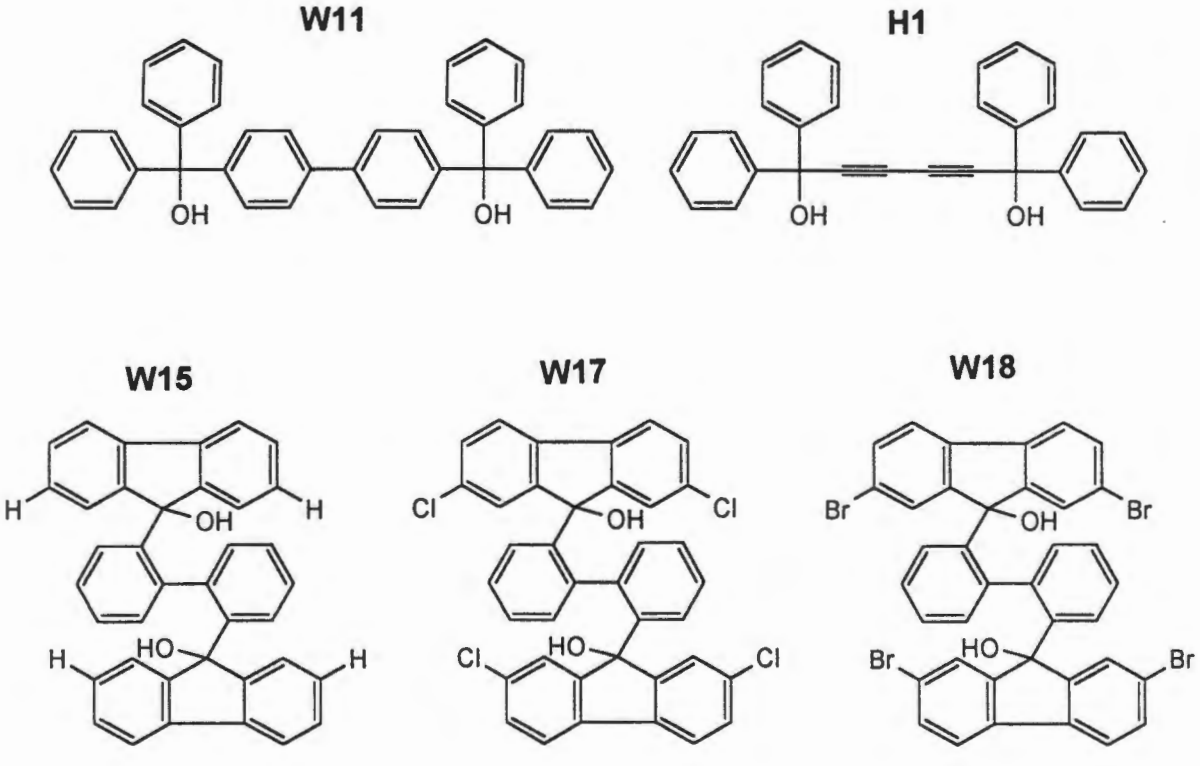

Figure 1.14 : Selected host compounds (rising temperature kinetic experiments).

Table 1.1 : Kinetics of desolvation obtained from rising temperature experiments for selected host compounds.

Host	Guest	Inclusion Mode	T_{on} (DSC) (°C)	T_b (°C)	$T_{on} - T_b$ (°C)	Ea ($kJ.mol^{-1}$)	Reference
W11	acetone	cavities	70	56.5	13.5	92-105	66[a]
	1,4-dioxane	cavities	112	101.1	10.9	136-163	66[a]
W15	diethyl ether	interconnected cavities	125.8	34.6	91.2	107-137	67[a]
H1	acetophenone	interconnected cavities	73	202	-129	42-51	68[a]
	1,4-dioxane	channels	123	101.1	-21.9	42-46	66[a]
	o-xylene	channels	87.1	144	-56.9	71-75	66[a]
	m-xylene	channels	66.8	139.3	-72.5	68-69	66[a]
	p-xylene	channels	102	137-138	-35.5	62-74	66[a]
W17	1,3-dioxane	channels	130	105-106	24.5	122(2)	69[b]
W18	1,3-dioxolane	channels	103	74-75	28.5	136(5)	69[b]

method of analysis : a) Flynn and Wall, b) Borchardt and Daniels.

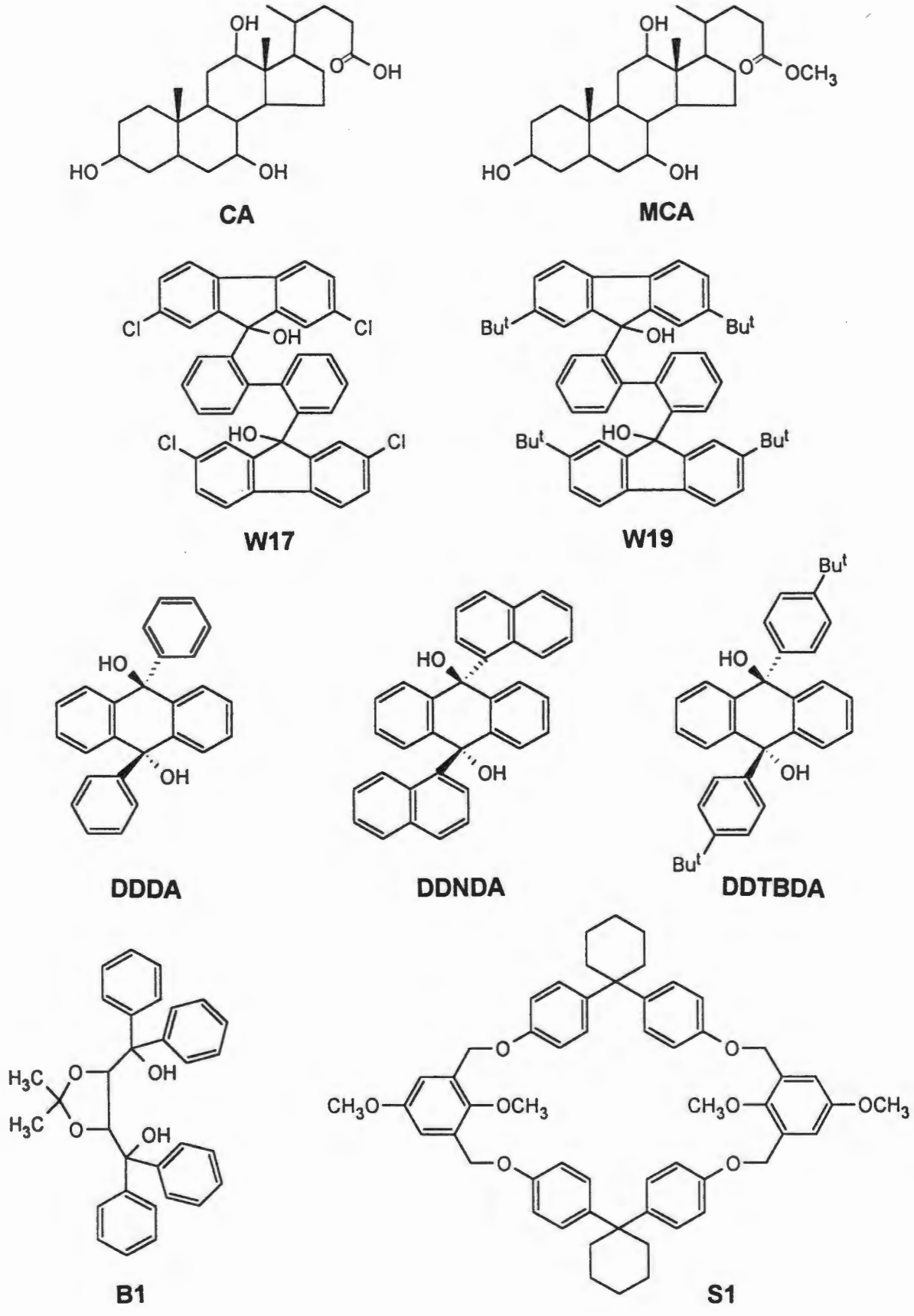

Figure 1.15 : Selected host compounds (isothermal kinetic experiments).

Table 1.2 : Kinetics of desolvation obtained from isothermal experiments for selected host compounds.

Host	Guest	Inclusion Mode	T_{on} (DSC) (°C)	T_b (°C)	$T_{on} - T_b$ (°C)	T-range (°C)	E_a (kJ.mol^{-1})	Reaction Mechanism*	Reference
CA	aniline	channels	142	184.4	-42.4	90-125	148(3)	B1	70
	benzonitrile	channels	144	189.6	-45.6	95-130	110(3)	B1	70
	nitrobenzene	channels	160	210.6	-50.6	110-145	151(2)	B1	70
	p-nitro toluene	channels	133	238.3	-105.3	98-132	117(5)	B1	70
	p-toluidine	channels	146	200.4	-54.4	95-125	151(8)	B1	70
	acetonitrile	cavities	101	81.6	19.4	78-112	244(9)	A2	71
MCA	acetonitrile	cavities	108	81.6	26.4	85-100	287(8)	D3	71
W17	acetone	channel	80	56.5	23.5	40-65	58(3)	D3	72
	1,4-dioxane	channel	66	101.1	-35.1	50-70	34(3)	F1	
			114			100-125	111(9)	F1	73
	1,3-dioxolane	channel	143	74-75	68.5	60-72	129(16)	R2	73
W19	acetone	constricted channel	175	56.5	118.5	125-145	147(4)	F1	72
	1,4-dioxane	constricted channel	179	101.1	77.9	148-160	150(6)	F1	69

Table 1.2 cont.

Host	Guest	Inclusion Mode	T_{on} (DSC) (°C)	T_b (°C)	$T_{on} - T_b$ (°C)	T-range (°C)	E_a (kJ.mol^{-1})	Reaction Mechanism*	Reference
DDDA	cyclohexanone	channels	128.5	155.6	-27.1	25-60	98(3)	R2	-
	2-methyl cyclohexanone	channels	80.1	162-163	-82.4	25-60	85(4)	R2	-
	3-methyl cyclohexanone	channels	81.4	169-170	-88.1	25-60	101(3)	R2	-
	4-methyl cyclohexanone	channels	108.8	169-171	-60.7	30-60	79(5)	R2	-
	1,3-dioxolane	channel	110	74-75	35.5	55-80	78(2)	R2	74
DDNDA	benzene	cavities	98	80.1	17.9	70-85	116(4)	B1	75
	1,3dioxolane	constricted channel	60 100	74-75	-14.5	55-75	50(10)	zero order	69
DDTBDA	benzene	channel	79	80.1	-1.1	50-70	89(4)	F1	75
	methanol	channel	60	64.7	-4.7	40-65	81(8)	F1	69
B1	methanol	cavities	135	64.7	70.3	100-130	170(1)	D4	76
	ethanol	cavities	131	78.5	52.5	100-130	179(1)	D4	76
S1	cyclohexanone	constricted channels	90	155.6	-65.6	90-100	180(20)	R2	77

* Described in detail in chapter 3. - unpublished results

It has been observed that the use of different experimental techniques and alternative methods of data analysis may result in variations in the kinetic data reported. Thus, comparisons between the kinetic data obtained from isothermal and rising temperature, and between the different methods of analysis, Flynn and Wall[64] and Borchardt and Daniels[65], will not be made.

A wide range of activation energies (E_a) is observed within each data set. From differential scanning calorimetry the onset temperature of the guest loss process can be determined. When this onset temperature (T_{on}) is compared with the boiling point (T_b) of the guest a crude measure of the thermal stability of the inclusion compound is obtained[78]. T_{on}-T_b and the mode of inclusion of the guest within the host framework are reported with the kinetic data. There does not appear to be a direct relationship between T_{on}-T_b and E_a. However, if T_{on}-T_b is negative, the E_a is much lower than if T_{on}-T_b is positive for respective hosts. This result is what we would expect since a negative T_{on}-T_b indicates a less stable inclusion compound.

A comparison of the kinetics of desolvation obtained for a particular host compound with different guest compounds suggests that E_a is higher when the mode of inclusion of the guest is in a cavity, rather than in a channel. This result would also be expected since in order to release the guest from within the cavity, the host framework must first collapse.

The kinetics of desolvation obtained for similar host compounds with the same guest also suggests that the activation energy is strongly dependent on the mode of inclusion, for example : W17 and W19 both form inclusion compounds with acetone and 1,4-dioxane. Both the inclusion compounds with W17 have a channel mode of inclusion, while for W19, the mode of inclusion is constricted channels. The activation energies obtained are greater for the W19 inclusion compounds. DDNDA and DDTBDA both include benzene. The DDNDA benzene inclusion compound has the higher activation energy, with cavities as the mode of inclusion, while DDTBDA has channels. When the mode of inclusion is the same, the stability of the inclusion compounds may explain a difference in activation energies, for example : MCA and CA are very similar host compounds both including acetonitrile within cavities found in the

host framework. However, the activation energy for MCA is greater than that obtained for CA. Looking at T_{on}-T_b, the MCA acetonitrile inclusion compound appears to be more stable than the CA inclusion compound, possibly explaining the difference in activation energies.

OBJECTIVES OF THIS STUDY

This study is concerned with the structure-reactivity relationship of selected inclusion compounds of three multipedal host compounds. The crystal structures of these inclusion compounds were elucidated and their physico-chemical properties studied. The kinetics of decomposition of some of these host-guest compounds were investigated.

The host compounds chosen for this study were hexakis(3-hydroxy-3,3-diphenyl-2-propynyl)benzene (**1**), 1,2,3,5,6,7-hexakis(3-hydroxy-3,3-diphenyl-2-propynyl)naphthalene (**2**) and tetra(3-hydroxy-3,3-diphenyl-2-propynyl) ethylene (**3**). The guest compounds were common organic solvents of varying size, shape, and hydrogen bond formation potential.

REFERENCES

1. J.-M. Lehn, *Angew. Chem., Int. Ed. Engl.*, 1990, **29**, 1304.
2. J. L. Atwood, J. E. D. Davies, D. D. MacNicol, F. Vögtle (exec. eds), *Comprehensive Supramolecular Chemistry*, Vols 1-11, Pergamon,1996.
3. J. L. Atwood, J. E. D. Davies, D. D. MacNicol (eds) *Inclusion Compounds*, Vols 1-3, Academic Press, London, 1984; Vols 4 and 5, Oxford University Press, Oxford, New York, 1991.
4. J.-M. Lehn, *Angew. Chem., Int. Ed. Engl.*, 1988, **27**, 89; J.-M. Lehn, *J. Inclusion Phenom.*, 1988, **6**, 351.
5. C. B. Aakeröy, K. R. Seddon, *Chem. Soc. Rev.*, 1993, 397.
6. G. R. Desiraju, *Crystal Engineering. The Design of Organic Solids*, Elsevier, Amsterdam, 1989.
7. J.-M. Lehn in *Frontiers in Supramolecular Organic Chemistry and Photochemistry*, (eds) H.-J. Schneider, H. Dürr, VCH Publishers, Weinheim, New York, 1991.
8. Y. Aoyama in *Supramolecular Chemistry*, (eds) V. Balzani, L. De Cola, Kluwer Academic Publishers, Dordrecht, 1992.
9. J.-M. Lehn, *Supramolecular Chemistry. Concepts and Perspectives*, VCH Publishers, Weinheim, 1995.
10. G. R. Desiraju in *Supramolecular Chemistry*. Vol. 6 - *Solid State Supramolecular Chemistry : Crystal Engineering*, (vol. eds) D. D. MacNicol, F. Toda, R. Bishop, Pergamon, 1996, chpt. 1.
11. R. Taylor, O. Kennard, *Acc. Chem. Res.*, 1984, **17**, 320.
12. M. C. Etter, *J. Phys. Chem.*, 1991, **95**, 4601.
13. J. Bernstein, M. C. Etter, L. Leiserowitz in *Structure Correlation*, Vol. 2, (eds) H.-B. Bürgi, J. D. Dunitz, VCH Publishers, Weinheim, 1994, chpt. 11.
14. S. Subramanian, M. J. Zaworotko, *Coord. Chem. Rev.*, 1994, **137**, 357.
15. W. Klemperer, *Nature*, 1993, **362**, 698.
16. H. Umeyama, K. Morokuma, *J. Am. Chem. Soc.*, 1977, 1316.
17. C. E. Dykstra, *Acc. Chem. Res.*, 1988, **21**, 355.
18. S. M. Cybulski, S. Scheiner, *J. Phys. Chem.*, 1990, **90**, 6106.
19. G. C. Pimetal, A. L. McClellan, *The Hydrogen Bond*, Freeman, San Francisco, 1960.

20. P. Schuster, G. Zundel, C. Sandorfy (eds), *The Hydrogen Bond. Recent Developments in Theory and Experiments.*, Vols 1-3, Elsivier, Amsterdam, 1976.
21. J. A. R. P. Sarma, G. R. Desiraju, *Acc. Chem. Res.*, 1986, **19**, 222.
22. G. R. Desiraju, *Acc. Chem. Res.*, 1991, **24**, 290.
23. T. Steiner, W. Saenger, *J. Am. Chem. Soc.*, 1992, **114**, 10146.
24. T. Steiner, W. Saenger, *J. Am. Chem. Soc.*, 1993, **115**, 4540.
25. T. Steiner, *J. Chem. Soc., Chem. Commun.*, 1994, 2341.
26. R. Taylor, O. Kennard, *J. Am. Chem. Soc.*, 1982, **104**, 5063.
27. N. Nishio, M. Hirota, *Tetrahedron*, 1989, **45**, 7201.
28. T. Steiner, E. B. Starikov, A. M. Amado, J. J. C. Teixeira-Dias, *J. Chem. Soc., Perkin Trans. 2*, 1995, 1321.
29. T. Steiner, E. B. Starikov, M. Tamm, *J. Chem Soc., Perkin Trans. 2*, 1996, 67.
30. T. Steiner, M. Tamm, A. Grzegorgzewski, N. Schulte, N. Veldman, A. M. M. Schreurs, J. A. Kanters, J. Kroon, J. van der Maas, B. Lutz, *J. Chem. Soc., Perkin Trans. 2*, 1996, 2441
31. M.-F. Fan, Z. Lin, J. E. McGrady, D. M. P. Mingos, *J. Chem. Soc., Perkin Trans. 2*, 1996, 563.
32. J. L. Atwood, F. Hamada, K. D. Robinson, G. W. Orr, R. L. Vincent, *Nature*, 1991, **349**, 683.
33. S. Ueji, K. Nakatsu, H. Yoshioka, K. Kinoshita, *Tetrahedron Lett.* 1982, **23**, 1173.
34. M. A. Viswamitra, R. Radhakrishna, J. Bandekar, G. R. Desiraju, *J. Am. Chem. Soc.*, 1993, **115**, 4868.
35. D. J. Cram, *Science*, 1983, **219**, 1177.
36. C. J. Pedersen, *Angew. Chem., Int. Ed. Engl.*, 1988, **27**, 1021; C. J. Pedersen, *J. Inclusion Phenom.*, 1988, **6**, 351.
37. D. J. Cram, *Angew. Chem., Int. Ed. Engl.*, 1988, **27**, 1009; D. J. Cram, *J. Inclusion Phenom.*, 1988, **6**, 397.
38. For review see : J. Szejtli, T. Osa (eds) *Comprehensive Supramolecular Chemistry*, Vol. 3, *Cyclodextrins*, Pergamon, 1996.
39. G. Wenz, *Angew. Chem., Int. Ed. Engl.*, 1994, **33**, 803.
40. H. Parrot-Lopez, E. Leray, A. W. Coleman, *Supramol. Chem.*, 1993, **3**, 37.

41. M. Selkti, H. Parrot-Lopez, J. Navaza, F. Villain, C. de Rango, *Supramol. Chem.*, 1995, **5**, 255.
42. D. J. Cram, *Angew. Chem., Int. Ed. Engl.*, 1986, **25**, 1039.
43. C. D. Gutsche, R. Muthukrishnan, *J. Org. Chem.*, 1982, **43**, 4905.
44. E. Weber, F. Vögtle in *Comprehensive Supramolecular Chemistry*, Vol. 2, *Molecular Recognition : Receptors for Molecular Guests.*, (ed.) F. Vögtle, Pergamon, 1996, chpt. 1.
45. G. D. Andreetti, R. Ungaro, A. Pochini, *J. Chem. Soc., Chem. Commun*, 1979, 1005.
46. For a review see : V. Böhmer, *Angew. Chem., Int. Ed. Engl.*, 1995, **34**, 713.
47. C. J. Pedersen, *J. Am. Chem. Soc.*, 1967, **89**, 2495.
48. B. Dietrich, J.-M. Lehn, J. P. Sauvage, *Tetrahedron Lett.*, 1969, 2885.
49. C. Pratt Brock, J. D. Dunitz, *Chem. Mater.*, 1994, **6**, 1118.
50. K. D. M. Harris, *Chemistry in Britain*, 1993, 132.
51. F. Toda in *Inclusion Compounds*, Vol. 4, (eds) J. L. Atwood, J. E. D. Davies, D. D. MacNicol, Oxford University Press, Oxford, New York, 1991.
52. E. Weber in *Top. Curr. Chem.*, Vol. 140, *Molecular Inclusion and Molecular Recognition - Clathrates 1*, (ed.) E. Weber, Springer-Verlag, Berlin-Heidelberg, 1987, chpt. 1.
53. H. Davy, Philos. Trans. R. Soc. Lond., 1811, 101, 155.
54. J. E. D. Davies, W. Kemula, H. M. Powell, N. O. Smith, *J. Inclusion Phenom.*, 1983, **1**, 3.
55. A. P. Dianin, *J. Russe. Phys. Chem. Soc.*, 1914, **46**, 1310.
56. For a review see : D. D. MacNicol in *Inclusion Compounds*, vol. 2, (eds) J. L. Atwood, J. E. D. Davies, D. D. MacNicol, Academic Press, London, 1984, chpt. 1; J. Szejtli, T. Osa in *Supramolecular Chemistry*. Vol. 6 - *Solid State Supramolecular Chemistry : Crystal Engineering*, (vol. eds) D. D. MacNicol, F. Toda, R. Bishop, Pergamon, 1996, chpt. 18.
57. A. D. U. Hardy, J. J. McKendrick, D. D. MacNicol, *J. Chem. Soc., Perkin Trans. 2*, 1979, 1072.
58. E. Weber in *Supramolecular Chemistry*. Vol. 6 - *Solid State Supramolecular Chemistry : Crystal Engineering*, (vol. eds) D. D. MacNicol, F. Toda, R. Bishop, Pergamon, 1996, chpt. 17.

59. D. D. MacNicol, D. R. Wilson, *J. Chem. Soc., Chem. Commun*, 1976, 494; A. D. U. Hardy, D. D. MacNicol, D. R. Wilson, *J. Chem. Soc., Perkin Trans. 2*, 1979, 1011.

60. For a review of these results : D. D. MacNicol in *Inclusion Compounds*, Vol. 2, (eds) J. L. Atwood, J. E. D. Davies, D. D. MacNicol, Academic Press, London, 1984, chpt. 5; D. D. MacNicol, G. A. Downing in *Supramolecular Chemistry.* Vol. 6 - *Solid State Supramolecular Chemistry: Crystal Engineering*, (vol. eds) D. D. MacNicol, F. Toda, R. Bishop, Pergamon, 1996, chpt. 14.

61. A. Freer, C. J. Gilmore, D. D. MacNicol, D. R. Wilson, *Tetrahedron Lett.*, 1980, **21**, 1159.

62. F. Toda, K. Akagi, *Tetrahedron Lett.*, 1968, **33**, 3695.

63. S. A. Bourne, M. R. Caira, L. R. Nassimbeni, M. Sakamoko, K. Tanaka, F. Toda, *J. Chem. Soc., Perkin Trans. 2*, 1994, 1899; O. Kakinoki, Bachelor Thesis, Ehime University, Japan, 1991; M. Sakamoto, Masters Thesis, Ehime University, Japan, 1994.

64. J. H. Flynn, L. A. Wall, *Polymer Lett.*, 1996, **4**, 323.

65. H. J. Borchardt, F. Daniels, *J. Am.Chem. Soc.*, 1957, **79**, 41.

66. L. Johnson, PhD Thesis, University of Cape Town, 1992.

67. M. R. Caira, L. R. Nassimbeni, N. Winder, E. Weber, A. Wierig, *Supramol. Chem.*, 1994, **4**, 135.

68. L. Johnson, L. R. Nassimbeni, *Acta Cryst.*, 1992, **B48**, 827.

69. A. Coetzee, PhD Thesis, University of Cape Town, 1996.

70. J. L. Scott, PhD Thesis, University of Cape Town, 1995.

71. J. L. Scott, *J. Chem. Soc., Perkin Trans. 2*, 1995, 495.

72. M. R. Caira, A. Coetzee, L. R. Nassimbeni, E. Weber, A. Wierig, *J. Chem. Soc., Perkin Trans. 2*, 1997, 237.

73. M. R. Caira, A. Coetzee, L. R. Nassimbeni, E. Weber, A. Wierig, *J. Chem. Soc., Perkin Trans. 2*, 1995, 281.

74. M. R. Caira, A. Coetzee, L. R. Nassimbeni, F. Toda, *J. Chem. Research (S),* 1996, 280.

75. L. J. Barbour, M. R. Caira, A. Coetzee, L. R. Nassimbeni, *J. Chem. Soc., Perkin Trans. 2*, 1995, 1345.

76. S. A. Bourne, B. M. Oom, F. Toda, *J. Chem. Soc., Perkin Trans. 2*, 1997, 585.

77. S. Apel, M. Czugler, V. J. Griffith, L. R. Nassimbeni, E. Weber, *J. Chem. Soc., Perkin Trans. 2*, in press.

78. S. A. Bourne, L. R. Nassimbeni, *J. Org. Chem.*, 1992, **57**, 2438.

CHAPTER 2

EXPERIMENTAL

The crystal structures described in this thesis have been divided into three groups based on the host compound.

Host 1 : hexakis(3-hydroxy-3,3-diphenyl-2-propynyl)benzene

Host 2 : 1,2,3,5,6,7-hexakis(3-hydroxy-3,3-diphenyl-2-propynyl)naphthalene

Host 3 : tetra(3-hydroxy-3,3-diphenyl-2-propynyl)ethylene

The compounds studied, with their code names, are listed in table 2.1. This table can also been found on the inserted bookmark.

HOST COMPOUNDS

The host compounds hexakis(3-hydroxy-3,3-diphenyl-2-propynyl)benzene (**1**)[1], 1,2,3,5,6,7-hexakis(3-hydroxy-3,3-diphenyl-2-propynyl)naphthalene (**2**)[2] and tetra(3-hydroxy-3,3-diphenyl-2-propynyl)ethylene (**3**)[2] were synthesised and supplied by Professor Fumio Toda, at the Ehime University, Japan.

INCLUSION COMPOUNDS AND CRYSTAL GROWTH

The amount of host material available was limited, and as a result, wherever possible the host compounds were recovered.

Inclusion compounds were obtained by dissolving the appropriate host compound in an excess of the solvent to be included. In some cases, it was necessary to warm the solution. A number of different crystallisation techniques were attempted, for example, slow cooling of the sample solution, maintaining the solution at an elevated temperature, reducing the rate of solvent evaporation by refrigeration, and removal of excess nucleation sites by filtration. The method which proved to be the most successful in obtaining suitable single crystals for X-ray diffraction data collection was filtration, followed by solvent evaporation at room temperature. The solutions were forced through 0.45μm teflon microfilters, via a syringe, and left to evaporate

slowly at room temperature until crystallisation occurred. At this point the vials were sealed to prevent further evaporation of the mother liquor.

All three of the host compounds were found to be soluble in ketones, esters, ethers, amines and amides. Single crystals of the non-porous α-phase of both hosts **1** and **3** were crystallised from benzene. The same α-phase of host **3** was also obtained on crystallisation from 2-hexanone.

Table 2.1 : Compounds studied.

Host	Guest	Code Name
1	-	SPBN
	acetonitrile, benzene	SPAB
	cyclohexanone	SPCHO
	cyclohexanone	SPDICHO
	diethyl ketone	SPDEK
	dimethyl acetamide	SPDMA
	1,4-dioxane	SPDIOX
	1,3-dioxolan-2-one	SPDIOXO
	ether	SPETH
	2-hexanone	SP2H
	methyl ethyl ketone	SPMEK
2	cyclohexanone	NAPCHO
	dimethyl acetamide	NAPDMA
	dimethyl formamide	NAPDMF
	2-hexanone	NAP2H
3	-	ETHBN
	cyclohexanone	ETHCHO
	dimethyl acetamide	ETHDMA

THERMAL ANALYSIS

The techniques used for thermal analysis are well established, and a number of books have been written on the subject[3-7].

Thermogravimetry (TG) and differential scanning calorimetry (DSC) were used to:

- establish the stoichiometry of the inclusion compound,
- determine the temperature of guest release from the crystal,
- observe the number of phase changes in the crystal structure and the temperatures at which they occur.

TG and DSC were performed using a Perkin Elmer PC7 Series system. The TG thermocouple and balance were calibrated using built in procedures for the furnace and weight calibration. Two point standard temperature calibration was performed by measuring the Curie points of alumel (163°C) and nickel (354°C). The DSC analyser was calibrated by measuring the melting points of indium (156.4°C) and zinc (419.5°C). The heat flow was calibrated using the enthalpy of melting of indium ($28.62 Jg^{-1}$).

Crystals were removed from the mother liquor, blotted dry and lightly crushed before analysis. Samples of 2 - 5mg were placed in an open platinum pan for TG experiments, while those for the DSC experiments were placed in a crimped, vented aluminium pan, with a sealed empty pan as the reference. Programmed temperature runs were performed over the temperature range 30 to 300°C at a heating rate of $10°C min^{-1}$ under dry nitrogen purge gas flowing at *ca* 40 $cm^3 min^{-1}$ (TG) and *ca* 30 $cm^3 min^{-1}$ (DSC).

TG was also used to determine the activation energy of guest release. Isothermal TG experiments were performed to obtain data for the kinetics of desolvation of the inclusion compounds studied which were characterised by single step guest loss reactions. Samples of similar mass, within 1mg, were heated rapidly to a specific temperature, which was then maintained until the guest release reaction was complete. The desorption reactions were done at

temperature intervals of 2 - 5°C over the range found to be isokinetic for that particular compound.

Finely powdered samples were used in these isothermal experiments. They were prepared by dissolving the host in the guest solvent. The solution was then continuously stirred, using a magnetic stirrer, until precipitation of the inclusion compound occurred. By stirring the solution continuously, the growth of larger crystals was prevented, and therefore, it was not necessary to crush the sample. The sample size distribution was determined using a Malvern Series 2600 laser particle sizer, and was found to be in the range 20 - 100μm. These powdered samples were prepared just prior to analysis, so the length of storage was kept to a minimum.

X-RAY POWDER DIFFRACTION

X-Ray powder diffraction (XRD) patterns were recorded on a Philips PW1050/80 vertical goniometer with a PW1394 motor control unit and PW1390 channel control unit mounted on a PW1130/90 X-ray generator operating at 40kV and 25mA. Powdered samples were packed into aluminium sample holders. Nickel-filtered CuK_α radiation (λ = 1.5418Å) was passed through 0.2° divergent and receiving slits, and a 1° anti-scatter slit. The samples were scanned over the range 6 - 35° 2θ at intervals of 0.1° with a 2s count.

Calculated XRD patterns for the corresponding crystal structures were produced using the computer program LAZYPULVERIX[8]. The input included the space group symmetry, refined unit cell parameters, atomic coordinates and thermal parameters.

HOTSTAGE MICROSCOPY

Melting points, temperatures of guest release and other interesting thermal events were observed visually on a Linkam TH600 hotstage mounted on a Nikon AFX microscope. The temperature was controlled by a Linkam CO600 temperature controller. The hotstage was calibrated using the melting points of azobenzene (68°C), benzil (95°C), benzanilide (163°C) and dicyanodiamide (210°C).

These observations were correlated with the thermal events recorded in the TG and DSC experiments. The temperatures at which the changes were observed were often slightly higher than those observed in the thermal analysis. The discrepancies between the temperatures are mainly due to the differences in the geometries of the instruments, and the use of different particle sizes. Single crystals, usually larger than 0.5mm in all dimensions, were observed on the hot-stage, whereas powdered samples were used for thermal analysis.

DENSITY MEASUREMENT

Densities were measured using the flotation method. A suitable crystal was blotted dry, and immersed in a solution of saturated potassium iodide and water. Further additions of KI or water were added until the density of the solution was the same as that of the crystal, that is, the crystal was suspended in the solution. The density of the solution was then determined using a Paar DMA digital density meter. This method is relatively slow, and as a result, only the densities of the sufficiently stable inclusion compounds could be determined.

MICROANALYSIS

C, H, and N (where appropriate) elemental analyses were performed in duplicate on a Carbo Erba elemental analyser Model 1106. Samples were not placed under vacuum as this could have resulted in loss of the guest. Even on removal from the mother liquor, some of the compounds started to decay owing to their low stability.

MASS SPECTROSCOPY

The mass spectrum of SPDIOXO was recorded using a VG-Micromass 16F mass spectrometer with a VG system 2000 PDP-8/a microprocessor. Accurate mass determination was performed by peak matching using a Kratos High Resolution mass spectrometer.

NUCLEAR MAGNETIC RESONANCE (NMR) SPECTROSCOPY

NMR spectroscopy was used to confirm guest composition, and stoichiometry in cases where possible ambiguities existed, such as when crystals were grown from mixed guest solutions.

Samples were dissolved in deuterated chloroform or acetone. ^{1}H and ^{13}C-NMR spectra were recorded at 200MHz on a Varian VXR-200 spectrometer with tetramethylsilane as the internal reference.

GAS CHROMATOGRAPHY

The 1,3-dioxolane used was analysed for impurities using a Carlo Erba Fractovap 4200 gas chromatograph equipped with a bp255 capillary column (0.25mm diameter, 25m length) and with a Spectra-Physics SP4290 integrator.

CRYSTAL STRUCTURE ANALYSIS

Suitable single crystals, typically between 0.2 and 0.5mm in all dimensions, were chosen for data collection. In some cases it was necessary to cleave the crystals to the appropriate size. Since all these compounds are relatively unstable, the crystals were firmly wedged and heat sealed into 0.3 or 0.5mm diameter Lindemann capillary tubes in order to protect them from the atmosphere. Crystals of SPBN and ETHBN were stable to the atmosphere, and were mounted on the end of glass fibres. The sealed Lindemann tube or glass fibre was then mounted on a brass pin and placed securely on a goniometer head.

Preliminary unit cell parameters, and space group symmetry were determined from oscillation and Weissenberg photographs taken on a Stoë goniometer, using Ni filtered CuKα radiation (λ = 1.5418Å).

X-Ray diffraction data were measured on an Enraf-Nonius CAD4 diffractometer, using graphite-monochromated MoKα radiation (λ = 0.71069Å). Most of the data collections were collected at low temperature, except for SPBN, SPDEK, SPDIOX and ETHBN, which were collected at room temperature. An FTS Systems Air Jet refrigeration unit (model XR-85-1) was used for the earlier low temperature collections. This system was later replaced by an Oxford Cryostream cooler[9].

Accurate unit cell parameters were obtained by least-squares analysis of the setting angles of 24 reflections collected in the θ range 16 - 17°. Intensity data were collected in the ω-2θ scan mode with a final acceptance limit of 20 σ at 20°min^{-1} and a maximum scan time of 40s. The vertical aperture length was fixed at 4mm, the aperture width at (1.12 + 1.05tanθ)mm, and the scan width ω = (x + 0.35tanθ)°, with x = 0.80 or 0.85. During each data collection three reference reflections were monitored periodically to check crystal stability and orientation. The data were corrected for Lorentz and polarisation effects. Absorption corrections were not applied, as the values for the product μR, where μ is the linear absorption coefficient and R the maximum radius of the crystal, were less than 0.1 for all crystals, and thus the values of the absorption correction factors are close to unity.

STRUCTURE SOLUTION AND REFINEMENT

The structures were solved by direct methods using the program SHELX86[10], which is based on a random start multisolution philosophy[11]. Subsequent refinements were done using SHELXL-93[12], which employs a full matrix least-squares refinement against F^2.

The residual index, R, is a measure of the agreement between the calculated (based on the model) and observed structure factors. The residual indices obtained for refinement against F^2, R_2, are larger than those obtained for refinement against F, R_1. In the past most crystal structures were refined against F, so for comparison with these structures R_1 is also calculated. Refinement against F^2 also tends to magnify the deviation of the Goodness of Fit, S, from unity.

R is defined as follows :

$$R_1 = \frac{\Sigma \, | \, |F_o| - |F_c| \, |}{\Sigma |F_o|}$$

$$wR_2 = \left(\frac{\Sigma \, w \, (F_o^2 - F_c^2)^2}{\Sigma \, w \, (F_o^2)^2} \right)^{1/2}$$

where w is the weighting scheme (a and b are refined for each structure) :

$$w = 1 / [\sigma^2 (F_o^2) + (aP)^2 + bP]$$

$$P = [\max(0, F_o^2) + 2F_c^2] / 3$$

S is defined as follows :

$$S = [\Sigma [w (F_o^2 - F_c^2)^2] / (n - p)]^{1/2}$$

where n is the number of reflections, and p is the total number of parameters refined.

If S is significantly higher than unity, the program may print out a warning that an extinction parameter should be refined. The extinction parameter, x, is refined by least squares, where

$$k\,[(1 + 0.001 \times x \times F_c^2 \times \lambda^3) / \sin(2\theta)]^{-1/4}$$

and k is the overall scale factor. This expression is empirical and represents a compromise to cover both primary and secondary extinction.

COMPUTATION

Molecular and packing diagrams were produced using the PC version of PLUTO[13]. The channel and cavity shapes and volumes formed by the host molecules were investigated using the program MOLMAP[14]. Guest co-ordinates were removed from the model and the host molecules are represented with spherical radii equal to their van der Waals radii.

The Cambridge Structural Database (CSD)[15] was used to investigate published crystal data, for comparison with the structures reported in this study.

REFERENCES

1. S. A. Bourne, M. R. Caira, L. R. Nassimbeni, M. Sakamoko, K. Tanaka, F. Toda, *J. Chem. Soc., Perkin Trans. 2*, 1994, 1899.
2. O. Kakinoki, Bachelor Thesis, Ehime University, 1991.
3. M. E. Brown, *Introduction To Thermal Analysis - Techniques and Applications*, Chapman and Hall, London, 1988.
4. E. L. Charsley, S. B. Warrington (eds), *Thermal Analysis - Techniques and Applications*, The Royal Society of Chemistry, 1992.
5. W. W. M. Wendlandt, *Thermal Analysis*, John Wiley and Sons, New York, 1964.
6. B. Wunderlich, *Thermal Analysis*, Academic Press Limited, London, 1990.
7. P. J. Haines, *Thermal Methods of Analysis*, Blackie Academic and Professional, 1995.
8. K. Yvon, W. Jeitschko, E. Parthe, *J. Appl. Crystallog.*, 1977, **10**, 73.
9. J. Cosier, A. M. Glazer, *J. Appl. Cryst.*, 1986, **19**, 105.
10. G. M. Sheldrick, *Acta. Crystallogr., Sect. A.*, 1990, **46**, 467.
11. *International Tables for Crystallography*, Vol. C, ed. A. J. C. Wilson, Kluwer Academic publishers, Dordrecht, 1992, 523.
12. G. M. Sheldrick, SHELXL-93 : Programme for Crystal Structure Determination, unpublished work.
13. W. D. S. Motherwell, PLUTO89, program for plotting molecular and crystal structures, University of Cambridge, England, 1989.
14. L. J. Barbour, *Clathration by Diol Hosts : Thermodynamics and Structure*, PhD Thesis, University of Cape Town, South Africa, 1994.
15. Cambridge Structural Database and Cambridge Structural Database System, Version 5.12, Cambridge Crystallographic Data Centre, University Chemical Laboratory, Cambridge, England.

CHAPTER 3

PHYSICAL CHARACTERISATION

The details of each of the structures elucidated in this study will be discussed in Chapters 4, 5 and 6. However, some of their physical characteristics are summarised below.

DECAY OF HOST 3

Approximately a year and a half after receiving the sample of host **3**, used in this study, it was found to have decayed. The decay mechanism is thought to be radical cleavage, reducing the steric strain induced in the host molecule by the ethylene group. This light catalysed reaction results in the possiblity of a number of products, one of which has been found to be the well known "wheel and axle" host, 1,1,6,6-tetraphenyl-2,4-hexadiyne-1,6-diol[1].

THERMAL ANALYSIS

The process of decomposition of an inclusion compound, without chemical change of either the host or guest, may be the sum of a number of steps each resulting in the existence of discrete, identifiable phases. Thermal events in a sample will appear as deviations from the DSC baseline in either an endothermic or exothermic direction, depending on whether more or less energy has to be supplied to the sample relative to the reference. Detectable changes in the DSC trace could be due to a guest loss reaction, a solid state phase change, melting or recrystallistion. Figure 3.1 shows a schematic DSC trace for some of the more commonly encountered phase changes associated with the decomposition of an inclusion compound. This trace may be interpreted as follows : β is the phase of the inclusion compound as grown from solution. This phase may on heating lose a portion of the included guest (endotherm A) resulting in the formation of a γ-phase with a different host to guest ratio. On further heating the γ-phase loses the remaining guest molecules (endotherm B) and the host compound usually collapses to the non-porous α-phase. The α-phase is defined as the host phase which is

stable at room temperature. However, other non-porous phases may exist in the form of stable, metastable or high temperature polymorphs. Endotherm C represents melting of the host compound. Endotherms A and B will be accompanied by a mass loss on TG analysis. Often only a single endotherm corresponding to guest loss and molecular rearrangement of the β-phase to the α-phase, followed by a host melt endotherm is observed. It should, however, be noted that the peaks obtained are not always well defined and may assume complex shapes due to the complex nature of phase-change mechanisms.

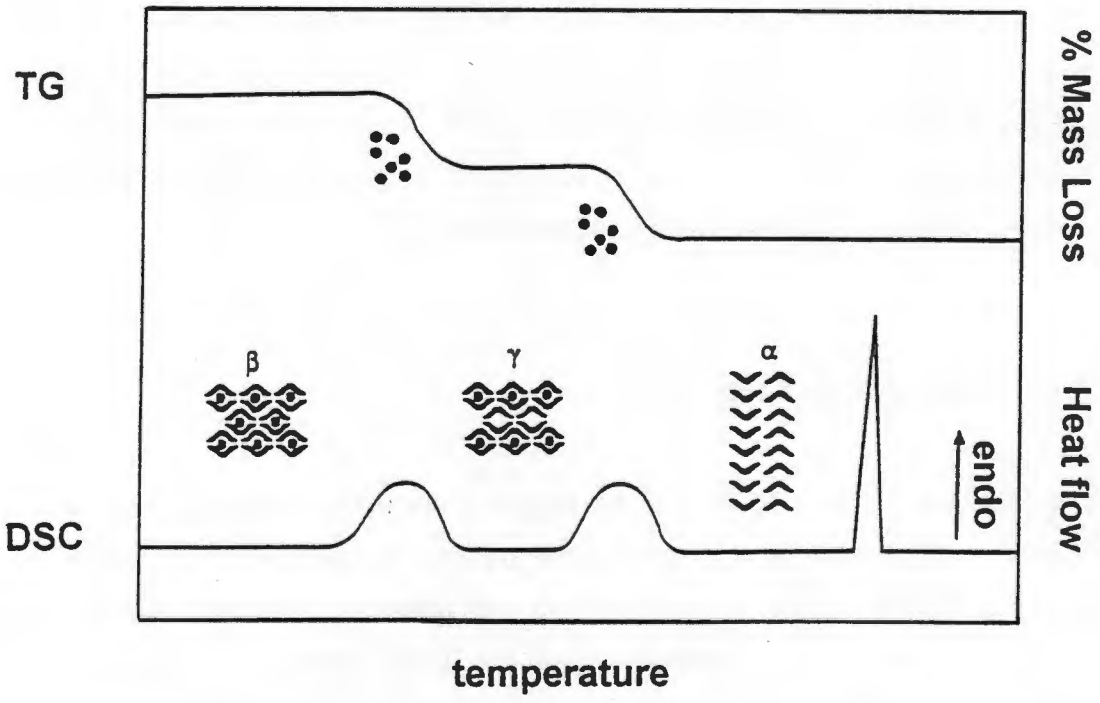

Figure 3.1 : A schematic DSC trace showing some of the possible phase changes (as endotherms) associated with inclusion compound decomposition. The TG curve follows the guest loss reaction. (modified from reference 2)

As with any instrumental technique TG and DSC have a large number of factors which affect the nature, precision and accuracy of the experimental results. The ΔH values measured using DSC are dependent on heating rates, purge gas flow rates, composition and geometry of the sample holder, geometry of the calorimeter, amount of sample, and most importantly, particle size. The particle size, particle size distribution and closeness of the size

fraction also influence the size, shape, position, resolution and even the number of peaks which are observed. In order to obtain reproducible results the samples should be crushed and sieved without loss of the guest. This is generally not possible owing to prompt decomposition of the inclusion compounds with volatile guests. For the purposes of this study, DSC was used qualitatively to gain information about the number and approximate temperatures of phase changes occurring during the decomposition process. The onset temperature of the guest loss process when compared with the boiling point of the guest is used as a crude measure of the thermal stability of the inclusion compound[3,4].

TG, and NMR spectroscopy, when the crystals were grown from mixed solutions, as for SPAB and SPDICHO, confirmed the host to guest ratios modelled in the crystal structures. The mass losses observed in the TG curves were used to calculate the host to guest ratios of the inclusion compounds formed, and were measured with an accuracy of 1%. The observed and calculated mass losses are tabulated in Appendix A. Not all the crystal structures of the inclusion compounds formed have been determined. Table 3.1(a) summarises the host to guest ratios of the inclusion compounds for which the crystal structures have been solved in this study. Other inclusion compounds formed by hosts **1** and **2** that have been characterised by thermal analysis are summarised in table 3.1(b).

The thermal analysis results obtained for the inclusion compounds studied will be discussed in detail with each structure. The TG and DSC curves are analysed together. The geometries and sample environments of the TG and DSC analysers are, however, significantly different, and as a result the onset temperatures of the thermal events observed do not always correspond exactly. Hotstage microscopy and X-ray powder diffraction were also used to aid in the assignment of the thermal events recorded.

Table 3.1(a) : Inclusion compounds studied.

Host	Guest	Observed mass loss (%)	Expected mass loss (%)	Host:Guest
1	-	-	-	-
	acetonitrile, benzene	14.8	15.3	1:2:2
	cyclohexanone	26.5	27.2	1:5
	cyclohexanone	12.8	13.0	1:2
	diethyl ketone	11.1	11.6	1:2
	dimethyl acetamide	20.3	20.1	1:4
	1,4-dioxane	24.3	25.1	1:5
	1,3-dioxolan-2-one	11.8	11.8	1:2
	ether	9.1	10.1	1:2
	2-hexanone	12.7	13.2	1:2
	methyl ethyl ketone	13.3	14.1	1:3
2	cyclohexanone	29.9	30.1	1:6
	dimethyl acetamide	26.9	27.7	1:6
	dimethyl formamide	24.8	24.3	1:6
	2-hexanone	21.8	22.7	1:4
3	-	-	-	-
	cyclohexanone	31.6	31.5	1:4
	dimethyl acetamide	16.7	17.0	1:2

Table 3.1(b) : Additional inclusion compounds of hosts **1-3**.

Host	Guest	H:G	Host	Guest	H:G
1	acetone	1:6	2	acetone	1:4
	acetonitrile	1:6		dimethyl formamide	1:4
	acetophenone	1:3		2,4-lutidine	1:6
	cyclopentanone	1:2		2,6-lutidine	1:4
	dimethyl sulfoxide	1:4		3,5-lutidine	1:6
	methyl acetate	1:5		2-picoline	1:6
	2-picoline	1:4		3-picoline	1:6
	3-picoline	1:3		4-picoline	1:6
	4-picoline	1:4		pyridine	1:6
	propyl acetate	1:2			
	pyridine	1:4			

KINETICS OF DESOLVATION

The thermal decomposition reaction of a single solid substance can be generalised as follows:

$$A\ (solid) \rightarrow B\ (solid) + C\ (gas)$$

The onset of the reaction involves the formation of the new phase **B** at certain discrete points in the lattice of **A**, called "germ" nuclei. Not all positions in a crystal are of the same intrinsic potential reactivity. It is generally accepted that the points at which the reaction will be initiated within the crystal are usually at the surface and generally associated with some type of lattice imperfection, for example, lattice defects, such as stoichiometric defects or impurities which disturb the regularity of the lattice, dislocations, and Smekal cracks[5,6]. These imperfections create the lattice strain necessary for a chemical attack to begin at that point. Germ nuclei are very unstable as a result of the high ratio of surface strain to volume, but some of these nuclei may develop into growth nuclei, which increase in size through the advance of the reactant-product interface into the bulk of lattice **A**, so reducing the relative importance of the surface strain. The reaction interface can be defined as the nominal boundary surface between the reactant and solid product. It is in this reaction interface that structural rearrangement occurs[7]. Further chemical reaction is localised at this interface, so that the nuclei grow in size as the reaction proceeds. However, as soon as the nuclei touch, their growth is interrupted at the surface of contact. This formation and growth of nuclei is illustrated in figure 3.2.

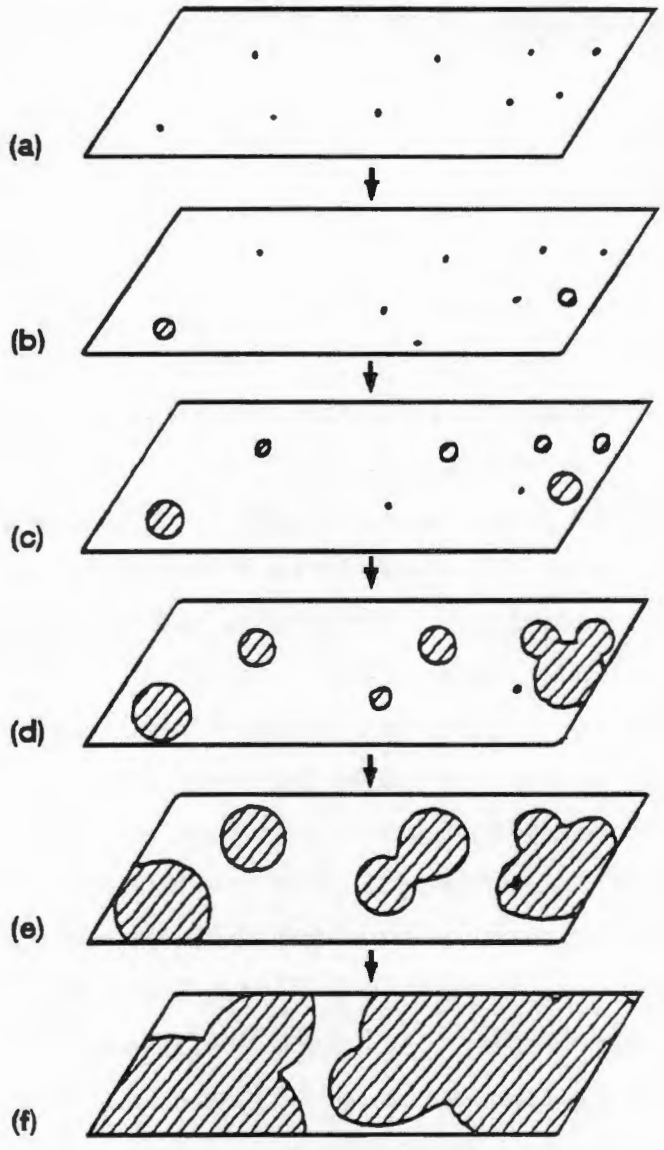

Figure 3.2 : Formation and growth of nuclei of product in the decomposition of solids. a) nucleation sites (germ nuclei); b) first nuclei formed; c) growth and further nucleation; d) overlap of nuclei; e) ingestion of nucleation sites; f) continued growth.[8]

The reactivity and chemical properties of solids are strongly influenced by the relative immobility of the constituent ions or molecules in the lattice of the reactant phase[5]. Interface advance represents the reactant consumed and product formed. The progress of this process is a measure of the reaction rate, and the controlling factors determine the kinetic characteristics of the chemical change under consideration. There are many cases possible for the mechanism of simple solid decomposition reactions depending on the rate of

the transformation of germ nuclei into growth nuclei, and depending on the rate of growth of the nuclei. The density of germ nuclei in the reactant crystal will have a direct effect on the measured rate of reaction not only in the initial stages but throughout the reaction, as a larger number of growing nuclei implies more rapid conversion to product and shortened path lengths for growing branches before intersection. During the development of the nuclei there may also be ingestion of other germ nuclei by the nuclei already formed[9]. This reduces the effective rate of nucleation.

It is well known that the kinetics of thermal decomposition of solids depends largely on the sample and reaction conditions[5,10,11]. The observed kinetic behaviour may be sensitive to the history of the sample, for example, method of sample preparation, length and conditions of storage, and any pretreatment before decomposition, such as damages to the crystal surface, for example, crushing, abrasion, or irradiation[12-15]. It is known that the crushing and grinding of whole crystals reduces the induction period[6]. The reactivity of a solid is often significantly influenced by its particle size, since thermal decomposition reactions are localised mostly on the surface of the reacting phase. The reaction rate usually increases with a decrease in the particle size, but this simple relationship is not always observed[13,16,17]. The shapes of the extent of reaction versus time curves for decomposition reactions have also been shown to be sensitive to changes in the distributions of sizes and shapes of the crystals which comprise the reactant[17]. This is due to variations in the geometry of the surface production of nuclei and the subsequent interface advance in the particles of different dimensions[5]. The kinetics of formation and growth of decomposition nuclei may also be influenced by the nature, concentration and distribution of crystal imperfections and impurities[13,18].

The rate determining step in any solid phase can be either (i) diffusion - transportation of participants to or from a zone of preferred reaction, or (ii) a chemical reaction - one or more bond redistribution steps generally occurring at the reaction interface[5]. The type of decomposition reaction considered here involves the loss of guest with the simultaneous or subsequent collapse of the crystal structure to the non-porous α-phase of the host compound. It was assumed that the guest release was the rate determining step of the

reaction. No chemical reaction occurs in terms of breaking or making covalent bonds. The guest vapour and host molecules remain chemically unchanged, and the general decomposition reaction can be rewritten in the form :

$$H.nG_{(\beta,s)} \rightarrow H_{(\alpha,s)} + nG_{(g)}$$

The desolvation of an inclusion compound involves the loss of a gaseous product, resulting in a reduction in the sample mass. The fractional reaction, α, is directly proportional to the extent of the reaction, and is usually defined in terms of the change in mass of the sample[8] :

$$\alpha = (m_o - m) / (m_o - m_f)$$

where m_o is the initial mass, and m_f the mass of the sample when the reaction is complete.

The extent of the reaction, α, can be measured using a variety of techniques[5,9], for example, TG, DSC, constant-rate thermal analysis (CRTA)[19], evolved gas analysis mass spectra (EGA-MS)[20], X-ray diffraction (XRD)[21] and infra-red (IR) spectroscopy. TG is often favoured and both isothermal and rising temperature kinetic experiments have been done. For non-isothermal experiments a number of assumptions need to be made and the data can be analysed by a number of different methods. The three methods usually applied to the analysis of non-isothermal data are (i) differential, (ii) difference differential, and (iii) integral methods, of which the last is the most widely used[8,22]. Treatment of isothermal kinetic data requires fewer assumptions, and the kinetic information obtained appears to be more consistent, and reliable[5,23].

The variations in reported kinetic data may also include effects arising from the use of different experimental techniques. Disagreements on the magnitude of the pre-exponential function, A, and activation energy, E_a, often arise in comparison between measurements made by isothermal techniques and those from rising temperature techniques. Further variations may also result from the use of alternative methods of data analysis[14,24-27].

Isothermal thermogravimetic analysis has often been used to determine the probable reaction mechanisms of solid state reactions[28], and was used in this study.

Temperature inhomogeneities within the reactant mass, usually when the sample mass is large, is another factor known to influence the kinetic characteristics of decomposition reactions[5]. The use of very small samples can, however, also lead to problems, since smaller samples need higher sensitivity of the measuring systems, and the composition of the sample may not be representative of the bulk of the material[13]. The TG apparatus allows the use of small sample masses, so the effect of heat and mass transfer processes are usually eliminated[22], but they are large enough for the sample to be considered representative.

The determination of kinetic data involved performing a series of runs in which the material was desolvated under isothermal conditions over a range of different temperatures. Strong evidence exists that for any given substance and crystal habit there is an isokinetic range of temperatures and concentrations, in which the characteristic kinetics of phase change remains the same[29]. The shapes of all the curves for a particular system should be similar if the same reaction mechanism dominates throughout, that is the system is isokinetic over the chosen temperature range. Table 3.2 shows the temperature ranges chosen for the compounds studied over which isokinetic behaviour was observed.

Table 3.2 : Temperature ranges studied for the kinetics of desolvation.

Compound	Temperature Range (°C)
SPDEK	55-80
SPETH	55-75
SPDIOX	56-75
SPMEK	62-72
SP2H	80-100
SPDMA	75-105
NAP2H	55-75
NAPDMA	65-80
ETHDMA	80-115

For each temperature, the resultant percentage mass loss versus time curve was reduced to an extent of reaction, α, versus time curve. The α-time curve obtained describes the kinetics of the solid state decomposition reaction. The shape of the curve is used to determine the probable reaction mechanism and a reaction rate constant for each temperature. The characteristic features of a generalised α-time curve are shown in figure 3.3. The curve can be divided up into six sections: A is an initial reaction, sometimes associated with unstable superficial material; B is the induction period, the length of which is determined by the rate of transformation of the germ nuclei to growth nuclei; C is the acceleratory period dominated by the rate of unimpeded expansion of the growth nuclei; D is the inflection point, the maximum rate of the reaction; E is the deceleratory or decay period characterised by a decrease in the rate of expansion of the nuclei due to impingement of the nuclei upon each other. The decrease in the overall reaction continues until F, completion of the reaction. In practice, some of these features may be absent for the different types of kinetic behaviour that are observed. The first consideration in selecting the kinetic mechanism is therefore to characterise the decomposition curve as acceleratory, deceloratory or sigmoidal.

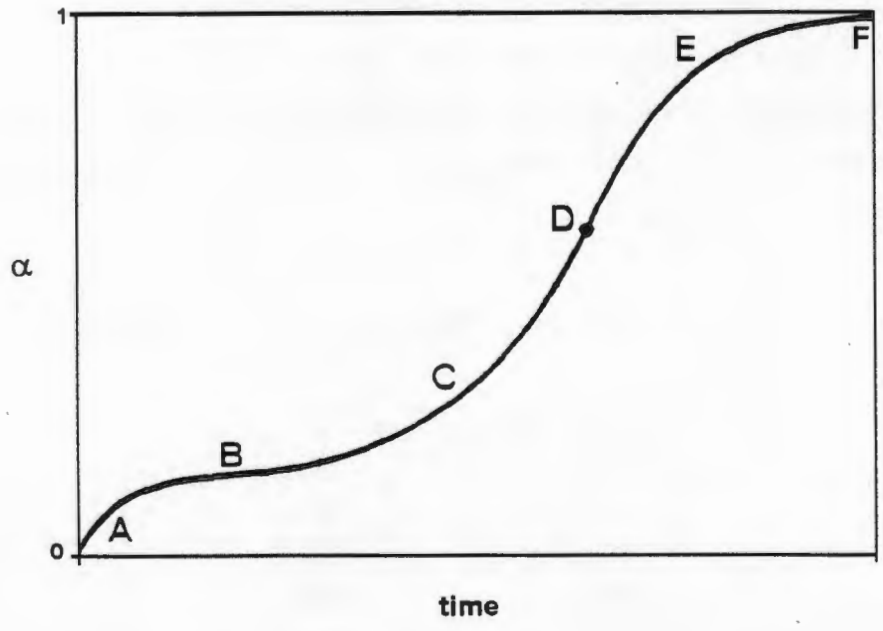

Figure 3.3 : Generalised α-time curve summarising the characteristic behaviour for the isothermal decomposition of solids. A: initial rapid reaction, B: induction period, C: acceleratory period, D: inflection point, E: deceleratory period, F: end of reaction.[5]

Several theoretical kinetic model functions for the α-time relationship have been derived, each describing a different reaction mechanism. The theory of the formulation of these rate equations has been given in the literature[5,6]. These expressions apply to single stage reactions, and those most commonly used are summarised in table 3.3. The expressions are grouped according to the shape of the α-time curves as sigmoidal, acceleratory, or deceleratory. The deceleratory group is further subdivided according to the controlling factors assumed in the derivation as geometric, diffusion or 'reaction order'. Most of these models use the concept of the formation of nuclei and their subsequent growth via the reaction interface[30].

Table 3.3 : Equations commonly used in kinetic analyses for solid state reactions.

	$f(\alpha) = kt$
1. Acceleratory α-time curves	
P1 power law	$\alpha^{1/n}$
E1 exponential law	$ln\alpha$
2. Sigmoid α-time curves	
A2 Avrami-Erofe'ev	$[-ln(1-\alpha)]^{1/2}$
A3 Avrami-Erofe'ev	$[-ln(1-\alpha)]^{1/3}$
A4 Avrami-Erofe'ev	$[-ln(1-\alpha)]^{1/4}$
B1 Prout-Tompkins	$ln[\alpha/(1-\alpha)]$
3. Deceleratory α-time curves	
3.1 based on geometrical models	
R2 contracting area	$1-(1-\alpha)^{1/2}$
R3 contracting volume	$1-(1-\alpha)^{1/3}$
3.2 based on diffusion mechanisms	
D1 one-dimensional	α^2
D2 two-dimensional	$(1-\alpha)ln(1-\alpha)+\alpha$
D3 three-dimensional	$[1-(1-\alpha)^{1/3}]^2$
D4 Ginstling-Brounshtein	$(1-2\alpha/3)-(1-\alpha)^{2/3}$
3.3 based on 'order of reaction'	
F1 first order	$-ln(1-\alpha)$
F2 second order	$1/(1-\alpha)$
F3 third order	$[1/(1-\alpha)]^2$

The rate laws describing sigmoid α-time curves were derived from consideration of the geometry of nucleation and growth of the product phase within the reactant phase. The Avrami-Erofe'ev models describe reactions which begin with the random and rapid evolution of nuclei which grow in two (A2), or three (A3) dimensions, or which proceed with two stages of nucleation (A4). The Prout-Tompkins model was derived to account for reactions that proceed via chain nucleation, with overlapping of the nuclei and ingestion of potential sites of nucleation. The rate equations R2 and R3 are geometrical models for the controlled advancement of the phase boundary towards the centre of the particles. The 'D' rate laws describe diffusion controlled reactions that result from the propagation of a reaction front towards the centre of a particle either in one-dimension, as a flat sheet (D1), in two-dimensions, that is, propagation towards the centre of a cylinder (D2), or in three-dimensions, where the reacting particle is envisaged as a sphere (D3). A more detailed treatment of three-dimensional diffusion was done by Ginstling and Brounshtein (D4). The third group of rate equations describing deceleratory α-time curves is based on the apparent 'order of reaction'. However, the concept of 'reaction order' must be applied with care to rate processes involving solids[31]. An acceptable solid state interpretation of F1 has been given as random nucleation followed by unimolecular decay of the active species[32]. All of these functions take the general form $f(\alpha) = kt$, where k is the rate constant.

Various appropriate kinetic models were fitted to the α-time data. There are no agreed criteria for the recognition of the 'best fit', for example, range of α applicable, statistical measurements of deviation, or behaviour at the limits[23]. The model which, for the temperature range considered, most nearly approached linearity over the largest α-range was chosen as the expression which most satisfactorily represents the reaction. The rate constant for each temperature is the slope of the resultant plot.

The assumption is made that solid state reactions are activated processes[32], therefore, the value of k, at different temperatures, for the same reaction can

be assumed to be governed by the Arrhenius equation :

$$k = A\exp(-E_a/RT)$$

where R is the gas constant, A is the pre-exponential factor and E_a is the activation energy. The pre-exponential factor provides a measure of the frequency of the occurrence of the reaction, while the activation energy is usually identified as the energy barrier that must be surmounted to enable the occurrence of the reaction.

By plotting the semilogarithmic graph of ln *k* versus 1/T, where T is the temperature in Kelvin, of the corresponding isothermal experiment, the Arrhenius terms, A and E_a, can be determined.

The Arrhenius equation has been widely accepted and successfully applied to numerous reactions involving solids. The validity of applying the Arrhenius equation to heterogeneous reactions has been questioned, but the parameters A and E_a do have practical value even if their theoretical interpretation is difficult[8,33]. It is also important to note that the β to α change in phase observed on desolvation of these inclusion compounds cannot be accounted for in the kinetic models obtained, because the extent of reaction was measured as a function of the guest loss.

The details of the kinetics of desolvation that were determined, will be discussed with the structure of the inclusion compound.

X-RAY POWDER DIFFRACTION

There was good agreement between the experimental XRD patterns for the powdered samples and the calculated patterns for the crystal structures. Thus, it was assumed that the powdered samples grown by continuous stirring were the same as the crystals grown by slow evaporation. For each of the inclusion compounds, for which the kinetics of desolvation were determined, the guest loss reaction was accompanied by a phase change to the non-porous α-phase of the relevant host. The experimental and calculated XRD patterns can be seen in Appendix B.

DENSITY MEASUREMENTS

Table 3.4 shows the calculated and experimental densities for the inclusion compounds studied which were sufficiently stable for determination by the flotation method.

Table 3.4 : Calculated and experimental densities.

Compound	D_c ($g.cm^{-3}$)	D_m ($g.cm^{-3}$)
SPBN	1.248	1.222
SPAB	1.209	1.196
SPCHO	1.089	1.077
SPDEK	1.195	1.170
SPDIOX	1.220	1.203
SPDIOXO	1.285	1.257
SPDMA	1.221	1.205
SPETH	1.206	1.185
SP2H	1.205	1.185
SPMEK	1.189	1.154
NAPCHO	1.186	1.168
NAPDMA	1.163	1.150
NAP2H	1.201	1.184
ETHBN	1.215	1.204
ETHCHO	1.180	1.167
ETHDMA	1.214	1.204

MICROANALYSIS

The elemental analysis results reported are the average of duplicate determinations. The host compounds show close agreement between the calculated and observed values, but a wider range was found for the inclusion compounds, due to their lower stability. The microanalysis results are shown in table 3.5.

Table 3.5 : C,H,N elemental analysis.

Code Name	Compound (Formula)	Observed			Calculated		
		%C	%H	%N	%C	%H	%N
SPBN	$C_{96}H_{66}O_6$	87.63	5.06		87.65	5.06	
SPAB	$C_{96}H_{66}O_6.2C_2H_3N.2C_6H_6$	86.44	5.47	1.76	86.57	5.45	1.80
SPCHO	$C_{96}H_{66}O_6.5C_6H_{10}0$	83.60	6.47		83.78	6.47	
SPDICHO*	$C_{96}H_{66}O_6.2C_6H_{10}0$	-	-		85.80	5.73	
SPDEK	$C_{96}H_{66}O_6,2C_5H_{10}O$	85.36	5.81		85.57	5.83	
SPDIOX	$C_{96}H_{66}O_6.5C_4H_8O_2$	79.65	6.00		79.34	6.08	
SPDIOXO*	$C_{96}H_{66}O_6.2C_3H_4O_3$	-	-		82.13	5.00	
SPDMA	$C_{96}H_{66}O_6.4C_4H_9ON$	80.64	6.42	3.47	80.84	6.18	3.37
SPETH	$C_{96}H_{66}O_6.2C_4H_{10}O$	85.20	5.97		85.33	5.92	
SP2H	$C_{96}H_{66}O_6.2C_6H_{12}O$	85.78	6.08		85.57	5.98	
SPMEK	$C_{96}H_{66}O_6.3C_4H_8O$	85.13	6.07		84.68	5.92	
NAPCHO	$C_{100}H_{68}O_6.6C_6H_{10}O$	83.65	6.65		83.58	6.60	
NAPDMA	$C_{100}H_{68}O_6.6C_4H_9NO$	78.72	6.70	4.52	78.87	6.51	4.45
NAPDMF	$C_{100}H_{68}O_6.6C_3H_7NO$	78.18	6.39	4.45	78.56	6.14	4.66
NAP2H	$C_{100}H_{68}O_6.4C_6H_{12}O$	84.37	6.76		84.32	6.62	
ETHBN	$C_{62}H_{44}O_4$	87.32	5.28		87.30	5.20	
ETHCHO	$C_{62}H_{44}O_4.4C_6H_{10}O$	83.30	6.78		82.93	6.80	
ETHDMA	$C_{62}H_{44}O_4.2C_4H_9NO$	81.71	6.26	2.78	81.85	6.08	2.73

* insufficient sample

STRUCTURE SOLUTION AND REFINEMENT

The crystal data, data collection parameters and final refinement data for each of the structures are given in table 3.6.

The structure solution and refinements were similar for all of the compounds studied. The positions of all of the host non-hydrogen atoms in the asymmetric unit were found by direct methods. The non-hydrogen atoms in the guest molecules were located in the difference electron density maps on subsequent refinement, using SHELXL-93[34]. All the host non-hydrogen

atoms were refined anisotropically. The non-hydrogen atoms of the guest molecules were also treated anisotropically, except where this led to unreasonably high temperature factors. Some of the guest molecules were disordered, and a few of the guests required bond length constraints to ensure sensible molecular geometry. All of the host phenyl hydrogen atoms were placed in geometrically calculated positions and linked to a common temperature factor. The guest hydrogen atoms were only included in calculated positions if the guest non-hydrogen atoms had reasonable temperature factors and exhibited no disorder. In most of the structures, the host hydroxyl hydrogen atoms were located in the difference electron density maps, and allowed to refine independently. A weighting scheme was employed in the final stages of the refinement, and where appropriate an extinction parameter was applied.

Particular details of the solution and refinement of individual structures, for example, bond length restraints and the modeling of disorder, are discussed in Chapters 4, 5 and 6. All bond lengths and angles, unless otherwise stated, lie within the expected ranges[35]. Final atomic co-ordinates, temperature factors, and bond lengths and angles are contained in Appendix C. Tables of observed and calculated structure factors are in Appendix D.

Table 3.6 : Crystal data, data collection parameters and final refinement data.

Parameter	SPBN	SPAB
Guest	-	acetonitrile, benzene
Molecular formula	$C_{96}H_{66}O_6$	$C_{96}H_{66}O_6.2C_2H_3N.2C_6H_6$
Molecular weight ($g.mol^{-1}$)	1315.57	1553.91
Crystal system	triclinic	monoclinic
Space Group	$P\bar{1}$	$P2_1/n$
a (Å)	10.683(2)	15.952(2)
b (Å)	11.065(1)	9.144(3)
c (Å)	15.442(3)	29.251(2)
α (°)	99.78(1)	90
β (°)	98.27(1)	89.917(8)
γ (°)	98.90(1)	90
Volume ($Å^3$)	1749.8(5)	4267(1)
Z	1	2
Linear absorption coefficient μ (mm^{-1})	0.077	0.074
F(000)	690	1636
Colour	colourless	colourless
Data collection		
Temperature (K)	293(2)	223(2)
Size of Crystal (mm)	0.44x0.44x0.40	0.44x0.31x0.31
θ range scanned (°)	1-25	1-25
Range of indices h,k,l	-12,12;-13,13;0,18	-19,19;0,10;0,34
Reflections measured	6406	8568
Unique reflections	6155	7482
R_{int}	0.018	0.161
Observed reflections $I_{rel}>2\sigma I_{rel}$	3986	4223
Decay of standard reflections (%)	-2.0	-3.4
Final refinement		
Number of restraints	0	0
Number of parameters	470	557
R_1 ($I_{rel}>2\sigma I_{rel}$)	0.0405	0.0465
R_1(all data)	0.0920	0.1329
wR_2 ($I_{rel}>2\sigma I_{rel}$)	0.1009	0.1095
wR_2 (all data)	0.1195	0.2192
w*	a=0.0515, b=0.32	a=0.0613, b=0.62
S	1.030	1.017
Extinction coefficient	-	-
Mean shift/esd	0	0
Max. height in difference electron density map ($eÅ^{-3}$)	0.146	0.189
Min. height in difference electron density map ($eÅ^{-3}$)	-0.191	-0.221

*$w = 1/[\sigma^2(F_o^2) + (aP)^2 + bP]$ where $P = (\max(0,F_o^2) + 2F_c^2)/3$

Table 3.6 : Crystal data, data collection parameters and final refinement data.

Parameter	SPDMA	SPMEK
Guest	dimethyl acetamide	methyl ethyl ketone
Molecular formula	$C_{96}H_{66}O_6.4C_4H_9ON$	$C_{96}H_{66}O_6.3C_4H_8O$
Molecular weight ($g.mol^{-1}$)	1664.06	1531.89
Crystal system	monoclinic	monoclinic
Space Group	$P2_1/n$	$P2_1/c$
a (Å)	16.230(9)	12.320(5)
b (Å)	9.611(2)	21.438(8)
c (Å)	29.015(8)	32.92(2)
α (°)	90	90
β (°)	90.47(3)	100.16(5)
γ (°)	90	90
Volume ($Å^3$)	4526(3)	8558(7)
Z	2	4
Linear absorption coefficient μ (mm^{-1})	0.078	0.074
F(000)	1764	3240
Colour	pale yellow	pale yellow
Data collection		
Temperature (K)	223(2)	248(2)
Size of Crystal (mm)	0.45x0.45x0.50	0.48x0.40x0.20
θ range scanned (°)	1-25	1-25
Range of indices h,k,l	-19,19;0,11;0,34	-14,14;0,25;0,39
Reflections measured	8133	15320
Unique reflections	7965	15035
R_{int}	0.089	0.038
Observed reflections $I_{rel}>2\sigma I_{rel}$	3610	8239
Decay of standard reflections (%)	-0.9	-21.0
Final refinement		
Number of restraints	5	0
Number of parameters	587	1053
R_1 ($I_{rel}>2\sigma I_{rel}$)	0.0735	0.0891
R_1 (all data)	0.2150	0.1714
wR_2 ($I_{rel}>2\sigma I_{rel}$)	0.1874	0.2230
wR_2 (all data)	0.2667	0.6097
w*	a=0.1413, b=0	a=0.1344, b=16.85
S	1.002	1.018
Extinction coefficient	-	-
Mean shift/esd	0.004	0.014
Max. height in difference electron density map ($eÅ^{-3}$)	0.363	0.579
Min. height in difference electron density map ($eÅ^{-3}$)	-0.330	-0.662

*$w = 1/[\sigma^2(F_o^2) + (aP)^2 + bP]$ where $P = (\max(0,F_o^2) + 2F_c^2)/3$

Table 3.6 : Crystal data, data collection parameters and final refinement data.

Parameter	SPDEK	SPETH
Guest	diethyl ketone	diethyl ether
Molecular formula	$C_{96}H_{66}O_6.2C_5H_{10}O$	$C_{96}H_{66}O_6.2C_4H_{10}O$
Molecular weight ($g.mol^{-1}$)	1487.74	1463.72
Crystal system	triclinic	triclinic
Space Group	P $\bar{1}$	P $\bar{1}$
a (Å)	10.912(4)	10.651(1)
b (Å)	12.651(3)	12.805(3)
c (Å)	15.705(4)	15.560(4)
α (°)	78.78(3)	78.06(2)
β (°)	87.94(3)	86.09(2)
γ (°)	76.42(3)	76.12(1)
Volume ($Å^3$)	2067(1)	2015.2(7)
Z	1	1
Linear absorption coefficient μ (mm^{-1})	0.075	0.075
F(000)	786	774
Colour	pale yellow	colourless
Data collection		
Temperature (K)	293(2)	223(2)
Size of Crystal (mm)	0.47x0.47x0.22	0.50x0.50x0.50
θ range scanned (°)	1-25	1-25
Range of indices h,k,l	-12,12;-15,15;0,18	-12,12;-15,15;0,18
Reflections measured	7532	7367
Unique reflections	7243	7080
R_{int}	0.021	0.021
Observed reflections $I_{rel}>2\sigma I_{rel}$	4416	5780
Decay of standard reflections (%)	-0.2	-2.6
Final refinement		
Number of restraints	1	0
Number of parameters	515	529
R_1 ($I_{rel}>2\sigma I_{rel}$)	0.0593	0.0450
R_1 (all data)	0.1310	0.0658
wR_2 ($I_{rel}>2\sigma I_{rel}$)	0.1503	0.1163
wR_2 (all data)	0.1882	0.1293
w*	a=0.0788, b=1.20	a=0.0569, b=0.84
S	1.013	1.025
Extinction coefficient	-	0.018(1)
Mean shift/esd	0.013	0.002
Max. height in difference electron density map ($eÅ^{-3}$)	0.387	0.471
Min. height in difference electron density map ($eÅ^{-3}$)	-0.425	-0.385

*$w = 1/[\sigma^2(F_o^2) + (aP)^2 + bP]$ where $P = (\max(0,F_o^2) + 2F_c^2)/3$

Table 3.6 : Crystal data, data collection parameters and final refinement data.

Parameter	SPDIOX	SPDIOXO
Guest	1,4-dioxane	1,3-dioxolan-2-one
Molecular formula	$C_{96}H_{66}O_6.5C_4H_8O_2$	$C_{96}H_{66}O_6.2C_3H_4O_3$
Molecular weight ($g.mol^{-1}$)	1756.10	1491.70
Crystal system	triclinic	monoclinic
Space Group	$P\bar{1}$	$P2_1/n$
a (Å)	12.203(2)	18.095(5)
b (Å)	14.384(3)	12.563(4)
c (Å)	15.827(3)	34.18(1)
α (°)	110.83(1)	90
β (°)	104.82(1)	97.14(3)
γ (°)	100.68(1)	90
Volume ($Å^3$)	2389.7(8)	7709(4)
Z	1	4
Linear absorption coefficient μ (mm^{-1})	0.080	0.083
F(000)	930	3128
Colour	pale yellow	pale orange
Data collection		
Temperature (K)	293(2)	223(2)
Size of Crystal (mm)	0.28x0.28x0.31	0.32x0.32x0.35
θ range scanned (°)	1-25	1-25
Range of indices h,k,l	-14,14;-17,17;0,18	-21,21;0,14;0,40
Reflections measured	8747	13779
Unique reflections	8415	13539
R_{int}	0.030	0.044
Observed reflections $I_{rel}>2\sigma I_{rel}$	4418	6598
Decay of standard reflections (%)	-1.12	-0.7
Final refinement		
Number of restraints	0	0
Number of parameters	575	1052
R_1 ($I_{rel}>2\sigma I_{rel}$)	0.076	0.066
R_1 (all data)	0.173	0.176
wR_2 ($I_{rel}>2\sigma I_{rel}$)	0.213	0.200
wR_2 (all data)	0.286	0.480
w*	a=0.1541, b=0.91	a=0.1413, b=6.01
S	1.034	1.037
Extinction coefficient	-	0.0009(3)
Mean shift/esd	0.023	0.001
Max. height in difference electron density map ($eÅ^{-3}$)	0.62	0.29
Min. height in difference electron density map ($eÅ^{-3}$)	-0.52	-0.35

*$w = 1/[\sigma^2(F_o^2) + (aP)^2 + bP]$ where $P = (\max(0,F_o^2) + 2F_c^2)/3$

Table 3.6 : Crystal data, data collection parameters and final refinement data.

Parameter	SPCHO	SPDICHO
Guest	cyclohexanone	cyclohexanone
Molecular formula	$C_{96}H_{66}O_6.5C_6H_{10}O$	$C_{96}H_{66}O_6.2C_6H_{10}O$
Molecular weight ($g.mol^{-1}$)	1686.19	1511.86
Crystal system	triclinic	triclinic
Space Group	$P\bar{1}$	$P\bar{1}$
a (Å)	8.957(4)	9.512(2)
b (Å)	16.69(1)	15.327(3)
c (Å)	17.201(4)	16.151(3)
α (°)	93.82(3)	114.89(2)
β (°)	97.61(3)	95.19(2)
γ (°)	93.13(5)	102.67(2)
Volume ($Å^3$)	2538(2)	2039.0(7)
Z	1	1
Linear absorption coefficient μ (mm^{-1})	0.074	0.076
F(000)	960	798
Colour	colourless	orange
Data collection		
Temperature (K)	223(2)	223(2)
Size of Crystal (mm)	0.50x0.41x0.50	0.28x0.38x0.38
θ range scanned (°)	1-25	1-25
Range of indices h,k,l	-10,10;-19,19;0,20	-11,11;-18,16;0,19
Reflections measured	9246	7438
Unique reflections	8921	7157
R_{int}	0.038	0.037
Observed reflections $I_{rel}>2\sigma I_{rel}$	4967	3896
Decay of standard reflections (%)	0.5	3.2
Final refinement		
Number of restraints	0	0
Number of parameters	599	537
R_1 ($I_{rel}>2\sigma I_{rel}$)	0.0892	0.0454
R_1 (all data)	0.1741	0.1396
wR_2 ($I_{rel}>2\sigma I_{rel}$)	0.2473	0.1073
wR_2 (all data)	0.3181	0.1386
w*	a=0.1829,b=1.93	a=0.0586, b=0.25
S	1.025	1.003
Extinction coefficient	0.009(3)	-
Mean shift/esd	0.011	0
Max. height in difference electron density map ($eÅ^{-3}$)	0.914	0.243
Min. height in difference electron density map ($eÅ^{-3}$)	-0.413	-0.194

*$w = 1/[\sigma^2(F_o^2) + (aP)^2 + bP]$ where $P = (\max(0,F_o^2) + 2F_c^2)/3$

Table 3.6 : Crystal data, data collection parameters and final refinement data.

Parameter	SP2H	NAPCHO
Guest	2-hexanone	cyclohexanone
Molecular formula	$C_{96}H_{66}O_6.2C_6H_{12}O$	$C_{100}H_{68}O_6.6C_6H_{10}O$
Molecular weight ($g.mol^{-1}$)	1515.89	1954.50
Crystal system	triclinic	monoclinic
Space Group	$P\bar{1}$	$P2_1/n$
a (Å)	8.886(5)	9.444(5)
b (Å)	16.283(9)	18.353(5)
c (Å)	16.386(6)	31.59(1)
α (°)	117.26(3)	90
β (°)	91.32(4)	92.18(3)
γ (°)	82.56(5)	90
Volume ($Å^3$)	2088(2)	5471(4)
Z	1	2
Linear absorption coefficient μ (mm^{-1})	0.075	0.074
F(000)	802	2080
Colour	pale yellow	pale yellow
Data collection		
Temperature (K)	223(2)	248(2)
Size of Crystal (mm)	0.25x0.35x0.45	0.25x0.34x0.38
θ range scanned (°)	1-28	1-25
Range of indices h,k,l	-10,10;-19,17;0,19	-11,11;0,21;0,37
Reflections measured	8009	9794
Unique reflections	7379	9612
R_{int}	0.364	0.050
Observed reflections $I_{rel}>2\sigma I_{rel}$	3405	3606
Decay of standard reflections (%)	1.0	-2.3
Final refinement		
Number of restraints	0	0
Number of parameters	503	577
R_1 ($I_{rel}>2\sigma I_{rel}$)	0.1043	0.1095
R_1 (all data)	0.2437	0.2914
wR_2 ($I_{rel}>2\sigma I_{rel}$)	0.2872	0.3116
wR_2 (all data)	0.3790	0.4642
w*	a=0.2096, b=2.27	a=0.2483, b=0
S	1.030	1.040
Extinction coefficient	-	-
Mean shift/esd	0.001	0.010
Max. height in difference electron density map ($eÅ^{-3}$)	0.967	0.861
Min. height in difference electron density map ($eÅ^{-3}$)	-0.633	-0.621

*$w = 1/[\sigma^2(F_o^2) + (aP)^2 + bP]$ where $P = (\max(0,F_o^2) + 2F_c^2)/3$

Table 3.6 : Crystal data, data collection parameters and final refinement data.

Parameter	NAPDMA	NAPDMF
Guest	dimethyl acetamide	dimethyl formamide
Molecular formula	$C_{100}H_{68}O_6.6C_4H_9NO$	$C_{100}H_{68}O_6.6C_3H_7NO$
Molecular weight ($g.mol^{-1}$)	1888.36	1804.21
Crystal system	triclinic	triclinic
Space Group	P $\bar{1}$	P $\bar{1}$
a (Å)	10.637(3)	10.390(6)
b (Å)	15.503(3)	15.641(2)
c (Å)	17.446(5)	17.459(6)
α (°)	106.71(2)	106.55(2)
β (°)	100.59(2)	104.35(3)
γ (°)	92.19(2)	92.98(2)
Volume ($Å^3$)	2696(1)	2612(2)
Z	1	1
Linear absorption coefficient μ (mm^{-1})	0.075	0.074
F(000)	1004	956
Colour	pale yellow	pale yellow
Data collection		
Temperature (K)	223(2)	223(2)
Size of Crystal (mm)	0.30x0.30x0.30	0.31x0.31x0.44
θ range scanned (°)	1-25	1-25
Range of indices h,k,l	-12,12;-18,17;0,20	-12,11;-18,17;0,20
Reflections measured	9828	9519
Unique reflections	9474	9191
R_{int}	0.039	0.031
Observed reflections $I_{rel}>2\sigma I_{rel}$	4416	5096
Decay of standard reflections (%)	1.1	-0.3
Final refinement		
Number of restraints	15	0
Number of parameters	567	587
R_1 ($I_{rel}>2\sigma I_{rel}$)	0.1152	0.0945
R_1 (all data)	0.2363	0.1803
wR_2 ($I_{rel}>2\sigma I_{rel}$)	0.3238	0.2729
wR_2 (all data)	0.4214	0.3411
w*	a=0.2318, b=2.55	a=0.1988, b=1.79
S	1.049	1.050
Extinction coefficient	0.007(3)	-
Mean shift/esd	0.001	0.001
Max. height in difference electron density map ($eÅ^{-3}$)	1.222	1.111
Min. height in difference electron density map ($eÅ^{-3}$)	-0.482	-0.510

*$w = 1/[\sigma^2(F_o^2) + (aP)^2 + bP]$ where $P = (\max(0,F_o^2) + 2F_c^2)/3$

Table 3.6 : Crystal data, data collection parameters and final refinement data.

Parameter	NAP2H	ETHBN
Guest	2-hexanone	-
Molecular formula	$C_{100}H_{68}O_6.4C_6H_{12}O$	$C_{62}H_{44}O_4$
Molecular weight ($g.mol^{-1}$)	1766.27	853.03
Crystal system	triclinic	triclinic
Space Group	P $\bar{1}$	P $\bar{1}$
a (Å)	8.539(1)	8.936(2)
b (Å)	16.907(3)	10.619(3)
c (Å)	18.907(3)	14.271(2)
α (°)	114.58(1)	110.88(2)
β (°)	97.65(1)	89.96(2)
γ (°)	92.90(1)	111.35(2)
Volume ($Å^3$)	2443.1(6)	1165.4(5)
Z	1	1
Linear absorption coefficient μ (mm^{-1})	0.075	0.075
F(000)	940	448
Colour	pale yellow	colourless
Data collection		
Temperature (K)	223(2)	293(2)
Size of Crystal (mm)	0.41x0.44x0.44	0.31x0.31x0.34
θ range scanned (°)	1-25	1-25
Range of indices h,k,l	-10,10;-20,18;0,22	-10,10;-12,11;0,16
Reflections measured	8865	4278
Unique reflections	8579	4098
R_{int}	0.0258	0.0157
Observed reflections $I_{rel}>2\sigma I_{rel}$	5324	2773
Decay of standard reflections (%)	-0.5	2.2
Final refinement		
Number of restraints	8	0
Number of parameters	757	307
R_1 ($I_{rel}>2\sigma I_{rel}$)	0.0638	0.0445
R_1 (all data)	0.1238	0.0871
wR_2 ($I_{rel}>2\sigma I_{rel}$)	0.1892	0.1107
wR_2 (all data)	0.2383	0.1287
w*	a=0.1499, b=1.54	a=0.0641, b=0.14
S	0.949	1.043
Extinction coefficient	0.011(2)	-
Mean shift/esd	0.16	0
Max. height in difference electron density map ($eÅ^{-3}$)	0.416	0.154
Min. height in difference electron density map ($eÅ^{-3}$)	-0.281	-0.244

*$w = 1/[\sigma^2(F_o^2) + (aP)^2 + bP]$ where $P = (\max(0,F_o^2) + 2F_c^2)/3$

Table 3.6 : Crystal data, data collection parameters and final refinement data.

Parameter	ETHCHO	ETHDMA
Guest	cyclohexanone	dimethyl acetamide
Molecular formula	$C_{62}H_{44}O_4.4C_6H_{10}O$	$C_{62}H_{44}O_4.2C_4H_9NO$
Molecular weight ($g.mol^{-1}$)	1245.60	1027.27
Crystal system	triclinic	triclinic
Space Group	P $\bar{1}$	P $\bar{1}$
a (Å)	14.208(2)	8.474(2)
b (Å)	14.710(4)	13.103(2)
c (Å)	17.915(2)	13.821(3)
α (°)	91.06(1)	67.16(2)
β (°)	89.98(1)	83.20(2)
γ (°)	110.60(2)	87.82(2)
Volume ($Å^3$)	3504(1)	1404.8(5)
Z	2	1
Linear absorption coefficient μ (mm^{-1})	0.074	0.077
F(000)	1328	544
Colour	colourless	colourless
Data collection		
Temperature (K)	223(2)	223(2)
Size of Crystal (mm)	0.50x0.38x0.50	0.28x0.28x0.34
θ range scanned (°)	1-25	1-25
Range of indices h,k,l	-16,16;-17,17;0,21	-9,10;-14,15;0,16
Reflections measured	12733	5154
Unique reflections	12299	4929
R_{int}	0.035	0.0309
Observed reflections $I_{rel}>2\sigma I_{rel}$	7181	3029
Decay of standard reflections (%)	-7.2	-2.0
Final refinement		
Number of restraints	0	0
Number of parameters	865	366
R_1 ($I_{rel}>2\sigma I_{rel}$)	0.0638	0.0519
R_1 (all data)	0.1367	0.1119
wR_2 ($I_{rel}>2\sigma I_{rel}$)	0.1793	0.1353
wR_2 (all data)	0.2399	0.1644
w*	a=0.1009, b=2.83	a=0.0759, b=0.41
S	1.020	1.053
Extinction coefficient	0.0095(10)	-
Mean shift/esd	0.001	0
Max. height in difference electron density map ($eÅ^{-3}$)	1.268	0.431
Min. height in difference electron density map ($eÅ^{-3}$)	-0.599	-0.229

*$w = 1/[\sigma^2(F_o^2) + (aP)^2 + bP]$ where $P = (\max(0,F_o^2) + 2F_c^2)/3$

REFERENCES

1. F. Toda, K. Akagi, *Tetrahedron Lett.*, 1968, **33**, 3695.
2. M. R. Caira, L. R. Nassimbeni in *Comprehensive Supramolecular Chemistry*. Vol. 6 - *Solid-state Supramolecular Chemistry : Crystal Engineering*, eds D. D. MacNicol, F. Toda, R. Bishop, Pregamon Press, 1996.
3. M. R. Caira, L. R. Nassimbeni, M. L. Niven, W.-D. Schubert, E. Weber, N. Dörpinghaus, *J. Chem. Soc. Perkin Trans. 2*, 1990, 2129.
4. S. A. Bourne, L. R. Nassimbeni, *J. Org. Chem.*, 1992, **57**, 2438.
5. M. E. Brown, D. Dollimore, A. K. Galwey in *Comprehensive Chemical Kinetics*, Vol. 22, *Reactions in the Solid State*, eds C. H. Bamford, C. F. H. Tipper, Elsevier, Amsterdam, 1980.
6. P. W. M. Jacobs, F. C. Tompkins in *Chemistry of the Solid State*, ed. W. E. Garner, Butterworth, London, 1955.
7. D. Dollimore, *Thermochim. Acta*, 1992, **203**, 7.
8. M. E. Brown, *Introduction To Thermal Analysis - Techniques and Applications*, Chapmann and Hall, London, 1988.
9. G. Pannetier, P. Souchay, *Chemical Kinetics*, Elsivier, Amsterdam, 1967.
10. J. Sestak, *Thermophysical Properties of Solids*, Elsivier, Amsterdam, 1984.
11. O. F. Shlensky, L. N. Aksenov, A. G. Shashkov, *Thermal Decomposition of Materials*, Elsivier, Amsterdam, 1991.
12. V. V. Boldyrev, M. Bulens, B. Delmon, *The Control of the Reactivity of Solids*, Elsivier, 1979.
13. M. E. Brown, A. K. Galwey, A. Li Wan Po, *Thermochimica Acta*, 1992, **203**, 221.
14. E. G. Prout, F. C. Tompkins, *Trans. Faraday Soc.*, 1944, **40**, 488.
15. E. G. Prout, F. C. Tompkins, *Trans. Faraday Soc.*, 1945, 468.
16. J. Pysiak, *J. Therm. Anal.*, 1995, **43**, 9.
17. N. Kogo, S. Takemoto, T. Nakamura, H. Tanaka, *Thermochimica Acta*, 1996, **282/283**, 81.
18. K. J. Laidler, *Chemical Kinetics*, McGraw-Hill, New York, 1965.
19. L. A. Pérez-Maqueda, A. Ortega, J. M. Criado, *Thermochimica Acta*, 1996, 277, 165.

20. M. Kamruddin, P. K. Ajikumar, S. Dash, R. Krishnan, A. K. Tyagi, K. Krishan, *Thermochimica Acta*, 1996, **287**, 13.
21. S. Mathew, N. Eisenreich, W. Engel, *Thermochimica Acta*, 1995, **269/270**, 475.
22. A. Romero, E. G. Calvo, P. Leton, M. A. Arranz, *Thermochimica Acta*, 1991, **182**, 235.
23. A. K. Galwey, M. E. Brown, *Thermochimica Acta*, 1995, **269/270**, 1.
24. A. K. Galwey, *Thermochimica Acta*, 1985, **96**, 259.
25. A. K. Galwey, *React. Solids*, 1990, **8**, 211.
26. El-H. M. Diefallah, A. Y. Obaid, A. H. Qusti, A. A. El-Bellihi, M. A. Wahab, M. M. Moustafa, *Thermochimica Acta*, 1996, **274**, 165.
27. S. D. Singh, P. S. Mazumdar, W. G. Devi, *Thermochimica Acta*, 1996, **284**, 389.
28. C. P. J. van Vuuren, J. B. Wagner, *Intelligent Instruments and Computers*, 1987, 72.
29. M. Avrami, *J. of Chemical Physics*, 1939, **7**, 1103.
30. D. Dollimore in ref. 2.
31. M. E. Brown, A. K. Galwey, *Thermochimica Acta*, 1979, **29**, 129.
32. J. M. Craido, A. Ortega, *Thermochimica. Acta*, 1994, **239**, 1.
33. K. Galwey, M. E. Brown, *Proc. R. Soc. Lond. A*, 1995, **450**, 501.
34. G. M. Sheldrick, SHELXL-93 : Programme for Crystal Structure Determination, unpublished work.
35. F. H. Allen, O. Kennard, D. G. Watson, L. Brammer, A. G. Orpen, R. Taylor, *J. Chem. Soc., Perkin Trans. 2*, 1987, S1.

CHAPTER 4

HOST 1 AND ITS INCLUSION COMPOUNDS.

The inclusion compounds formed by host **1** will be discussed in this chapter. Each inclusion compound is discussed in terms of crystal structure (refinement and molecular structure), thermal analysis, and kinetics of desolvation, where applicable. The molecular formula, space group and cell parameters are summarised at the beginning of the discussion of each inclusion compound.

The structures of SPAB, SPDMA, SPMEK and SPDIOXO were refined in monoclinic space groups, while the structures of SPBN, SPDEK, SPETH, SP2H, SPCHO, SPDIOX and SPDICHO were all refined in the triclinic space group P $\bar{1}$. For the triclinic structures, preliminary oscillation and Weissenberg X-ray photography established the crystal system. P $\bar{1}$ was chosen as the space group, rather than P1, based on the intensity statistics of the crystal reflection data. The mean $|E^2-1|$ values for the 0kl, h0l, hk0, as well as for the remainder of the reflections were all close to the theoretical value of 0.968. Successful refinements confirmed the choice of the centric space group.

The atomic labelling scheme for host **1** can be seen in Figure 4.1. In all cases half the host was located in the asymmetric unit, except for SPMEK and SPDIOXO, where the whole host molecule was found. The atomic labelling scheme used for the guests is shown at the beginning of the discussion of each structure. The guest molecules were labelled with a suffix G, J, or K.

The inclusion compound of host **1** with dimethyl formamide has already been reported[1]. This inclusion compound has a host to guest ratio of 1:6, and the structure was refined in the triclinic space group P $\bar{1}$.

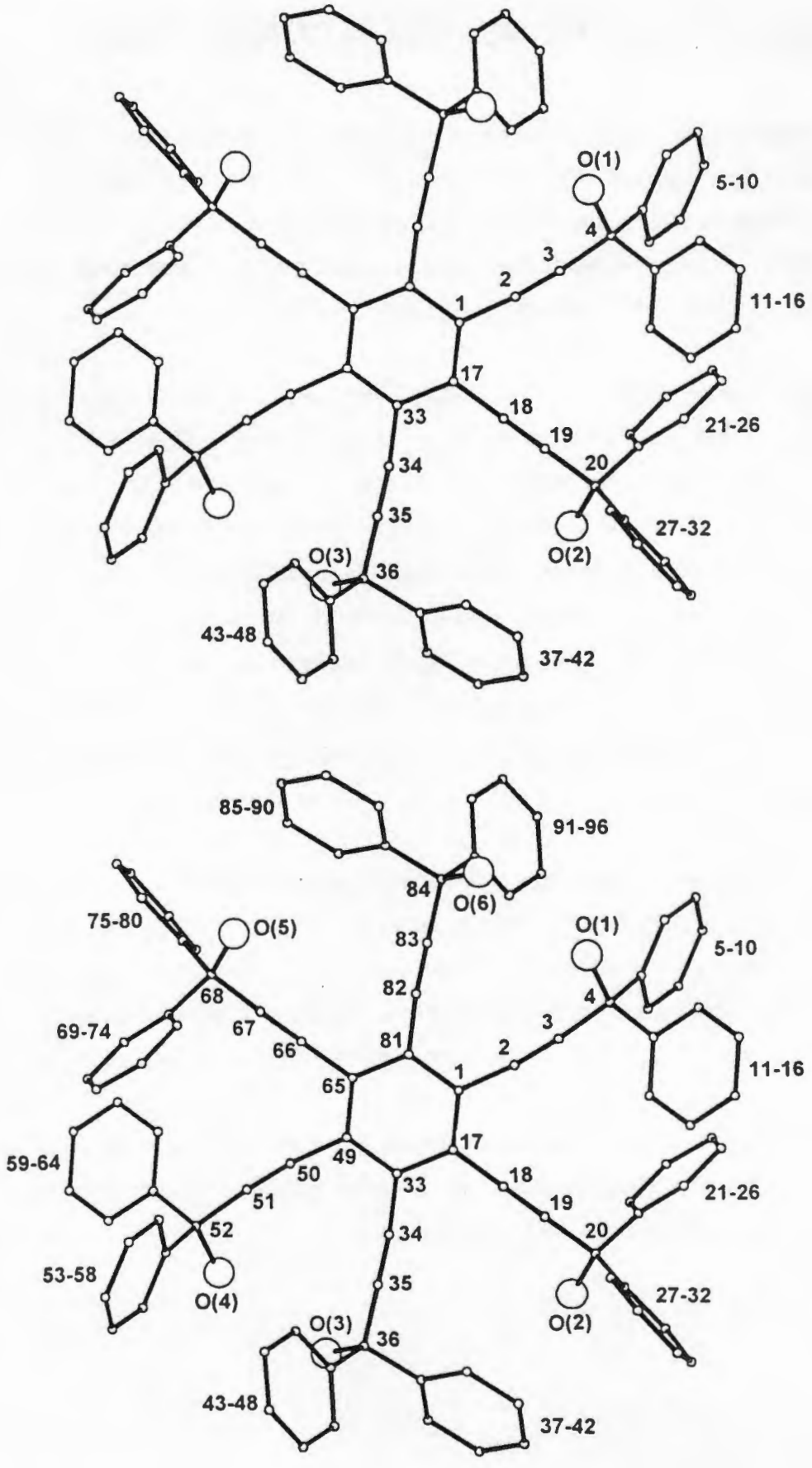

Figure 4.1 : Atomic labelling scheme used for host 1.

SPBN

$C_{96}H_{66}O_6$ (Host **1**)	
Space Group : P $\bar{1}$	
a = 10.683(2)Å	α = 99.78(1)°
b = 11.065(1)Å	β = 98.27(1)°
c = 15.442(3)Å	γ = 98.90(1)°
Volume = 1749.8(5)Å^3	
Z = 1	

Crystal Structure :

The structure of host **1** was refined in the centrosymmetric space group P $\bar{1}$.

Refinement :

All the non-hydrogen atoms were refined anisotropically. The hydroxyl hydrogens were located in the difference electron density maps, and H(2O) and H(3O) were refined isotropically. H(1O) was placed in a geometrically calculated position, and allowed to refine with an isotropic temperature factor linked to O(1). *U* values for the geometrically generated phenyl hydrogen atoms refined to 0.084(2)Å^2, and the structure refined to a final R_1 = 0.0405.

Molecular Structure :

The molecular structure of SPBN is shown in figure 4.2. There is a weak intramolecular hydrogen bond between O(3) and O(1), and between O(2) and an adjacent phenyl ring. Details of these hydrogen bonds are given in table 4.1. The host molecules pack in layers parallel to [100], with the interlinking phenyl rings forming a hydrophobic region between adjacent layers, figure 4.3. There is no intermolecular OH...OH hydrogen bonding. Host to host hydrogen bonding is prevented due to the bulky phenyl groups, which cause steric crowding around the hydroxyl groups. A number of short CH...O distances are observed.

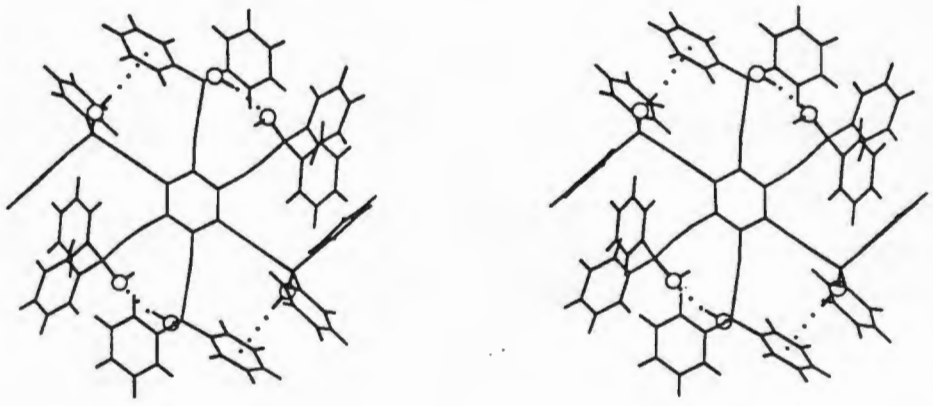

Figure 4.2 : Stereoview of SPBN.

Table 4.1 : Intramolecular hydrogen bonds details of SPBN.

(D)onor	(A)cceptor	D-H (Å)	D...A (Å)	D-H...A (°)
O(3)	O(1)	0.87(3)	3.097(2)	169(3)
O(2)	centroid (C(37)-C(42))	1.0(2)	3.611(9)	145(9)

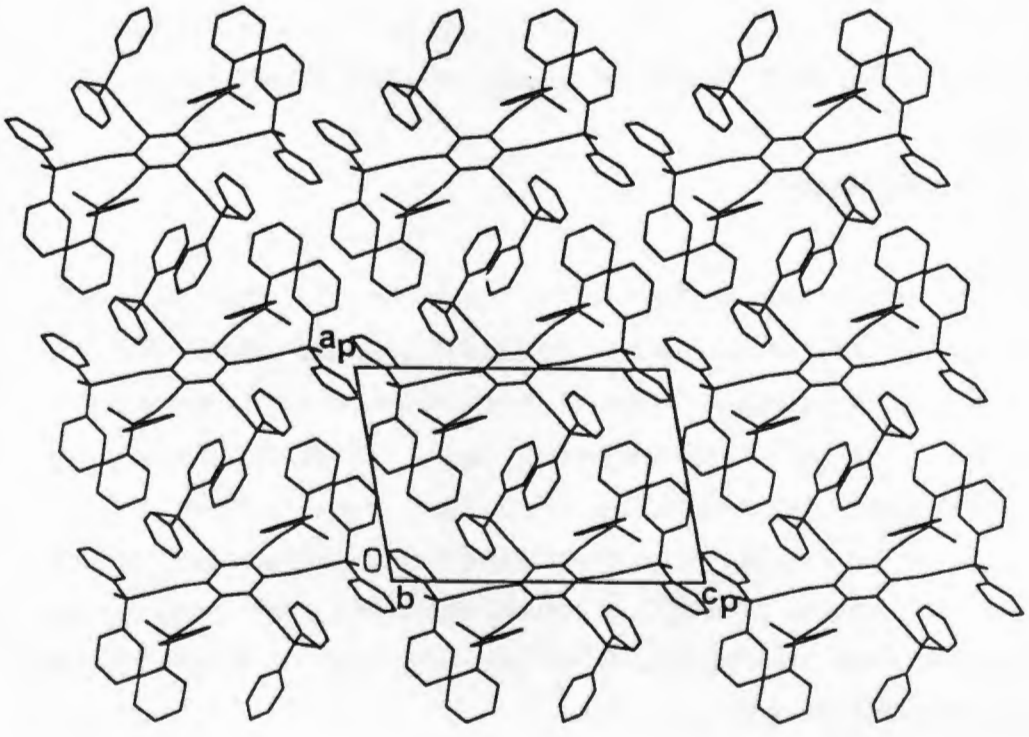

Figure 4.3a : Crystal packing in SPBN, viewed down [010].

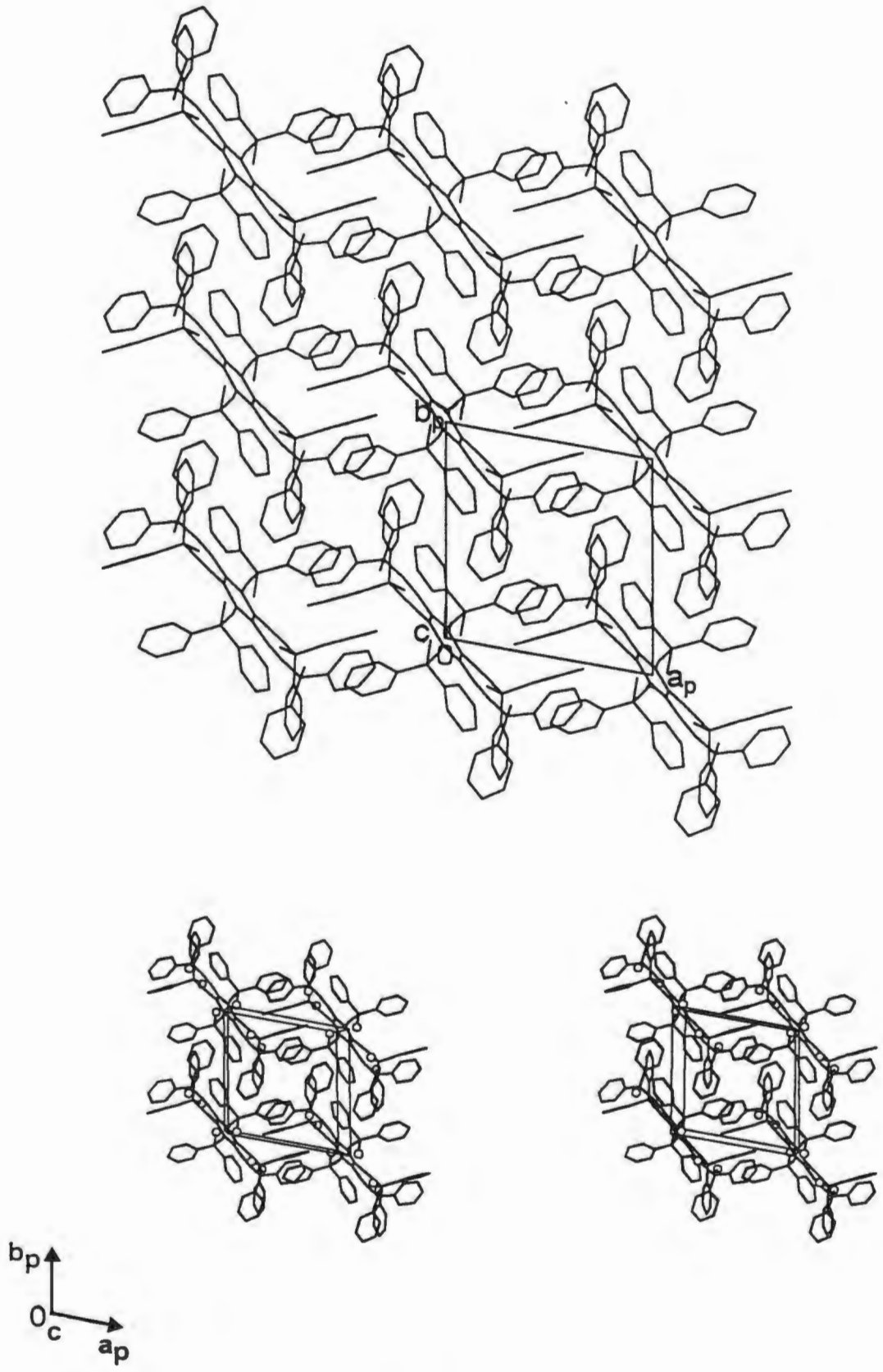

Figure 4.3b : Crystal packing in SPBN, viewed down [001].

Thermal Analysis :

There is no mass loss on heating, and the DSC trace shows a single melt endotherm at 262°C, followed immediately by decomposition of the compound (figure 4.4).

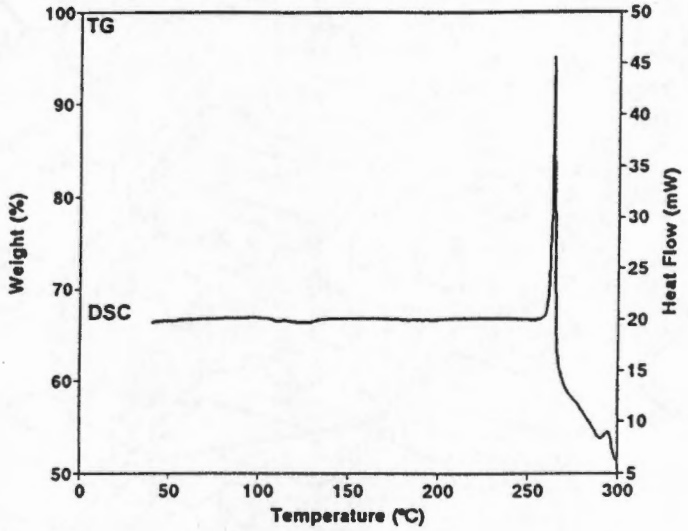

Figure 4.4 : TG and DSC traces for SPBN.

SPAB

$C_{96}H_{66}O_6.2C_2H_3N.2C_6H_6$
Guest : acetonitrile, benzene
Space Group : $P2_1/n$

a = 15.952(2)Å	$\alpha = 90°$
b = 9.144(3)Å	$\beta = 89.917(8)°$
c = 29.251(2)Å	$\gamma = 90°$

Volume = 4267(1)Å^3
Z = 2

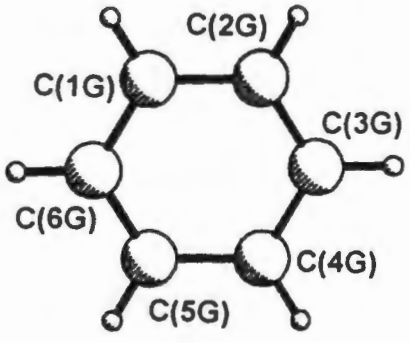

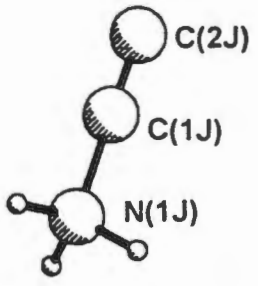

This inclusion compound was obtained unexpectedly from a host **1** and benzene solution, which was subsequently found to contain a small acetonitrile impurity. Nuclear magnetic resonance spectroscopy and C,H,N elemental analysis were used to confirm the presence of the benzene and acetonitrile guests modelled in the crystal structure. The ^{1}H-NMR spectrum of SPAB clearly shows two singlet peaks at δ = 2.03 and 7.37ppm corresponding to the presence of acetonitrile and benzene, respectively. The elemental results are reported in table 3.5 (pg. 51).

On further investigation, a simple competition experiment showed that only a very small impurity, *ca* 5% molar, of either solvent was all that was required to result in the crystallisation of SPAB.

Crystal Structure :

The structure of SPAB was refined in the monoclinic space group, $P2_1/n$.

Oscillation and Weissenberg photography established the unit cell dimensions and crystal system (monoclinic). The crystal reflection data exhibited non-extinction conditions corresponding to the space group $P2_1/n$.

h0l : h + l = 2n

0k0 : k = 2n

(h00 : h = 2n)

(00l : l = 2n)

Refinement :

All the non-hydrogen atoms were refined anisotropically. The hydroxyl hydrogens were located in the difference electron density maps and allowed to refine isotropically. *U* values for the geometrically generated hydrogen atoms refined to CH (phenyl) : 0.064(2)Å^2, and CH (benzene) : 0.105(6)Å^2. The hydrogen atoms of the acetonitrile methyl group were generated geometrically and allowed to refine with an isotropic temperature factor linked to C(2J). The structure refined successfully to $R_1 = 0.0465$.

Molecular Structure :

The crystal packing is shown in figure 4.5. The host molecules are packed in staggered layers parallel to [100] and [010], with the central aromatic ring parallel to the (010) plane. The guest molecules are located in cavities between the central aromatic rings of adjacent host molecules within each [100] layer. An examination of the volume of these cavities showed that these cavities are approximately 9 x 7 x 13.5Å in dimension (figure 4.6). The acetonitrile guests are held in position by co-operative hydrogen bonding. The hydrogen bonds observed in SPAB are detailed in table 4.2, and illustrated in figure 4.7.

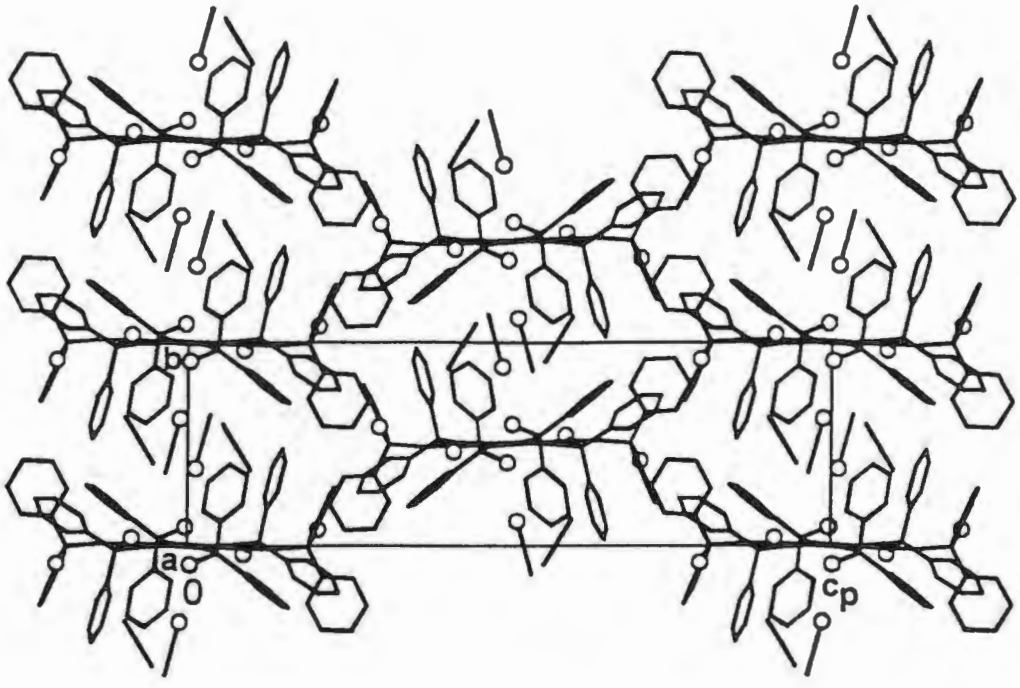

Figure 4.5a : Crystal packing in SPAB, viewed down [100].

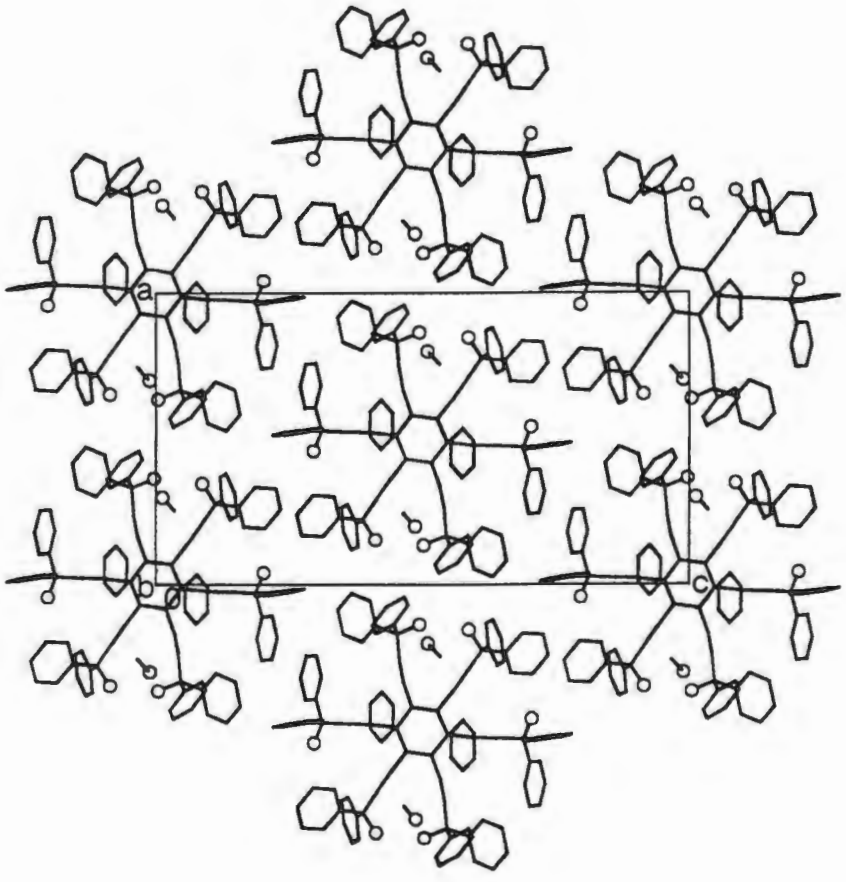

Figure 4.5b : Crystal packing in SPAB, viewed down [010].

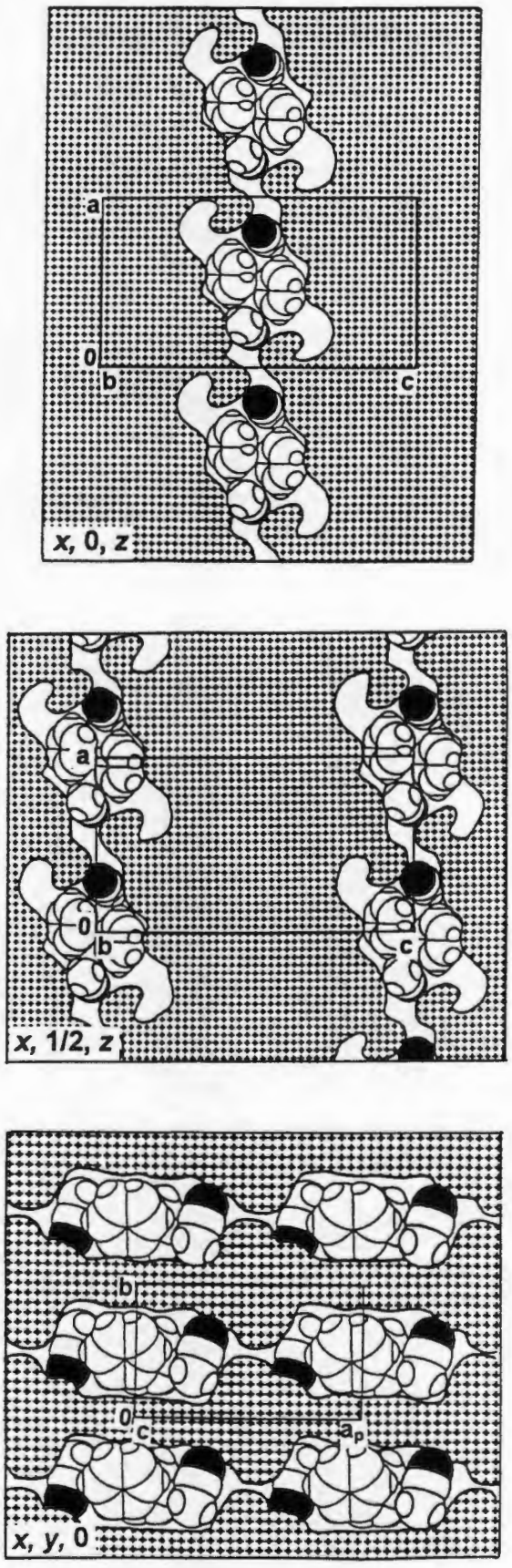

Figure 4.6 : Cross section of SPAB viewed (a) along [010], and (b) along [001]. The hatched region is that occupied by the host molecules. The guest molecules (with the nitrogens shaded) are located within the cavities.

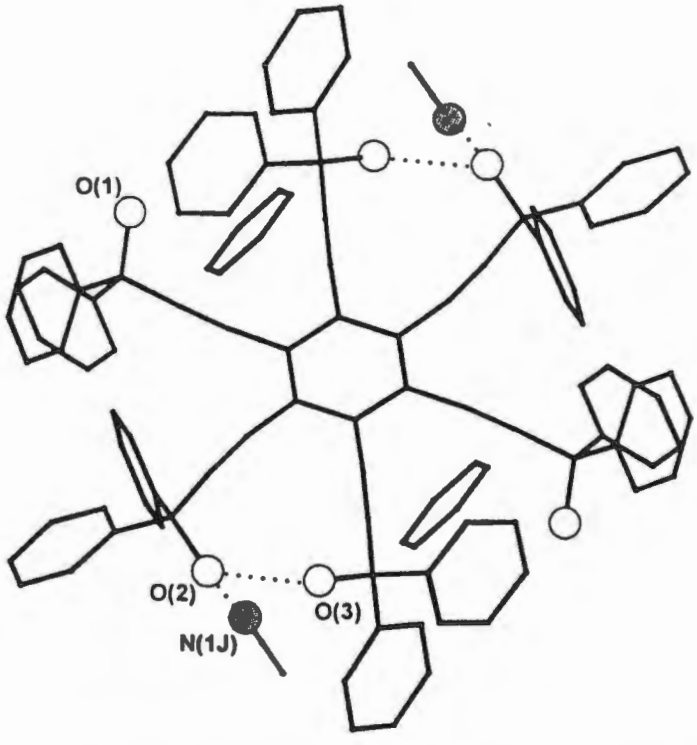

Figure 4.7 : Hydrogen bonding scheme of SPAB (hydrogens are omitted and the hydrogen bonds are indicated as dotted lines).

Table 4.2 : Hydrogen bonding details of SPAB.

(D)onor	(A)cceptor	D-H (Å)	D...A (Å)	D-H...A (°)
O(3)	O(2)	0.82(3)	2.926(3)	175(3)
O(2)	N(1J)	0.96(4)	2.836(4)	172(3)

Thermal Analysis :

The thermograms for SPAB are shown in figure 4.8. The DSC curve shows a single endotherm associated with guest loss at *ca* 92°C. The benzene and acetonitrile guest molecules are situated within the same cavity. On structural collapse of the β-phase to the non-porous α-phase, both the benzene and acetonitrile molecules are released simultaneously, resulting in a single step guest loss. The host then melts with decomposition at 263°C. The TG curve confirms the single step guest loss, and the host to guest ratio refined in the crystal structure (expected mass loss : 15.34%, observed mass loss : 14.88%). Figure 4.9 is a series of photographs of crystals of SPAB under slow heating; the crystals begin to decay with nuclei, probably of the α-phase, at points of defects. These nuclei grow rapidly as the guest release temperature is approached. The α-phase then melts at 272°C.

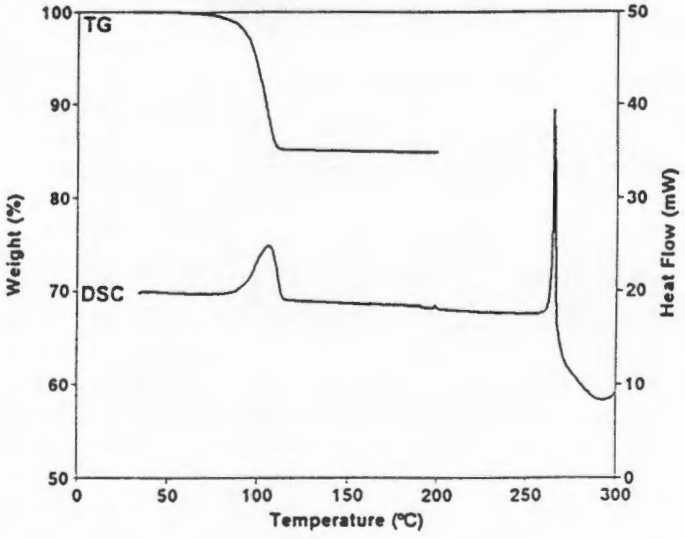

Figure 4.8 : TG and DSC traces for SPAB.

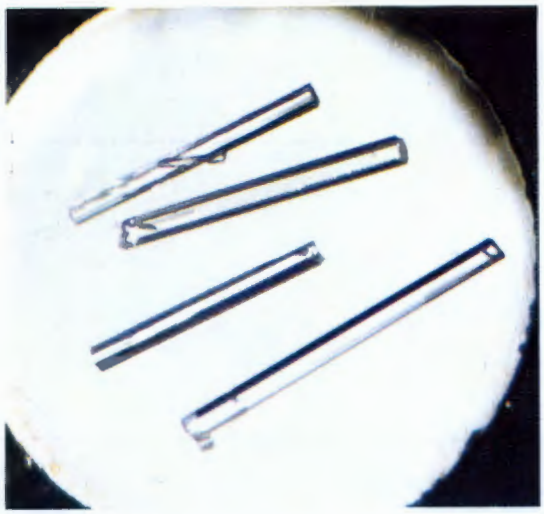

(a) room temperature

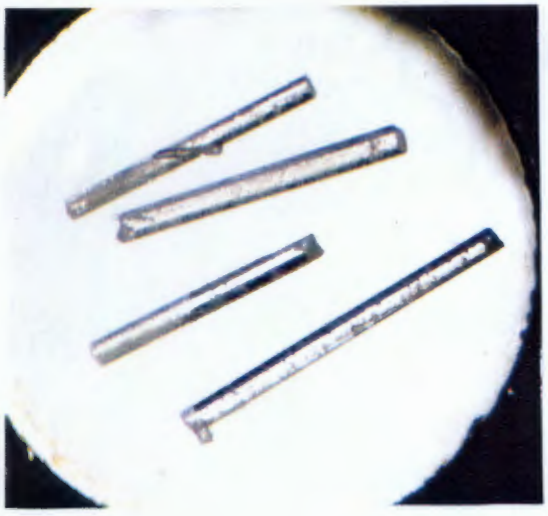

(b) 90°C

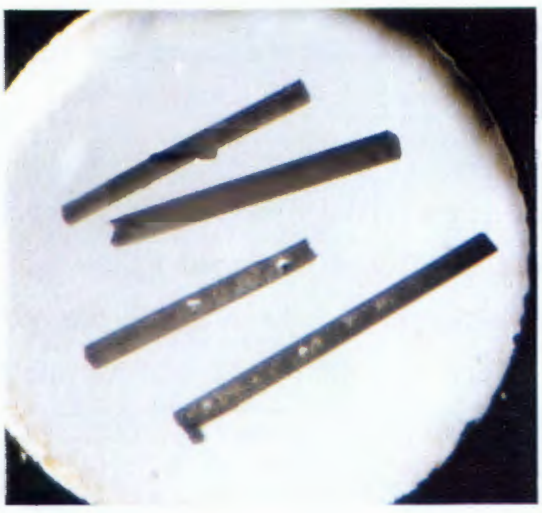

(c) 97°C

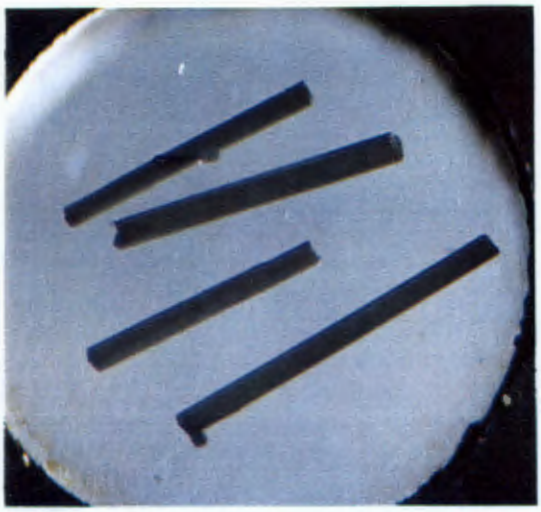

(d) 100°C

(e) 272°C

Figure 4.9 : Thermal decay of SPAB, heating rate 10°C.min^{-1} (magnification : 30X).

SPDMA

$C_{96}H_{66}O_6.4C_4H_9NO$
Guest : dimethyl acetamide
Space Group : $P2_1/n$

a = 16.230(9)Å	α = 90°
b = 9.611(2)Å	β = 90.47(3)°
c = 29.015(8)Å	γ = 90°

Volume = 4526(3)Å^3
Z = 2

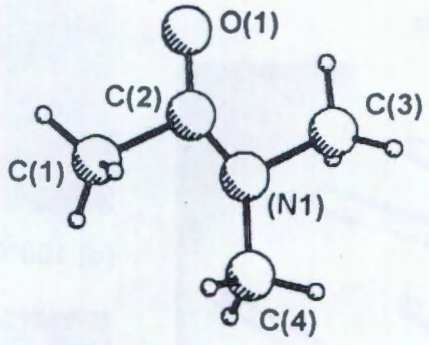

Guests labelled : G, J.

Crystal Structure :

The crystal structure of SPDMA was also refined in the monoclinic space group, $P2_1/n$.

Preliminary X-ray photography established the crystal system (monoclinic) and cell parameters. The space group ($P2_1/n$) was confirmed by the non-extinction conditions of the crystal reflection data. As in SPAB, the host molecule is situated on a centre of inversion. Half a host and two guest molecules are located in the asymmetric unit.

Refinement :

All the non-hydrogen atoms were refined anisotropically. The hydroxyl hydrogens were located in the difference electron density maps, and refined with isotropic temperature factors. The phenyl hydrogens were placed in geometrically calculated positions and refined with a common temperature factor (*U* (CH) : 0.069(3)Å^2). The guest hydrogens were placed in calculated positions and refined with a temperature factor linked to the parent carbon. Guest J was located unambiguously in the difference electron density maps, but required bond length and distance restraints to retain a reasonable molecular geometry. The distances restrained were : C(1J) - C(2J) : 1.50(3)Å, C(2J) - N(1J) : 1.30(3)Å, and N(1J) - C(3J) : 1.40(3)Å. The final values obtained were 1.67(1)Å, 1.15(1)Å and 1.62(1)Å respectively. The bond length C(2J) - N(1J) is relatively short, but a search of the CSD[2] revealed that for other reported dimethyl acetamide inclusion complexes, the C2 - N1 bond length ranged from 1.05Å to 1.45Å , as shown in the histogram (figure 4.10).

The structure refined to a final R_1 = 0.0735.

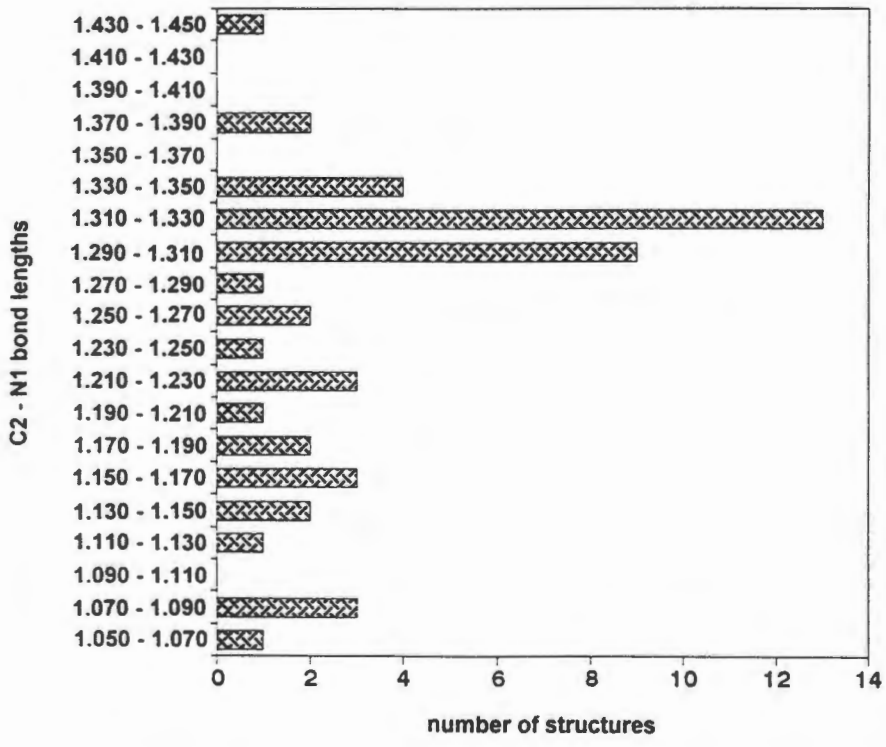

Figure 4.10 : Histogram showing the C2 - N1 bond lengths for forty-nine reported dimethyl acetamide inclusion complexes.

Molecular Structure :

The molecular structure of SPDMA is shown in figure 4.11, and the hydrogen bond details are given in table 4.3. Figure 4.12 shows the crystal packing in SPDMA, which resembles the crystal packing observed in SPAB. The host molecules pack in layers parallel to the (020) plane, with the central aromatic region of the host molecules inclined in opposite directions in alternate layers. The guests are located in cavities between adjacent host molecules within each layer (figure 4.13), with an approximate volume of (14 x 10 x 6.5)$Å^3$.

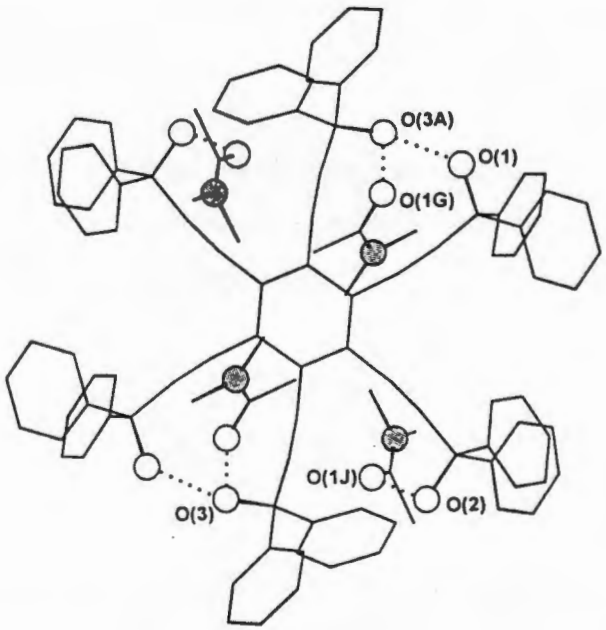

Figure 4.11 : Molecular structure of SPDMA (nitrogen atoms are shaded, hydrogens are omitted and the hydrogen bonds are indicated as dotted lines).

Table 4.3 : Hydrogen Bond data for SPDMA.

(D)onor	(A)cceptor	D-H (Å)	D...A (Å)	D-H...A (°)
O(1)	O(3)[a]	0.89(5)	2.839(5)	162(5)
O(3)	O(1G)	0.86(5)	2.641(5)	171(4)
O(2)	O(1J)	0.77(7)	2.707(6)	153(7)

a : 2-*x*, 2-*y*, -*z*

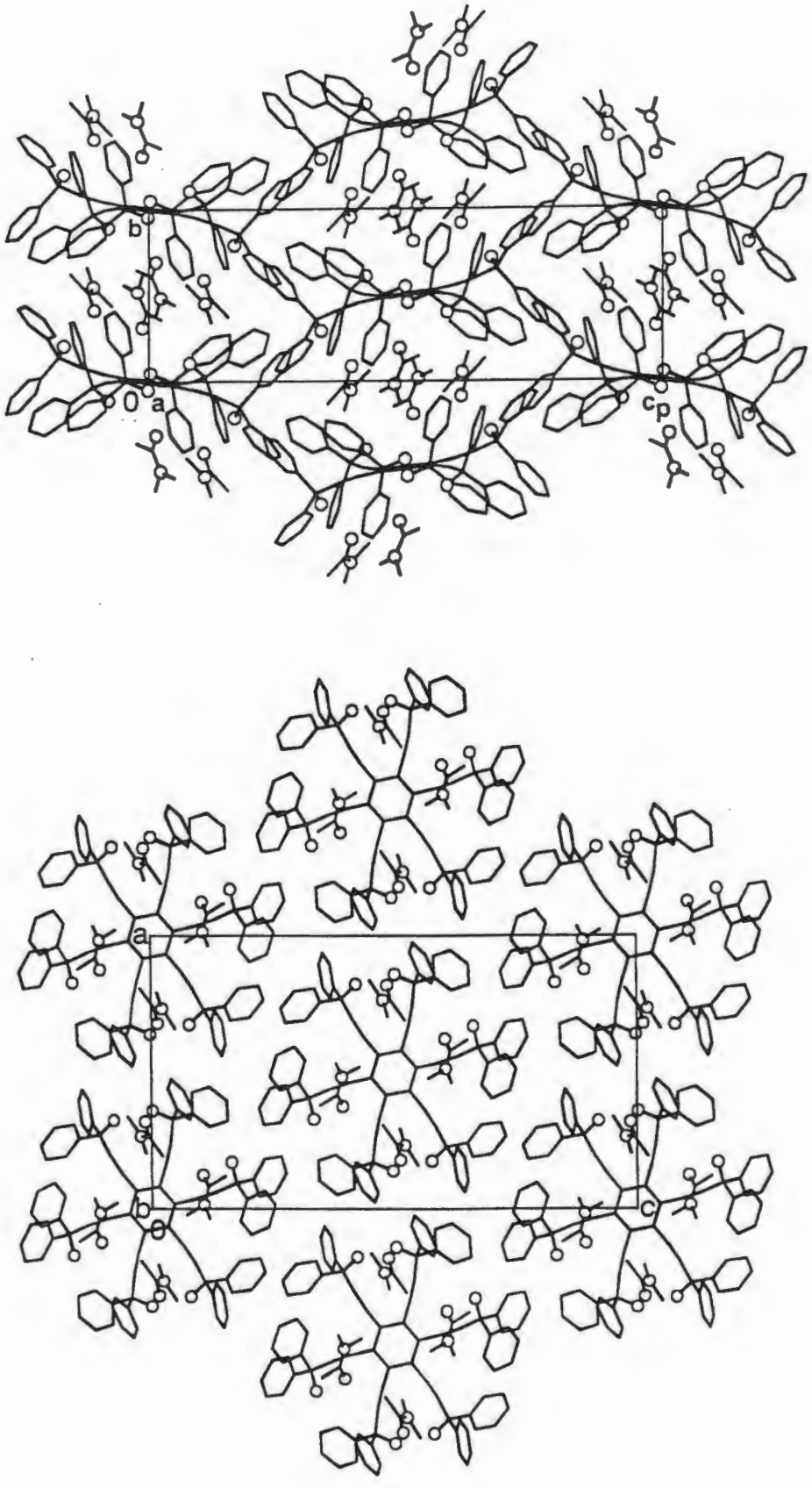

Figure 4.12 : Crystal packing in SPDMA, viewed down (a) [100], and (b) [010].

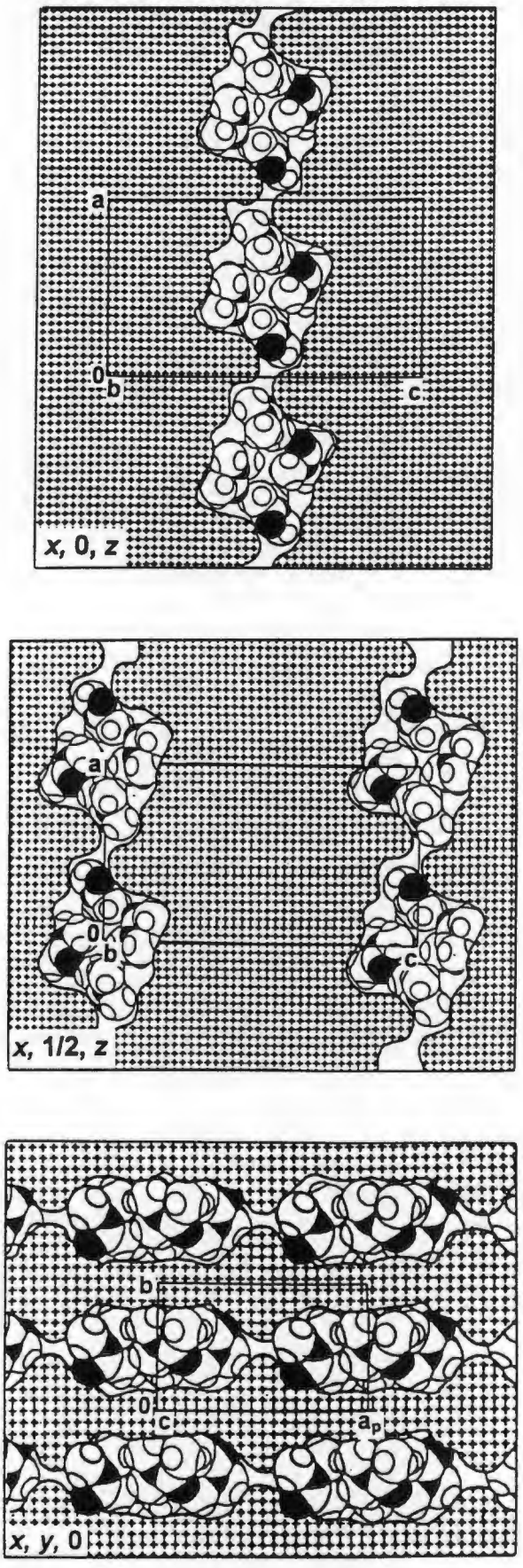

Figure 4.13 : Cross section of SPDMA, viewed down (a) [010], and (b) [001]. The hatched region is that occupied by the host molecules, and the guest molecules (with the oxygens and nitrogens shaded) are located within the cavities.

Thermal Analysis :

The host to guest ratio of 1:4 modelled in the crystal structure is confirmed by TG analysis (expected mass loss : 20.1%, observed mass loss : 20.3%). The guest is lost in a single step, and this is reflected in a single guest loss endotherm at *ca* 135°C, on DSC analysis (figure 4.14). The host then melts and decomposes at 254°C.

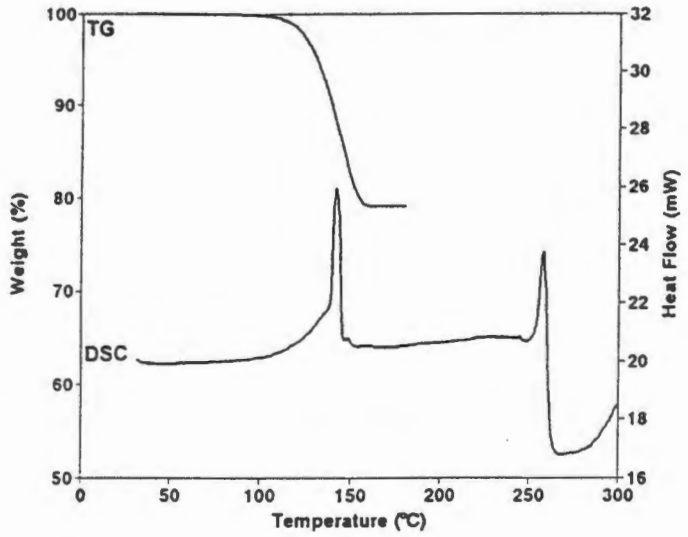

Figure 4.14 : TG and DSC curves of SPDMA.

Kinetics of Desolvation :

Data for the kinetics of desolvation of SPDMA was obtained over the temperature range 75 - 105°C. The α-time curves, which are truncated sigmoidal in shape (figure 4.15), are best described by the Avrami-Erofeev (A2) equation. The semilogarithmic plot of ln *k vs.* 1/T was linear over the investigated temperature range, and is shown in figure 4.16. An activation energy of 154(3) kJ.mol^{-1} was obtained for this desolvation reaction (α-range 0.05 - 0.95).

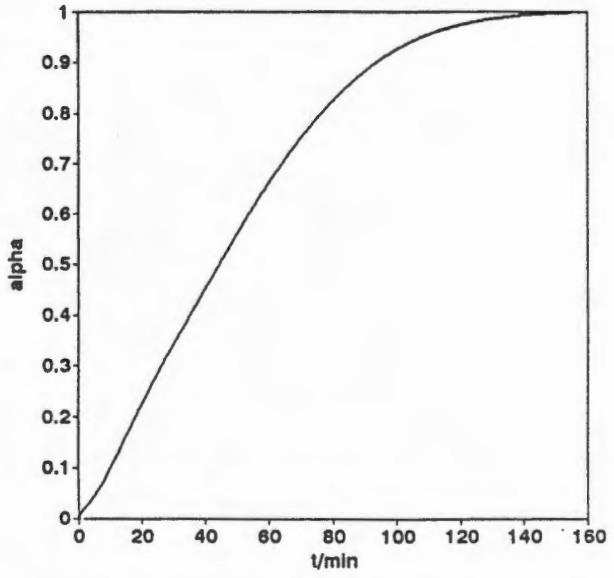

Figure 4.15 : An example of an α vs. time curve for SPDMA.

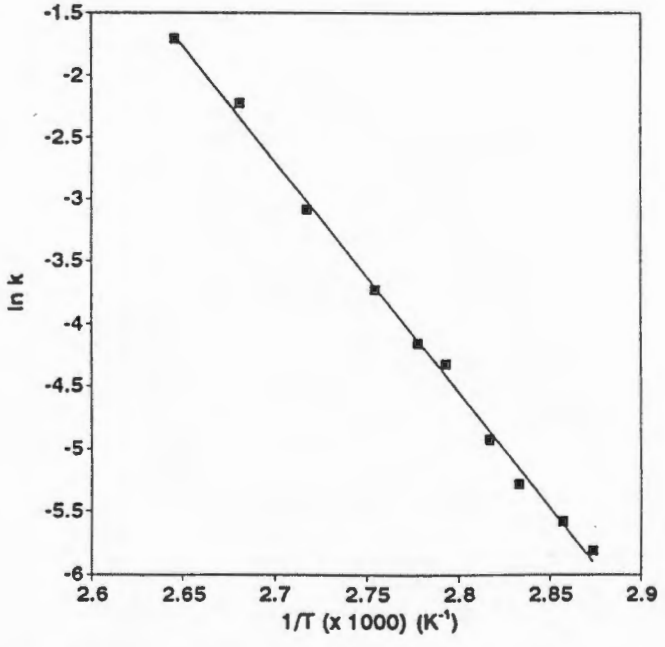

Figure 4.16 : Arrhenius plot for the desolvation of SPDMA.

SPMEK

$C_{96}H_{66}O_6.3C_4H_8O$
Guest : methyl ethyl ketone
Space Group : $P2_1/c$

a = 12.320(5)Å	α = 90°
b = 21.438(8)Å	β = 100.16(5)°
c = 32.92(2)Å	γ = 90°

Volume = 8558(7)Å^3
Z = 4

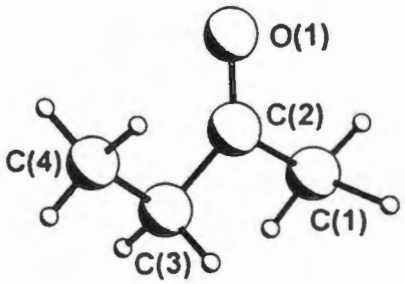

Guests labelled : G, J, K.

Crystal Structure :

The crystal structure of SPMEK was refined in the monoclinic space group $P2_1/c$. This was established from preliminary oscillation and Weissenberg photography, and from the non-extinction conditions observed in the crystal reflection data, namely :

h0l : l = 2n

0k0 : k = 2n

(00l : l = 2n)

The host molecules are not situated on a centre of inversion, resulting in one host molecule and three guests being located in the asymmetric unit.

Refinement :

All the non-hydrogen atoms of the host molecules were refined anisotropially. Some of the carbons on the phenyl rings, namely C(46), C(47), C(73), C(74), C(78), C(94) and C(95), have relatively high temperature factors. A disorder model of these carbons was attempted but was unsuccessful, since it resulted in poor geometry of the phenyl rings. The phenyl hydrogens were placed in

geometrically calculated positions and refined with a common isotropic temperature factor (*U* (CH) : 0.088(3)Å^2). The hydroxyl hydrogens were not found in the difference electron density maps and were omitted from the model. The non-hydrogen atoms of guest G were refined anisotropically, while those for guests J and K were refined isotropically, owing to their high temperature factors. The guest hydrogens were placed in calculated positions. The methyl hydrogens were refined with a common temperature factor for each of the two chemically distinct methyl groups, while the CH_2 hydrogens were refined with a temperature factor linked to the parent carbon.

U (CH_3 - C(1G/J/K)) : 0.048(5)Å^2

U (CH_3 - C(4G/J/K)) : 0.067(6)Å^2

There is a residual electron density of 0.58eÅ^{-3} in the region of guest K; this is ascribed to an imperfect model. The structure refined to a final R_1 = 0.0891.

Molecular Structure :

The molecular structure of SPMEK is shown in figure 4.17. Three different types of hydrogen bonding are observed; guest G is hydrogen bonded to O(5), guests J and K are held in position by co-operative hydrogen bonds and O(2) forms a short contact to an adjacent phenyl ring within the same host molecule (C37-C42). These hydrogen bonding details are given in table 4.4. The host molecules pack in a herringbone pattern, and this packing motif is clearly shown in figure 4.18. The guests J and K are situated in zigzag channels parallel to [100], while guest G is situated in cavities adjacent to the channels (figure 4.19).

Table 4.4 : Hydrogen bond data for SPMEK.

(D)onor	(A)cceptor	D...A (Å)
O(5)	O(1G)	2.807(6)
O(3)	O(4)	2.834(5)
O(4)	O(1J)	2.684(7)
O(6)	O(1)	2.769(5)
O(1)	O(1K)	2.665(8)
O(2)	centroid (C37-C42)	3.446(7)

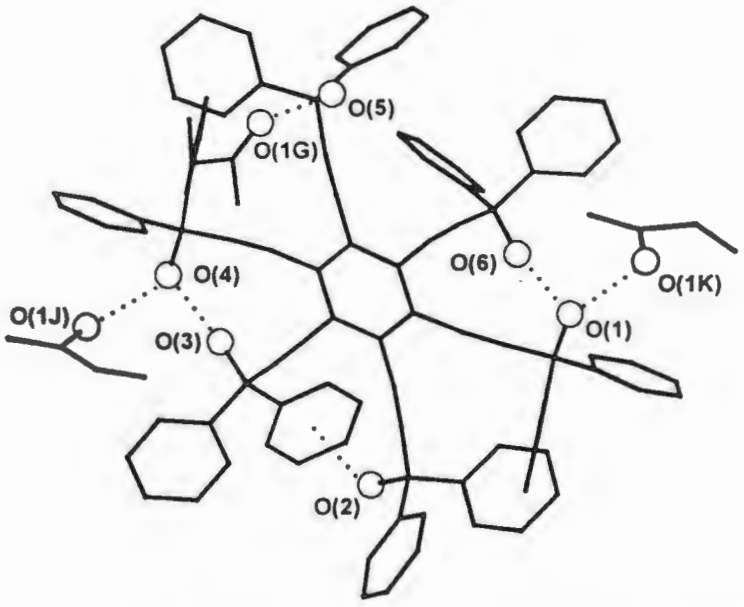

Figure 4.17 : Molecular structure of SPMEK (hydrogen atoms are omitted, and hydrogen bonds are represented as dotted lines).

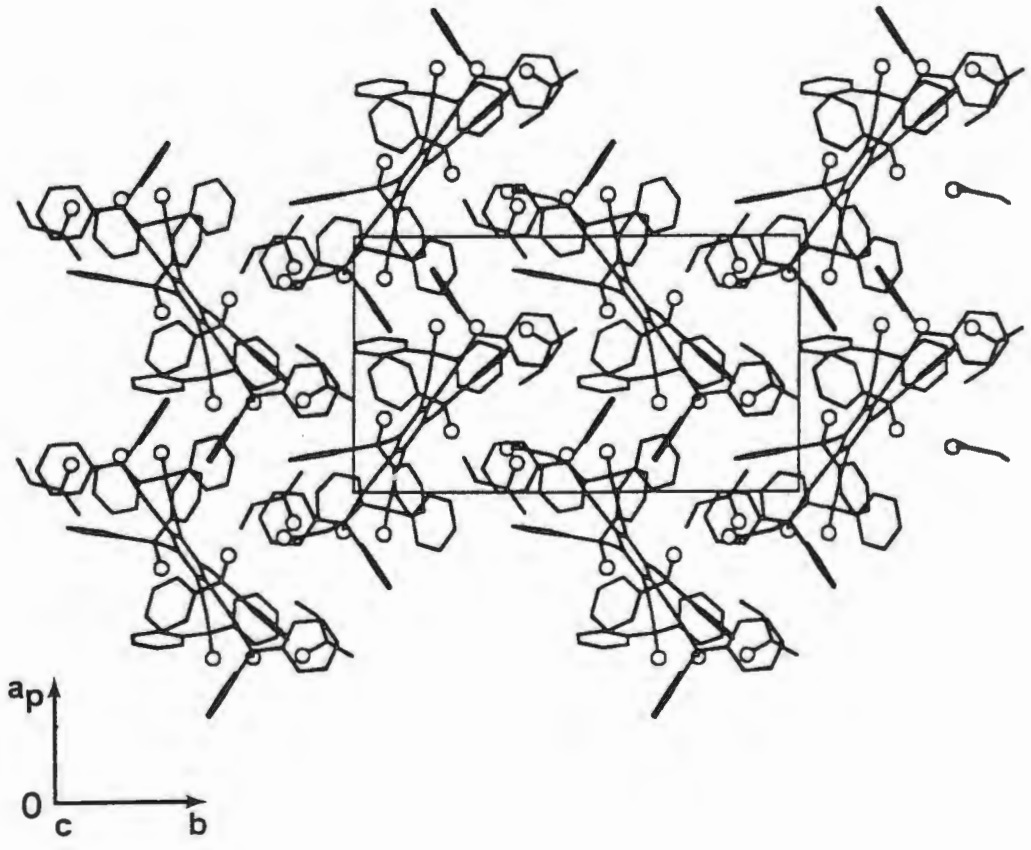

Figure 4.18 : Crystal packing in SPMEK, viewed down [001].

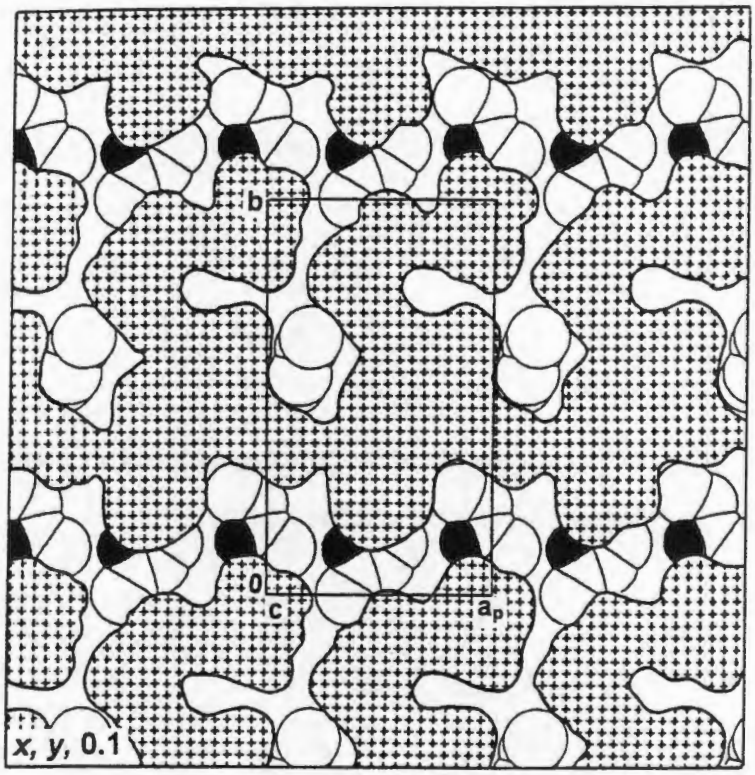

Figure 4.19 : Cross-section of SPMEK viewed along [001]. The hatched region is that occupied by the host molecules, and the guests are shown in the voids.

Thermal Analysis :

TG analysis shows that the guest loss occurs in a single step (figure 4.20), and confirms the host to guest ratio of 1:3 modelled in the crystal structure (calculated mass loss : 14.1%, observed mass loss : 13.3%). The DSC trace, however, is more complex, and shows a broad double endotherm at *ca* 75°C, corresponding to guest loss and β to α phase change. The host then melts with decomposition at 260°C.

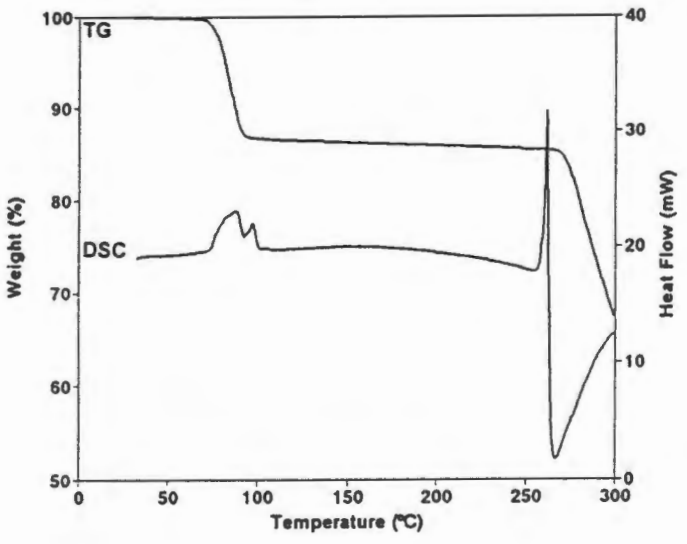

Figure 4.20 : TG and DSC traces of SPMEK.

Kinetics of Desolvation :

A series of isothermal TG experiments were carried out over the temperature range 62 - 72°C. Figure 4.21 shows an example of a resultant α vs. time curve. These curves are best described in two parts. The first part (α-range 0 - 0.2) is linear, and corresponds to surface evaporation. The Prout-Tompkins kinetic model (B1) fits the second part of the reaction (α-range 0.2 - 0.95). The Prout-Tompkins rate law is derived from the branching growth of nuclei, arising from the stresses which result from the formation of a new phase with a significantly different volume. In this case the host framework collapses to the non-porous α-phase, which has a

significantly different crystal structure with new molecular orientations. The semilogarithmic plot of ln k vs. 1/T, shown in figure 4.22, yields an activation energy of 156(9) $kJmol^{-1}$ for this reaction.

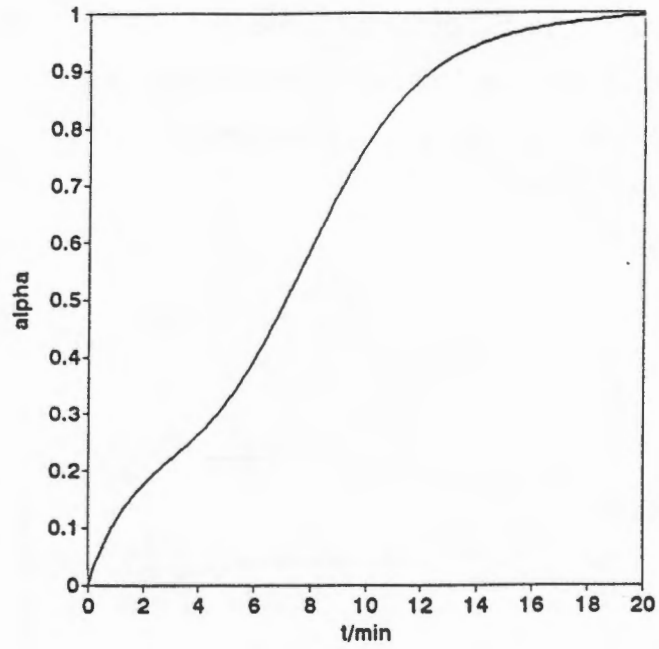

Figure 4.21 : An example of an α *vs.* time curve for SPMEK.

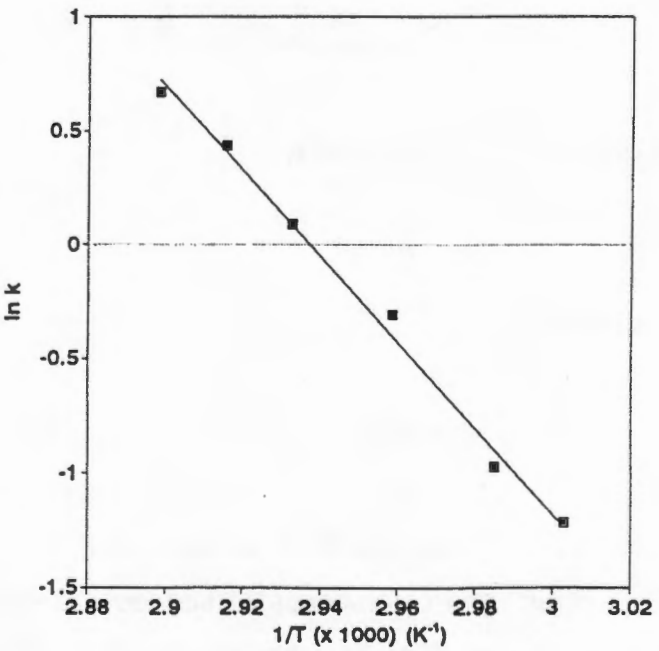

Figure 4.22 : Arrhenius plot for the desolvation of SPMEK.

SPDEK

$C_{96}H_{66}O_6.2C_5H_{10}O$
Guest : diethyl ketone
Space Group : P $\bar{1}$

a = 10.912(4)Å	α = 78.78(3)°
b = 12.651(3)Å	β = 87.94(3)°
c = 15.705(4)Å	γ = 76.42(3)°

Volume = 2067(1)Å^3
Z = 1

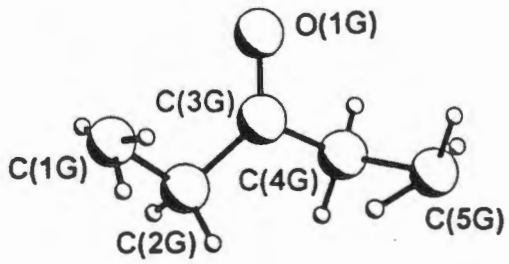

Crystal Structure :

The structure of SPDEK was refined in the triclinic space group P $\bar{1}$, and the structure was successfully solved by direct methods.

Refinement :

All of the host non-hydrogen atoms, and oxygen atoms of the guests were refined anisotropically. C(14), C(15), C(29), C(30) and C(31) show comparatively high temperature factors. A disorder model for these carbons was investigated, but was unsatisfactory, since it resulted in poor geometry of the respective phenyl rings. The hydroxyl hydrogens were located in the electron density maps. H(2O) and H(3O) were refined isotropically, while H(1O) was refined with a bond length restraint and temperature factor linked to O(1). The host phenyl and guest hydrogen atoms were placed in geometrically calculated positions, with a common isotropic temperature factor (*U*) for similar hydrogens. The final *U* values obtained were :

CH : 0.097(2)Å^2 CH_2 : 0.17(1)Å^2 CH_3 : 0.079(4)Å^2

The structure refined to a final R_1 = 0.0593.

Molecular Structure :

The molecular structure of SPDEK can be seen in figure 4.23. Co-operative hydrogen bonding between O(2), O(3) and O(1G) is observed, the details of which are given in table 4.5. The crystal packing is shown in figure 4.24. The host molecules pack in layers parallel to [100] with the central aromatic ring parallel to [110]. The guest molecules are situated in cavities between these layers. These cavities have dimensions of approximately 7 x 9 x 8.5Å, and can be seen in projection in figure 4.25.

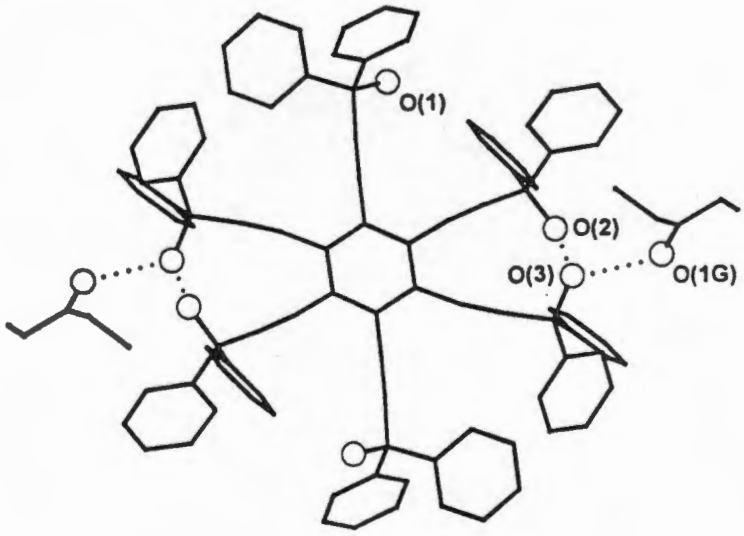

Figure 4.23 : Molecular structure of SPDEK (hydrogen atoms are omitted for clarity, and the hydrogen bonds are indicated as dashed lines).

Table 4.5 : Hydrogen bonding details of SPDEK.

(D)onor	(A)cceptor	D-H (Å)	D...A (Å)	D-H...A(°)
O(2)	O(3)	0.85(4)	2.768(3)	175(4)
O(3)	O(1G)	0.80(4)	2.69(2)	165(4)

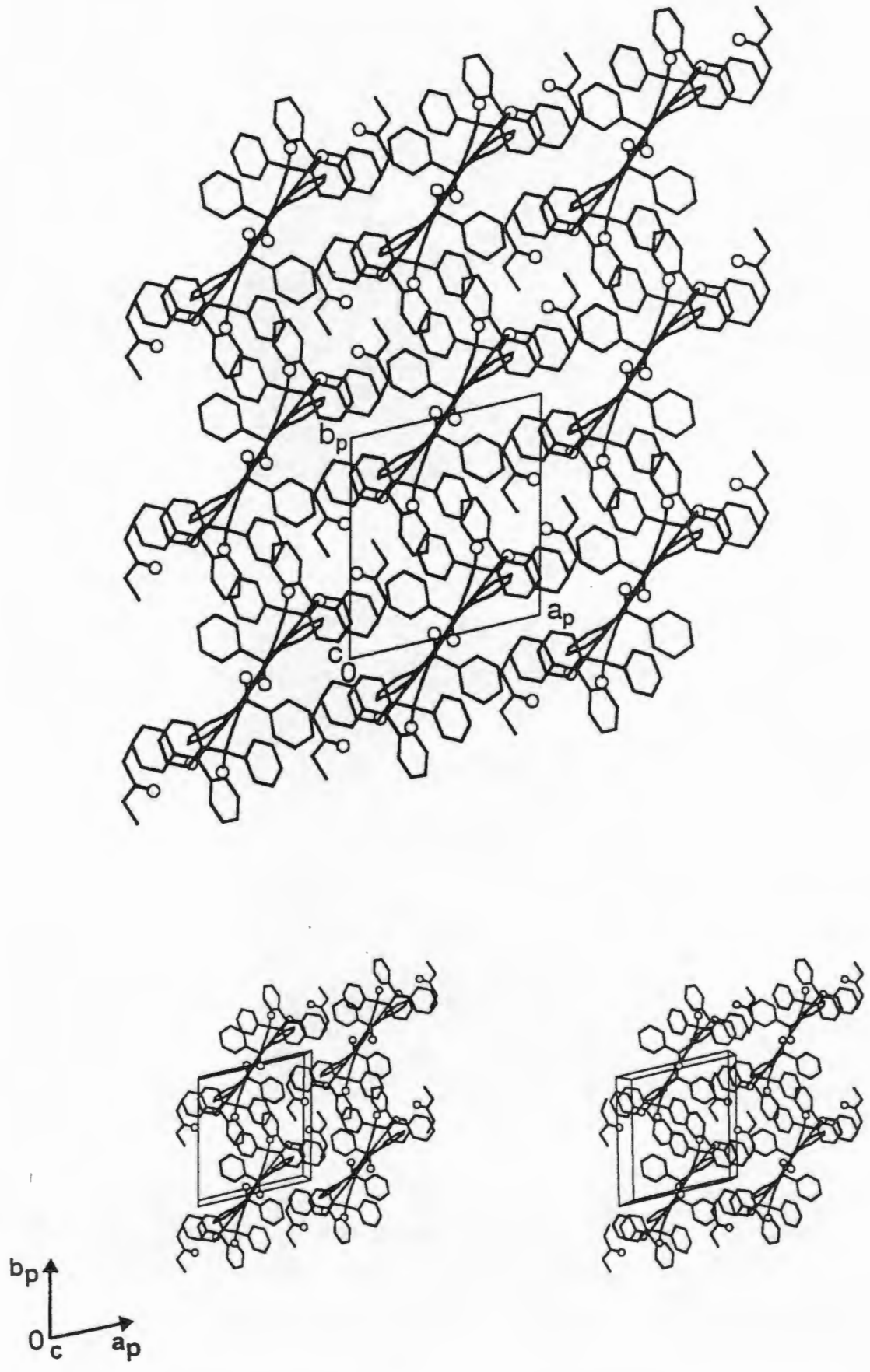

Figure 4.24 : Crystal packing in SPDEK, viewed down [001].

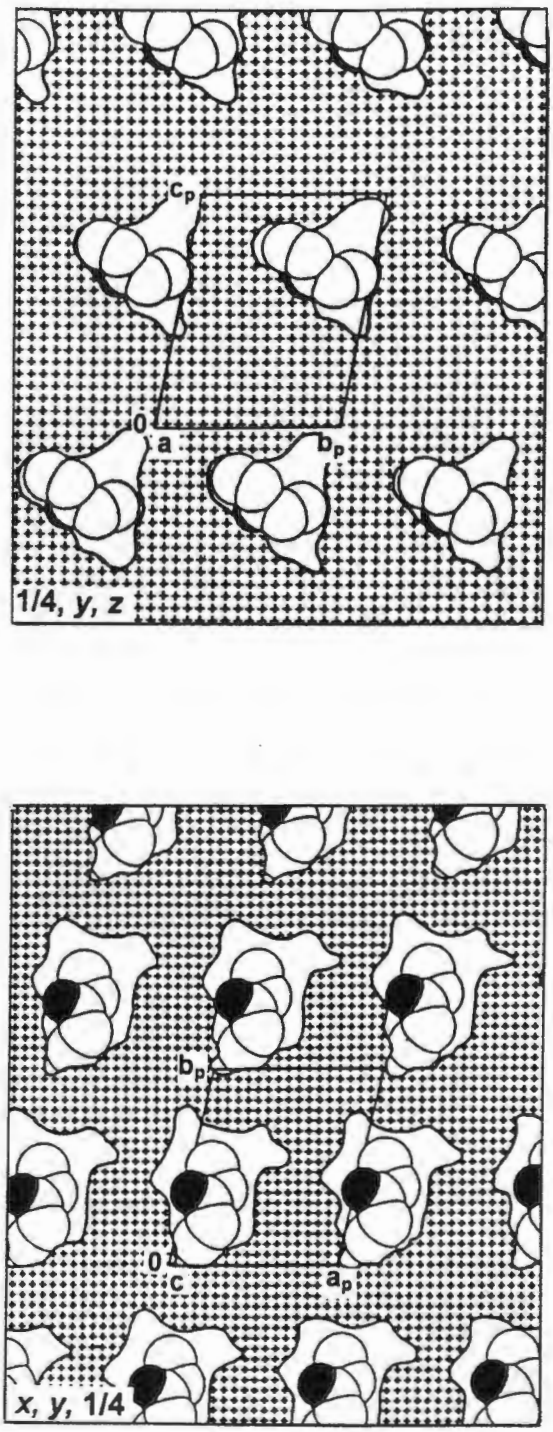

Figure 4.25 : Cross-section of SPDEK viewed along a) [100], and b) [001]. The hatched region is that occupied by the host molecules. The guest molecules (with the oxygens shaded) are shown in the cavities.

Thermal Analysis :

The TG curve (figure 4.26) clearly shows a single step guest loss, and confirms the host to guest ratio of 1:2 modelled in the crystal structure (expected mass loss : 11.6%, observed mass loss : 11.1%). The DSC trace shows a small broad endotherm at *ca* 86°C, corresponding to the guest loss, followed by a sharper endotherm at 258°C caused by the host melting. This is followed by the exothermic decomposition of the host. Figure 4.27 is a series of photographs showing the decomposition of SPDEK. It was noted that on heating the crystals of SPDEK fracture prior to significant guest loss.

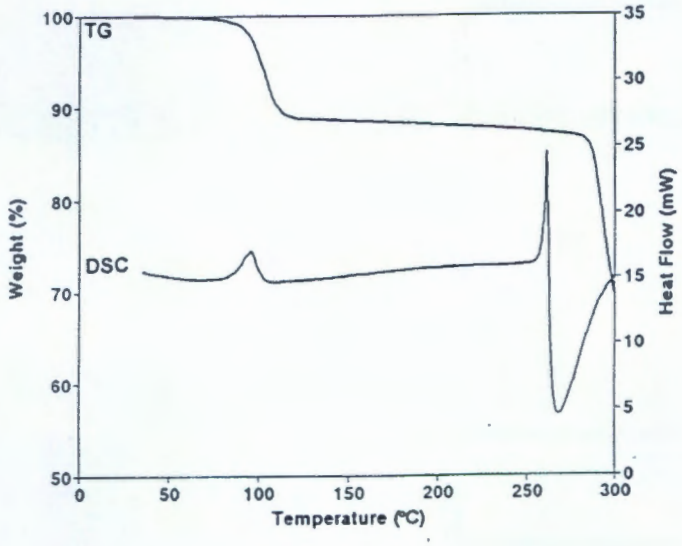

Figure 4.26 : TG and DSC traces of SPDEK.

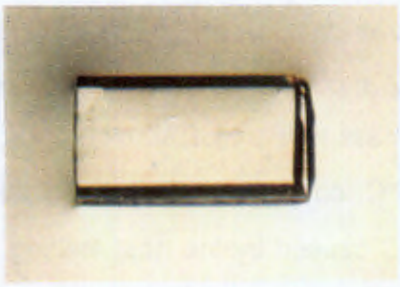

(a) room temperature

(e)106.5

(b) 65°C

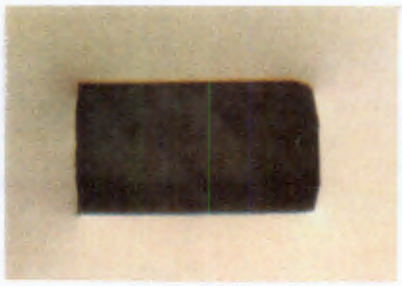

(f) 116°C

(c) 79°C

(d) crystal begins to discolour, 157°C

(d) 100°C

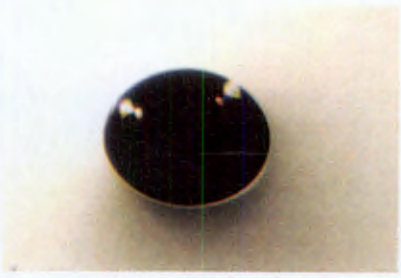

(h) melt with decomposition, 272°C

Figure 4.27 : Thermal decomposition of SPDEK, heating rate 10°C.min^{-1} (magnification : 36X).

Kinetics of Desolvation :

Data for the kinetics of desolvation were obtained from isothermal experiments carried out at temperature intervals of 2 - 5°C over the temperature range of 55 to 80°C. An example of the α-time curves obtained is shown in figure 4.28. The curves are sigmoidal in shape, clearly consisting of an induction period, an acceleratory stage and a deceleratory stage. The mechanism of guest release and structural collapse of the host to its uncomplexed form is best described by the Avrami-Erofeev (A2) equation. An activation energy of 163(5) kJ.mol^{-1} was obtained for this reaction over the α-range 0.05 - 0.95. The semilogarithmic plot of ln *k vs.* 1/T is shown in figure 4.29.

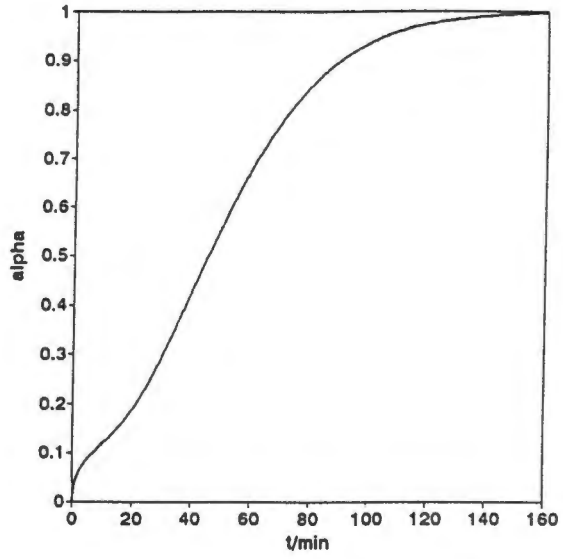

Figure 4.28 : An example of an α *vs.* time curve obtained for SPDEK.

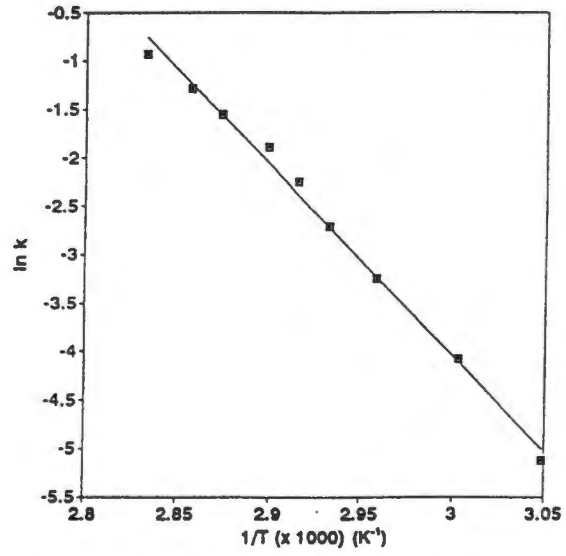

Figure 4.29 : Arrhenius plot for the desolvation of SPDEK.

SPETH

$C_{96}H_{66}O_6.2C_4H_{10}O$
Guest : diethyl ether
Space Group : P $\bar{1}$

a = 10.651(1)Å	α = 78.06(2)°
b = 12.805(3)Å	β = 86.09(2)°
c = 15.560(4)Å	γ = 76.12(1)°

Volume = 2015.2(7)Å^3
Z = 1

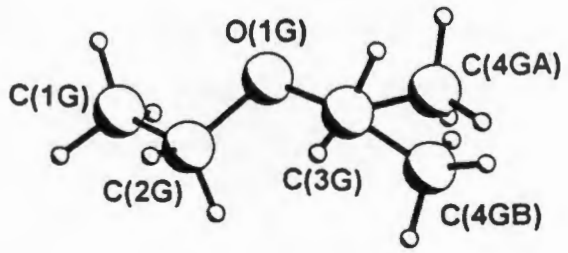

Crystal Structure :

The crystal structure of SPETH was refined in the space group P $\bar{1}$. SPETH and SPDEK are isostructural in that they have similar cell parameters and host skeletons[3].

Refinement :

All of the non-hydrogen atoms were refined anisotropically. One of the end carbons of the guest, C(4G), was found to be disordered over two positions, with site occupancy factors of 0.46 and 0.54. The hydroxyl hydrogens were located in the difference electron density maps. H(1O) and H(3O) were refined independently with isotropic temperature factors. H(2O) was placed in a geometrically calculated position and refined with a temperature factor linked to O(2). All the remaining hydrogen atoms were placed in calculated positions. The phenyl hydrogens were allowed to refine with a common temperature factor, which refined to 0.079(1)Å^2, while the guest hydrogens were refined with temperature factors linked to the parent carbons. An extinction coefficient of 0.018(1) was applied, and the structure refined to R_1 = 0.0450.

Molecular Structure :

Figure 4.30 shows the molecular structure of SPETH. The hydrogen bond details are tabulated in table 4.6. Both SPETH and SPDEK exhibit similar packing with respect to both the host and guest molecules. The crystal packing is shown in figure 4.31; when viewed down [001], layers of host molecules parallel to [100], with the central aromatic ring parallel to [110], can be seen. As in SPDEK, the diethyl ether guest molecules are found in the cavities located between adjacent layers of host molecules, with dimensions of approximately 7.5 x 8.5 x 8Å.

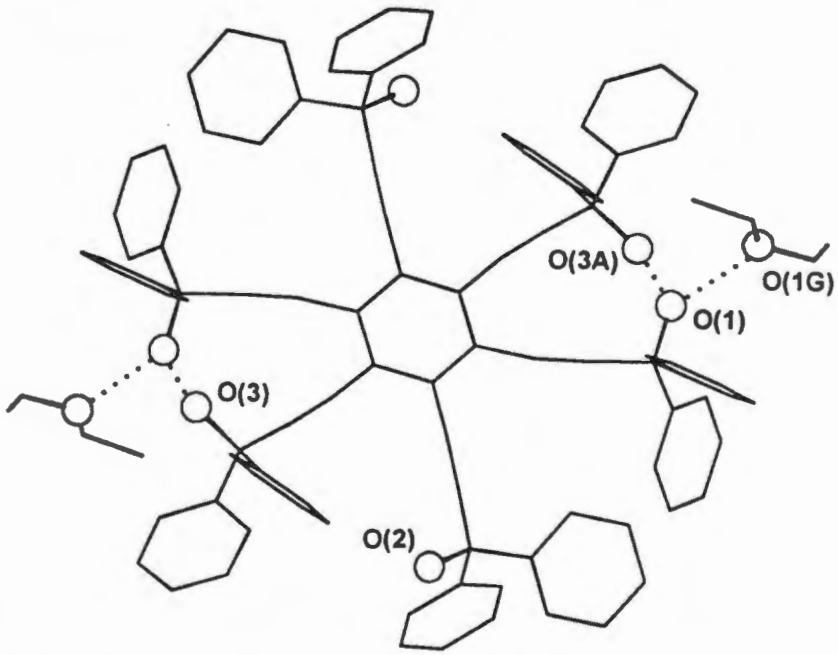

Figure 4.30 : Molecular structure of SPETH (the hydrogen atoms and C(4GA) are omitted; hydrogen bonds are represented as dashed lines).

Table 4.6 : Hydrogen bonding details of SPETH.

(D)onor	(A)cceptor	D-H (Å)	D...A (Å)	D-H...A(°)
O(3)	O(1) [a]	O.89(3)	2.770(2)	171(2)
O(1)	O(1G)	0.89(3)	2.691(2)	164(2)

a : 1-*x*, 2-*y*, 1-*z*

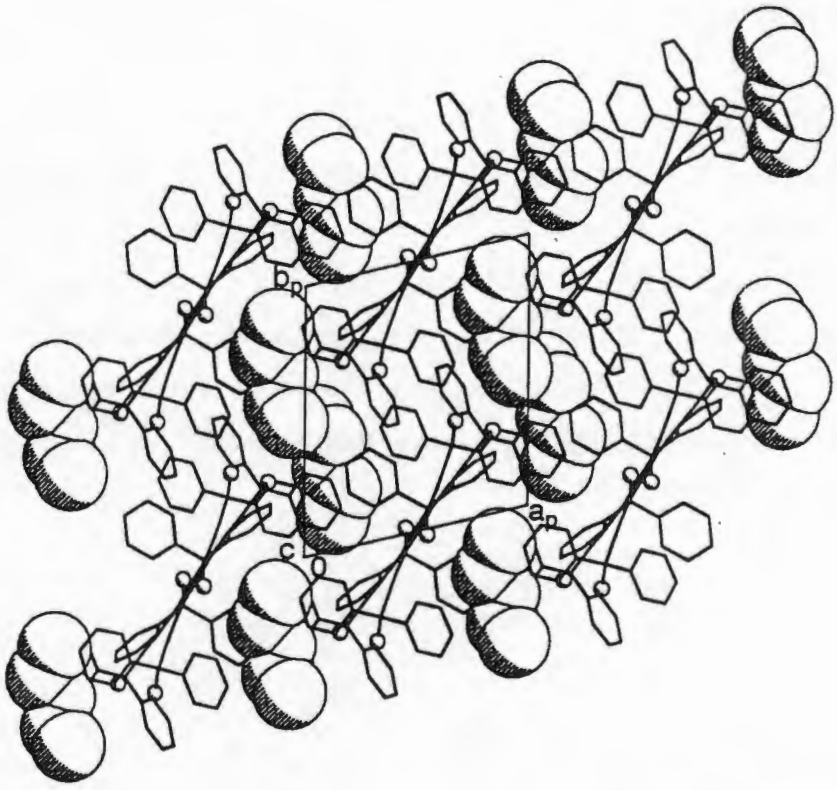

Figure 4.31a : Crystal packing in SPETH as viewed down [001]. The host is represented by stick figures, while the guests are shown as space-filled models.

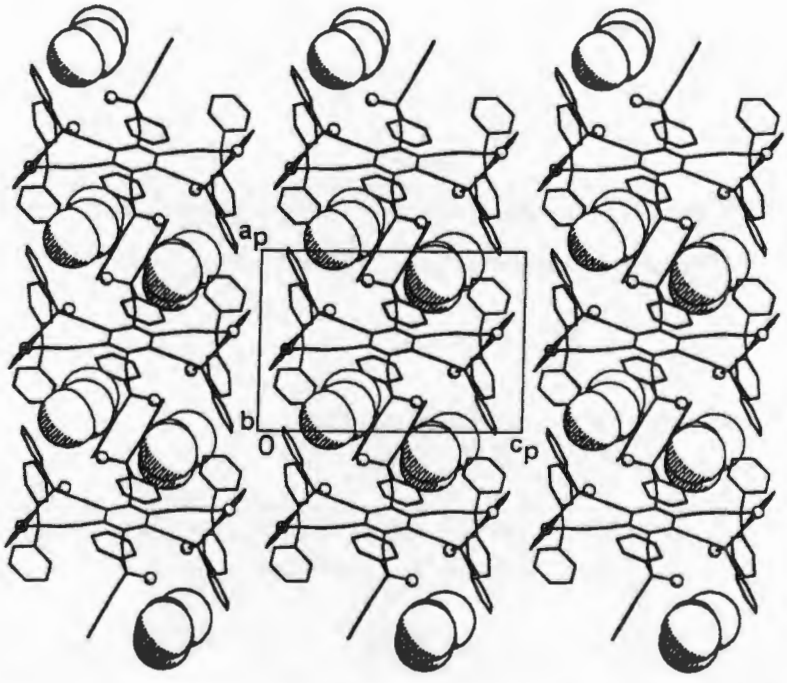

Figure 4.31b : Crystal packing in SPETH as viewed down [010]. The host is represented by stick figures, while the guests are shown as space-filled models.

Thermal Analysis :

The host to guest ratio (1:2) modelled in the crystal structure was confirmed by TG (calculated mass loss : 10.1%, observed mass loss : 9.1%). Guest loss occurs in a single step. A single guest loss endotherm at *ca* 77°C, followed by the host melting with decomposition at 264°C was observed on DSC analysis (figure 4.32). Figure 4.33 shows the slow heating of a single crystal of SPETH. The crystal was immersed in a drop of silicon oil, which is an inert, high boiling liquid, allowing for the detection of the escape of guest vapours, as these result in bubble formation. The crystal started to desolvate slowly at first and then more rapidly as the temperature of guest release and β to α-phase change is approached. The guest loss was clearly observed as bubbles in the silicon oil. The crystal then started to decompose at 234°C, and finally melted at 272°C.

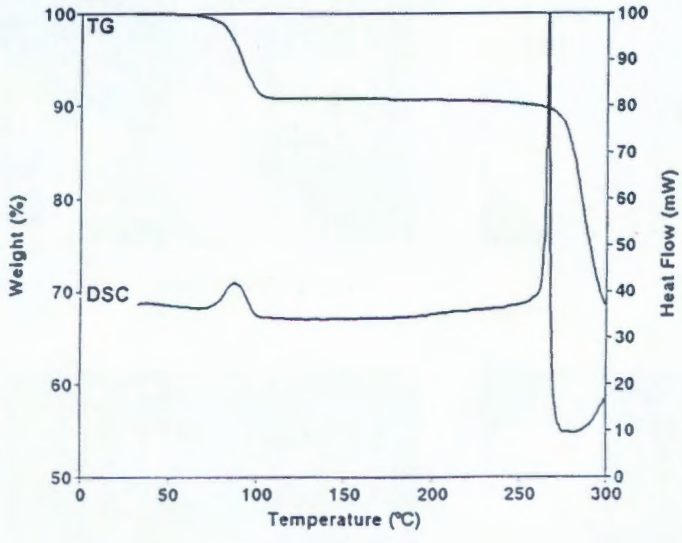

Figure 4.32 : TG and DSC traces of SPETH.

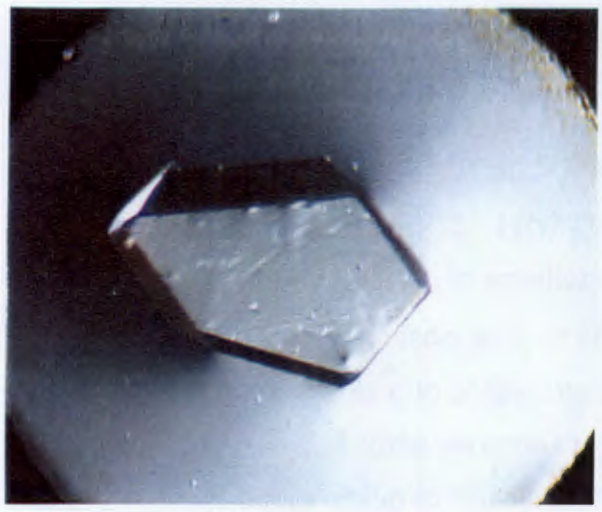

(a) room temperature

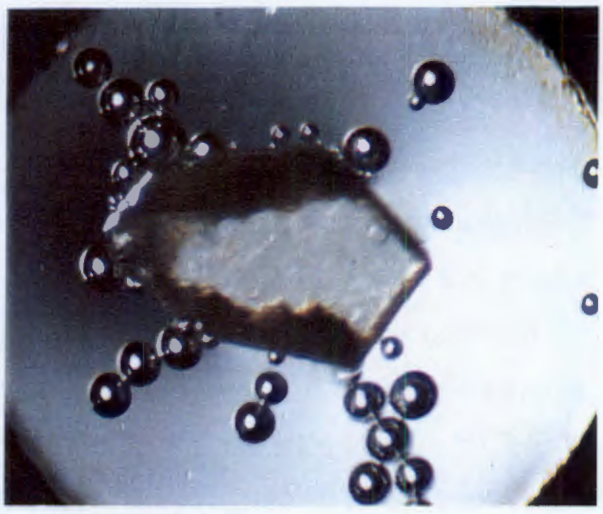

(d) 101°C

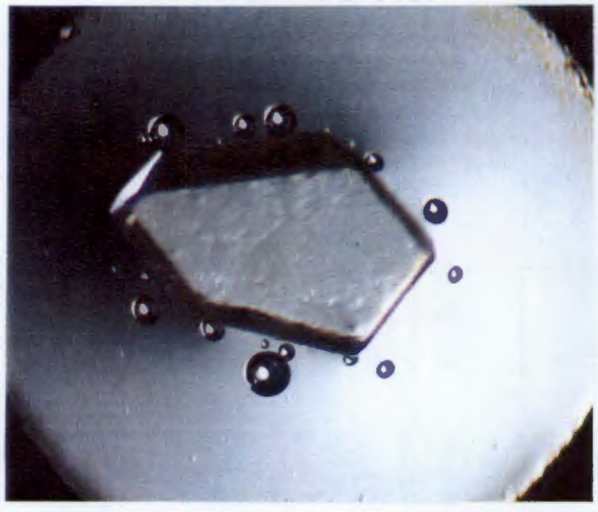

(b) 97°C

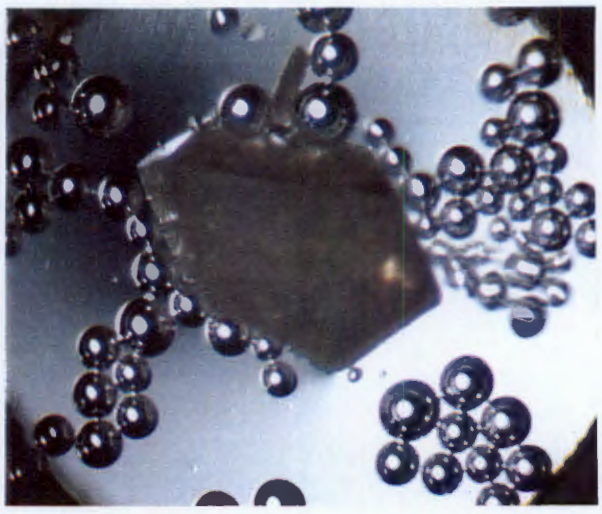

(e) 102°C

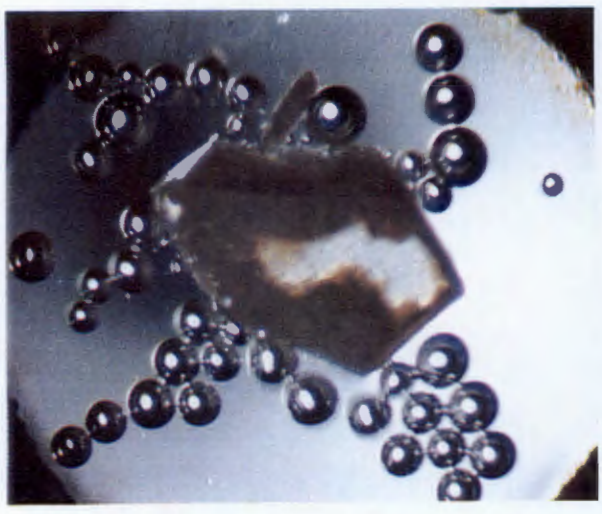

(c) 100°C

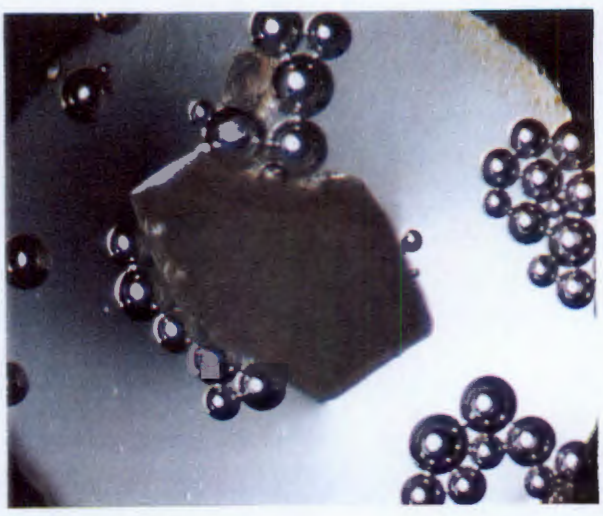

(f) 104°C

Figure 4.33 : Thermal decay of SPETH, heating rate 10°C.min^{-1} (magnification : 33X).

Kinetics of Desolvation :

An example of the α-time curves obtained for SPETH over the temperature range 55 - 75°C is shown in figure 4.34. These α-time curves have a truncated sigmoidal shape since they consist of an acceleratory and deceleratory period, but do not possess a significant induction period. The Avrami-Erofeev (A2) equation, derived to model two dimensional nucleation and growth of the product phase, fits the data over the α-range of 0.05 - 0.95. Isokinetic behaviour over the temperature range chosen is confirmed by the linearity of the semilogarithmic plot of ln *k* *vs.* 1/T (figure 4.35), and an activation energy of 190(6) kJ.mol^{-1} was obtained.

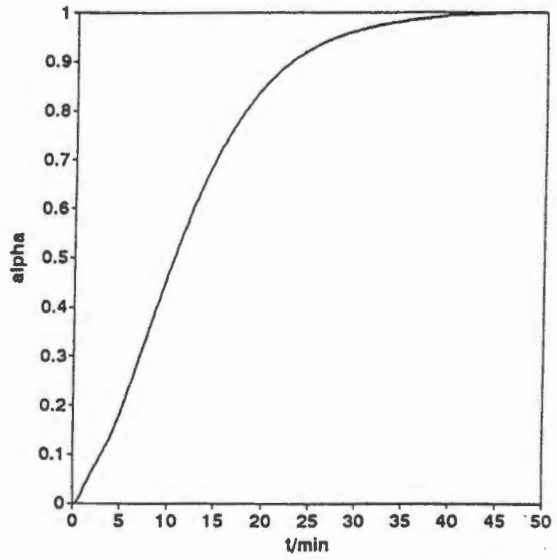

Figure 4.34 : An example of an α *vs.* time curve obtained for SPETH.

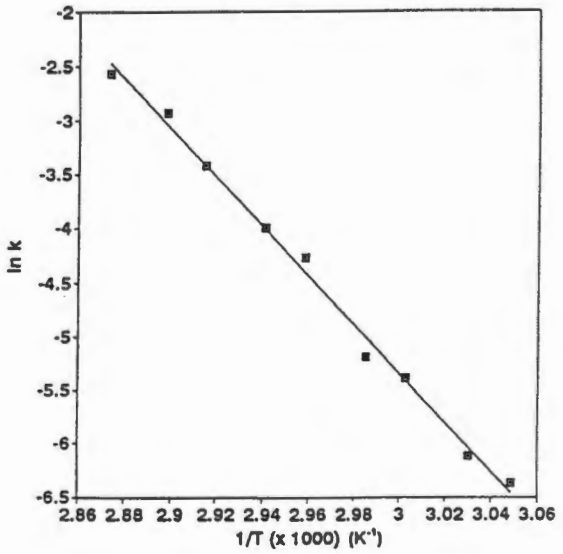

Figure 4.35 : Arrhenius plot for the desolvation of SPETH.

SP2H

$C_{96}H_{66}O_6.2C_6H_{12}O$
Guest : 2-hexanone
Space Group : P $\bar{1}$

a = 8.886(5)Å	α = 117.26(3)°
b = 16.283(9)Å	β = 91.32(4)°
c = 16.386(6)Å	γ = 82.56(5)°

Volume = 2088(2)Å^3
Z = 1

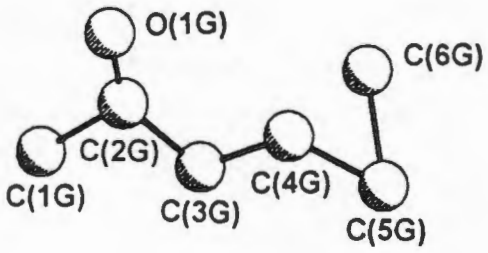

Crystal Structure :

The structure of SP2H was refined in the centrosymmetric triclinic space group, P $\bar{1}$, with the host molecule situated on a centre of inversion.

Refinement :

All the host non-hydrogen atoms and the guest oxygen atom were refined anisotropically. The guest carbon atoms were refined isotropically, because of their relatively high temperature factors. The hydroxyl hydrogens were located in the difference electron density map. H(1O) and H(2O) were refined independently with isotropic temperature factors, while H(3O) was refined with a temperature factor linked to O(3). The phenyl hydrogen atoms were placed in calculated positions, and refined with a common temperature factor (U (CH) : 0.064(4)Å^2). The guest hydrogens were omitted from the final model. A residual electron density of 0.96eÅ^{-3} is located close to the guest, but could not be incorporated into the model sensibly. The structure refined to a final R_1 = 0.1043.

Molecular Structure :

The molecular structure of SP2H is shown in figure 4.36. A co-operative hydrogen bonding scheme is seen between O(1), O(2) and O(1G). The details are given in table 4.7. O(3) does not appear to be involved in any hydrogen bonding. The crystal packing, shown in figure 4.37, is different from all the other triclinic structures, in that the central aromatic ring is parallel to the (100) planes, and not at an angle to the axes, as previously observed. The host molecules still pack in layers parallel to [100], and the guests are located in elongated cavities, situated between adjacent host molecules within each layer. These cavities are shown in projection in figure 4.38. The dimensions of these cavities were found to be approximately 6 x 14.5 x 10Å.

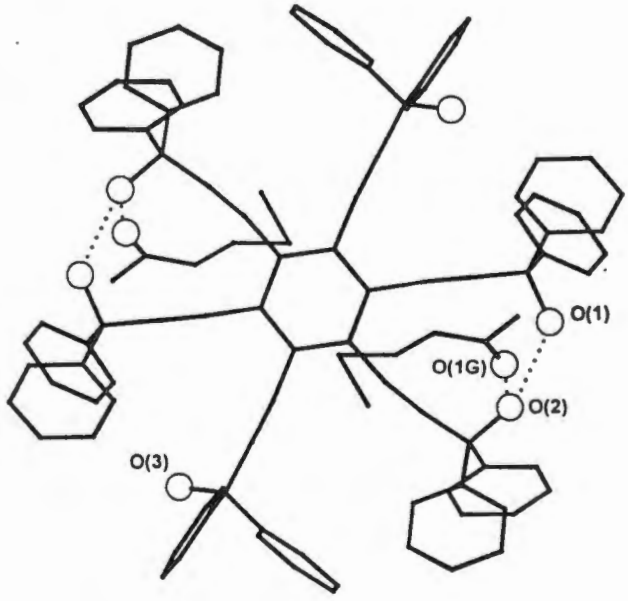

Figure 4.36 : Molecular structure of SP2H (the hydrogens are omitted and the hydrogen bonds are indicated as dotted lines).

Table 4.7 : Hydrogen bond details for SP2H.

(D)onor	(A)cceptor	D-H (Å)	D...A (Å)	D-H...A (°)
O(1)	O(2)	1.00(8)	2.893(6)	162(6)
O(2)	O(1G)	0.87(8)	2.689(8)	156(8)

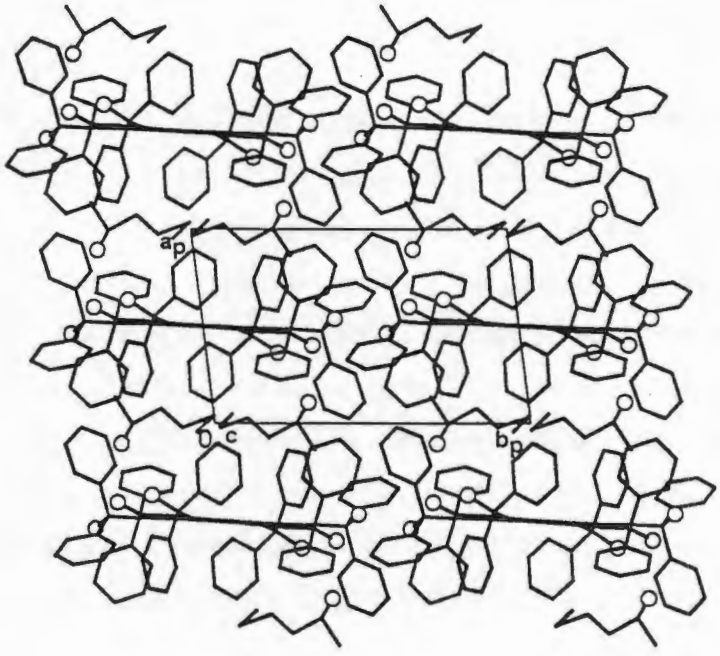

Figure 4.37 : Crystal packing in SP2H, viewed down [001].

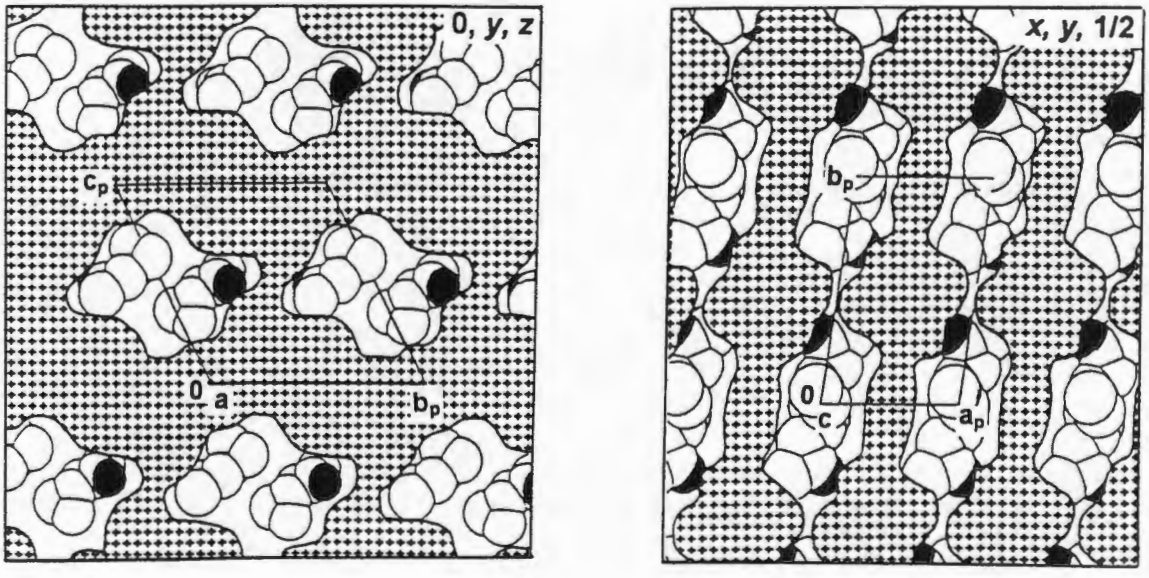

Figure 4.38 : Cross-section of the host molecules (hatched region) of SP2H viewed down a) [100] and b) [001], showing the guest molecules (with oxygen atoms shaded) in the cavities.

Thermal Analysis :

The thermograms obtained on decomposition of SP2H are shown in figure 4.39. From the TG curve, a single step guest loss is observed with a mass loss of 12.7% corresponding to a 1:2 stoichiometry (calculated mass loss : 13.2%). The DSC curve shows a broad double endotherm at *ca* 99°C, corresponding to guest loss and structural collapse of the host's β-phase to the non-porous α-phase. A sharper endotherm at 263°C corresponds to the melt of the host, which then decomposes.

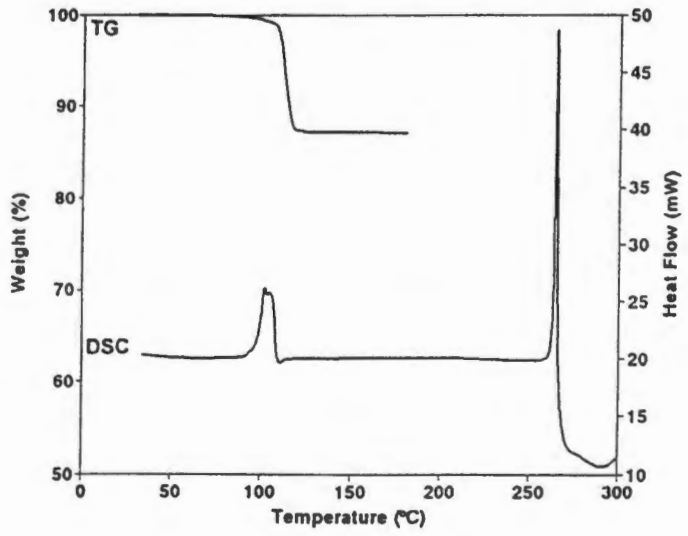

Figure 4.39 : TG and DSC traces of SP2H.

Kinetics of Desolvation :

Isothermal TG experiments were done over the temperature range 80 - 100°C, at intervals of 2 - 3°. The shape of all the α-time curves obtained are similar (figure 4.40), thus it was assumed that the system is isokinetic over this temperature range. The curves are sigmoidal in shape, consisting of an induction period, an acceleratory period and a deceleratory period. The Avrami-Erofeev (A2) equation fits the data over the α-range 0.05-0.95. An activation energy of 264(3) $kJ.mol^{-1}$ was obtained. The semilogarithmic plot of ln *k vs.* 1/T is shown in figure 4.41.

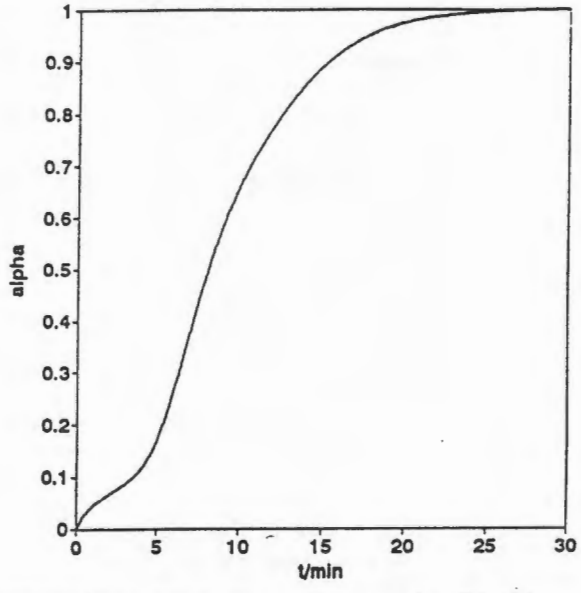

Figure 4.40 : An example of an α *vs.* time curve for SP2H.

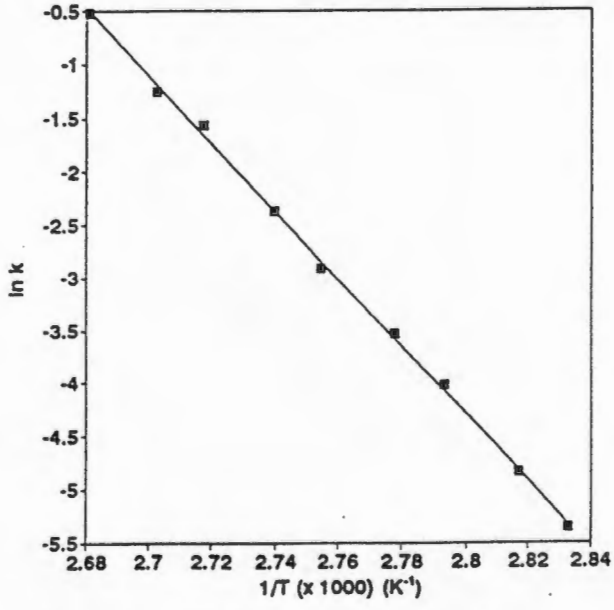

Figure 4.41 : Arrhenius plot for the desolvation of SP2H.

SPCHO

$C_{96}H_{66}O_6.5C_6H_{10}O$
Guest : cyclohexanone
Space Group : P $\bar{1}$

a = 8.957(4)Å	α = 93.82(3)°
b = 16.69(1)Å	β = 97.61(3)°
c = 17.201(4)Å	γ = 93.13(5)°

Volume = 2538(2)Å^3
Z = 1

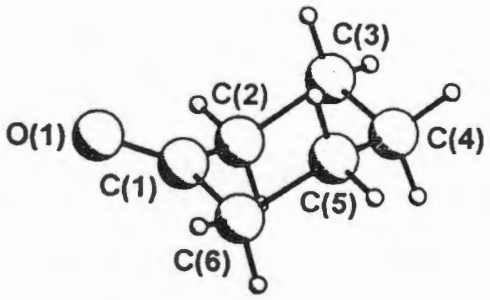

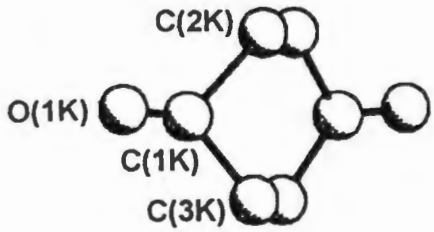

Guests labelled : G, J.

Crystal Structure :

The structure of SPCHO was refined in the space group P $\bar{1}$. The host molecules are located on a centre of inversion, as is guest K, at Wyckoff position *a*.

Refinement :

All the host non-hydrogen atoms of the host molecule and guest G were refined anisotropically. The hydroxyl hydrogens were located in the difference electron density maps and refined isotropically with a temperature factor linked to the parent oxygen. The remaining hydrogen atoms on the host and the hydrogen atoms on guest G were placed in geometrically calculated positions and allowed to refine with a common temperature factor for similar atoms (*U* (phenyl) : 0.089(4)Å^2 ; *U* (CH_2 - guest G) : 0.128(9)Å^2). The oxygen atom on guest J was refined anistropically, while the carbon atoms were refined isotropically. The carbon atoms C(2J), C(3J) and C(6J) were disordered over two positions. The disorder model of guest J is shown in figure 4.42. All the non-hydrogen atoms on guest K had high temperature

factors (> 0.18Å^2), and were refined isotropically. The oxygen atom was refined with a site occupancy factor of 0.5. There is a residual electron density of 0.91eÅ^{-3} in the middle of guest K, which could not be modelled sensibly. The hydrogen atoms on guests J and K were omitted from the final model. The structure refined to a final R_1 = 0.0892.

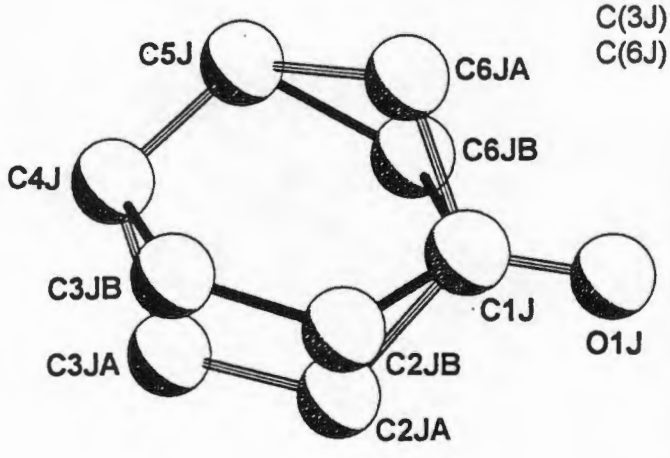

Site occupancy factors :
C(2J) : A = 0.64(3), B = 0.36(3)
C(3J) : A = 0.56(2), B = 0.44(2)
C(6J) : A = 0.52(2), B = 0.48(2)

C(1J) - C(2JA) : 1.48(2)Å
C(1J) - C(2JB) : 1.48(2)Å
C(2JA) - C(3JA) : 1.59(2)Å
C(2JB) - C(3JB) : 1.46(3)Å
C(3JA) - C(4J) : 1.47(2)Å
C(3JB) - C(4J) : 1.33(2)Å
C(5J) - C(6JA) : 1.62(2)Å
C(5J) - C(6JB) : 1.64(2)Å
C(6JA) - C(1J) : 1.48(2)Å
C(6JB) - C(1J) : 1.55(2)Å

C(4J) - C(5J) - C(6JA) : 106(1)°
C(4J) - C(5J) - C(6JB) : 114(1)°

Figure 4.42 : Disorder in guest J in SPCHO.

Molecular Structure :

The molecular structure of SPCHO is shown in figure 4.43. Guests G and J are held in position by hydrogen bonds, the details of which are given in table 4.8. Guest K does not appear to be involved in a hydrogen bonding scheme. The host molecules pack in layers parallel to [100], with the central aromatic region at an angle to the (100) plane (figure 4.44). Guest G is located within a cavity, centred at *z*=0, between the host molecules within each layer (figure 4.45). Guest K is located within a channel between the layers of host molecules, parallel to [100] and centred at *z*=0.5. Guest J is located in pockets along the channel, with the oxygen directed towards the host molecule (figure 4.45). Guest J causes an obstruction within the channel, preventing the movement of guest K along the channel.

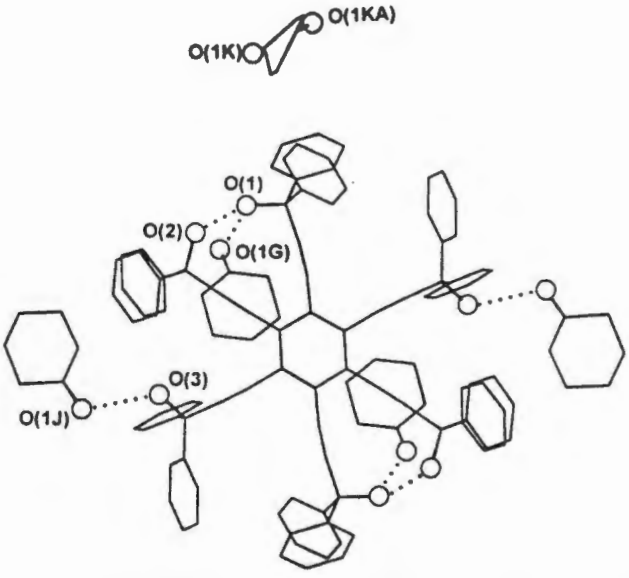

Figure 4.43 : Molecular structure of SPCHO (the hydrogen atoms are omitted and the hydrogen bonds are represented as dotted lines).

Table 4.8 : Hydrogen bond details of SPCHO.

(D)onor	(A)cceptor	D-H (Å)	D...A (Å)	D-H...A (°)
O2	O1	0.89(6)	2.862(5)	176(5)
O1	O1G	0.85(5)	2.649(5)	160(5)
O3	O1J	0.90(6)	2.821(5)	155(5)

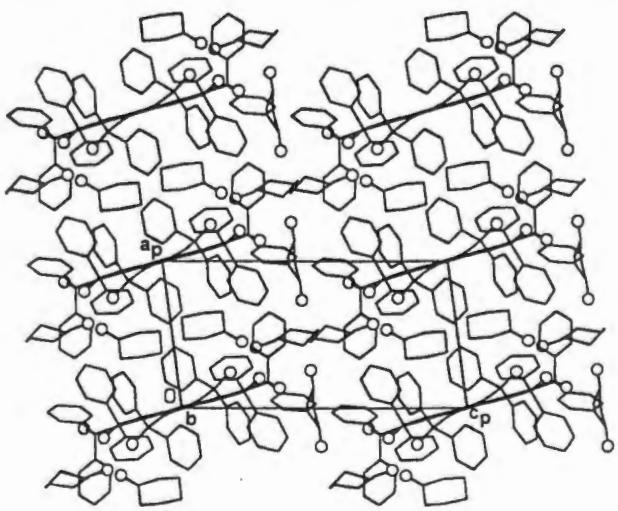

Figure 4.44a : Crystal packing in SPCHO viewed down [010].

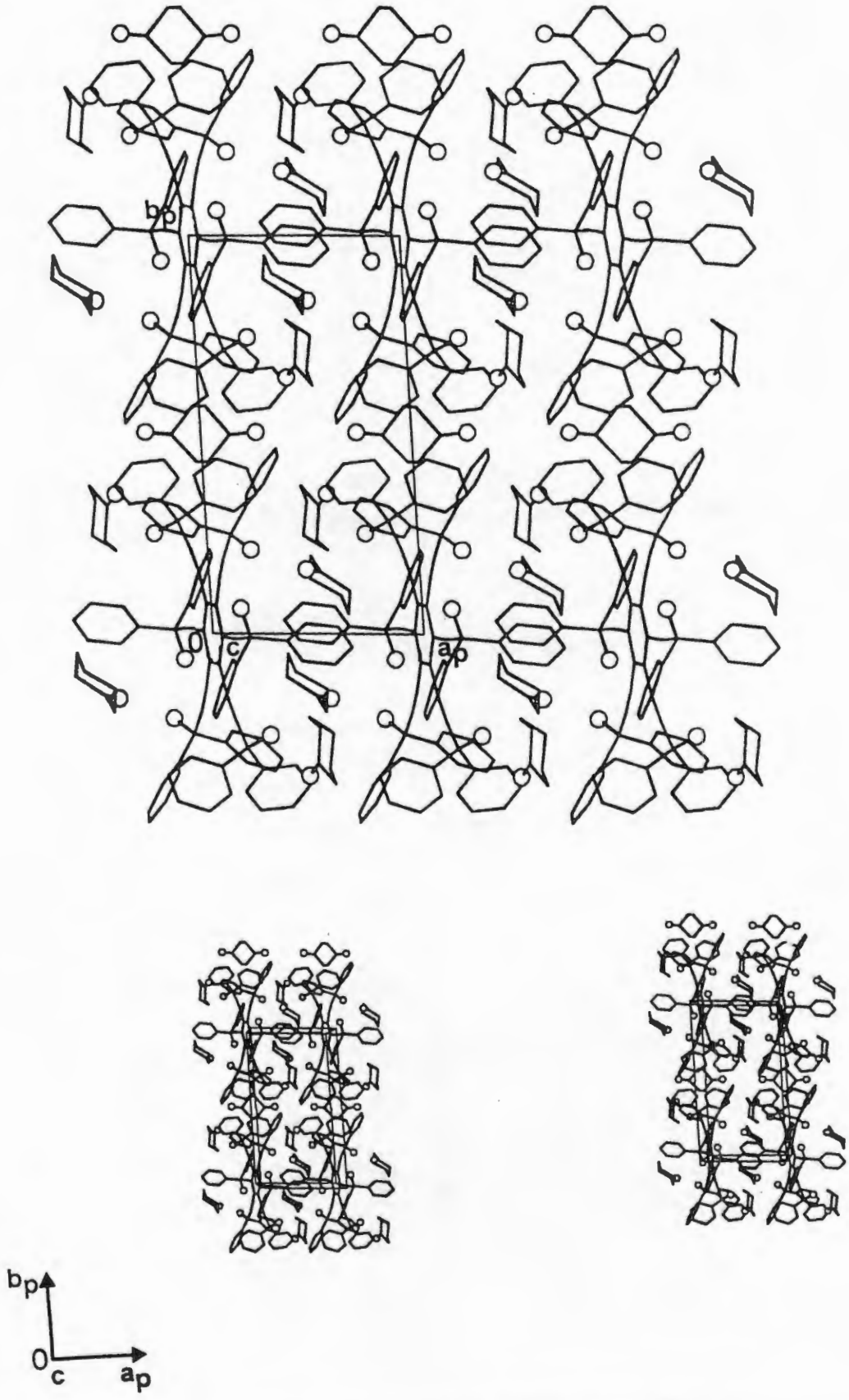

Figure 4.44b : Crystal packing in SPCHO viewed down [001].

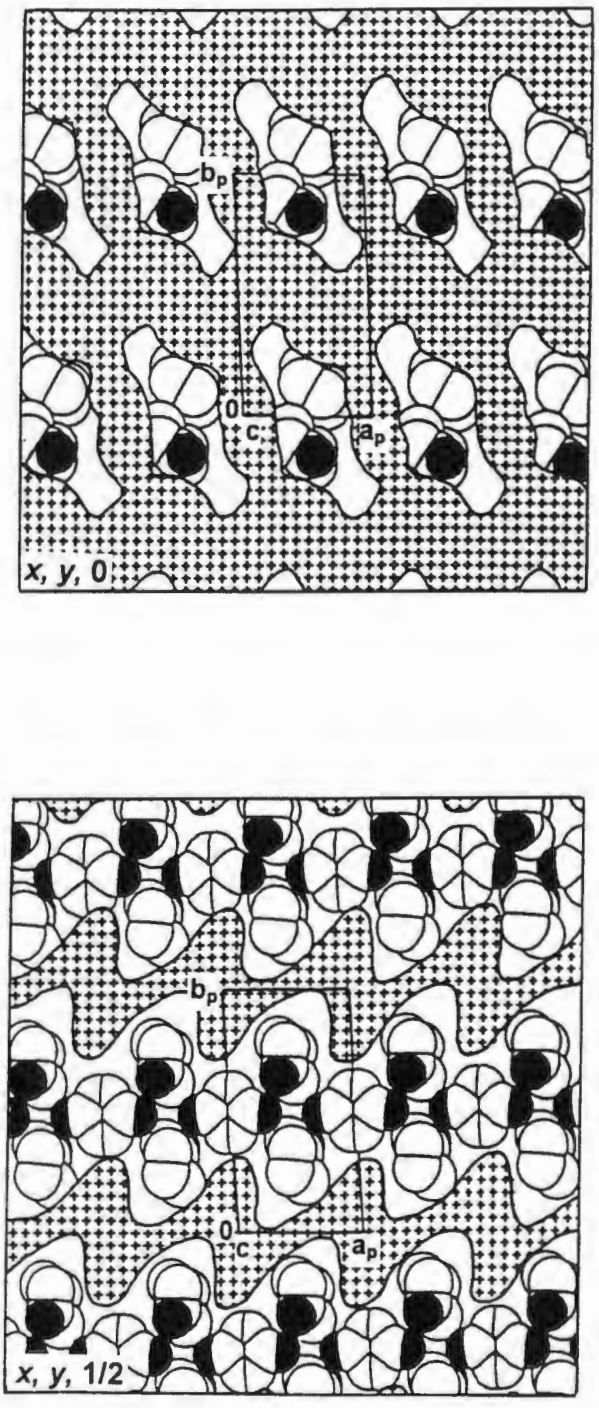

Figure 4.45 : Cross-section of SPCHO viewed along [001]. The hatched region is that occupied by the host molecules. The guest molecules (oxygens shaded) are shown in the channels, and cavities.

Thermal Analysis :

The traces obtained on TG and DSC analysis are shown in figure 4.46. The TG curve shows a two step guest loss. The 1:5 stoichiometry modelled in the crystal structure is confirmed by the overall guest loss (expected mass loss : 27.2%, observed mass loss : 26.5%). The individual guest loss steps were not stoichiometric. The DSC trace also shows two guest loss endotherms with onset temperatures at 70°C and 125°C. The second endotherm is sharper than the first, and is followed by a step, possibly due to recrystallisation of the host to the non-porous α-phase on desolvation. The host then melts with decomposition at 263°C. Figure 4.47 shows the thermal decay of a SPCHO crystal, immersed in a drop of silicon oil and heated at $10°.min^{-1}$. The crystal starts to decay at 66°C, slowly at first and then more rapidly as the temperature of guest release is approached. At 106°C, the beginnings of host recrystallisation are observed. At 179°C there is a sudden loss of the guest with partial recrystallisation of the desolvated crystal. The host melts with decomposition at 272°C.

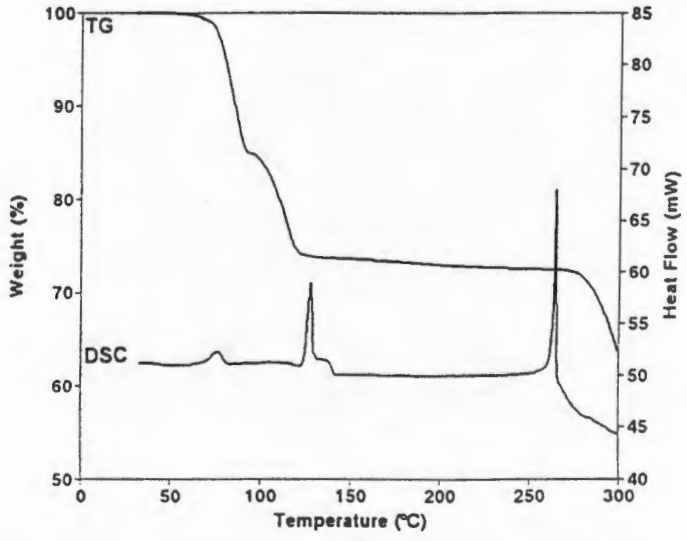

Figure 4.46 : TG and DSC trace of SPCHO.

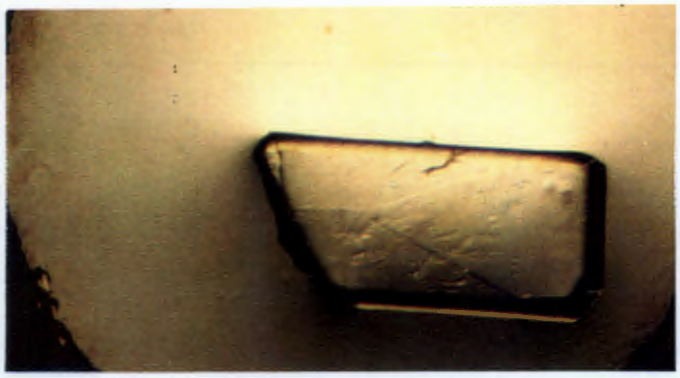

(a) room temperature

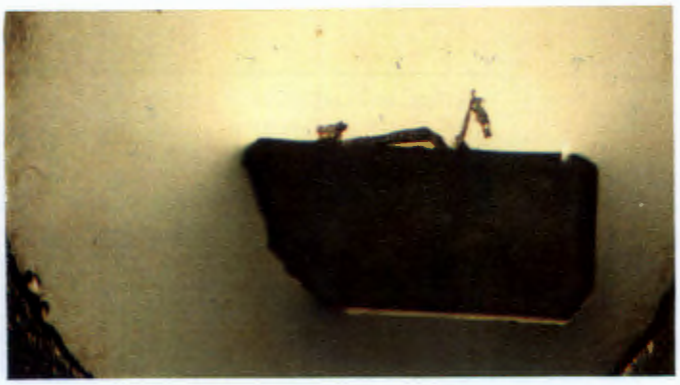

(d) 141°C

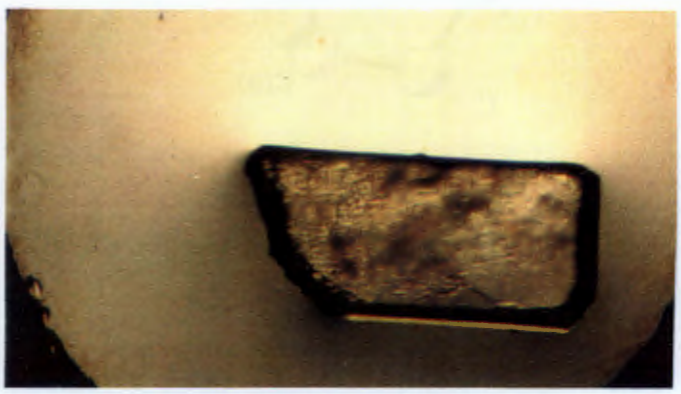

(b) 72°C

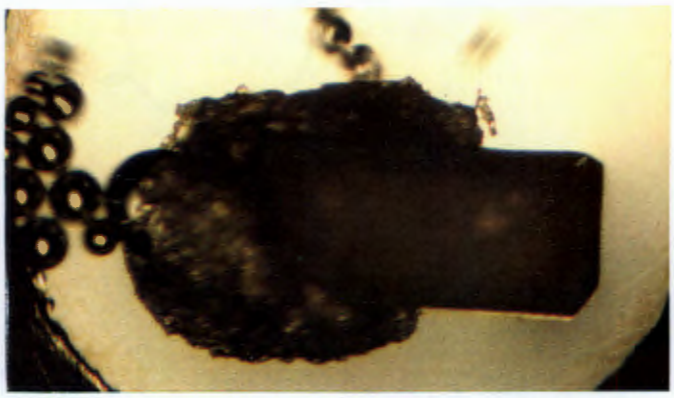

(e) 179°C

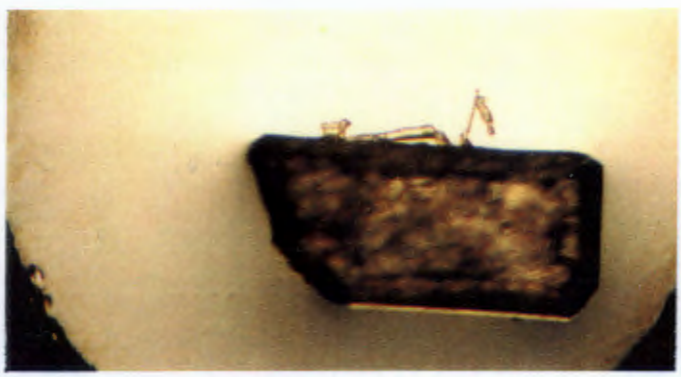

(c) 112°C

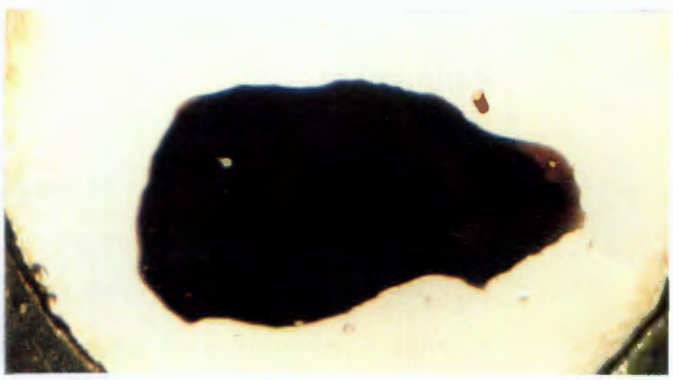

(f) 272°C

Figure 4.47 : Thermal decay of SPCHO (magnification : 36X).

SPDIOX

$C_{96}H_{66}O_6.5C_4H_8O_2$
Guest : 1,4-dioxane
Space Group : P $\bar{1}$
a = 12.203(2) Å α = 110.83(1)°
b = 14.384(3) Å β = 104.82(1)°
c = 15.827(3)Å γ = 100.68(1)°
Volume = 2389.7(8)Å^3
Z = 1

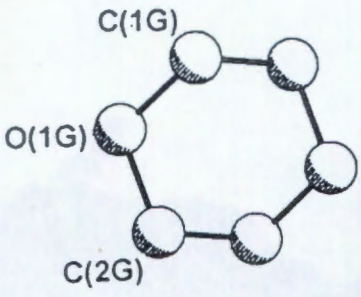

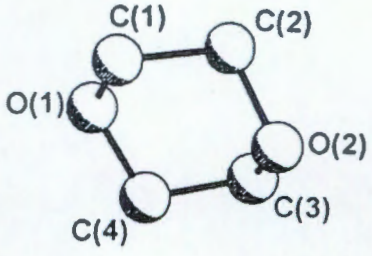

Guests labelled : J,K.

Crystal Structure :

The structure of SPDIOX was refined in the centrosymmetric triclinic space group, P $\bar{1}$, and like all the previous triclinic structures, the host molecule is located on a centre of inversion. One of the guest molecules (G) is located on a centre of inversion at Wyckoff position *b*.

Refinement :

All the non-hydrogen atoms of the host molecule were refined anisotropically. The aromatic hydrogens were placed in geometrically calculated positions and linked to a common temperature factor, which refined to 0.078(3)Å^2. The hydroxyl hydrogens were located in the difference electron density maps and allowed to refine isotropically. The non-hydrogen atoms of guest G and oxygen atoms of guest J were refined with anisotropic temperature factors. The carbons of guest J were found to be disordered over two positions, with site occupancy factors of A: 0.48(2), B: 0.52(2), as shown in figure 4.48.

They were refined isotropically. Both the carbon and oxygen atoms of guest K had high temperature factors and as a result were refined isotropically. All the guest hydrogens were omitted from the final model. The residual electron density of $0.62eÅ^{-3}$ in the region of guest K was ascribed to an imperfect model, and the structure refined to a final R_1= 0.0762.

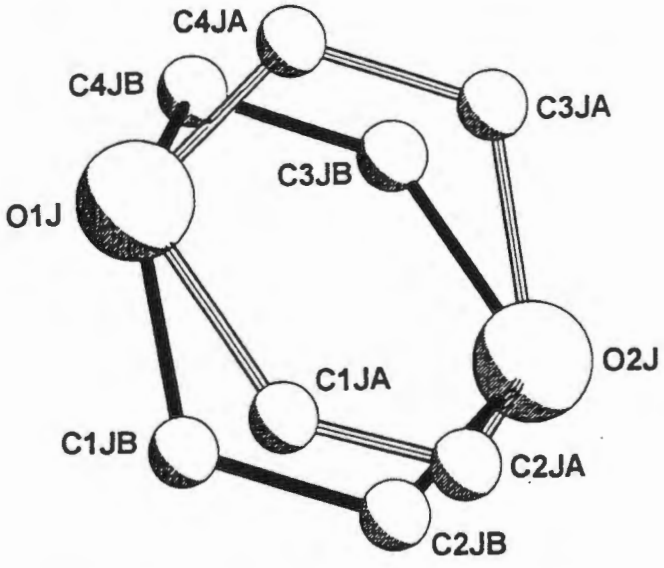

O(1J) - C(1JA) : 1.59(2)Å
O(1J) - C(1JB) : 1.44(1)Å
O(1J) - C(4JA) : 1.50(2)Å
O(1J) - C(4JB) : 1.41(1)Å
O(2J) - C(2JA) : 1.51(1)Å
O(2J) - C(2JB) : 1.38(2)Å
O(2J) - C(3JA) : 1.47(1)Å
O(2J) - C(3JB) : 1.44(2)Å

Figure 4.48 : Disorder in guest J of SPDIOX.

Molecular Structure :

The molecular structure of SPDIOX is shown in figure 4.49. The host molecules pack in layers parallel to [100] (figure 4.50). Phenyl rings interlink adjacent layers, forming a hydrophobic region between the layers. The guests are situated in constricted channels between the host molecules, centred at z=0.5 and parallel to [110]. They can be seen in projection in figure 4.51. Within the channels, the guests are located between adjacent host molecules in each layer. The hydrogen bonding scheme for SPDIOX is different to that observed in the previous structures of host **1** inclusion compounds, in that although guest J is held in position by co-operative hydrogen bonding, guest G is hydrogen bonded so as to link adjacent host molecules, and guest K shows no short contacts. The hydrogen bonding details are shown in table 4.9.

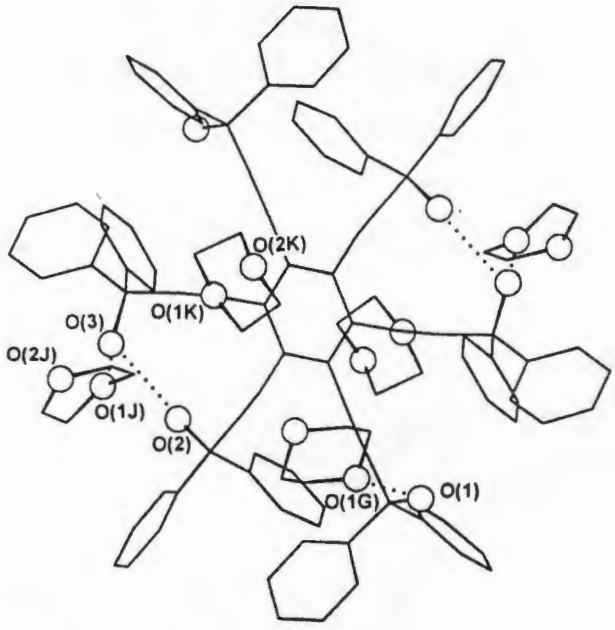

Figure 4.49 : Molecular structure of SPDIOX (hydrogens are omitted and the hydrogen bonds are represented as dotted lines).

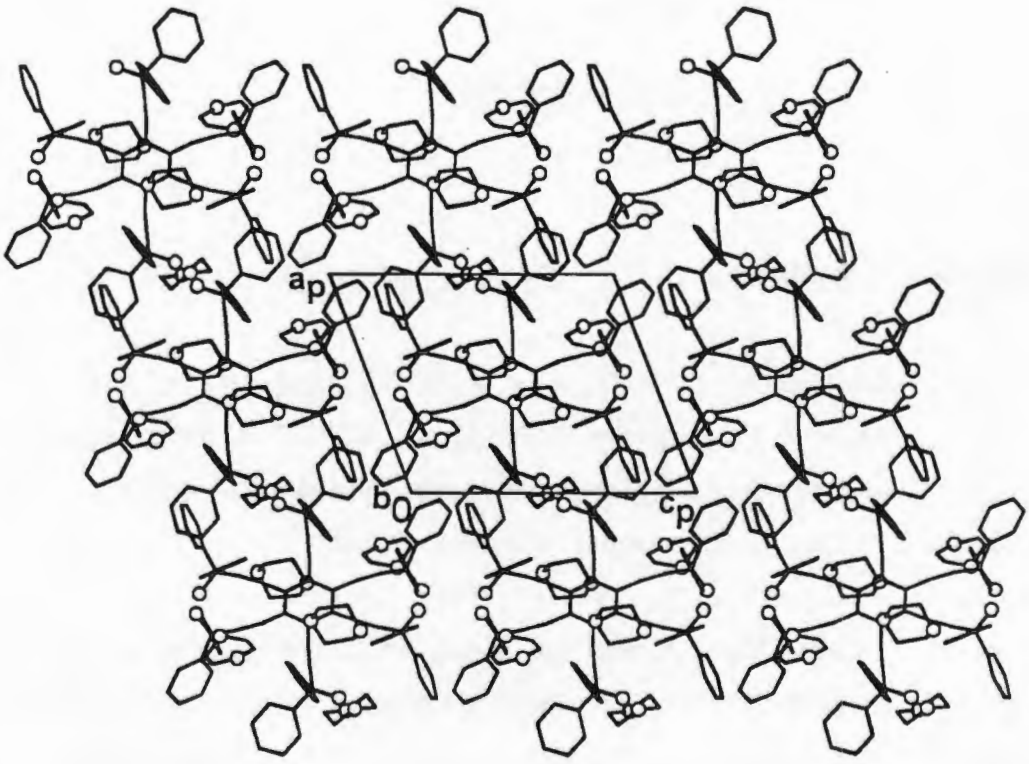

Figure 4.50a : Crystal packing in SPDIOX viewed down [010].

Table 4.9 : Hydrogen bonding details of SPDIOX.

(D)onor	(A)cceptor	D-H (Å)	D...A (Å)	D-H...A (°)
O(1)	O(1G)	0.74(5)	2.809(5)	172(5)
O(2)	O(3)	0.87(5)	2.958(4)	158(4)
O(3)	O(1J)	0.83(6)	2.759(5)	171(6)

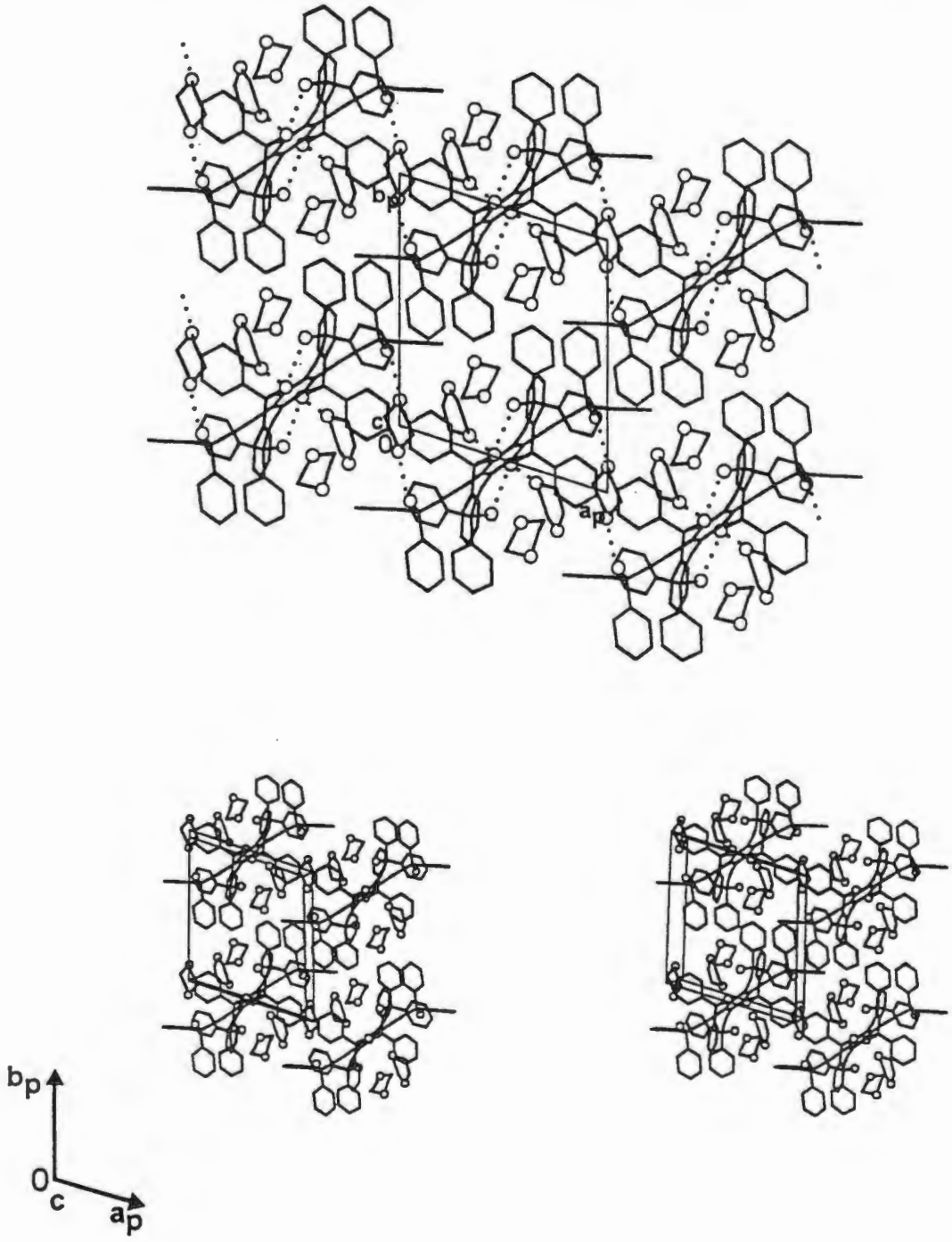

Figure 4.50b : Crystal packing in SPDIOX viewed down [001]. The hydrogen bonds are indicated by dotted lines.

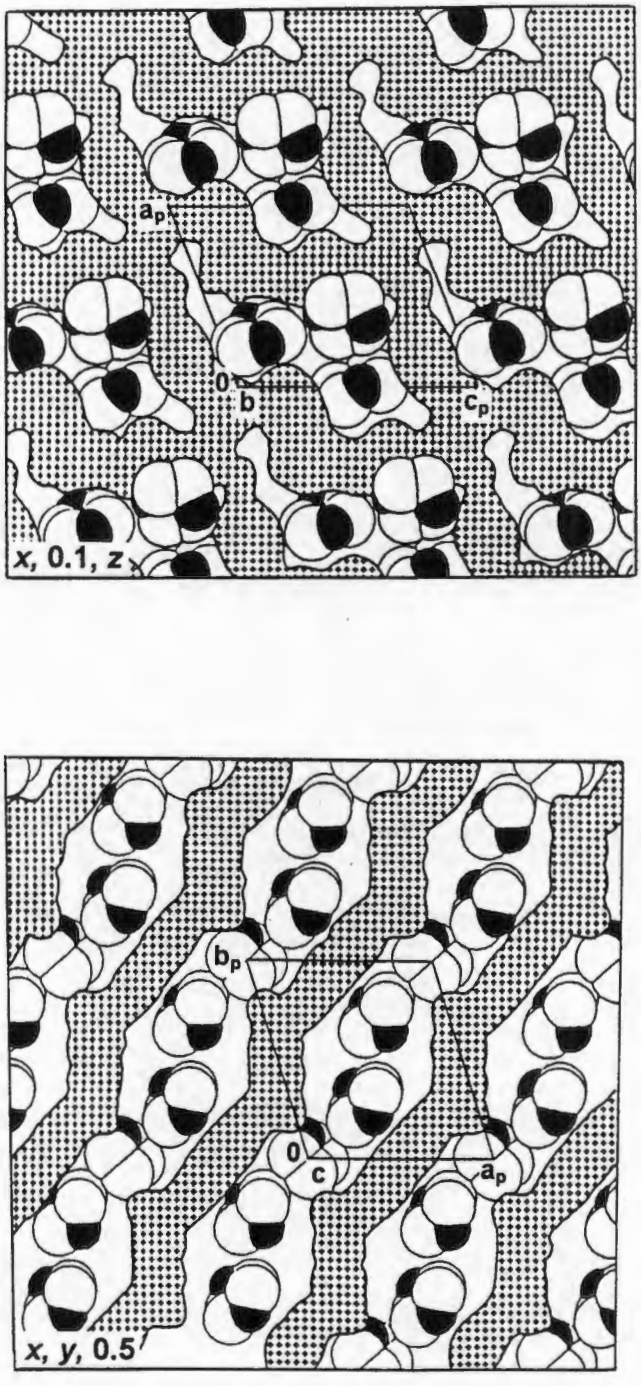

Figure 4.51 : Cross-section of SPDIOX viewed along a) [010] and b) [001]. The hatched region is that occupied by the host molecules. The guest molecules (oxygens shaded) are shown in the channels.

Thermal Analysis :

The thermograms of SPDIOX are shown in figure 4.52. The DSC curve shows a single step guest loss at *ca* 100°C, followed by an exothermic rearrangement of the host at *ca* 115°C. The host then melts with decomposition at 259°C. The TG curve confirms the single step guest loss and the host to guest ratio of 1:5 refined in the crystal structure (expected mass loss : 25.1%, observed mass loss: 24.3%).

The guests G, J and K are all located within the same channel, but each of them are held in position by different forces. On desolvation these positional forces are broken, and the guest molecules escape along the channel, resulting in a single step guest loss. This is followed by the structural collapse of the β-phase to the non-porous α-phase.

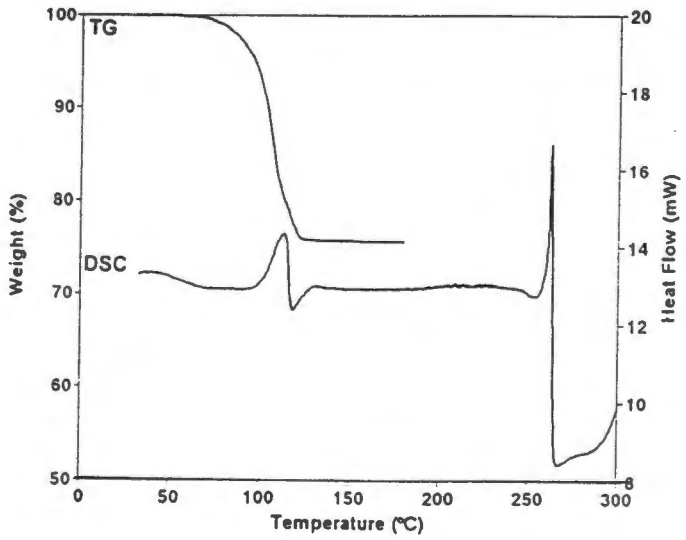

Figure 4.52 : TG and DSC traces of SPDIOX.

Kinetics of Desolvation :

The kinetics of desolvation and structural collapse to the non-porous α-phase of the host was determined by a series of isothermal TG experiments over the temperature range 56 - 75°C. Guest loss was found to take place in a single deceleratory step (figure 4.53), and the first order (F1) reaction mechanism (-ln(1-α)) fits the data (α-range 0.05 - 0.95). The semilogarithmic plot of ln *k* *vs.* 1/T, shown in figure 4.54, yields an activation energy of 148(2) kJ.mol^{-1}.

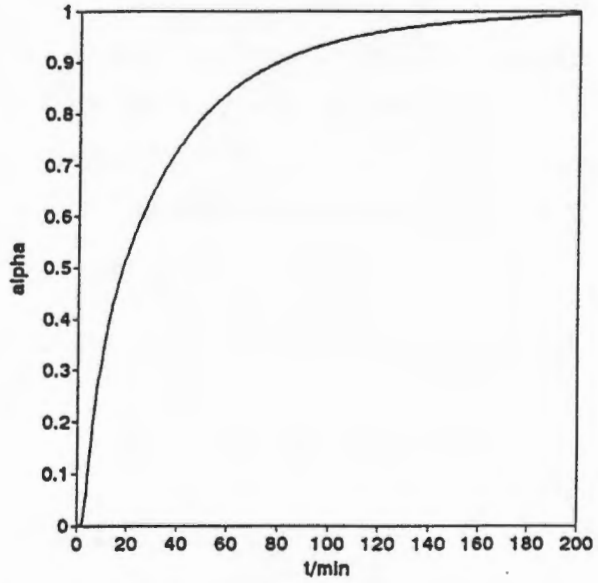

Figure 4.53 : An example of an α *vs.* time curve obtained for SPDIOX.

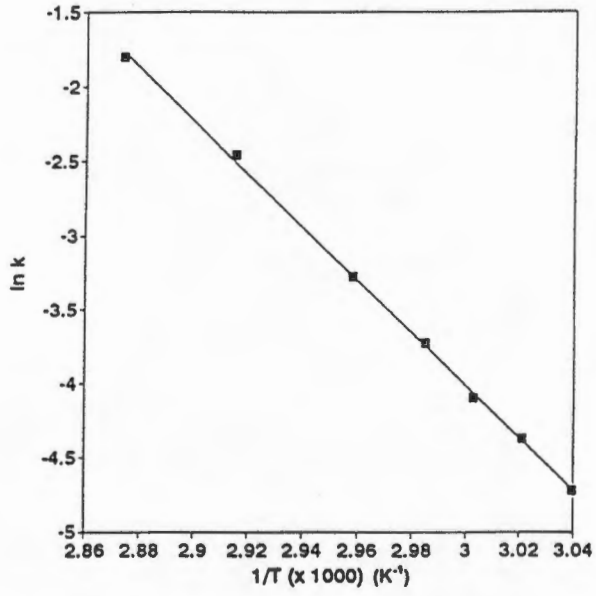

Figure 4.54 : Arrhenius plot for the desolvation of SPDIOX.

SPDIOXO

$C_{96}H_{66}O_6.2C_3H_4O_3$
Guest : 1,3-dioxolan-2-one
Space Group : $P2_1/n$

a = 18.095(5)Å	α = 90°
b = 12.563(4)Å	β = 97.14(3)°
c = 34.18(1)Å	γ = 90°

Volume = 7709(4) $Å^3$
Z = 4

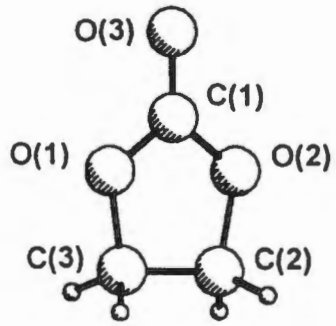

Guests labelled : G, J.

Crystals of SPDIOXO were grown from a solution of host **1** in 1,3-dioxolane. Direct methods located the host and two guest molecules. However, the guests proved not to be 1,3-dioxolane as expected, but 1,3-dioxolan-2-one. These two compounds are shown in figure 4.55. Several analytical techniques were performed on the crystals to confirm the identity of the guest compound. Both ^1H and ^{13}C-NMR spectroscopy established that 1,3-dioxolane was not present as the guest. 1,3-Dioxolane is a puckered molecule, and as a result none of the hydrogens are equivalent. If the guest had been 1,3-dioxolane very complicated coupling should have been visible in the ^1H NMR spectrum. The hydrogens on 1,3-dioxolan-2-one are, however, equivalent since the molecule is far more rigid and planar. The measured ^1H NMR spectrum showed only one singlet for the guest compound (δ = 3.28), suggesting that it is 1,3-dioxolan-2-one. In the ^{13}C-NMR spectrum only one guest peak was observed. If the guest had been 1,3-dioxolane two peaks should have been observed for C(a) and C(b). However, if C(a) were a carbonyl carbon, as in 1,3-dioxolan-2-one, the peak would have been shifted far down field, and difficult to detect. Mass spectroscopy confirmed the guest compound's identity. The mass spectrum was recorded at 70eV, 50°C. This

temperature was chosen so that the guest was volatised before the host compound. The M^+ peak and route of decomposition corresponds to 1,3-dioxolan-2-one : m/z 88 (M^+, 100), 43 (M-COOH, 68), 29 (M-CH_2COOH, 62).

Gas chromatography was performed to analyse a sample of the 1,3-dioxolane that had been used to grow these crystals. Two peaks were observed. The first which was for the 1,3-dioxolane (b.p. = 78°C), was followed by a much smaller second peak (*ca* 2%). 1,3-dioxolan-2-one (b.p.= 152°C) is not commercially available, so its retention time under these conditions could not be determined. Nevertheless, it was concluded that it was this small impurity found in the 1,3-dioxolane solvent that was selectively included by the host.

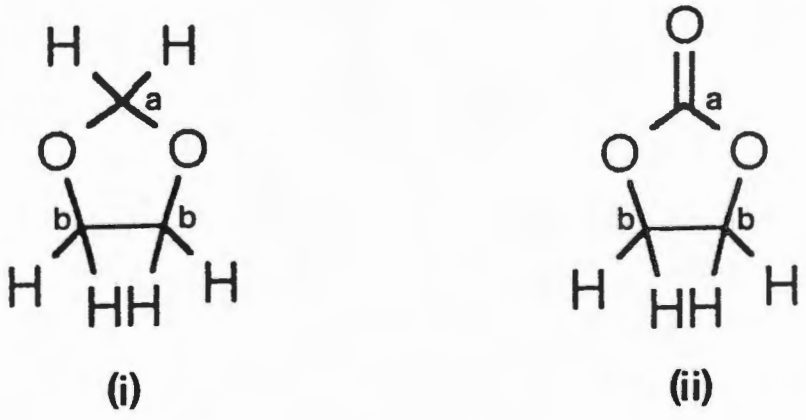

Figure 4.55 : (i) 1,3-dioxolane, (ii) 1,3-dioxolan-2-one.

Crystal Structure :

The crystal structure of SPDIOXO was refined in the monoclinic space group, $P2_1/n$. As in SPMEK, the host molecules are not situated on a centre of inversion. One host molecule and two guest molecules are located in the asymmetric unit.

Refinement :

All the non-hydrogen atoms were allowed to refine anisotropically. The hydroxyl hydrogens were located in the difference electron density map, and allowed to refine independently, except for H(1O), which was placed in a

geometrically calculated position and refined with an isotropic temperature factor linked to O(1). The aromatic and guest hydrogens were placed in geometrically calculated positions. *U* values refined to :

CH : 0.065(2)Å^2 CH_2 (guest G) : 0.081(9)Å^2 CH_2 (guest J) : 0.080(9)Å^2

An extinction coefficient of 0.0009(3) was applied, and the structure refined successfully to a final R_1 = 0.0661.

Molecular Structure :

The molecular structure and hydrogen bonding scheme observed are shown in figure 4.56. The guests are held in position by hydrogen bonds from two of the host hydroxyl moieties. There is also a short contact between O(2) and an adjacent phenyl ring (C(5)-C(10)) and O(5) and an adjacent phenyl ring (C(59)-C(64)) within the same host molecule. Details of the hydrogen bonds are given in table 4.10. The host molecules are packed in a herringbone pattern (figure 4.57), with the guests situated in cavities between them (figure 4.58). An examination of the volume of these cavities showed that they are approximately (6 x 6 x 12)Å^3.

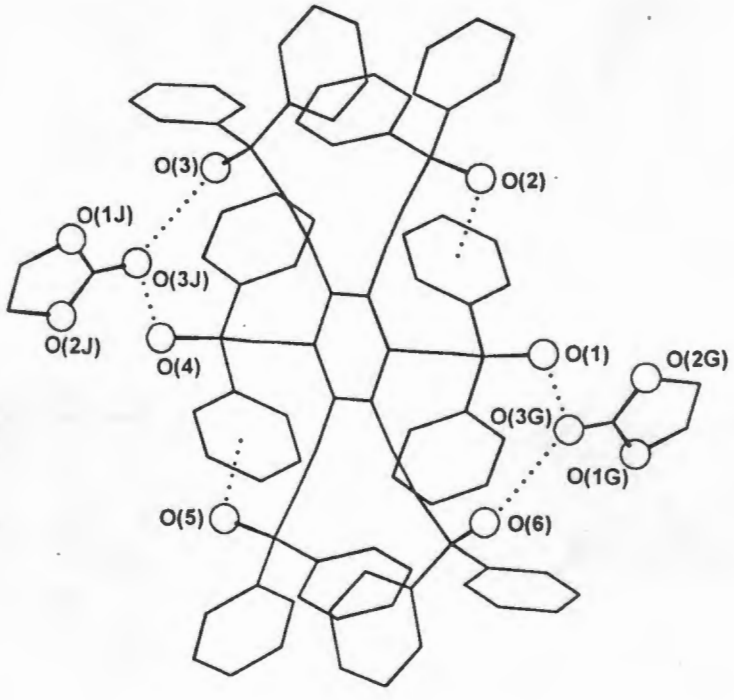

Figure 4.56 : Hydrogen bonding scheme of SPDIOXO (hydrogens are omitted and the hydrogen bonds are represented as dotted lines).

Table 4.10 : Hydrogen bond details of SPDIOXO.

(D)onor	(A)cceptor	D-H (Å)	D...A (Å)	D-H...A (°)
O(1)	O(3G)	0.83	2.873(5)	172(5)
O(6)	O(3G)	0.92(7)	3.053(6)	173(6)
O(3)	O(3J)	0.88(5)	2.995(6)	174(5)
O(4)	O(3J)	0.99(6)	2.881(5)	156(5)
O(2)	centroid (C5-C10)	0.84(6)	3.55(1)	143(13)
O(5)	centroid (C59 -C64)	0.87(6)	3.50(1)	164(17)

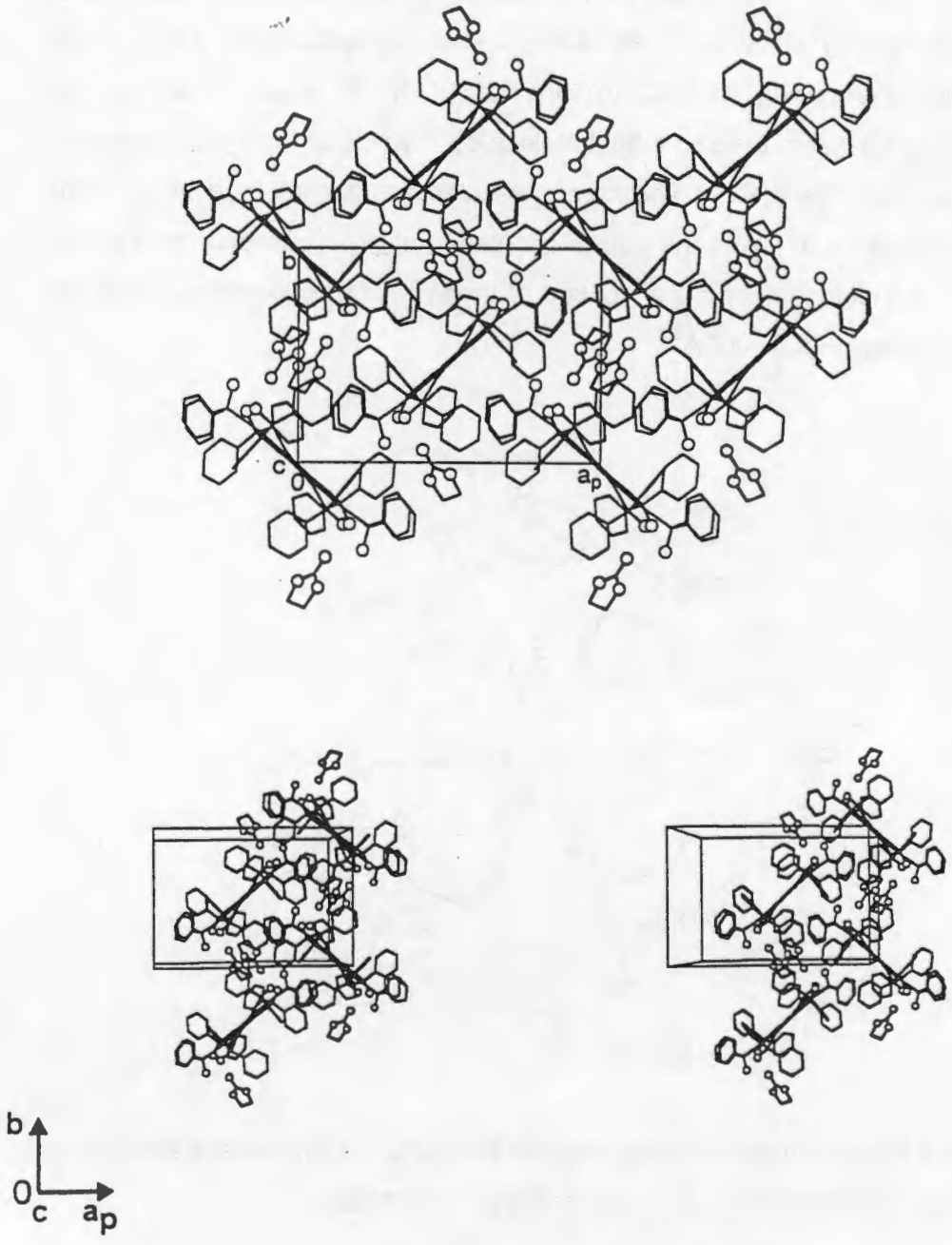

Figure 4.57 : Crystal packing in SPDIOXO viewed down [001].

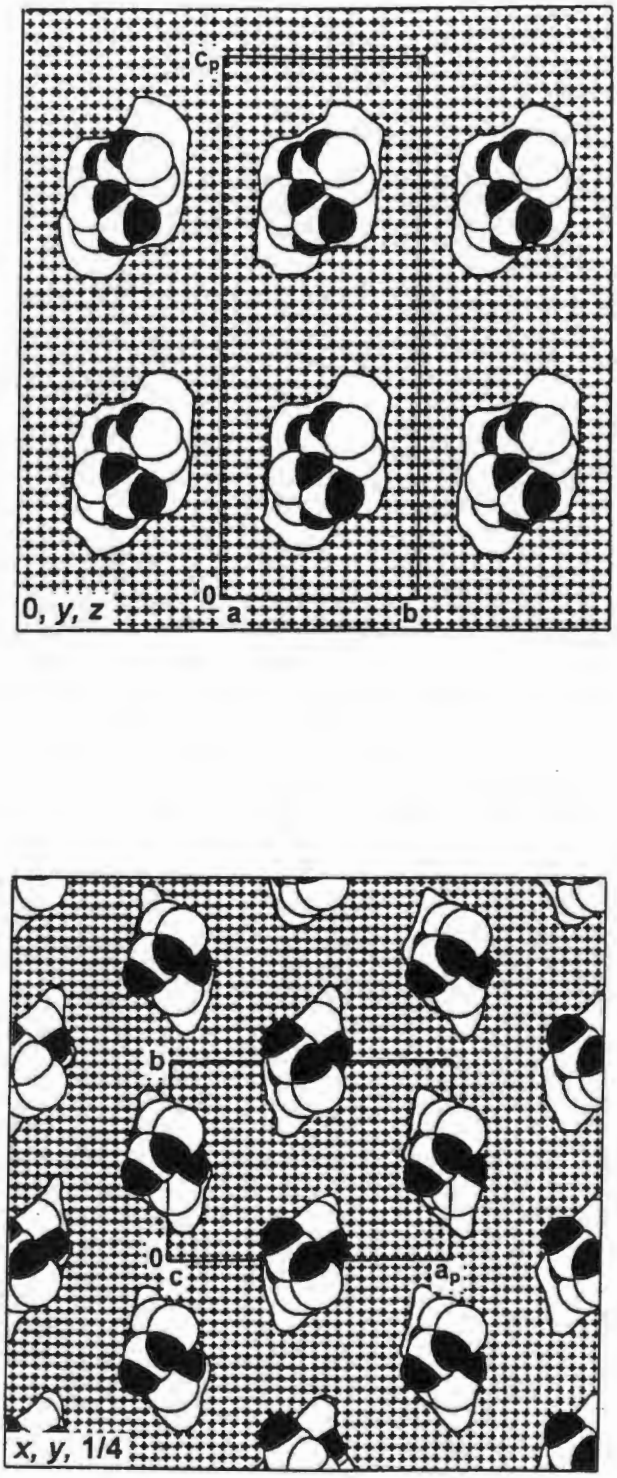

Figure 4.58 : Cross section of the host molecules (hatched area) of SPDIOXO viewed along a) [100], and b) [001]. The guest molecules (with the oxygens shaded) are located in cavities.

Thermal Analysis :

The TG curve shows a single step guest loss and confirms the 1:2 stoichiometry modelled in the crystal structure (calculated mass loss : 11.8%, observed mass loss : 11.8%). The DSC curve shows a broad endotherm at *ca* 150°C corresponding to guest loss, followed by a sharper endotherm at 240°C due to the host melting. The host then immediately decomposes exothermically. The TG and DSC traces can be seen in figure 4.59.

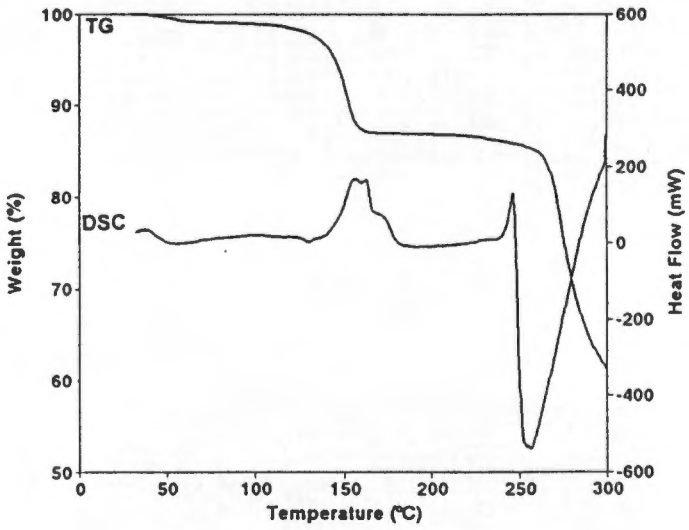

Figure 4.59 : TG and DSC traces of SPDIOXO.

SPDICHO

$C_{96}H_{66}O_6.2C_6H_{10}O$
Guest : cyclohexanone
Space Group : P $\bar{1}$

a = 9.512(2)Å	α = 114.89(2)°
b = 15.327(3)Å	β = 95.19(2)°
c = 16.151(3)Å	γ = 102.67(2)°

Volume = 2039.0(7)Å^3
Z = 1

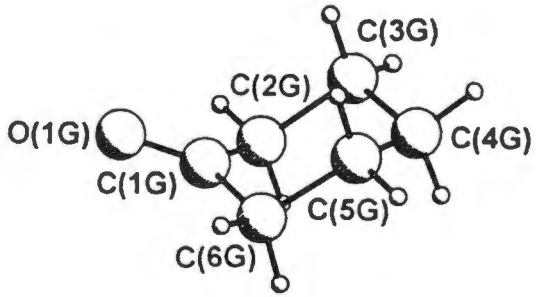

The result obtained from SPDIOXO suggests that host **1** has a higher selectivity for molecules with a carbonyl oxygen over those with an ether oxygen. In order to confirm this selectivity of host **1**, a crystallisation experiment of the host in a 50:50 molar ratio solution of cyclohexanone and 1,4-dioxane was set-up. Crystals of SPDICHO were obtained. On NMR analysis, both the ^{1}H- and ^{13}C-spectra confirmed that host **1** had selectively included cyclohexanone. This cyclohexanone inclusion compound obtained from the mixed solvent crystallisation is different to the cyclohexanone inclusion compound obtained on crystallisation of host **1** from cyclohexanone alone (SPCHO).

Crystal Structure :

The structure of SPDICHO was refined in the centrosymmetric space group P $\bar{1}$.

Refinement :

All the non-hydrogen atoms were refined anisotropically. The host hydroxyl hydrogens were located in the difference electron density maps and allowed to refine independently. All the remaining hydrogen atoms were placed in geometrically calculated positions and refined with a common isotropic temperature factor for similar groups. The final *U* values for the geometrically placed hydrogens were : CH : 0.063(2)Å^2 CH_2 : 0.103(4)Å^2
The structure refined successfully to R_1 = 0.0454.

Molecular Structure :

The molecular structure of SPDICHO is shown in figure 4.60. O(2), O(1) and O(1G) are involved in a co-operative hydrogen bond. The details are tabulated in table 4.11. There is a distance of 3.75(2)Å (150(26)°) between O(3) and the centroid of C(21)-C(26). The host molecules pack in layers parallel to [100], with the central aromatic ring parallel to [110], figure 4.61. The guests are located in interconnected cavities situated between adjacent host molecules within each layer (figure 4.62). An examination of the volume occupied by the guests showed that these cavities are approximately (6 x 11 x 10)Å^3.

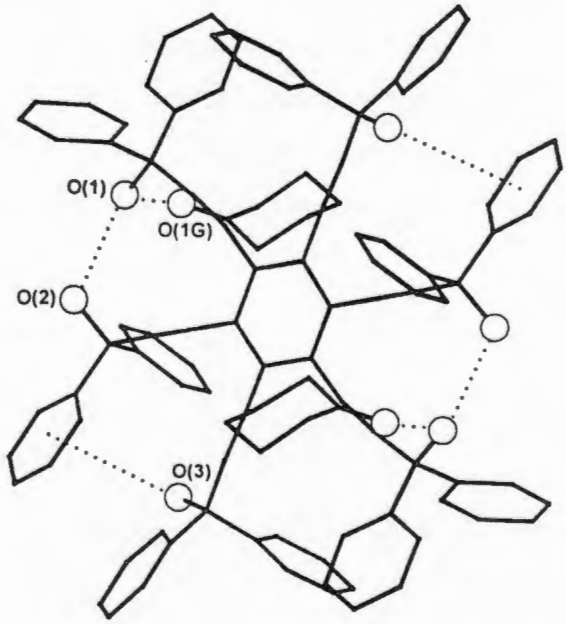

Figure 4.60 : Molecular structure of SPDICHO (hydrogens are omitted and hydrogen bonds are represented as dotted lines).

Table 4.11 : Hydrogen bond data for SPDICHO.

(D)onor	(A)cceptor	D-H (Å)	D...A (Å)	D-H...A (°)
O(2)	O(1)	0.86(3)	2.878(3)	175(2)
O(1)	O(1G)	0.97(3)	2.718(3)	177(3)

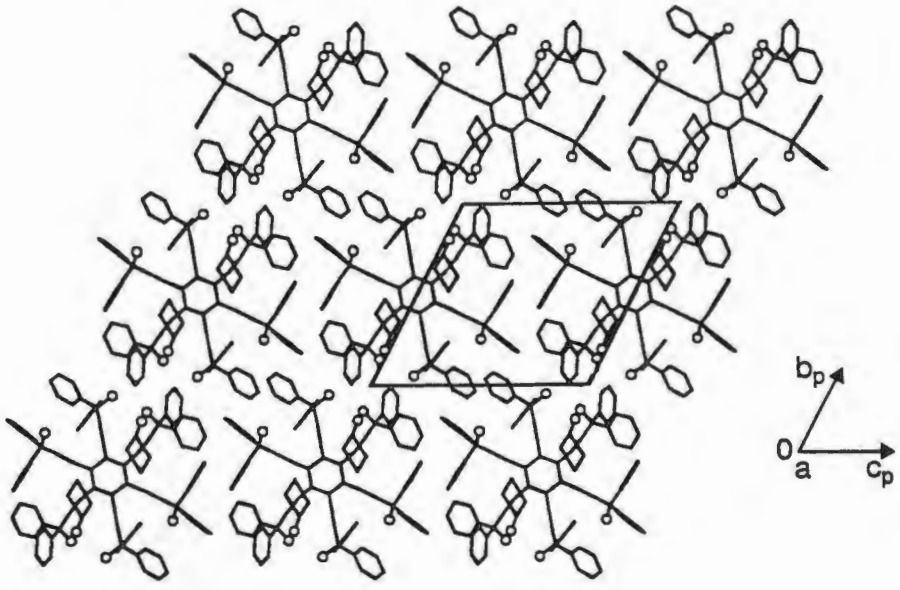

Figure 4.61a : Crystal packing in SPDICHO viewed along [100].

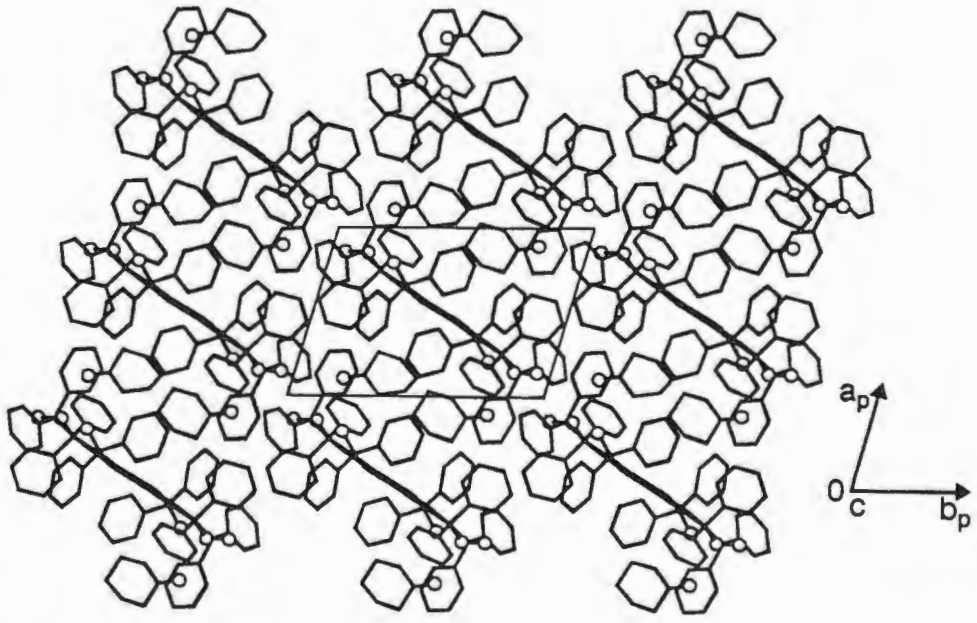

Figure 4.61b : Crystal packing in SPDICHO viewed along [001].

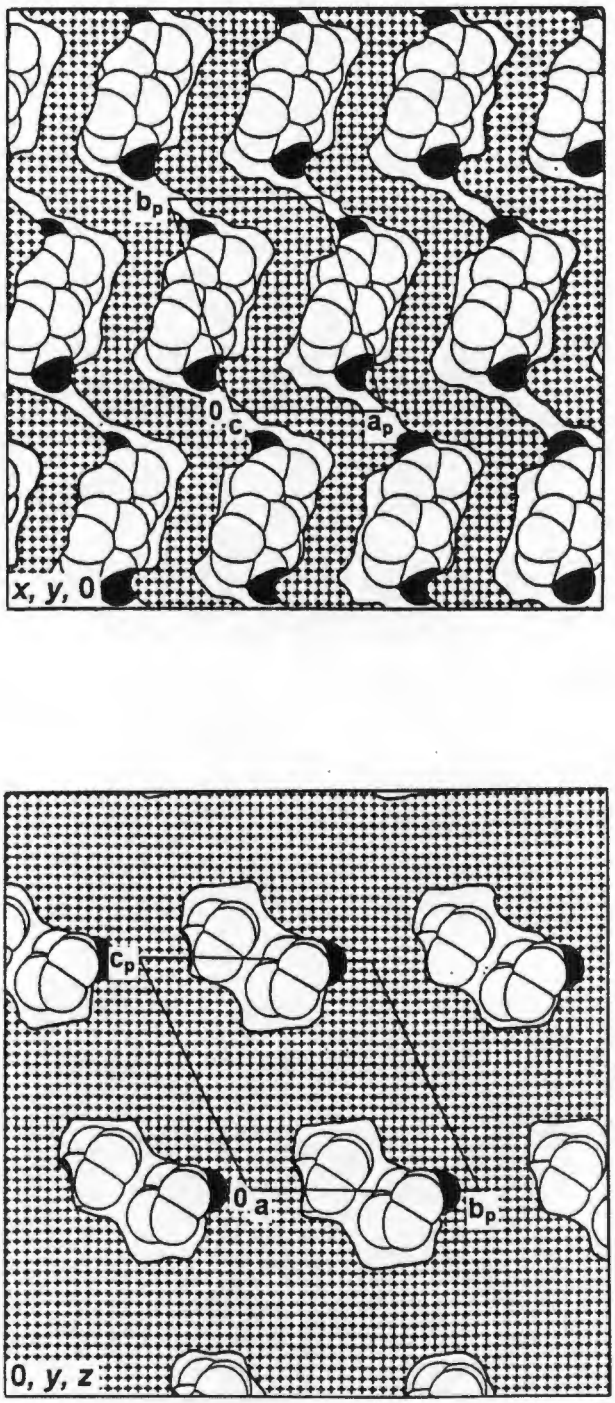

Figure 4.62 : Cross-section of SPDICHO viewed along a) [100], and b) [001]. The hatched region is that occupied by the host atoms. The guest molecules (with the oxygens shaded) are shown in the cavities.

Thermal Analysis :

The thermograms for SPDICHO are shown in figure 4.63. The TG curve shows a single step guest loss, followed by a gradual mass loss due to decomposition of the sample. The mass loss corresponding to guest release confirms the 1:2 host to guest ratio modelled in the crystal structure (expected mass loss : 13.0%, observed mass loss : 12.8%). The DSC trace, however, is more complex with three consecutive endotherms related to guest loss and structural collapse of the β to α-phase. The sample then melts with decomposition at 260°C.

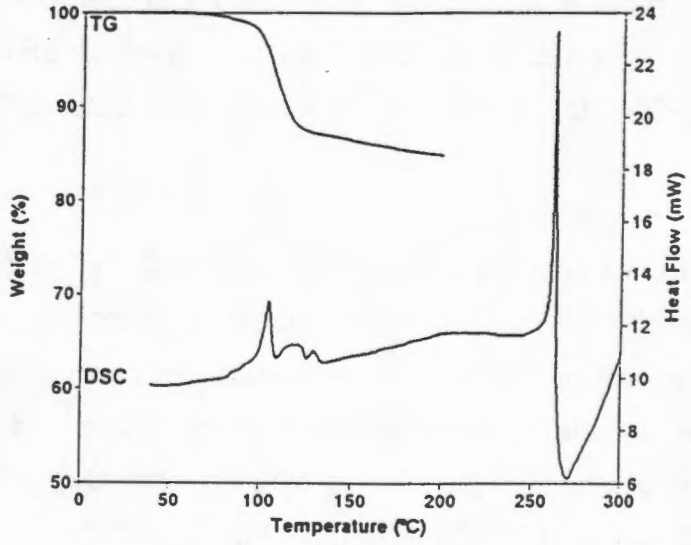

Figure 4.63 : TG and DSC curves of SPDICHO.

DISCUSSION

Initially the X-ray diffraction data were collected at room temperature. SPDEK and SPDIOX were refined successfully on this data, with relatively little disorder of either the host or guest molecules. However, the room temperature data for SPCHO and SPMEK was poor, and the guest molecules, in particular, could not be modelled successfully, owing to high thermal motion. It was decided that it was necessary to recollect the data at a lower temperature. SPMEK was repeated at 248K, using the FTS Systems Air Jet refrigeration unit, and the structure solution improved dramatically. The FTS Systems Air Jet refrigeration unit was then replaced by an Oxford Cryostream cooler, which is more efficient, and enabled future data collections to be done at 223K. All of the subsequent data collections were performed at 223K, except for SPBN, for which a low temperature data collection was unnecessary.

From the structures reported above, it is clear that the hexapedal host, hexakis(3-hydroxy-3,3-diphenyl-2-propynyl)benzene (host **1**), is a very versatile host compound, forming inclusion compounds with a wide range of volatile organic solvents. The solvents vary in size, shape, and capability to form hydrogen bonds. A number of different host to guest ratios are observed : 1:2 - SPDEK, SPETH, SP2H, SPDICHO, SPDIOXO; 1:3 - SPMEK; 1:4 - SPDMA; 1:5 - SPDIOX, SPCHO; and 1:6 - host **1** with dimethyl formamide[1]. Host **1** has also shown a preference for including molecules with a carbonyl functional group over those with only an ether oxygen, as indicated by the surprise inclusion of the 1,3-dioxolan-2-one impurity in 1,3-dioxolane, and the selective inclusion of cyclohexanone from a mixture of cyclohexanone and 1,4-dioxane. Another interesting result was that obtained from SPAB. It was found that on crystallisation from benzene alone the non-porous α-phase of host **1** was obtained, while a very unstable 1:6 acetonitrile inclusion compound was grown from acetonitrile. However, on crystallisation from a mixture of benzene and acetonitrile a relatively stable mixed guest inclusion compound, SPAB, was obtained. The benzene molecule is probably just the right size to pack into the cavity formed when two acetonitrile molecules

crystallise with a host molecule, thereby forming and stabilising the 1:2:2 inclusion compound.

A number of different hydrogen bonding patterns and packing motifs are noted. All the inclusion compounds investigated here are stabilised by hydrogen bonding. In none of the structures was host to host hydrogen bonding observed. The bulky end phenyl groups cause steric crowding around the hydroxy groups, thereby preventing host to host hydrogen bonding. Small organic molecules with suitable functional groups with the potential to act as hydrogen bond acceptors have, however, been found to hydrogen bond to the host hydroxyl groups. A number of different hydrogen bonding patterns are observed, as illustrated in figure 4.64, and the strengths of hydrogen bonds observed are either medium (2.65-2.80Å) or weak (>2.80Å)[4]. In all of the structures, where the host molecules are located on a centre of inversion, a co-operative hydrogen bonding scheme is observed. One of the host hydroxyl groups is involved in a hydrogen bond to the hydroxyl group on the adjacent 'leg', which in turn is hydrogen bonded to a guest molecule. In SPMEK, two co-operative hydrogen bonds are observed, while in SPDIOXO, the guest molecules are held in position by two hydrogen bonds from the hydroxyl groups on adjacent 'legs'. The only guests not involved in hydrogen bonding are guests K in SPCHO and SPDIOX.

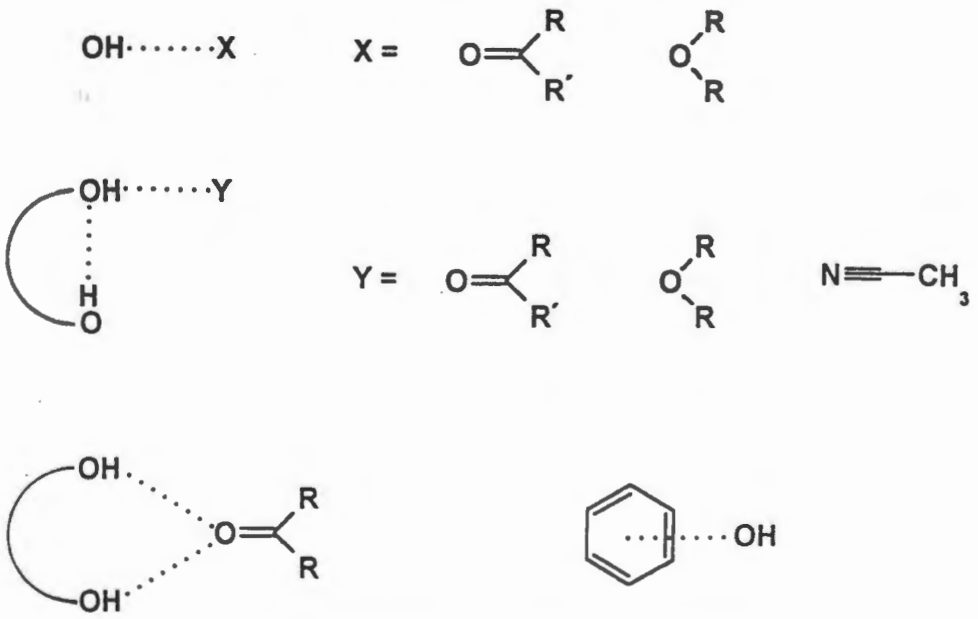

Figure 4.64 : Hydrogen bonding patterns observed in the inclusion compounds of host **1** studied here.

Four of the inclusion compounds were found to crystallise in the monoclinic crystal system, namely SPAB, SPDMA, SPMEK and SPDIOXO, while the rest of the structures belonged to the triclinic crystal system. Of all the structures investigated in this study only two of them were isostructural[3], namely SPDEK and SPETH. If the packing of the host molecules is viewed parallel to the central aromatic ring, there appear to be only three different packing motifs of host **1** observed in all of the above structures. These motifs are shown schematically in figure 4.65. The first is the herringbone packing seen in SPMEK and SPDIOXO. The second is that observed in SPBN, SPDEK, SPETH and SPDIOX. The host molecules pack in staggered layers parallel to the central aromatic region. The guest molecules, where present, are located between the bulky phenyl rings of adjacent host molecules within each layer; and above ,or below the central aromatic region of the host molecules. In SPDIOX, the 1,4 dioxolane guest molecules push the host molecules far enough apart to establish a channel between the off-set layers of host molecules. Guest G stabilises the structure by hydrogen bonding to two of the host molecules, and thereby linking the layers of host molecules. The third type of packing motif observed can be seen in the structures of SPAB, SPDMA, SPCHO, SPDICHO, and SP2H. The host molecules are stacked on top of each other, with the guest molecules located in the cavities created between the central aromatic regions of adjacent host molecules. In SPCHO, one of the guest molecules is also located between the layers of stacked host molecules.

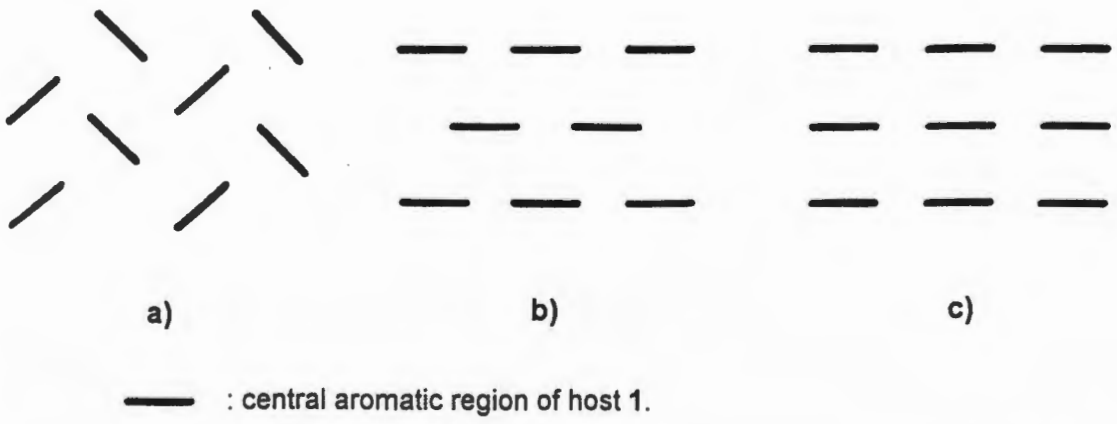

Figure 4.65 : A schematic representation of the packing motifs observed in host **1** inclusion compounds : a) herringbone pattern, b) staggered layers, and c) stacked hosts (the host molecules are viewed parallel to the central aromatic region).

The kinetics of desolvation for some of the inclusion compounds studied were obtained using isothermal thermogravimetry. The kinetic data, along with the mode of inclusion and onset temperature of guest release, obtained from the DSC analysis, is tabulated in table 4.12. All the inclusion compounds in which the guests are situated in cavities, were found to obey the Avrami-Erofeev (A2) kinetic model. It is interesting to note that although SPDEK and SPETH are isostructural, and the strengths of their hydrogen bonds similar, SPETH has a significantly greater activation energy than SPDEK. Looking at the onset temperatures (T_{on}) of the guess loss reaction and boiling points (T_b) of the guests, T_{on} - T_b for SPDEK is -15.5°C, while T_{on} - T_b for SPETH is 42.4°C. It has been suggested that T_{on} - T_b is a crude measure of the thermal stability of an inclusion compound[5], and as a result SPETH appears more thermally stable than SPDEK, which may account for the difference in their activation energies of desolvation. The activation energy of SP2H is notably higher than any of the activation energies obtained for the other host **1** inclusion compounds. A possible explanation for this could be that the size of the guest molecules may also influence the activation energy of desolvation of an inclusion compound, since 2-hexanone is a much larger molecule than the other guests investigated.

Table 4.12 : Kinetics of desolvation of host **1** inclusion compounds.

Compound	Inclusion mode	T_{on} (°C)	T_b (°C)	T_{on}-T_b (°C)	T-range (°C)	E_a (kJ.mol^{-1})	Reaction mechanism
SPDIOX	constricted channels	115	101.1	13.9	56-75	148(2)	F1
SPMEK	channels/ cavities	75	79.6	-4.6	62-72	156(9)	B1
SPDMA	cavities	135	164	-29	75-105	154(3)	A2
SPDEK	cavities	86	101.5	-15.5	55-80	163(5)	A2
SPETH	cavities	77	34.6	42.4	55-75	190(6)	A2
SP2H	cavities	99	128	-29	80-100	264(3)	A2

HOST CONFORMATION

Host **1** is a large, bulky molecule, and at first glance the overall conformation appears to be similar for all the structures investigated in this study. For the structures in which the host molecules are located on a centre of inversion, two of the hydroxyl groups on adjacent 'legs' are directed towards each other. Symmetry forces the opposite ends of the host molecule to be alike, while for SPMEK and SPDIOXO, there is no symmetry relationship within the host molecules, but the conformation seen is similar. For both SPMEK and SPDIOXO, two pairs of adjacent 'legs', on opposite sides of the central aromatic ring, have the hydroxyl groups directed towards each other (figure 4.66).

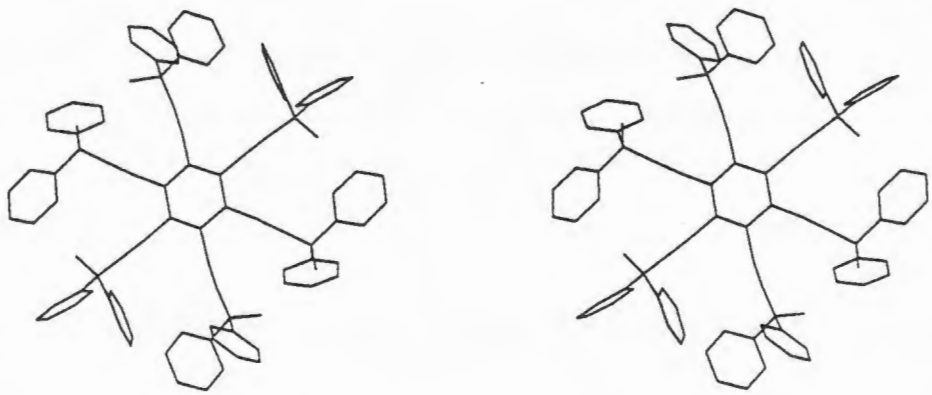

Figure 4.66a : Host con formation of SPBN, viewed perpendicular to the C(1)-C(17)-C(33) plane.

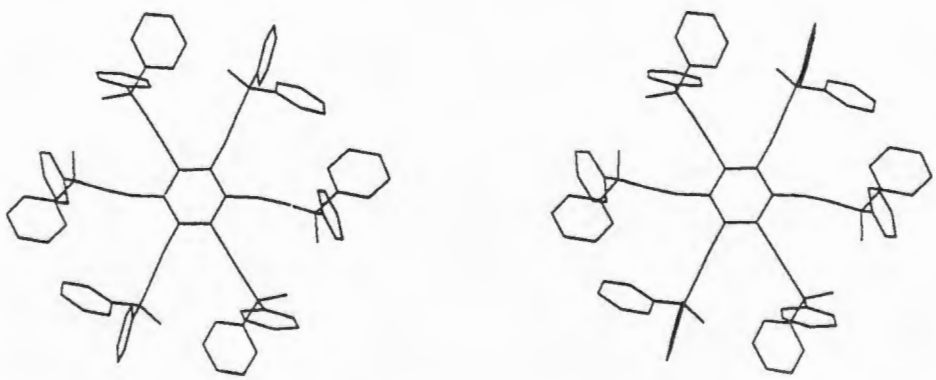

Figure 4.66b : Host con formation of SPAB, viewed perpendicular to the C(1)-C(17)-C(33) plane.

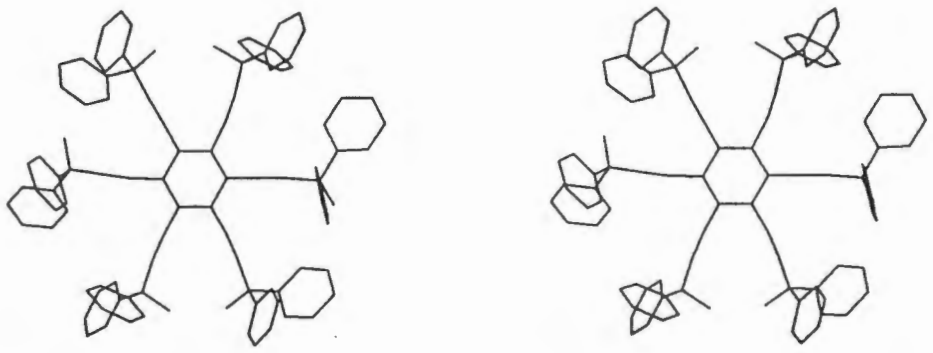

Figure 4.66c : Host con formation of SPMEK, viewed perpendicular to the C(1)-C(17)-C(33) plane.

However, on closer inspection, the conformation of host **1** is not the same in any of the structures investigated. The hydroxyl and bulky phenyl groups at the end of each 'leg' are free to rotate relative to the central aromatic region and also relative to each other, resulting in the possibilty of a large number of host conformations. This rotational freedom allows for the adjustment of the host molecules to accommodate a variety of guest molecules, differing in size and shape, within its framework. The torsion angles defining the relative position of the phenyl rings to the central aromatic region are indicated in the scheme below. The labelling of the host molecules in each structure, although carried out cyclically, was initially done arbitrarily, therefore it is not possible to compare the torsion angles directly. For each 'leg', τ_1 will define the smallest torsion angle, and τ_3 will define the smaller of the two angles observed for the second phenyl ring. Table 4.13 reports the torsion angles obtained for each of the structures.

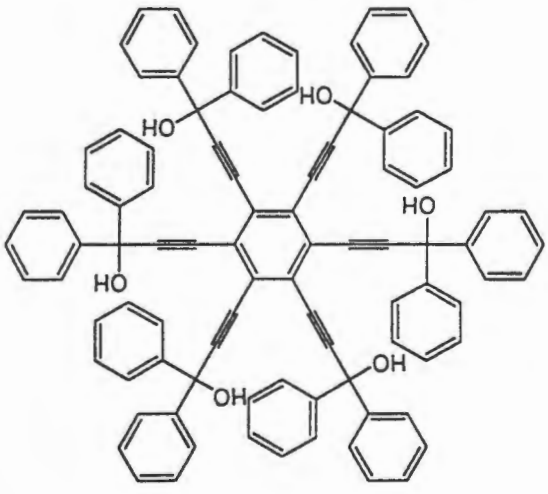

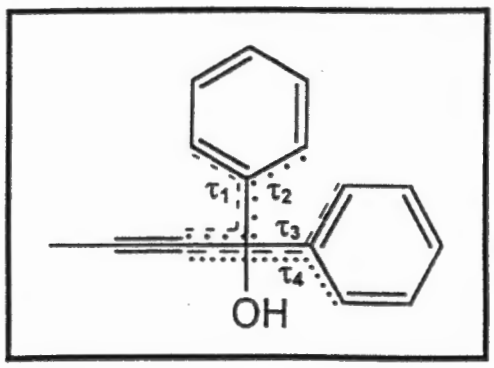

Table 4.13 : Torsion angles for the structures of host **1**.

Compound	τ_1 (°)	τ_2 (°)	τ_3 (°)	τ_4 (°)
SPBN	9.2(3)	-170.4(2)	-40.0(2)	143.5(2)
	-7.6(3)	171.4(2)	-86.2(2)	90.1(2)
	29.3(2)	-154.1(2)	52.0(2)	-129.3(2)
SPDEK	-1.7(4)	178.5(3)	-76.1(3)	103.2(3)
	-22.3(4)	158.5(3)	52.6(4)	-128.0(3)
	-35.4(4)	148.8(3)	-44.7(4)	134.8(3)
SPETH	-27.7(2)	155.3(2)	-58.1(2)	119.6(2)
	0.0(2)	178.0(2)	80.1(2)	-98.7(2)
	24.5(2)	-155.0(2)	-51.4(2)	127.5(2)
SPDIOX	-27.1(5)	157.0(4)	32.8(5)	-149.2(4)
	8.8(3)	-171.1(2)	45.5(3)	-134.6(2)
	29.2(5)	-151.3(4)	61.7(5)	-117.9(4)
SPAB	11.7(3)	-168.7(2)	-64.7(3)	113.4(3)
	4.8(3)	-175.2(2)	52.2(3)	-129.1(2)
	0.7(3)	-179.1(2)	48.1(3)	-175.2(2)
SPDMA	-22.9	157.4(4)	44.4(6)	-138.0(5)
	12.7(6)	-169.3(4)	-53.0(6)	130.7(5)
	-27.0(6)	154.9(4)	39.2(5)	-143.2(4)
SPCHO	18.6(6)	-162.6(4)	-73.0(5)	106.4(5)
	29.0(6)	-152.6(4)	-37.0(6)	143.9(4)
	1.4(5)	-177.7(4)	-85.7(5)	91.6(5)
SPDICHO	-25.1(5)	158.7(2)	42.0(3)	-141.9(2)
	8.8(3)	-171.1(2)	45.5(3)	-134.6(2)
	-9.9(3)	168.5(2)	80.1(3)	-95.4(3)
SP2H	16.1(8)	-167.7(6)	-42.9(8)	142.2(6)
	21.3(8)	-164.6(6)	-46.3(7)	136.1(6)
	-5.4(8)	172.8(5)	-41.1(7)	-93.3(8)

Compound	τ_1 (°)	τ_2 (°)	τ_3 (°)	τ_4 (°)
SPMEK	17.2(6)	-169.3(5)	70.8(5)	-108.4(5)
	5.3(7)	-174.9(5)	-49.0(6)	131.4(6)
	-32.1(6)	149.6(5)	-54.4(6)	127.6(5)
	-17.1(6)	166.9(4)	-65.0(5)	111.3(5)
	2.6(8)	-178.3(6)	75.2(6)	-102.7(6)
	-34.9(7)	148.3(6)	45.5(7)	-138.0(6)
SPDIOXO	32.3(5)	-152.1(4)	-36.1(5)	148.3(4)
	-13.9(6)	166.7(4)	42.6(5)	-140.6(4)
	41.9(6)	-143.0(5)	55.0(6)	-122.3(5)
	33.5(5)	-151.3(4)	-35.0(5)	149.9(4)
	15.7(6)	-164.9(4)	-47.2(5)	135.8(4)
	-52.9(5)	126.7(5)	75.2(5)	141.0(4)

In all cases the aromatic rings can be considered to be planar, the maximum deviations from their least squares planes are all below 0.03Å. The angle between the planes of the phenyl rings, on the each 'leg', was also found to be fairly consistent, only varying between 3.5° and 13.8° for each structure (table 4.14).

Table 4.14 : Angle between the planes of the phenyl rings on each 'leg' of host **1**.

Angle between	SPBN	SPDEK	SPETH	SPDIOX
C(5)-C(10)/C(11)-C(16)	75.24(7)	81.9(1)	81.78(7)	76.4(2)
C(21)-C(26)/C(27)-C(32)	84.99(7)	74.1(1)	77.69(7)	80.6(2)
C(37)-C(42)/C(43)-C(48)	85.01(7)	87.0(1)	86.94(6)	89.4(2)

Angle between	SPAB	SPDMA	SPCHO	SPDICHO	SP2H
C(5)-C(10)/C(11)-C(16)	81.88(9)	78.6(2)	84.3(2)	81.02(8)	82.9(2)
C(21)-C(26)/C(27)-C(32)	85.65(8)	83.9(1)	75.4(2)	83.68(9)	80.6(2)
C(37)-C(42)/C(43)-C(48)	82.14(8)	70.1(2)	80.2(1)	84.90(9)	89.4(3)

Table 1.14 cont.

Angle between	SPMEK	SPDIOXO
C(5)-C(10)/C(11)-C(16)	82.3(2)	80.4(1)
C(21)-C(26)/C(27)-C(32)	80.2(2)	77.2(1)
C(37)-C(42)/C(43)-C(48)	79.5(2)	76.8(2)
C(53)-C(58)/C(59)-C(64)	84.4(2)	80.3(1)
C(69)-C(74)/C(75)-C(80)	83.4(2)	78.8(1)
C(85)-C(90)/C(91)-C(96)	74.1(2)	78.0(2)

The orientation of the hydroxyl groups in relation to the central aromatic region is also important in defining each structure's host conformation. The torsion angles defining the positions of the hydroxyl groups relative to the central aromatic ring are shown in the scheme below and tabulated in table 4.15. Foces-Foces[6] has investigated the possible conformations of related compounds, the 'aromatic propellenes', with respect to the orientation of the nitrogen atoms bearing the lone pair placed up (*u*) and down (*d*) in relation to the central benzene ring. The most stable conformation was found to be *ududud*. Using this concept, the orientation of the hydroxyl groups in relation to the central aromatic region was found to be *ududud* for SPAB, SPDMA, SPCHO, SPDICHO, and SP2H, while for SPBN, SPMEK, SPDEK, SPETH, SPDIOX and SPDIOXO, it was *uuuddd*. This can be clearly seen in figure 4.67.

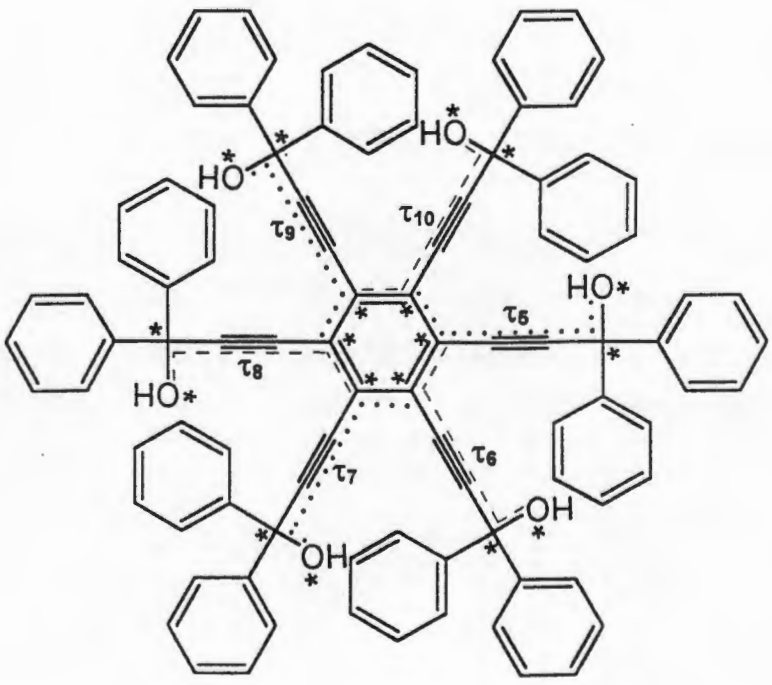

Table 4.15 : Torsion angles defining the position of the hydroxyl groups relative to the central aromatic ring.

Torsion angles (°)	SPBN	SPAB	SPDMA	SPDEK	SPETH
τ_5	25.1(2)	145.0(2)	-152.0(4)	169.0(2)	169.4(2)
τ_6	52.6(2)	-22.7(2)	19.6(4)	35.0(3)	33.3(2)
τ_7	152.1(2)	152.7(2)	-11.4(4)	18.1(3)	18.4(2)
τ_8	-25.1(2)	-145.0(2)	152.0(4)	-169.0(2)	-169.4(2)
τ_9	-52.6(2)	22.7(2)	-19.6(4)	-35.0(3)	-33.3(2)
τ_{10}	-152.1(2)	-153.7(2)	11.4(4)	-18.1(3)	-18.4(2)

Torsion angles (°)	SPMEK	SPCHO	SP2H	SPDIOX	SPDIOXO	SPDICHO
τ_5	175.5(4)	19.9(4)	26.0(6)	9.7(3)	-94.8(4)	19.9(4)
τ_6	12.3(4)	-160.5(4)	-159.3(6)	37.2(2)	-159.1(4)	-160.5(4)
τ_7	23.0(4)	147.0(3)	26.3(6)	159.4(3)	-3.4(4)	147.0(3)
τ_8	-175.6(4)	-19.9(4)	-26.0(6)	-9.7(3)	96.2(4)	-19.9(4)
τ_9	-41.0(4)	160.5(4)	159.3(6)	-37.2(2)	159.4(4)	160.5(4)
τ_{10}	-24.2(4)	-147.0(3)	-26.3(6)	-159.4(3)	5.0(4)	-147.0(3)

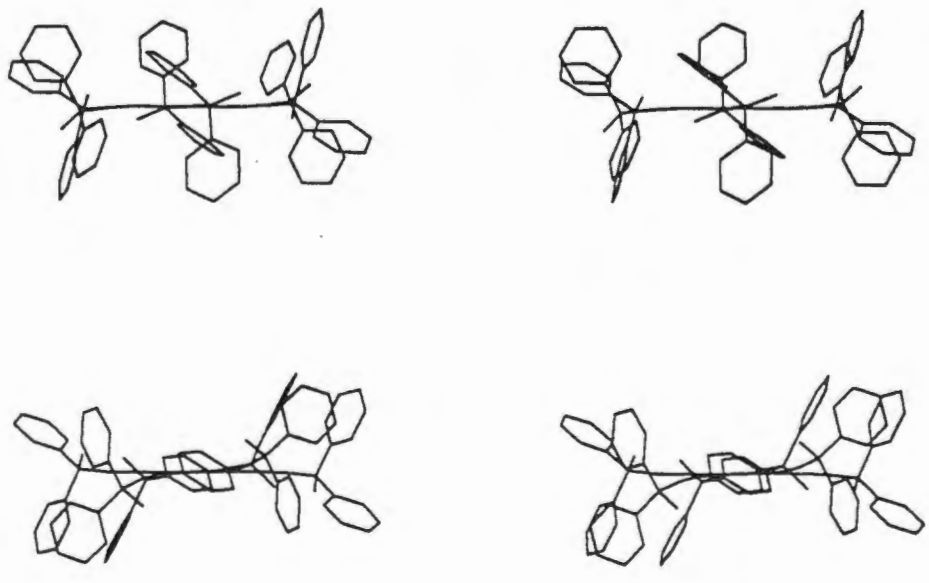

Figure 4.67 : Host conformation of a) SPAB and b) SPBN viewed parallel to the central aromatic region, clearly showing the orientation of the hydroxyl groups as *ududud* and *uuuddd* respectively.

The different bond types observed in host **1** are indicated in the scheme below. The bond length ranges observed in each of the structures are tabulated in table 4.16, and are comparable with known values[7]. For all of the structures investigated the lengths of the $C_{ar} \simeq C_{ar}$ bonds for the central aromatic ring are noticeably longer than the bond lengths observed in the phenyl rings. This is presumably in order to maximise the space between adjacent 'legs'.

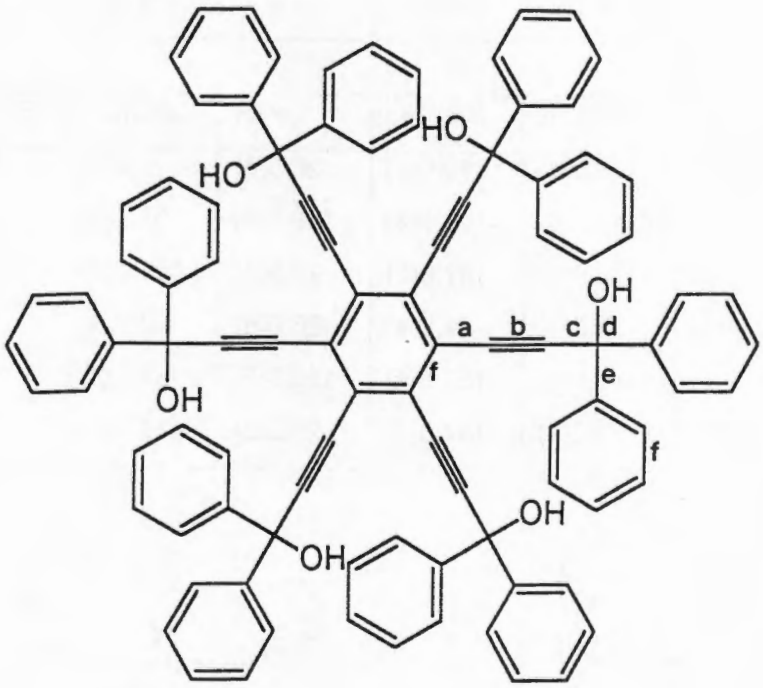

Table 4.16 : Bond length ranges observed in host **1** (bond lengths in angstroms).

Bond		SPBN	SPDEK	SPETH	SPDIOX	SP2H	SPCHO	SPDICHO	SPAB	SPDMA	SPMEK	SPDIOXO	Ref 7 (median)
a = C_{ar} - C_{sp}	min	1.425(2)	1.425(4)	1.429(2)	1.427(5)	1.426(8)	1.418(5)	1.430(3)	1.425(3)	1.425(6)	1.422(6)	1.428(6)	1.43(1)
	max	1.432(2)	1.434(4)	1.435(2)	1.434(5)	1.441(7)	1.432(5)	1.432(3)	1.440(3)	1.439(5)	1.439(6)	1.440(5)	
b = C ≡ C	min	1.188(2)	1.187(4)	1.191(2)	1.191(5)	1.184(8)	1.194(5)	1.188(3)	1.182(3)	1.191(6)	1.180(6)	1.182(5)	1.19(1)
	max	1.192(3)	1.195(4)	1.197(2)	1.194(5)	1.197(8)	1.203(6)	1.192(3)	1.195(3)	1.192(6)	1.203(6)	1.198(5)	
c = C_{sp} - C_{sp}^3	min	1.476(3)	1.475(4)	1.479(2)	1.476(5)	1.471(8)	1.469(6)	1.474(3)	1.473(3)	1.459(6)	1.471(7)	1.470(6)	1.47(1)
	max	1.486(2)	1.477(4)	1,482(2)	1.480(5)	1.486(8)	1.485(6)	1.486(3)	1.487(3)	1.500(5)	1.495(6)	1.496(6)	
d = C_{sp}^3 - O	min	1.432(2)	1.418(3)	1.423(2)	1.414(4)	1.432(7)	1.424(5)	1.428(3)	1.432(3)	1.415(5)	1.427(6)	1.414(6)	1.43(1)
	max	1.447(2)	1.442(4)	1.440(2)	1.444(5)	1.447(7)	1.433(5)	1.438(3)	1.438(3)	1.435(5)	1.440(6)	1.436(6)	
e = C_{sp}^3 - C_{ar}	min	1.520(3)	1.515(4)	1.525(3)	1.523(5)	1.501(9)	1.521(6)	1.517(3)	1.524(3)	1.522(6)	1.520(7)	1.522(6)	1.53(2)
	max	1.535(3)	1.533(4)	1.534(2)	1.540(6)	1.531(9)	1.543(6)	1.540(3)	1.535(3)	1.543(6)	1.544(7)	1.542(6)	
f = C_{ar} ≃ C_{ar}	min	1.353(4)	1.347(9)	1.357(5)	1.341(7)	1.34(1)	1.341(8)	1.360(4)	1.355(4)	1.344(7)	1.34(1)	1.350(8)	1.38(1)
	max	1.393(3)	1.394(5)	1.393(3)	1.394(6)	1.396(9)	1.395(7)	1.395(4)	1.392(3)	1.399(7)	1.397(6)	1.395(6)	
f = C_{ar} ≃ C_{ar}	min	1.401(2)	1.401(4)	1.402(2)	1.403(5)	1.383(8)	1.404(5)	1.404(3)	1.403(3)	1.385(6)	1.395(6)	1.390(6)	1.40(1)
(central ring)	max	1.407(2)	1.410(3)	1.409(2)	1.407(5)	1.415(7)	1.413(5)	1.410(3)	1.404(3)	1.432(5)	1.418(6)	1.415(5)	

REFERENCES

1. S. A. Bourne, M. R. Caira, L. R. Nassimbeni, M. Sakamoko, K. Tanaka, F. Toda, *J. Chem. Soc., Perkin Trans. 2*, 1994, 1899
2. Cambridge Structural Database and Cambridge Structural Database System, Version 5.12, Cambridge Crystallographic Data Centre, University Chemical Laboratory, Cambridge, England.
3. A. Kálmán, L. Parkanyi, G. Argay, *Acta Crystallogr.*, 1993, **B49**, 1039.
4. P. Gilli, V. Bertolasi, V. Ferretti, G. Gilli, *J. Am. Chem. Soc.*, 1994, **116**, 909.
5. S. A. Bourne, L. R. Nassimbeni, *J. Org. Chem.*, 1992, **57**, 2438.
6. C. Foces-Foces, A. L. Llamas-Saiz, R. M. Claramunt, N. Jagerovic, M. L. Jimeno, J. Elguero, *J. Chem. Soc., Perkin Trans. 2*, 1995, 1359.
7. F. H. Allen, O. Kennard, D. G. Watson, L. Brammer, A. G. Orpen, R. Taylor, *J. Chem. Soc., Perkin Trans. 2*, 1987, S1.

CHAPTER 5

HOST 2 INCLUSION COMPOUNDS.

The inclusion compounds formed by host **2** will be discussed in this chapter. Each inclusion compound is discussed in terms of crystal structure (refinement and molecular structure), thermal analysis, and kinetics of desolvation, where applicable. The molecular formula, space group and cell parameters are summarised at the beginning of the discussion of each inclusion compound.

The structure of NAPCHO was refined in the monoclinic space group $P2_1/n$, while the structures of NAP2H, NAPDMA and NAPDMF were all refined in the triclinic space group $P\bar{1}$. For the triclinic structures, preliminary oscillation and Weissenberg X-ray photography established the crystal system. $P\bar{1}$ was chosen as the space group, rather than P1, based on the intensity statistics of the crystal reflection data. The mean $|E^2-1|$ values for the 0kl, h0l, hk0, as well as for the remainder of the reflections were all close to the theoretical value of 0.968. Successful refinements confirmed the choice of the centric space group.

In all four of the inclusion compounds studied, the host molecules are situated on a centre of inversion, resulting in half the host and half the guest molecules being located in the asymmetric unit. The atomic labelling scheme for host **2** can be seen in Figure 5.1, while the atomic labelling scheme used for the guests is shown at the beginning of the discussion of each structure. The guest molecules were labelled with a suffix G, J, or K.

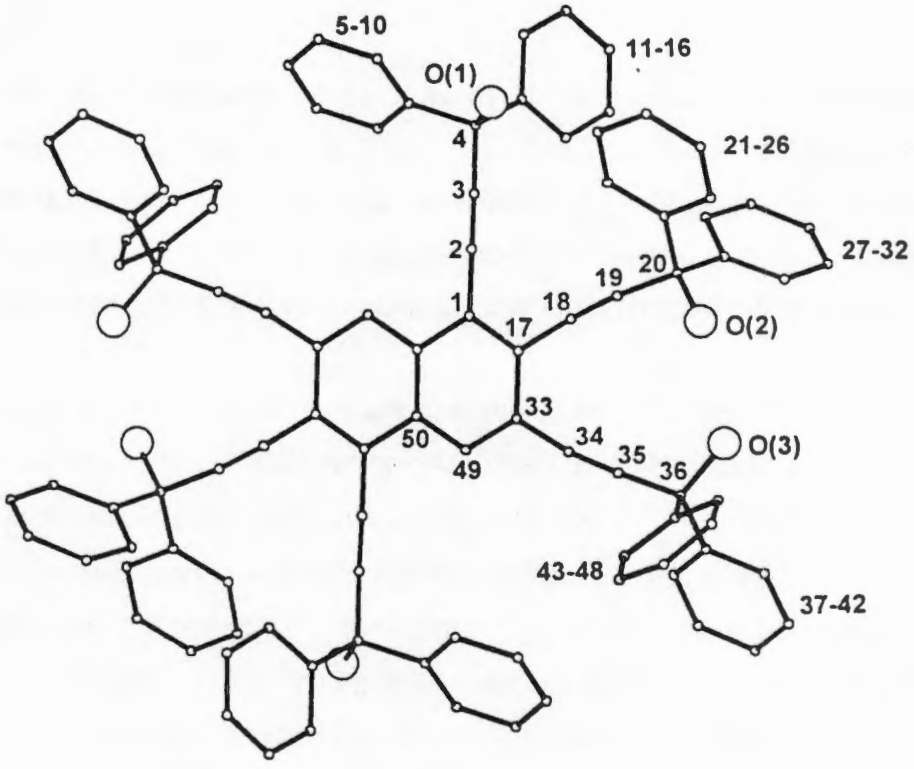

Figure 5.1 : Atomic labelling scheme used for host **2**.

The structure of the α-phase of host **2** could not be determined since suitable single crystals for X-ray diffraction were not obtained during the course of this study. Thermal analysis results for this host showed no mass loss on heating, and the DSC trace showed a single melt endotherm at 256°C. The host then decomposes exothermically.

NAPCHO

$C_{100}H_{68}O_6 \cdot 6C_6H_{10}O$	
Guest : cyclohexanone	
Space Group : $P2_1/n$	
a = 9.444(5)Å	$\alpha = 90°$
b = 18.353(5)Å	$\beta = 92.18(3)°$
c = 31.59(1)Å	$\gamma = 90°$
Volume = 5471(4)Å^3	
Z = 2	

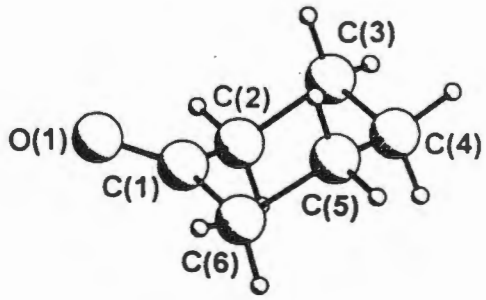

Guests labelled : G, J, K.

Crystal Structure :

Preliminary X-ray photography established that NAPCHO displays 2/*m* Laue symmetry and therefore crystallises in the monoclinic crystal system. The crystal reflection data exhibited the following non-extinction conditions :

h0l : h + l = 2n

0k0 : k = 2n

(h00 : h = 2n)

(00l : l = 2n)

Based on these non-extinction conditions, the structure of NAPCHO was refined in the centrosymmetric monoclinic space group, $P2_1/n$.

Refinement :

All the host non-hydrogen atoms were refined anisotropically. The phenyl hydrogens were placed in geometrically calculated positions, and refined isotropically linked to a common temperature factor (*U* (CH) : 0.085(5)Å^2), except for H(49) which was linked to C(49) (H(49) is the aromatic hydrogen on the central naphthalene ring). The hydroxyl hydrogens were not located in

the difference electron density maps, and were omitted from the final model. The oxygen atoms on guests G and J were refined anisotropically, while O(1K) and all the carbon atoms were refined isotropically, owing to their relatively high temperature factors. The hydrogen atoms on guests G and J were placed in calculated positions and allowed to refine with a common temperature factor for each guest.

U (CH_2 - guest G) : 0.14(1)Å^2 *U* (CH_2 - guest J) : 0.12(1)Å^2

There is a residual electron density of 0.86eÅ^{-3} in the region of guest J, which could not be modelled successfully; this is ascribed to an imperfect model. The structure refined to a final R_1 = 0.1095.

Molecular Structure :

The molecular structure of NAPCHO is shown in figure 5.2, and the hydrogen bond data is reported in table 5.1. Guest G is held in position by a co-operative hydrogen bond between O(2), O(3) and O(1G), guest J is held in position by a hydrogen bond between O(1) and O(1J), while guest K does not appear to be involved in a hydrogen bonding scheme. The host molecules are stacked in columns parallel to [100], with the central naphthalene moieties lying in the (200) plane (figure 5.3). The guests are located in interconnected cavities, centred at *x*=0 and *x*=0.5, shown in figure 5.4. The approximate dimensions of the cavities are 6 x 15.5 x 24.5Å.

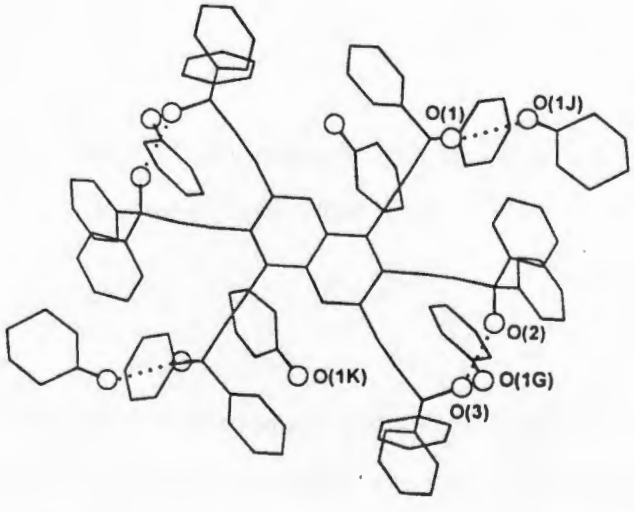

Figure 5.2 : Molecular structure of NAPCHO (the hydrogen atoms are omitted for clarity, and the hydrogen bonds are represented as dotted lines).

Table 5.1 : Hydrogen bond data for NAPCHO.

(D)onor	(A)cceptor	D...A (Å)
O(2)	O(3)	2.882(7)
O(3)	O(1G)	2.686(8)
O(1)	O(1J)	2.741(9)

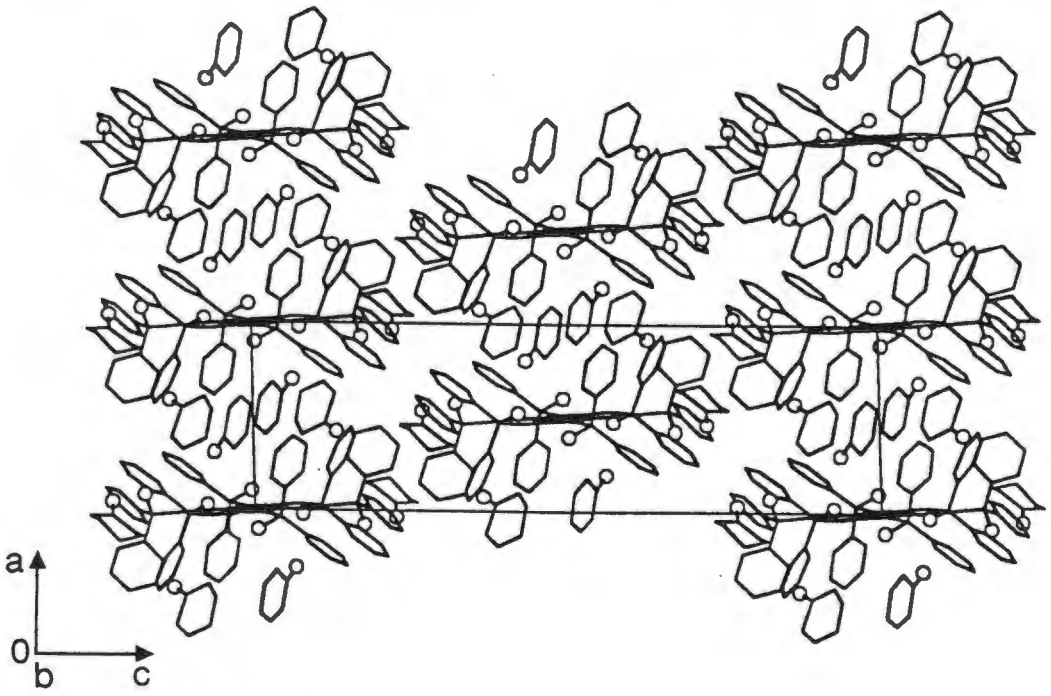

Figure 5.3a : Crystal packing in NAPCHO viewed along [010].

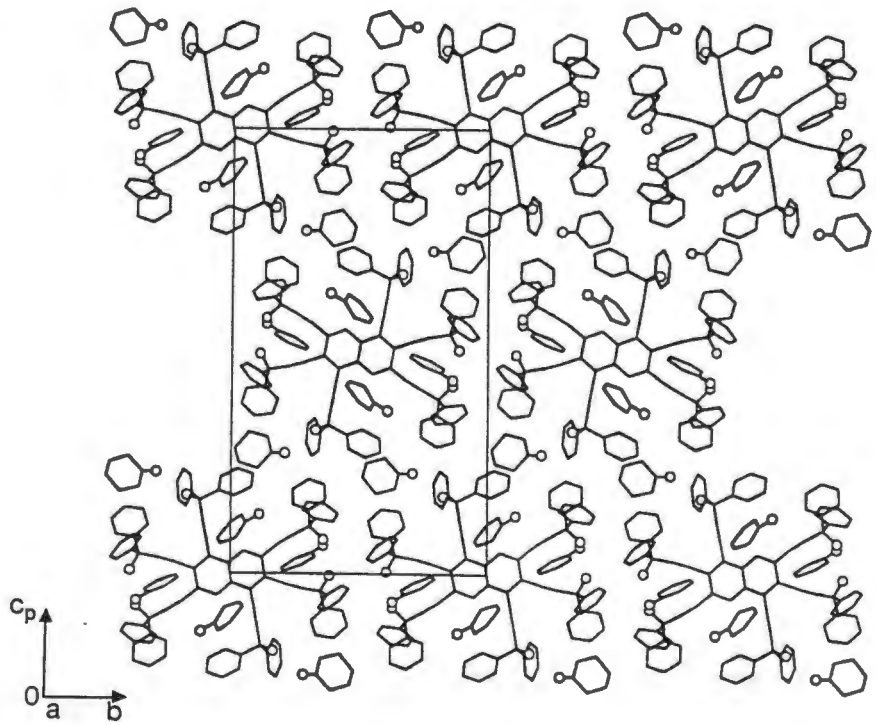

Figure 5.3b : Crystal packing in NAPCHO viewed along [100].

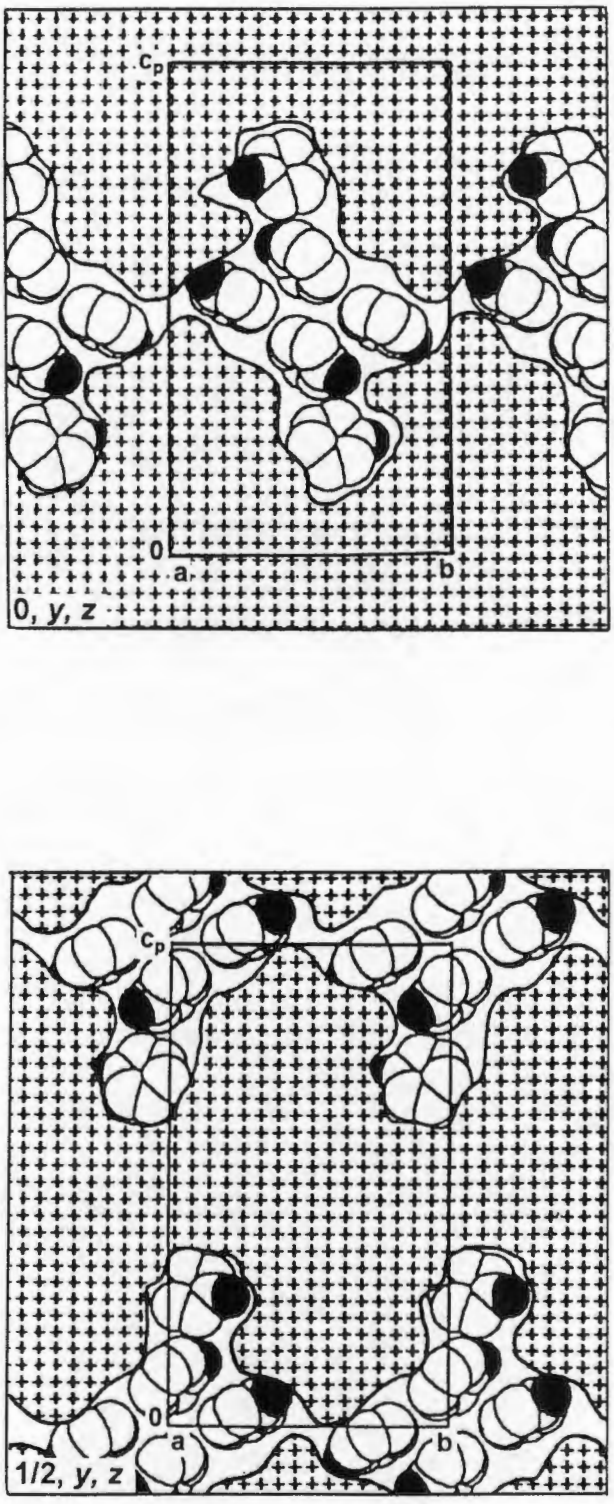

Figure 5.4 : Cross-section of NAPCHO viewed along [100]. The hatched region is that occupied by the host molecules, and the guests are shown in the cavities (the oxygen atoms are shaded).

Thermal Analysis :

The thermograms of NAPCHO are shown in figure 5.5. The TG curve does not show a smooth single step guest loss, but rather a multiple step guest loss, where the steps are not clearly defined. The guest molecules are located in different environments within the host framework and held in position by different forces, suggesting that, on desolvation of NAPCHO, a multiple step guest loss will result. The overall guest loss confirms the host to guest ratio, 1:6, modelled in the crystal structure (expected mass loss : 30.1%, observed mass loss : 29.9%). The DSC trace is characterised by four endotherms. The multiple step guest loss is confirmed by the endotherms, A and B, at 100°C and 119°C. B is followed by a step, similar to that observed in the DSC trace of SPCHO, and then by endotherms C and D. This trace is indicative of a concomitant phase change with the loss of the guest molecules to a polymorph of host **2**. This polymorph converts to the α-phase at 235°C, which in turn melts and decomposes at 256°C. Figure 5.6 shows the thermal decay of a single crystal of NAPCHO; the crystal begins to decay at 75°C, at points of defects on the crystal surface. The reaction interface proceeds rapidly as the guest release temperature approaches. The crystal then melted with decomposition at 263°C, no evidence for the polymorph was observed.

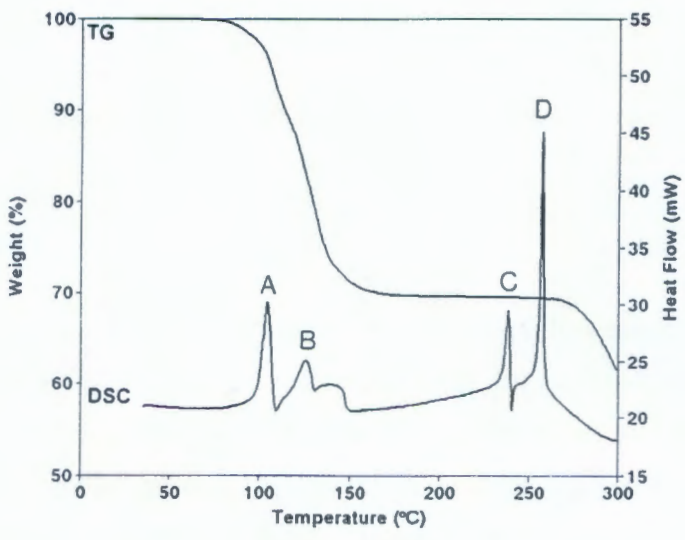

Figure 5.5 : TG and DSC traces for NAPCHO.

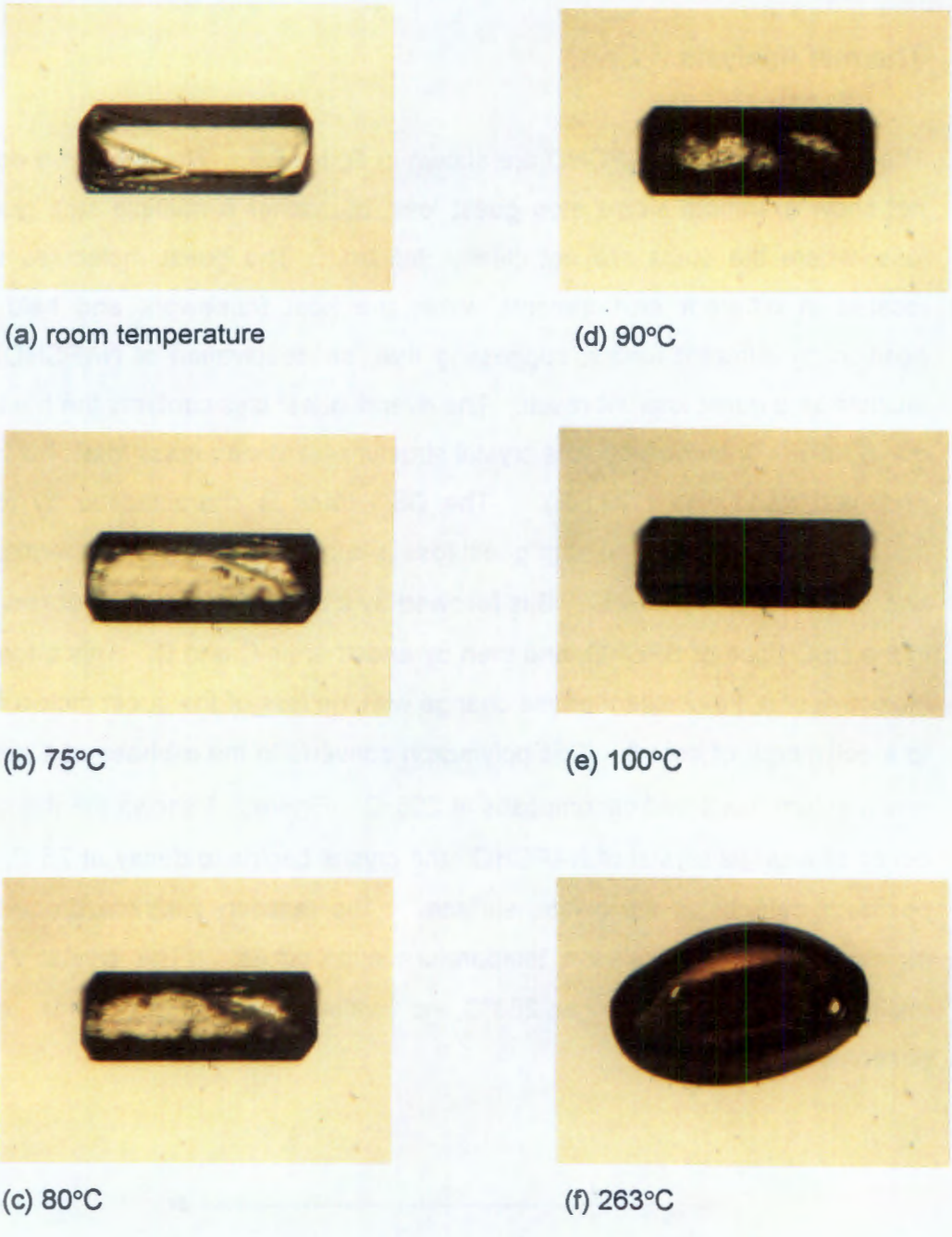

Figure 5.6 : Thermal decay of a single NAPCHO crystal, under slow heating (magnification : 36X).

The polymorph was not observed during hotstage microscopy since the eye is much less sensitive than the DSC to crystal changes. Unless a gross change in the microcrystalline structure of the sample occurs, a polymorphic change will not be observed by hotstage microscopy. Due to insufficient sample and the fact that X-ray powder diffraction analysis requires at least 50mg of sample, it was not possible to isolate and characterise this polymorph.

NAP2H

$C_{100}H_{68}O_6.4C_6H_{12}O$
Guest : 2-hexanone
Space Group : P $\bar{1}$

a = 8.539(1)Å	α = 114.58(1)°
b = 16.907(3)Å	β = 97.65(1)°
c = 18.907(3)Å	γ = 92.90(1)°

Volume = 2443.1(6)Å^3
Z = 1

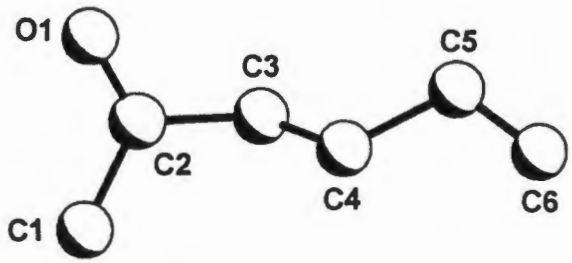

Guests labelled : G, J.

Crystal Structure :

The crystal structure of NAP2H was refined in the triclinic space group P $\bar{1}$.

Refinement :

All the non-hydrogen atoms were refined anisotropically. The hydroxyl hydrogens were located in the difference electron density maps and refined isotropically. The phenyl hydrogens were placed in geometrically calculated positions and refined with a common temperature factor (*U* (CH) : 0.083(3)Å^2). The guest hydrogens were omitted from the final model.

Two of the phenyl rings on one of the 'legs', C(5)-C(10) and C(11)-C(16), and both guests were found to be disordered. The disorder was modelled as shown in figure 5.7. Guest G was also refined with bond length restraints.

An extinction coefficient of 0.011(2) was applied and the structure refined to a final R_1 = 0.0638.

site occupancy factors - A : 0.57(2) B: 0.43(2)

Bond lengths (Å)

C(4) - C(5A) :	1.677(8)	C(4) - C(5B) :	1.39(1)
C(5A) - C(6) :	1.260(7)	C(5B) - C(6) :	1.53(1)
C(6) - C(7) :	1.397(6)	C(6) - C(7) :	1.397(6)
C(7) - C(8A) :	1.304(8)	C(7) - C(8B) :	1.55(2)
C(8A) - C(9A) :	1.38(1)	C(8B) - C(9B) :	1.35(2)
C(9A) - C(10A) :	1.381(9)	C(9B) - C(10B) :	1.39(2)
C(10A) - C(5A) :	1.390(9)	C(10B) - C(5B) :	1.38(1)
C(4) - C(11A) :	1.38(1)	C(4) - C(11B) :	1.79(1)
C(11A) - C(12A) :	1.38(1)	C(11B) - C(12B) :	1.41(1)
C(12A) - C(13A) :	1.40(1)	C(12B) - C(13B) :	1.38(2)
C(13A) - C(14A) :	1.38(1)	C(13B) - C(14B) :	1.37(2)
C(14A) - C(15A) :	1.38(2)	C(14B) - C(15B) :	1.37(2)
C(15A) - C(16A) :	1.39(2)	C(15B) - C(16B) :	1.37(3)
C(16A) - C(11A) :	1.43(1)	C(16B) - C(11B) :	1.41(2)

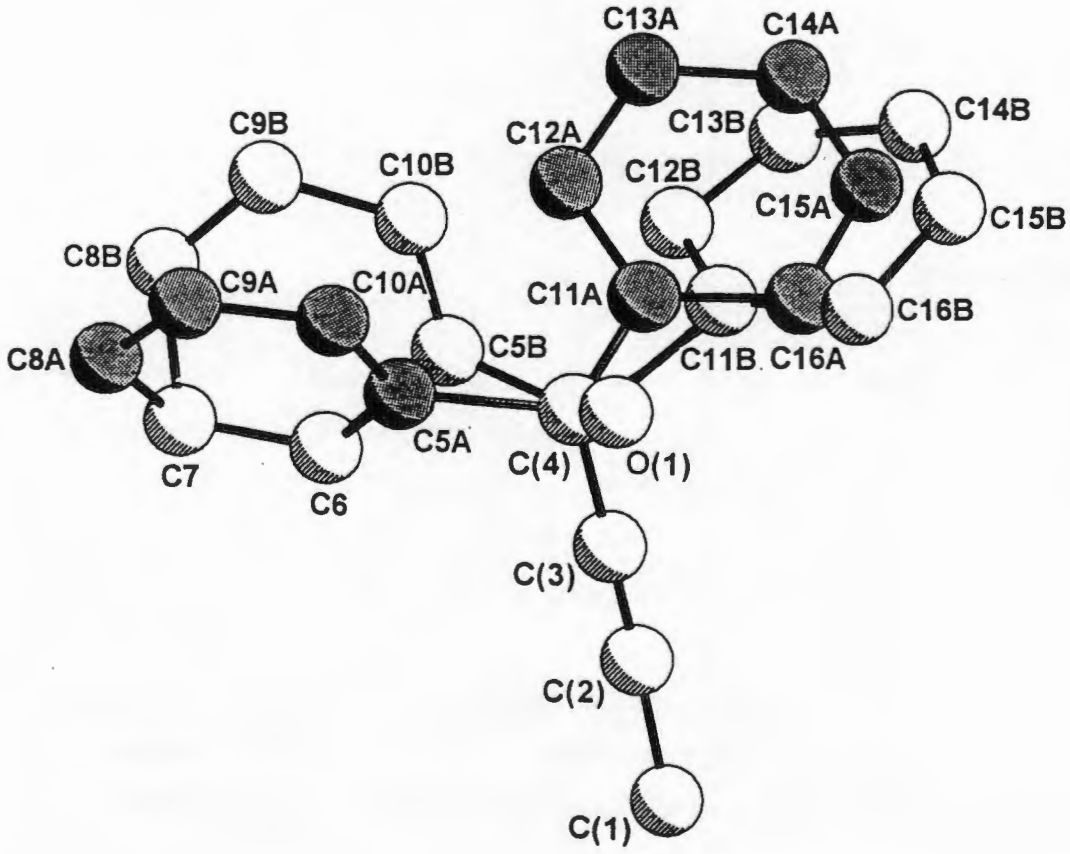

Figure 5.7a : Disorder model for host.

site occupancy factors - A : 0.57(2) B: 0.43(2)

C(3G) - C(4GA) : 1.28(1)Å
C(3G) - C(4GB) : 1.34(2)Å
C(5G) - C(4GA) : 1.72(1)Å
C(5G) - C(4GB) : 1.54(2)Å
C(5G) - C(6GA) : 1.23(2)Å
C(5G) - C(6GB) : 1.18(2)Å

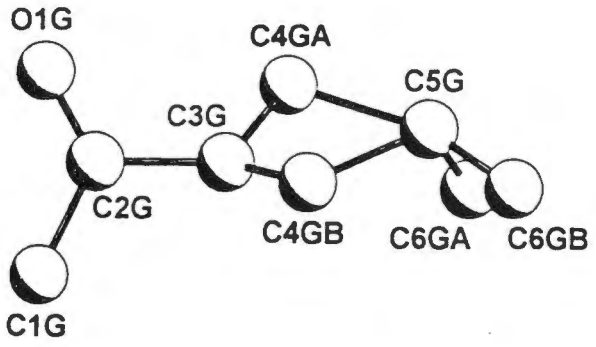

Figure 5.7b : Disorder model for guest G.

site occupancy factors - A : 0.46(1) B : 0.54(1)

C(1JA) - C(2J) : 1.59(1)Å
C(1JB) - C(2J) : 1.62(1)Å
C(3J) - C(4JA) : 1.59(1)Å
C(3J) - C(4JB) : 1.52(1)Å
C(4JA) - C(5JA) : 1.55(2)Å
C(4JB) - C(5JB) : 1.48(2)Å
C(5JA) - C(6J) : 1.56(1)Å
C(5JB) - C(6J) : 1.74(2)Å

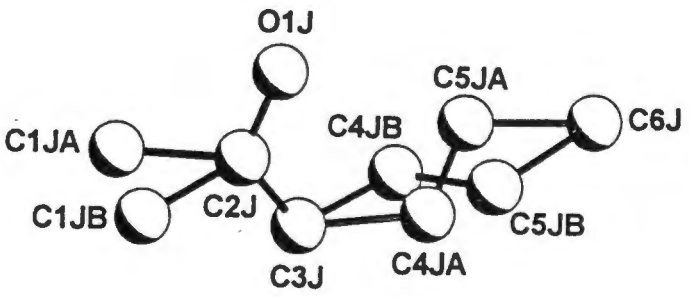

Figure 5.7c : Disorder model for guest J.

Molecular Structure :

The molecular structure of NAP2H is shown in figure 5.8. Guest J is held in position by one hydrogen bond, while guest G is held in position by two, the details of which are given in table 5.2. Figure 5.9 shows the crystal packing in NAP2H. The host molecules pack in layers parallel to [100], with guest J located between adjacent host molecules, above and below the central aromatic region. Guest G is located in the area between the layers of host molecules, in between the interlinking phenyl groups. The guests are located in interconnected cavities centred at x=0.25 and x=0.75 (figure 5.10).

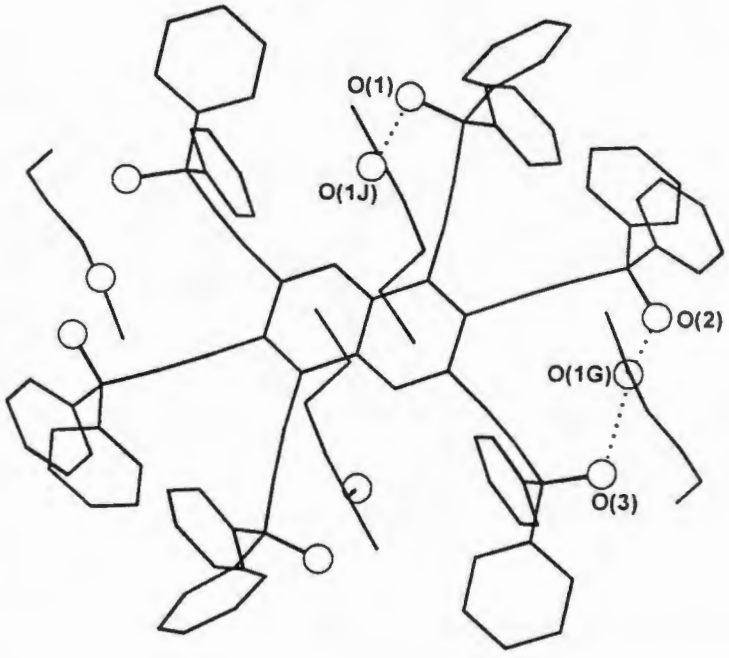

Figure 5.8 : Molecular structure of NAP2H (the hydrogen atoms are omitted and the hydrogen bonds are shown as dotted lines).

Table 5.2 : Hydrogen bond data for NAP2H.

(D)onor	(A)cceptor	D-H (Å)	D...A (Å)	D-H...A (°)
O(1)	O(1J)	0.97(5)	2.797(4)	168(4)
O(2)	O(1G)	0.86(4)	2.845(4)	168(4)
O(3)	O(1G)	0.92(5)	2.827(4)	171(4)

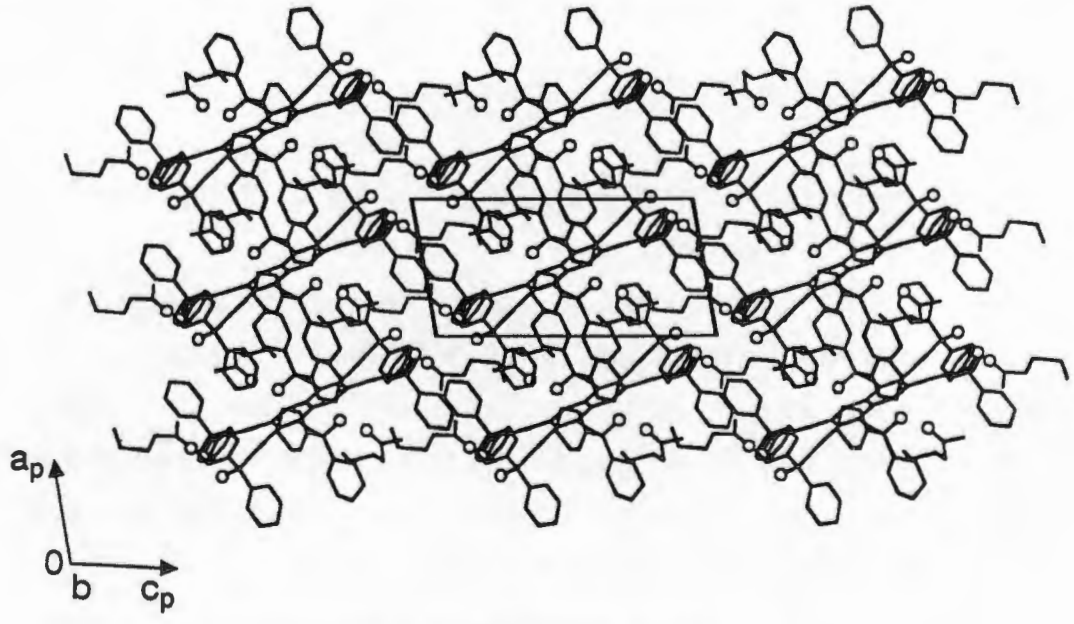

Figure 5.9 : Crystal packing in NAP2H viewed along [010].

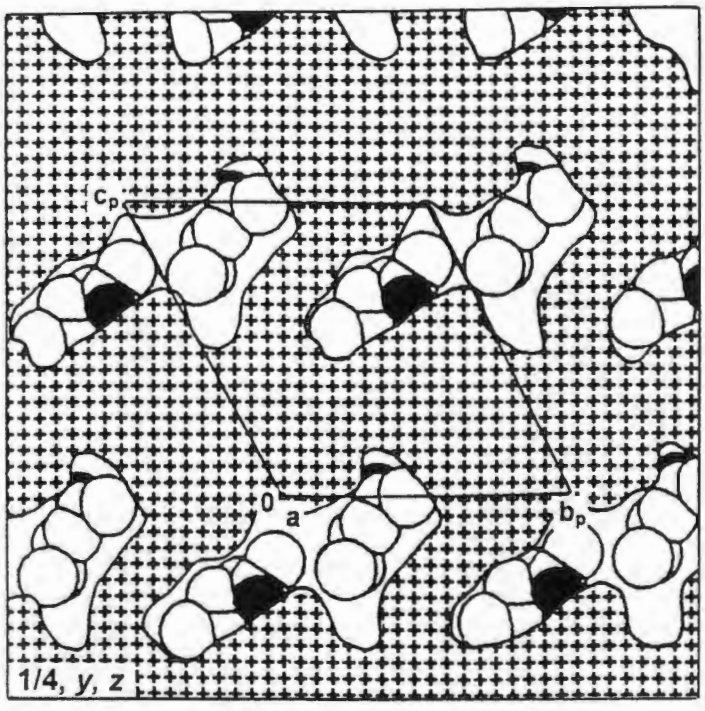

Figure 5.10 : Cross section of NAP2H viewed along [100]. The hatched region is that occupied by the host molecules, and the guests are shown in the cavities (the oxygen atoms are shaded).

Thermal Analysis :

The TG curve shows a rapid single step guest loss reaction, figure 5.11. The mass loss confirms the host to guest ratio of 1:4 modelled in the crystal structure (expected mass loss : 22.7%, observed mass loss : 21.8%). The DSC trace confirms the single step guest loss reaction with an endotherm at 74°C, which is followed by a long step. The trace then shows two endotherms at 234°C and 256°C. The β-phase of NAP2H may desolvate and change phase into that of a polymorph of host **2**, which converts at 234°C into the α-phase of host **2**. The α-phase then melts and decomposes at 256°C. Hotstage microscopy of a single crystal of NAP2H, showed that the crystal became opaque almost instantaneously at 82°C, and then melted with decomposition at 263°C. As for NAPCHO, no evidence of the polymorph was observed.

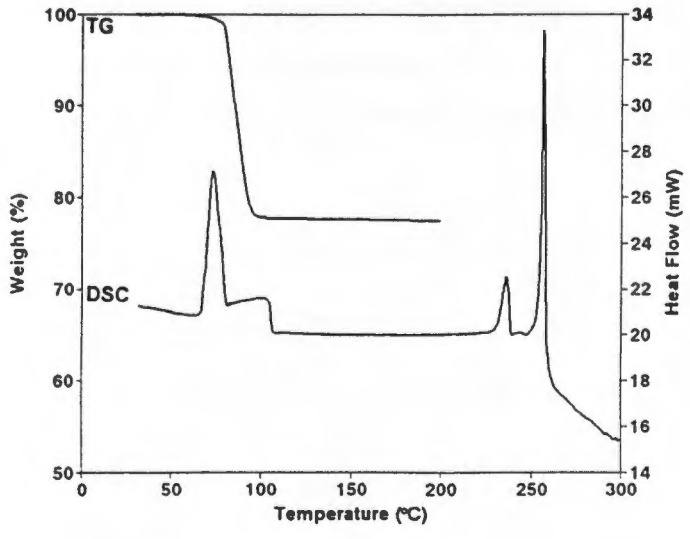

Figure 5.11 : TG and DSC traces of NAP2H.

Kinetics of Desolvation :

Data for the kinetics of desolvation were obtained from isothermal experiments carried out at temperature intervals of 2-3°C over the temperature range of 55-75°C. The shape of all of the α-time curves obtained are similar, thus the system was isokinetic over this temperature range. An example of the α-time curves is shown in figure 5.12. The curves are deceleratory, and the best-fit kinetic model was found to be the first order reaction mechanism, which fits the data over the α-range 0.05-0.95. The semilogarithmic plot of ln *k* *vs.* 1/T, shown in figure 5.13, yields an activation energy of 256(4) $kJ.mol^{-1}$.

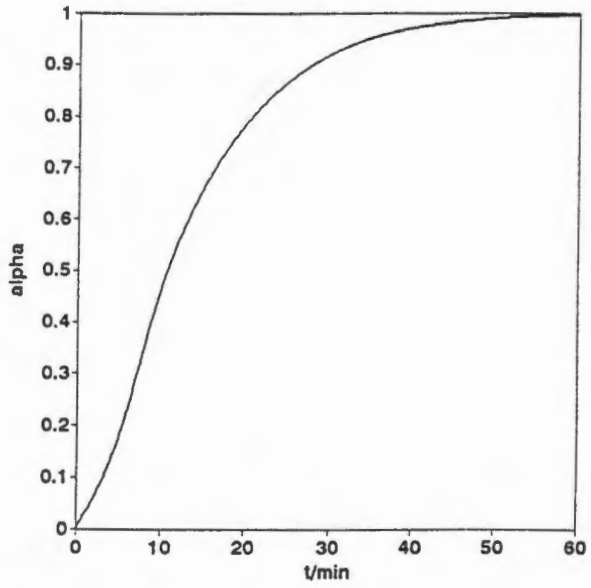

Figure 5.12 : An example of an α vs. time curve obtained for NAP2H.

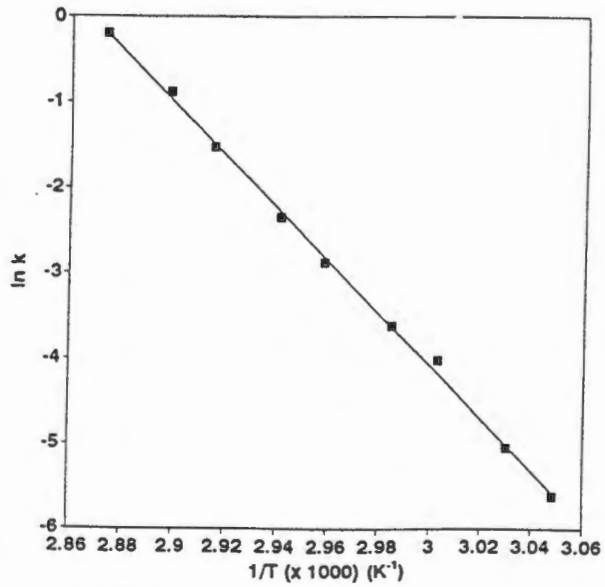

Figure 5.13 : Arrhenius plot for the desolvation of NAP2H.

NAPDMA

$C_{100}H_{68}O_6.6C_4H_9NO$
Guest : dimethyl acetamide
Space Group : P $\bar{1}$

a = 10.637(3)Å	α = 106.71(2)°
b = 15.503(3)Å	β = 100.59(2)°
c = 17.446(5)Å	γ = 92.19(2)°

Volume = 2696(1)Å^3
Z = 1

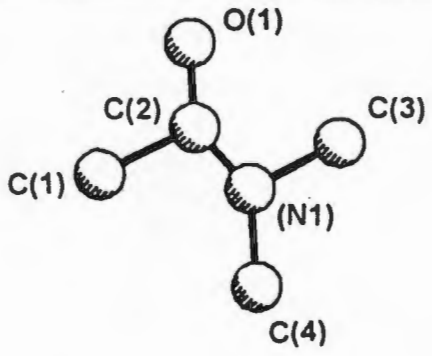

Guests labelled : G, J, K.

Crystal Structure :

The structure of NAPDMA was also refined in the triclinic space group, P $\bar{1}$, with half a host molecule and three guest molecules located in the asymmetric unit.

Refinement :

All of the host molecule non-hydrogen atoms were refined anisotropically. C(39), C(40), C(41) and C(42) had relatively high temperature factors, and a disorder model was attempted, but was unsatisfactory. The hydroxyl hydrogens were not located in the difference electron density maps, and were therefore omitted from the final model. The phenyl hydrogens were placed in geometrically calculated positions and allowed to refine with a common temperature factor (*U* (CH) : 0.106(5)Å^2), except for H(49) which was linked to C(49). The guest oxygens were refined anisotropically, while the carbon and nitrogen atoms were refined isotropically due to their relatively high temperature factors. The guest hydrogen atoms were omitted from the final model.

Both guest J and K required bond length restraints to obtain a reasonable molecular geometry. The distances restrained were : C(2J) - N(1J) : 1.30(3)Å, N(1J) - C(3J) : 1.40(3)Å, N(1J) - C(4J) : 1.40(3)Å, and C(2K) - N(1K) : 1.30(3)Å. The values obtained were 1.08(2)Å, 1.51(2)Å, 1,59(2)Å and 1.19(2)Å. As for SPDMA, the final C(2J)-N(1J) distance was significantly shorter than the expected value for this type of C-N bond. However, it did fall within the range for other reported dimethyl acetamide inclusion structures found in the CSD[1] (figure 4.10, pg. 79).

A residual electron density of $1.22eÅ^{-3}$ is found in the region of guest J. A suitable disorder model incorporating this peak proved to be impossible due to the rigid structure of the dimethyl acetamide molecule. An extinction coefficient of 0.007(3) was applied, and the structure refined to a final $R_1 = 0.1152$.

Molecular Structure :

The molecular structure and hydrogen bonding scheme of NAPDMA is shown in figure 5.14 O(1G) is hydrogen bonded to O(2), O(1J) to O(1) and O(1K) to O(3), and the distances are reported in table 5.3. The host molecules pack in layers parallel to the axes, with the central naphthalene section inclined (figure 5.15). Guest J is located within a cavity centred at *y*=0.5. The cavity is created by the bulky phenyl groups of adjacent host molecules in the (100) plane. Guests G and K are situated in a channel parallel to [101] and centred at *y*=0, clearly shown in figure 5.16.

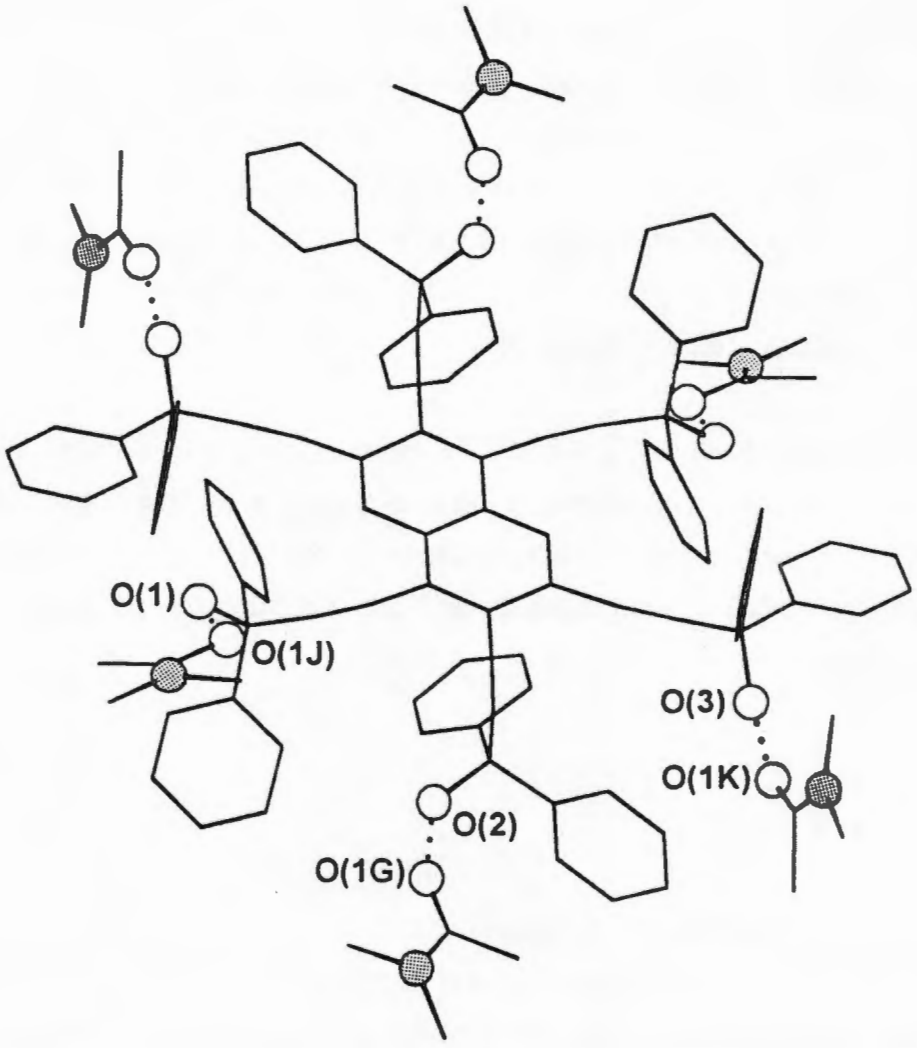

Figure 5.14 : Molecular structure of NAPDMA (hydrogen atoms are omitted and the hydrogen bonds are represented as dotted lines).

Table 5.3 : Hydrogen bond data for NAPDMA.

(D)onor	(A)cceptor	D-A (Å)
O(1)	O(1J)	2.700(8)
O(2)	O(1G)	2.692(8)
O(3)	O(1K)	2.694(9)

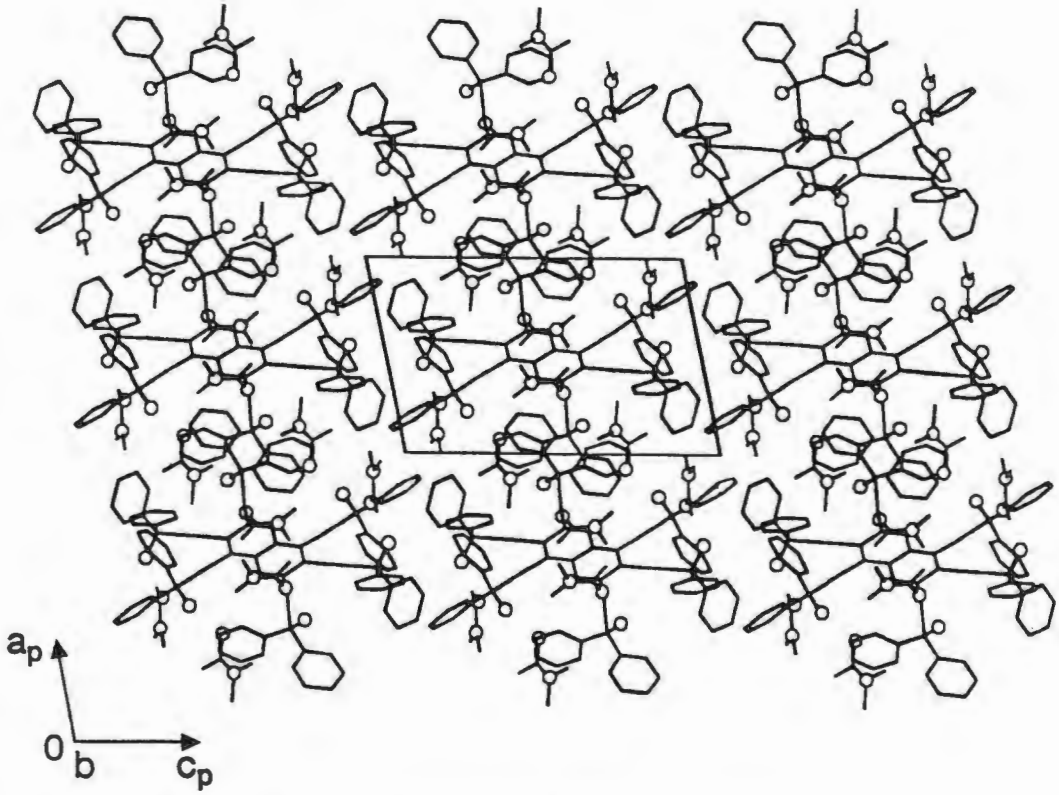

Figure 5.15a : Crystal packing in NAPDMA viewed down [010].

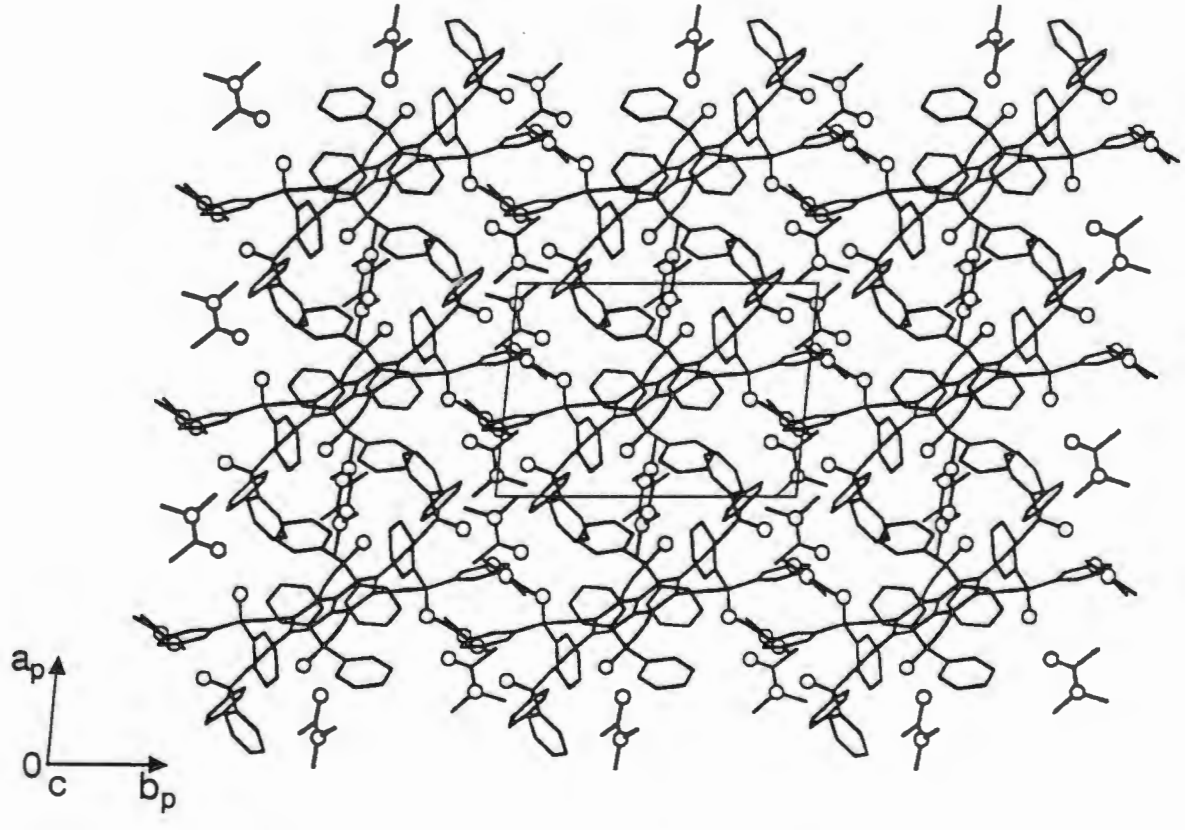

Figure 5.15b : Crystal packing in NAPDMA viewed down [001].

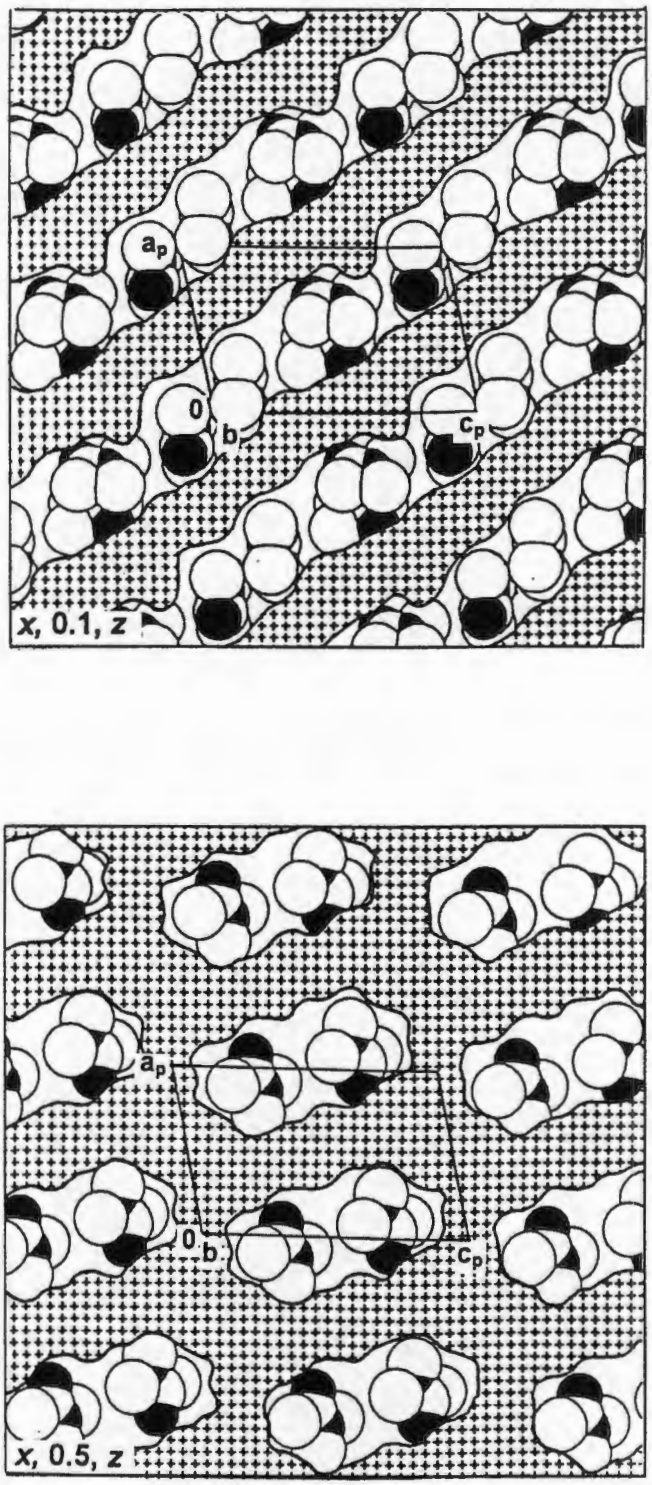

Figure 5.16 : Cross-section of NAPDMA viewed along [010]. The hatched region is that occupied by the host molecules, and the guests G and K are shown in the channels and guest J is located in the cavities (the oxygen and nitrogen atoms are shaded).

Thermal Analysis :

The TG and DSC traces are shown in figure 5.17. The TG curve shows a single step guest loss, and confirms the host to guest ratio of 1:6 that was modelled in the crystal structure (expected mass loss : 27.7%, observed mass loss : 26.9%). The DSC trace shows two endotherms. The first endotherm is at 123°C, which is followed by a small exotherm, probably due to the structural rearrangement of the host molecules. The second endotherm is at 155°C. No endotherm was observed at a higher temperature suggesting that the host must have dissolved in the guest (dimethyl acetamide is not a particularly volatile solvent (b.p. = 163-165°C) and may not have been removed by the purge gas). TG is performed in an open pan, and as a result the dimethyl acetamide is more likely to be removed by the purge gas, so host dissolution is not a complicating step in the desolvation process.

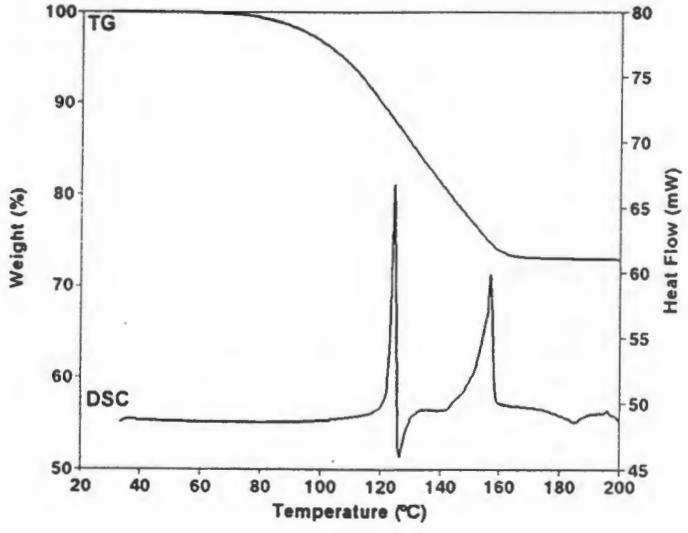

Figure 5.17 : TG and DSC traces for NAPDMA.

Kinetics of Desolvation :

Isothermal TG experiments were carried out over the temperature range 65-80°C, and one of the α-time curves is shown in figure 5.18. The guest loss reaction occurs in a single deceleratory step, and the D3 kinetic model for three dimensional diffusion controlled reactions fitted the data over the largest α-range (0.05-0.95). The semilogarithmic curve of ln *k* *vs.* 1/T yielded an activation energy of 148(5) $kJ.mol^{-1}$ (figure 5.19).

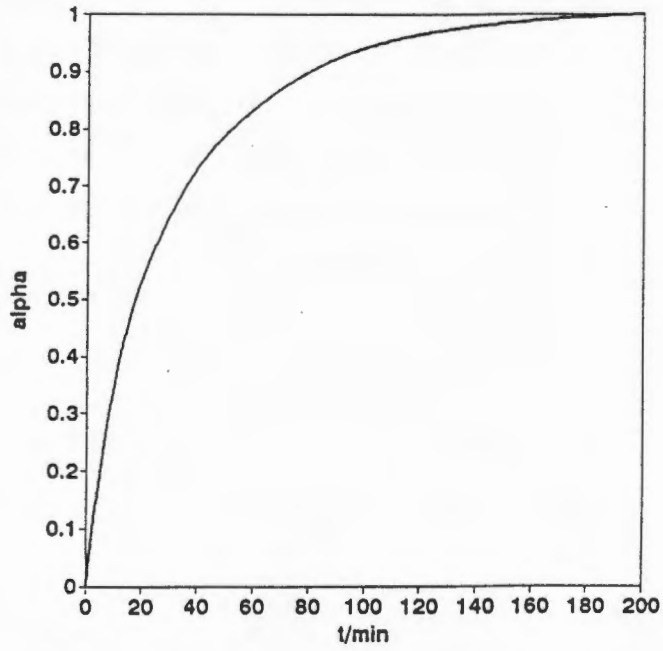

Figure 5.18 : An example of an α vs. time curve obtained for NAPDMA.

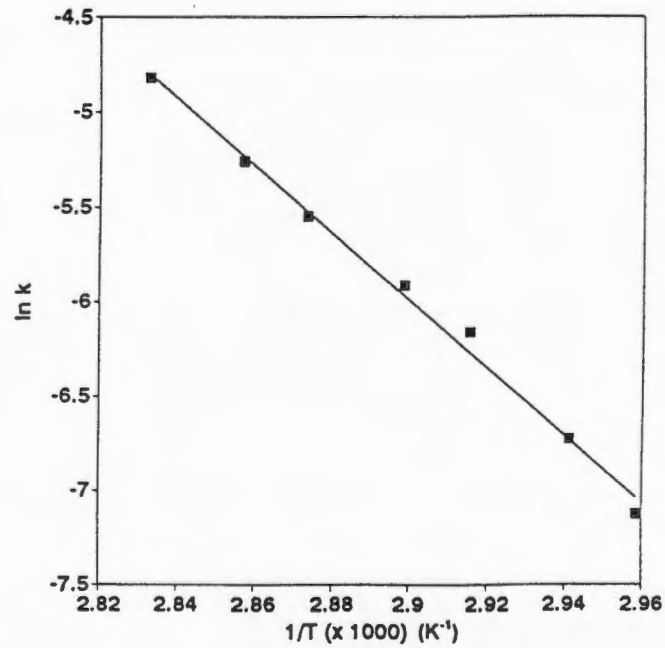

Figure 5.19 : Arrhenius plot for the desolvation of NAPDMA.

NAPDMF

$C_{100}H_{68}O_6.6C3H7NO$	
Guest : dimethyl formamide	
Space Group : P $\bar{1}$	
a = 10.390(6)Å	α = 106.55(2)°
b = 15.641(2)Å	β = 104.35(3)°
c = 17.459(6)Å	γ = 92.98(2)°
Volume = 2612(2)Å^3	
Z = 1	

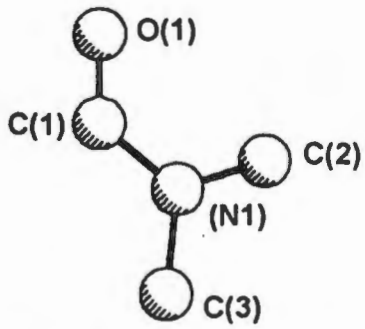

Guests labelled : G, J, K.

Crystal Structure :

The crystal structure of NAPDMF was refined in the space group P $\bar{1}$. NAPDMF and NAPDMA are isostructural in that they have very similar cell dimensions and host framework[2].

Refinement :

All of the non-hydrogen atoms of the host and guest G were refined anisotropically. Some of the phenyl carbon atoms, namely C(15), C(16), C(45), C(46) and C(47), have high temperature factors relative to the other phenyl carbons. A disorder model was attempted for the phenyl rings C(11)-C(16) and C(43)-C(48), but this resulted in poor geometry of the rings and was, therefore, not applied. The hydroxyl hydrogens were located in the difference electron density maps and refined isotropically. The host phenyl hydrogens were placed in geometrically calculated positions and refined with a common temperature factor (U (CH) : 0.098(4)Å^2), except for H(49), which was refined independently (U (CH) : 0.04(1)Å^2). Both the oxygen and nitrogen

atoms of guest J were refined anisotropically. The carbon atoms of guest J and all the non-hydrogen atoms of guest K were refined isotropically due to their relatively high temperature factors. All of the guest hydrogen atoms were omitted from the final model. Although the maximum peak height in the final electron density map was 1.11eÅ^{-3}, this was very close to guest K. This peak could not be modelled sensibly, and as a result is ascribed to an imperfect model of guest K. The structure refined to a final R_1 = 0.0945.

Molecular Structure :

The molecular structure of NAPDMF is shown in figure 5.20, and the hydrogen bond data is reported in table 5.4. NAPDMF and NAPDMA are isostructural. The host framework and position of the guest molecules are almost identical. The host molecules pack in layers parallel to the axes, as shown in figure 5.21. Guest G is located within cavities centred at *y*=0.5, while guests J and K are located with in channels parallel to [101] and centred at *y*=0.

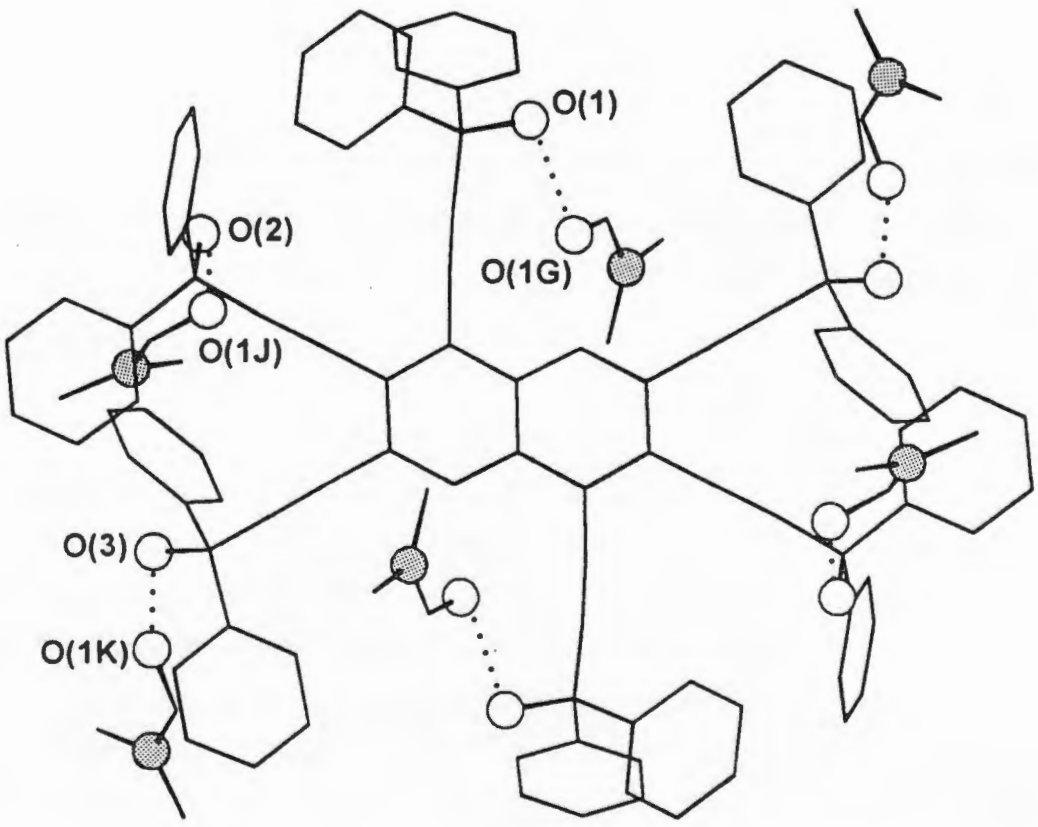

Figure 5.20 : Molecular structure for NAPDMF (hydrogen atoms are omitted and the hydrogen bonds are represented as dotted lines).

Table 5.4 : Hydrogen bond data for NAPDMF.

(D)onor	(A)cceptor	D-H (Å)	D...A (Å)	D-H...A (°)
O(1)	O(1G)	0.83(7)	2.696(6)	161(7)
O(2)	O(1J)	0.90(5)	2.732(6)	165(4)
O(3)	O(1K)	0.84(5)	2.712(8)	153(5)

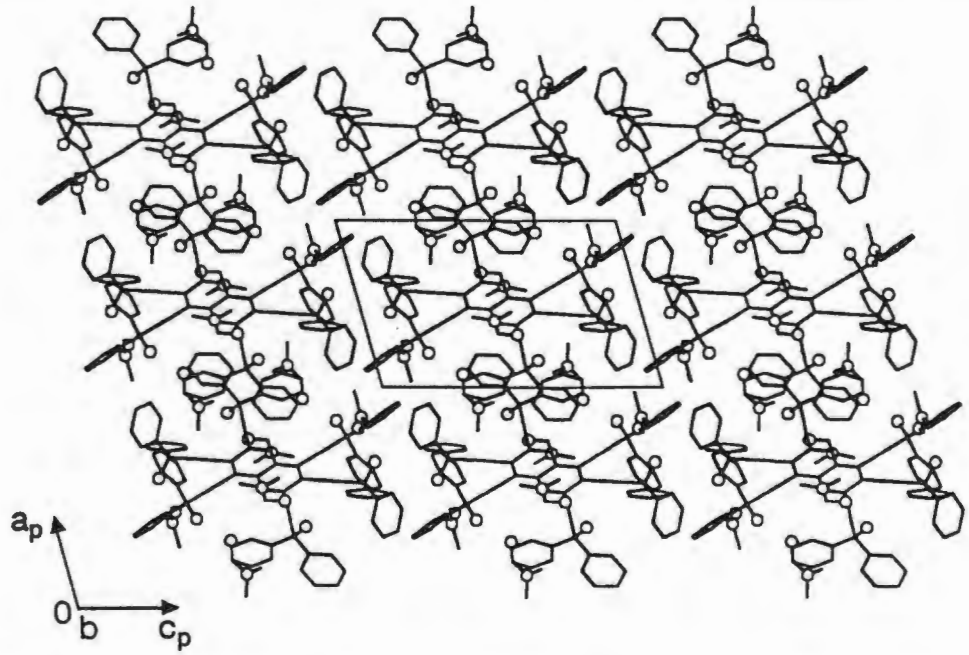

Figure 5.21a : Crystal packing in NAPDMF, viewed along [010].

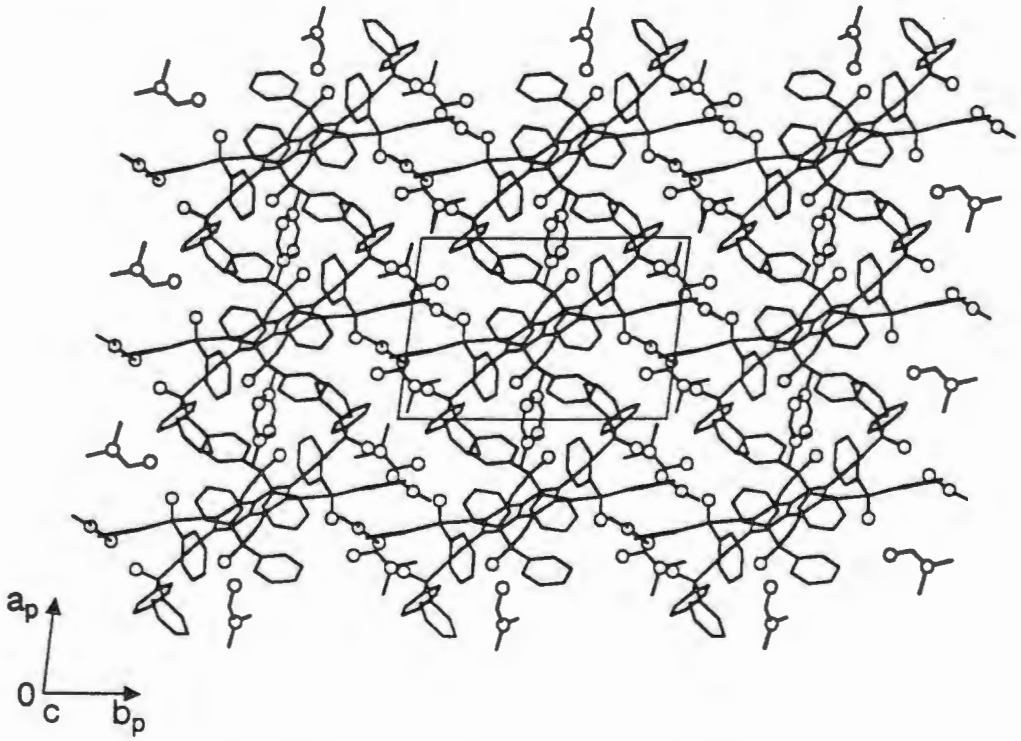

Figure 5.21b : Crystal packing in NAPDMF, viewed along [001].

Thermal Analysis :

The thermograms of NAPDMF are shown in figure 5.22.

NAPDMF is a particularly unstable inclusion compound. The crystals of NAPDMF begin to crack and desolvate seconds after being removed from the mother liquor, (figure 5.23). On TG analysis, the crystals were rapidly removed from the mother liquor, blotted dry and placed in the sample holder. The TG experiment was started immediately. The resultant mass loss was not a smooth single step mass loss, as for NAPDMA, but a multiple step guest loss, where the steps are not clearly defined. The mass loss confirmed the host to guest ratio modelled in the crystal structure (expected mass loss : 24.3%, observed mass loss : 24.8%). The DSC trace is complicated showing a number of endotherms. The first is at *ca* 92°C followed by a smaller second endotherm at *ca* 106°C, due to guest loss. These peaks are followed by a much larger and sharper one, with an onset temperature of *ca* 146°C, possibly due to the collapse of the β-phase to a non-porous polymorph of host **2**, which melts at 238°C and recrystallises. Host **2** then melts again with decomposition at 251°C.

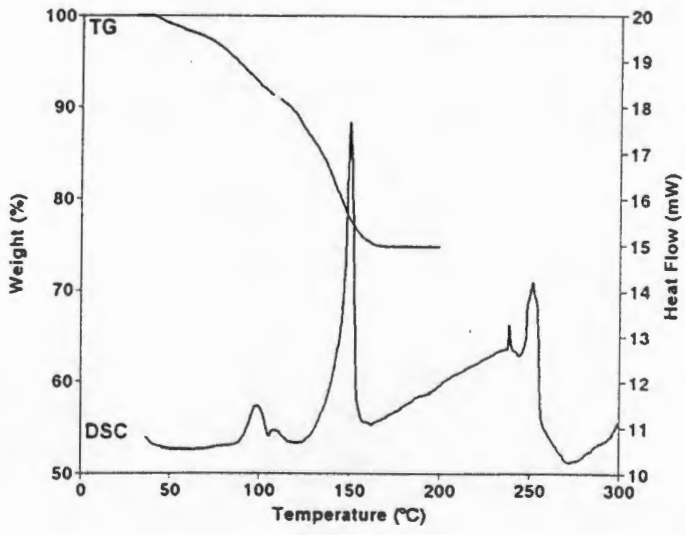

Figure 5.22 : TG and DSC traces of NAPDMF.

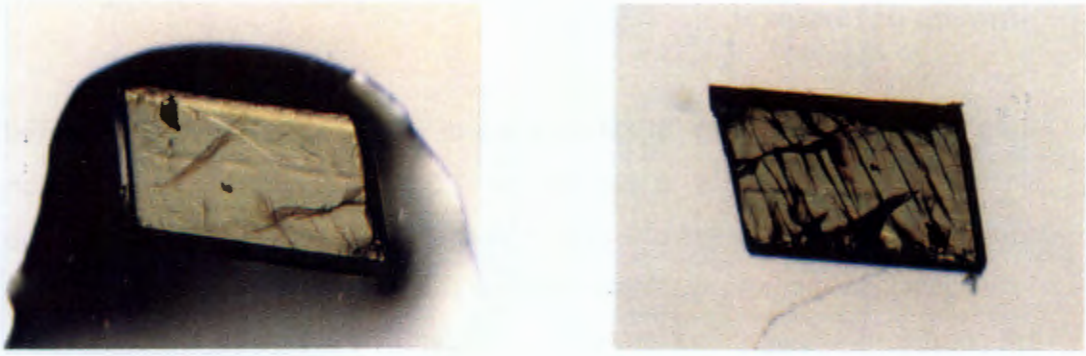

(a) in mother liquor (b) 1 minute later

Figure 5.22 : NAPDMF crystal: (magnification : 40X).

Figure 5.24 shows a series of photographs of the thermal decay of a single crystal of NAPDMF, immersed in a drop of silicon oil, and heated at $10°.min^{-1}$. The crystal begins to fracture at room temperature. At 86°C, the crystal starts to desolvate at the surface defects and along the fractures, and at 103°C a few small bubbles (the guest) are released from the crystal. At 158°C the crystal suddenly recrystallises, confirming that the large sharp endotherm observed at 146°C in the DSC trace is probably due to the structural collapse of the β-phase. The crystal then begins to discolour at 234°C, partial melting is observed at 245°C, and at 268°C the crystal finally melts and decomposes.

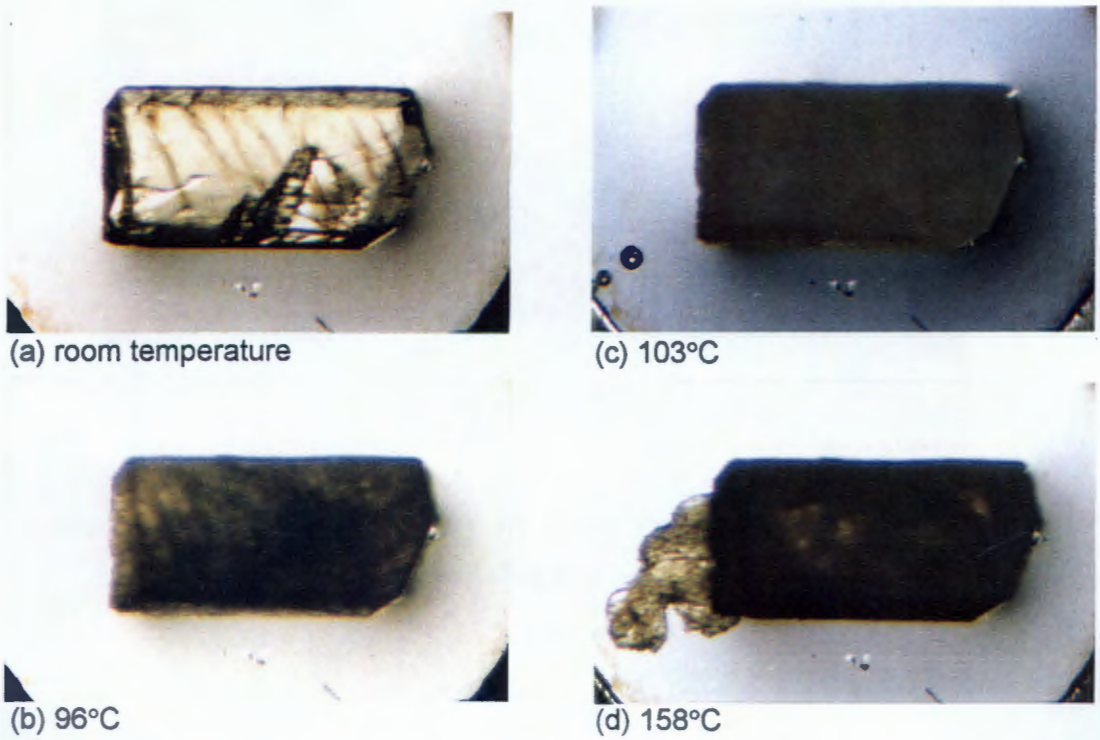

(a) room temperature (c) 103°C

(b) 96°C (d) 158°C

Figure 5.24 : Thermal decay of a single crystal of NAPDMF (magnification : 30X).

Kinetics of Desolvation :

Unfortunately the kinetics of desolvation of NAPDMF was not determined since all future attempts to regrow the 1:6 dimethyl formamide inclusion compound were unsuccessful. The original conditions of crystallisation of the 1:6 inclusion compound were repeated as closely as possible. Changes in the conditions of crystallisation, such as different cooling rates and different starting concentrations, were also tried. On all occasions, a more stable 1:4 inclusion compound was obtained. This crystal structure has not been determined since only needle-like crystals, less than 0.1mm thick, have been grown (figure 5.25). On preparation of a powdered sample, the 1:4 inclusion compound was also obtained. This problem is not unknown, there are numerous reports of laboratories around the world being unable to regrow a particular polymorph once another was grown.[3]

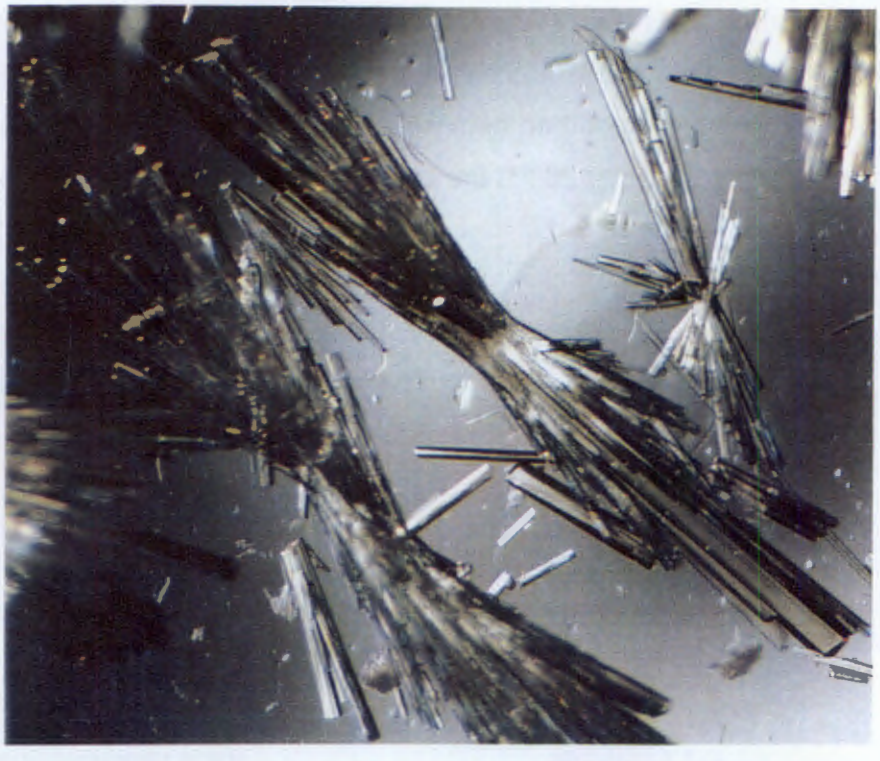

Figure 5.25 : Needle-like crystals of the 1:4 dimethyl formamide inclusion compound (magnification : 50X).

DISCUSSION

The hexapedal host, hexakis(3-hydroxy-3,3-diphenyl-2-propynyl)naphthalene (host **2**), forms inclusion compounds with a number of small, volatile organic solvents. In order for the solvent to be included on crystallisation, a suitable functional group which can act as a possible hydrogen bond acceptor, is required. The host to guest ratios were found to be either 1:4 or 1:6, which is considerably richer in guest than is usually observed for organic host compounds. As for host **1**, the non-porous α-phase of host **2** was obtained on crystallization from benzene. Unfortunately however, single crystals suitable for X-ray diffraction were not obtained during the course of this study.

The structures of four inclusion compounds of host **2** have been reported above. All the X-ray diffraction data were collected at low temperature, in order to minimise the predicted high thermal motion of the atoms. The data for NAPCHO was collected at 248K, using the FTS Systems Air Jet refrigeration unit, while the data for the next three structures were collected later, and done at 223K using an Oxford Cryostream cooler. All four structures refined well. For NAPCHO, NAPDMA and NAPDMF possible disorder was observed in the region of the guests, but could not be modelled satisfactorily. NAP2H was harder to model, since both the host and guests were found to be disordered. The disorder of the guest molecules, and the two phenyl rings, C(5)-C(10) and C(11)-C(16), was modelled successfully.

All four structures are stabilised by hydrogen bonding. Direct host-guest hydrogen bonding was expected in the 1:6 structures, yet was only observed for NAPDMA and NAPDMF. In NAPCHO, guest J is held in position by a direct hydrogen bond, guest G is held in position by a co-operative hydrogen bond, while guest K does not appear to be involved in any hydrogen bonding scheme, and is held in position by van der Waals forces. 2-Hexanone is a much longer guest molecule than the other guest molecules investigated. NAP2H has a 1:4 host to guest ratio, with guest G held in position by two hydrogen bonds and guest J, by one. All of the hydrogen bond interactions are either of weak (>2.80Å) or medium strength (2.65-2.80Å)[4].

Figure 5.26 shows the packing motif of each of the above structures, viewed parallel to the plane of the central aromatic region. Since NAPDMA and NAPDMF are isostructural, their packing motifs are the same. However, different packing motifs are observed for NAPCHO, NAP2H and NAPDMA, clearly indicating the adaptability of host 2 to accommodate different guest molecules. The host molecules in NAPCHO are stacked one on top of each other, with adjacent columns of host molecules staggered with respect to each other. In NAP2H, the host molecules are all staggered with respect to each other, while in NAPDMA and NAPDMF, the host molecules pack almost in layers parallel to the central naphthalene ring. These layers are staggered with respect to each other.

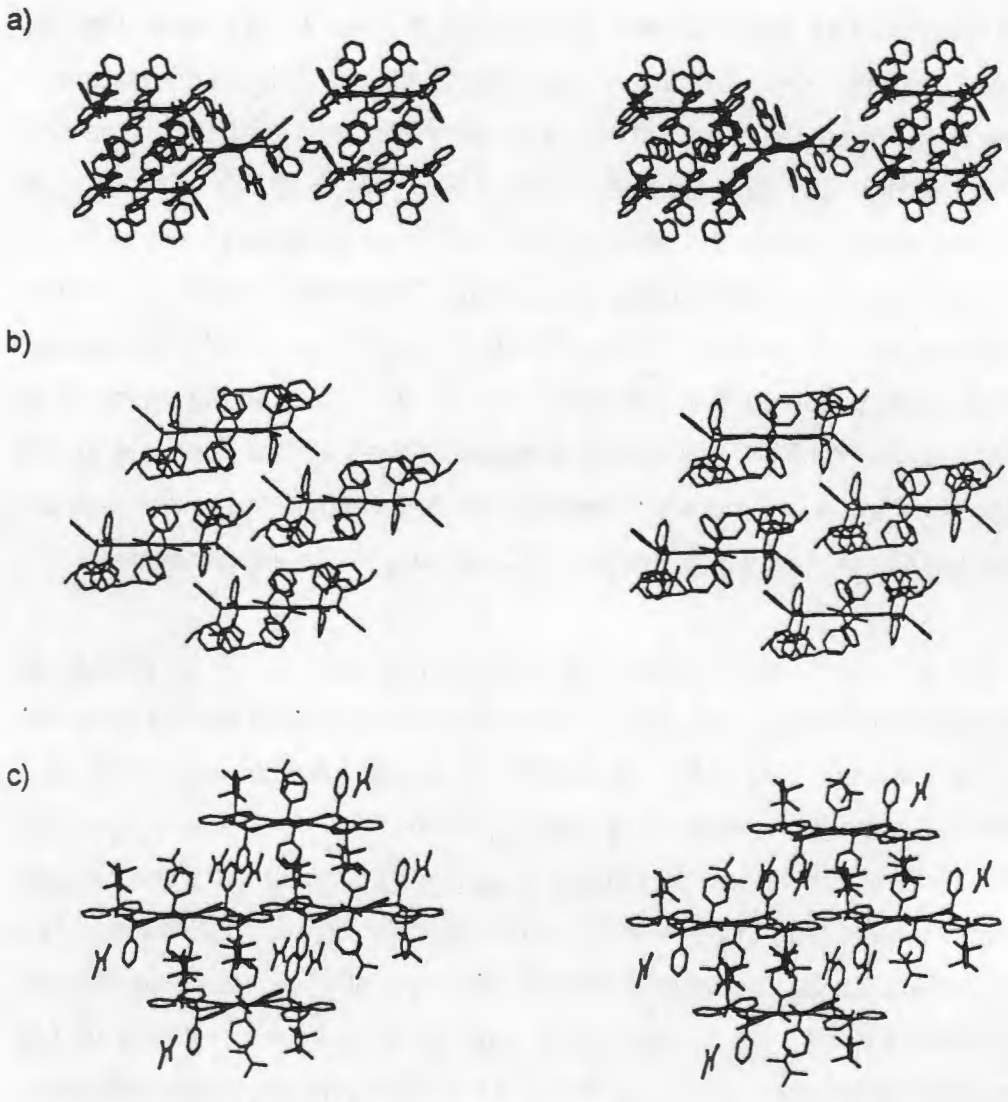

Figure 5.26 : Packing motifs of a) NAPCHO, b) NAP2H, c) NAPDMA, viewed parallel to the central naphthalene ring.

The kinetics of desolvation for NAP2H and NAPDMA were determined (table 5.5). The desolvation reactions were found to be deceleratory. NAP2H follows the first order (F1) reaction mechanism, while NAPDMA follows the three dimensional diffusion controlled (D3) mechanism. The activation energy obtained for NAP2H is significantly higher than that for NAPDMA. In NAP2H the guests are located within cavities, whereas in NAPDMA they are located within channels and cavities, suggesting that NAP2H is the more stable inclusion compound, and thereby confirming the higher activation energy.

Table 5.5 : Kinetic data for host **2** inclusion compounds.

Compound	Inclusion mode	T_{on} (°C)	T_b (°C)	T_{on}-T_b (°C)	T-range (°C)	E_a (kJ.mol^{-1})	Reaction mechanism
NAPDMA	channels/ cavities	123	164	-41	65-80	148(5)	D3
NAP2H	cavities	74	128	-54	55-75	256(4)	F1

HOST CONFORMATION

Host **2** is a very large, awkward molecule, with a large number of possible conformations. Like host **1**, host **2** has a high degree of rotational freedom of the bulky end phenyl groups relative to the central aromatic region, and relative to each other. By altering its conformation slightly, host **2** is able to accommodate a number of different guest molecules within its framework. Therefore, the main aspect of the conformation of host **2** which needs to be considered involves the orientation of the phenyl rings relative to the central aromatic region. This can be defined by the torsion angles indicated in the scheme below. The labelling of the host molecule in each structure, although carried out cyclically, was initially done arbitrarily. As a result it is not possible to compare the torsion angles obtained directly, so for each 'leg', τ_1 will define the smallest torsion angle, and τ_3 will define the smaller of the two angles observed for the second phenyl ring. For NAP2H, the host conformation will be analysed with the dominating component of the disorder model.

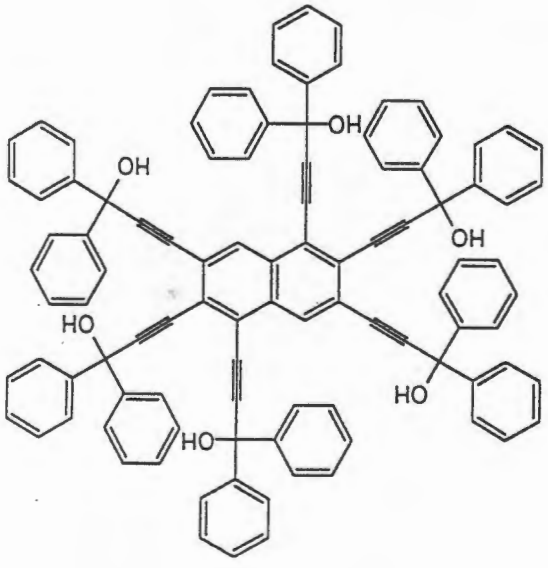

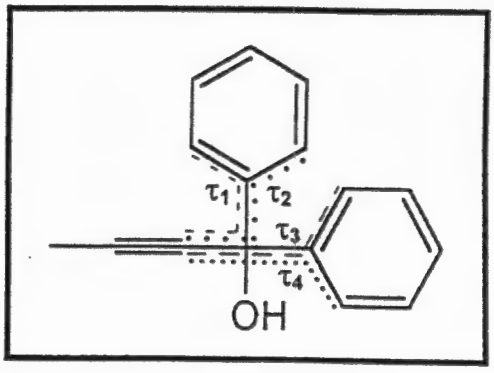

A wide range of torsion angles is observed, only for NAPDMA are all four torsion angles similar for each of the 'legs'. Table 5.6 reports the torsion angles for each of the structures.

Table 5.6 : Torsion angles defining the conformation of host **2**.

Compound	τ_1	τ_2	τ_3	τ_4
NAPCHO	9(1)	-171.5(7)	51(1)	-127.1(9)
	15.5(9)	-165.5(6)	-51.7(9)	130.1(7)
	3.3(9)	-177.5(6)	-46.8(8)	133.8(7)
NAP2H	-35.5(6)	148.4(5)	-59.2(9)	121.6(7)
	-29.1(5)	152.2(3)	62.8(4)	-115.8(4)
	-13.5(4)	167.7(3)	-48.4(4)	134.0(3)
NAPDMA	9.5(8)	-173.2(5)	-81.2(7)	99.1(8)
	3.4(8)	-176.1(5)	-68.1(7)	112.5(6)
	2(1)	-176.1(7)	-81.1(8)	95.3(8)
NAPDMF	8.3(6)	-172.7(4)	-83.5(5)	94.0(8)
	-6.0(6)	178.5(4)	-72.7(5)	104.4(5)
	69.3(6)	-116.0(6)	-74.3(6)	100.2(5)

In all four structures the central naphthalene ring can be considered planar, the maximum deviations from the least squares planes are all below 0.02Å. All the phenyl rings, can also be considered planar, with the maximum deviations also being less than 0.02Å. In the asymmetric unit, the angle between the planes of the phenyl rings for NAPDMA and NAPDMF are similar for all three 'legs', while for NAPCHO and NAP2H, the angle between the planes of the phenyl rings on the second 'leg' is notably smaller than the angle observed for the other two legs, which were almost the same. The angles between the planes of the phenyl rings for all four structures are tabulated in table 5.7.

Table 5.7 : Angle between the planes of the phenyl rings on each 'leg' of host **2**.

Angle between	NAPCHO (°)	NAP2H (°)	NAPDMA (°)	NAPDMF (°)
C(5)-C(10)/C(11)-C(16)	85.7(3)	87.4(2)	83.4(2)	85.2(2)
C(21)-C(26)/C(27)-C(32)	75.0(3)	72.7(2)	88.0(3)	86.9(2)
C(37)-C(42)/C(43)-C(48)	84.6(2)	89.8(1)	84.2(3)	86.6(2)

The conformation of host **2** can also be described by the position of the hydroxyl groups. The torsion angles defining the positions of the hydroxyl groups relative to the central naphthalene ring are shown in the scheme below, and are tabulated in table 5.8. As for host **1**, the orientation of the hydroxyl groups relative to the central aromatic region can be defined as either up (*u*) or down (*d*). Although this *u-d* nomenclature is simplistic, since the torsion angles are variable, it is still useful in describing the host comformation. If one of the naphthyl rings is considered, the position of the hydroxyl groups can be defined relative to the ring as being *uuu* (for NAPDMA and NAPDMF) or *uud* (for NAPCHO and NAP2H). Due to symmetry, the reverse situation is observed for the other napthyl ring.

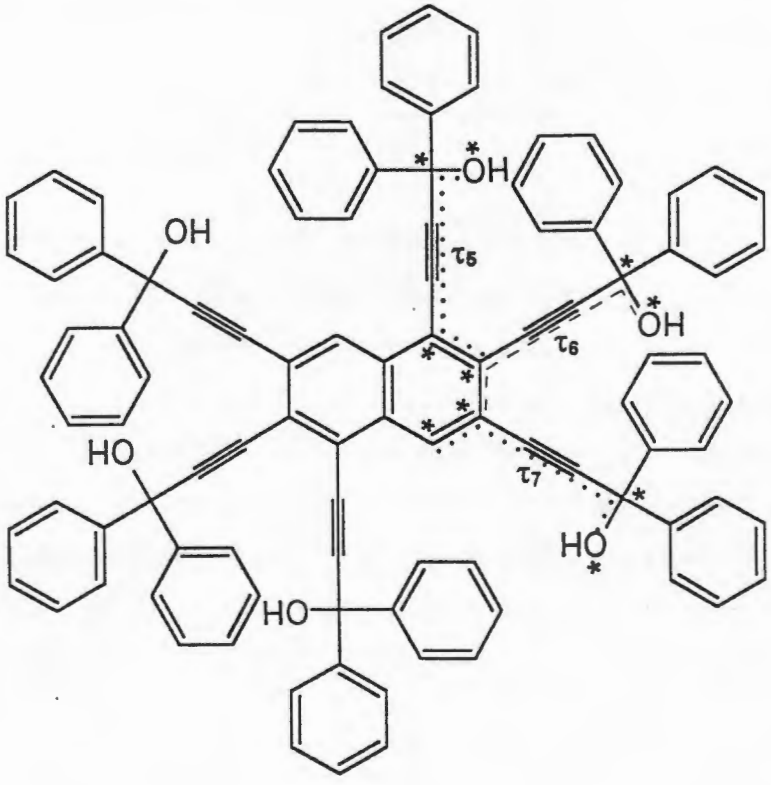

Table 5.8 : Torsion angles defining the position of the hydroxyl groups relative to the central naphthalene ring.

Torsion angles (°)	NAPCHO	NAP2H	NAPDMA	NAPDMF
τ_5	48.0(7)	-163.0(3)	-164.9(5)	-165.8(4)
τ_6	22.2(6)	9.8(3)	-145.5(5)	-147.1(3)
τ_7	-159.0(6)	156.8(3)	-135.6(5)	-132.4(4)

The different bond types observed in host **2** are indicated in the scheme below, and the bond length ranges observed in each structure are summarised in table 5.9. All the bond lengths and angles are comparable with known values[5], with the exception of the bonds related to the disorder of the phenyl rings on the one 'leg' of the host in NAP2H. In the naphthalene ring, the bond lengths between the carbons with a 'leg' bonded to them, C(1)-C(17) and C(17)-C(33), are noticeably longer than the remaining bonds in the naphthalene ring. Presumably these bonds are longer in order to maximise the space between the adjacent 'legs'.

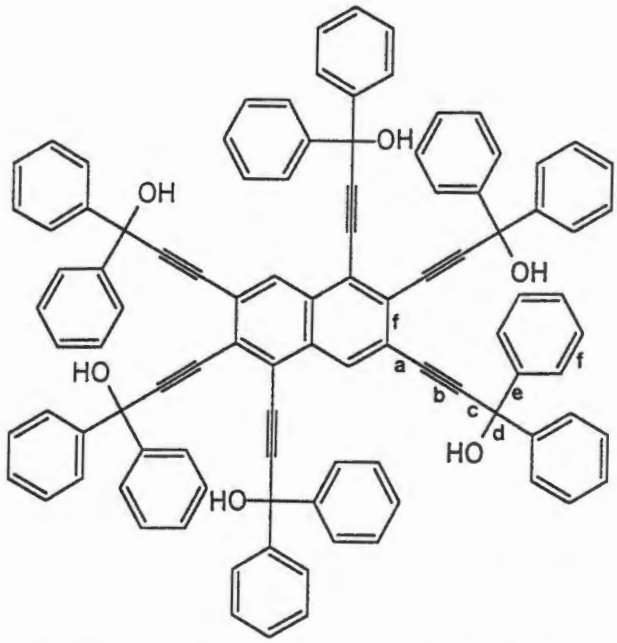

Table 5.9 : Bond length ranges for host 2 (bond lengths in angstroms).

Bond		NAPCHO	NAP2H	NAPDMA	NAPDMF	Ref 5 (median)
a = C_{ar} - C_{sp}	min	1.429(9)	1.425(4)	1.422(7)	1.430(5)	1.43(1)
	max	1.434(9)	1.438(4)	1.435(7)	1.436(6)	
b = C ≡ C	min	1.181(9)	1.193(4)	1.189(7)	1.189(6)	1.19(1)
	max	1.193(9)	1.204(4)	1.194(7)	1.194(5)	
c = C_{sp} - C_{sp}^3	min	1.476(9)	1.476(4)	1.476(7)	1.481(6)	1.47(1)
	max	1.481(9)	1.481(7)	1.488(8)	1.488(6)	
d = C_{sp}^3 - O	min	1.431(9)	1.429(4)	1.427(7)	1.413(5)	1.43(1)
	max	1.449(7)	1.430(4)	1.440(6)	1.429(5)	
e = C_{sp}^3 - C_{ar}	min	1.51(1)	1.39(1)	1.514(8)	1.522(7)	1.53(2)
	max	1.54(1)	1.79(1)	1.540(9)	1.533(8)	
f = C_{ar} ≃ C_{ar}	min	1.32(2)	1.26(1)	1.30(2)	1.33(1)	1.38(1)
	max	1.41(1)	1.55(2)	1.39(1)	1.396(8)	
f = C_{ar} ≃ C_{ar}	min	1.371(9)	1.372(4)	1.368(7)	1.372(5)	1.36(1) to
(naphthalene)	max	1.438(9)	1.432(4)	1.441(7)	1.434(5)	1.42(1)

REFERENCES

1. Cambridge Structural Database and Cambridge Structural Database System, Version 5.12, Cambridge Crystallographic Data Centre, University Chemical Laboratory, Cambridge, England.
2. A. Kálmán, L. Parkanyi, G. Argay, *Acta Crystallogr.*, 1993, **B49**, 1039.
3. J. D. Dunitz, J. Bernstein, *Acc. Chem. Res.*, 1995, **28**, 193.
4. P. Gilli, V. Bertolasi, V. Ferretti, G. Gilli, *J. Am. Chem. Soc.*, 1994, **116**, 909.
5. F. H. Allen, O. Kennard, D. G. Watson, L. Brammer, A. G. Orpen, R. Taylor, *J. Chem. Soc., Perkin Trans. 2*, 1987, S1.

CHAPTER 6

HOST 3 AND ITS INCLUSION COMPOUNDS.

The α-phase and two inclusion compounds formed by host **3** have been investigated in this study. They will be discussed in terms of crystal structure (refinement and molecular structure), and thermal analysis. For ETHDMA, the kinetics of desolvation have been determined, and will also be discussed in this chapter. The molecular formula, space group and cell parameters are summarised at the beginning of the discussion of each compound.

All three structures were refined in the triclinic space group P $\bar{1}$. Preliminary oscillation and Weissenberg photography established the unit cell parameters and crystal system (triclinic). The space group P $\bar{1}$ was chosen based on the mean $|E^2-1|$ values for the 0kl, h0l, hk0 projections, as well as for the remainder of the reflections, all of which were close to the theoretical value of 0.968. The choice of P $\bar{1}$ was further justified by the successful refinement of these structures.

The atomic labelling scheme for host **3** can be seen in Figure 6.1. For ETHBN and ETHDMA half the host was located in the asymmetric unit. For ETHCHO, the host molecule was not located on a centre of inversion, and a whole host molecule was found in the asymmetric unit. The atomic labelling scheme used for the guests is shown at the beginning of the discussion of each structure. The guest molecules were labelled with a suffix G, J, K or L.

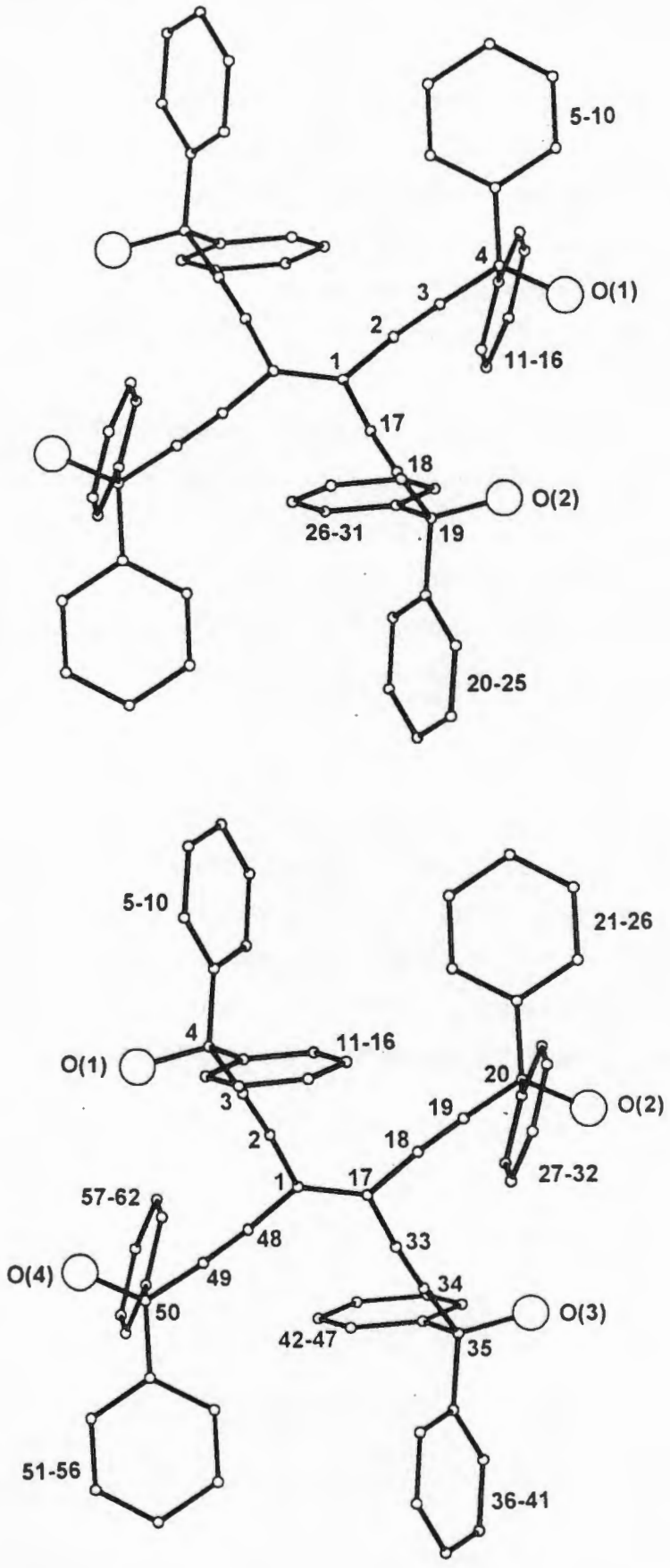

Figure 6.1 : Atomic labelling scheme used for host **3**.

ETHBN

$C_{62}H_{44}O_4$ (Host **3**)	
Space Group : P $\bar{1}$	
a = 8.936(2)Å	α = 110.88(2)°
b = 10.619(3)Å	β = 89.96(2)°
c = 14.271(2)Å	γ = 111.35(2)°
Volume = 1165.4(5)Å^3	
Z = 1	

The α-phase of host **3** was obtained on crystallisation from benzene. Later, it was also obtained on crystallisation of host **3** from 2-hexanone.

Crystal Structure :

The host molecules are located on a centre of inversion, resulting in half a host molecule in the asymmetric unit.

Refinement :

All the non-hydrogen atoms were refined anisotropically. The hydroxyl hydrogens were located in the difference electron density map, and refined isotropically. The phenyl hydrogens were placed in geometrically calculated positions linked to a common temperature factor (U (CH) : 0.085(2)Å^2). The structure refined to a final R_1 = 0.0445.

Molecular Structure :

A stereoview of the molecular structure of ETHBN is shown in figure 6.2. The host molecules pack in layers, with the central ethylene bond parallel to [010] (figure 6.3). Intermolecular hydrogen bonds linking adjacent host molecules within each of the layers parallel to [010] are observed, showing that the bulky phenyl groups do not prevent interaction between the hydroxyl groups. The hydrogen bonding details are reported in table 6.1.

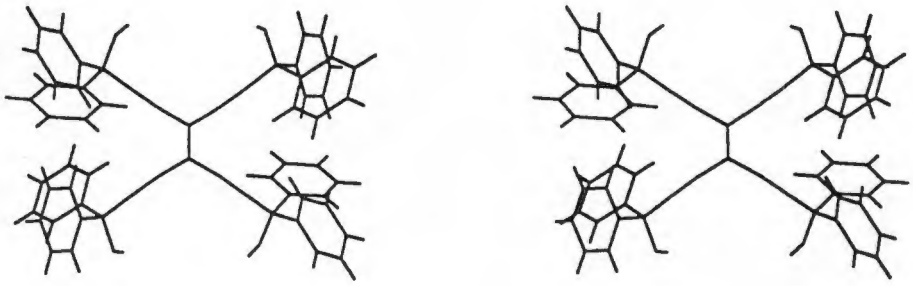

Figure 6.2 : Stereoview of the molecular structure of ETHBN.

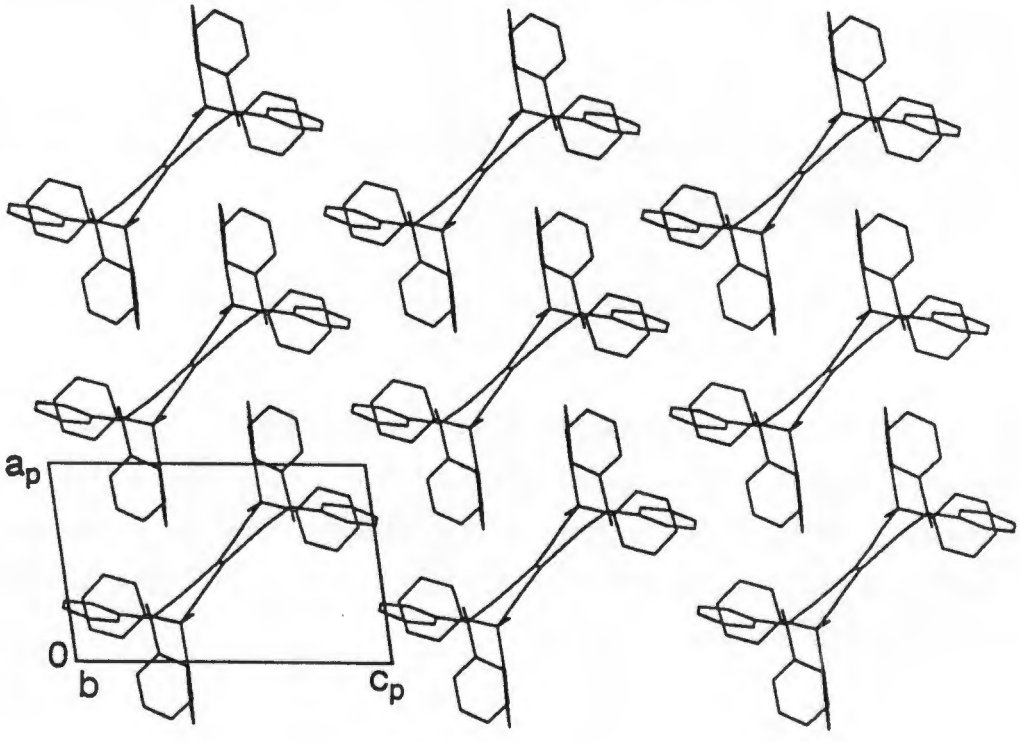

Figure 6.3a : Crystal packing in ETHBN, viewed down [010].

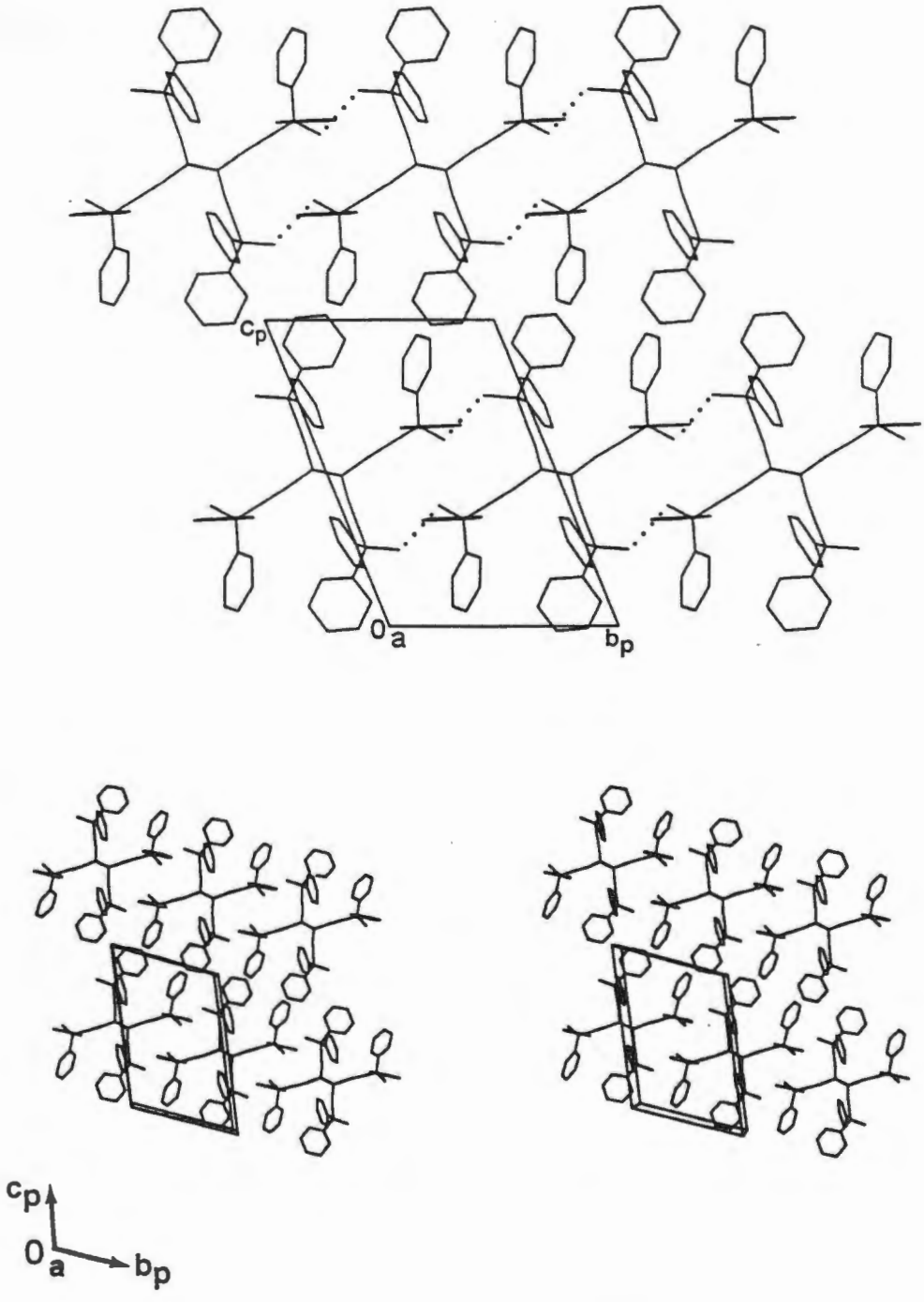

Figure 6.3b : Crystal packing in ETHBN viewed down [100] (the hydrogen bonds are represented as dotted lines).

Table 6.1 : Intermolecular hydrogen bonding details of ETHBN.

(D)onor	(A)cceptor	D-H (Å)	D...A (Å)	D-H...A (°)
O(2)	O(1)[a]	0.92(3)	2.899(2)	165(3)

a : 1-*x*, 1-*y*, 1-*z*

Thermal Analysis :

On TG analysis, no mass loss was observed. The DSC trace shows a single sharp endotherm at 198°C, corresponding to the melt of host 3 (figure 6.4). The compound then decomposes exothermically.

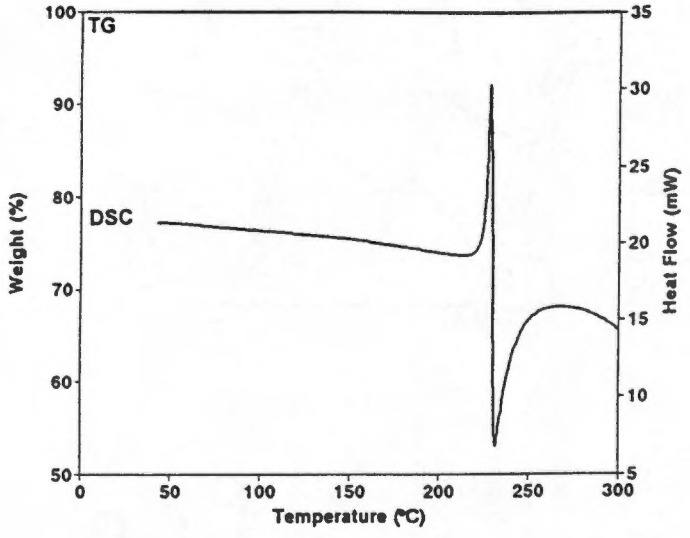

Figure 6.4 : TG and DSC trace of ETHBN.

ETHCHO

$C_{62}H_{44}O_4.4C_6H_{10}O$
Guest : cyclohexanone
Space Group : P $\bar{1}$

a = 14.208(2)Å	α = 91.06(1)°
b = 14.710(4)Å	β = 89.98(1)°
c = 17.915(2)Å	γ = 110.60(2)°

Volume = 3504(1)Å^3
Z = 2

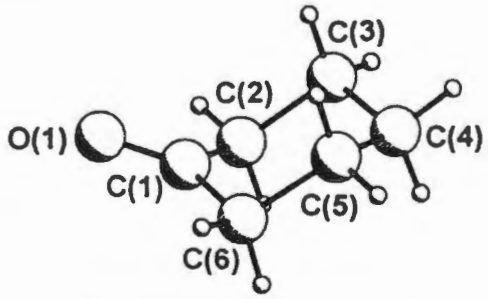

Guests labelled : G. J, K, L.

Crystal Structure :

ETHCHO was refined in the triclinic space group P $\bar{1}$. Unlike ETHBN, the host molecule is not situated on a centre of inversion, and a whole host molecule and four guest molecules are found in the asymmetric unit.

Refinement :

All the non-hydrogen atoms, except for O(1L), were refined anisotropically. The hydroxyl hydrogens were located in the difference electron density map, and refined isotropically. All the remaining hydrogen atoms were placed in geometrically calculated positions and allowed to refine with a common temperature factor for similar atoms. The final *U* values obtained were :

CH : 0.079(2)Å^2

CH_2 - guest G : 0.070(4)Å^2

CH_2 - guest J : 0.160(8)Å^2

CH_2 - guest K : 0.159(8)Å^2

CH_2 - guest L : 0.158(9)Å^2

There is a residual electron density of 1.27eÅ^{-3} in the region of guest L, fairly close to C(6L) (1.63Å) and within hydrogen bonding distance of O(4) (2.98Å). A disorder model of O(1L) was attempted, and is shown schematically in figure 6.5. The resultant geometry of the guest molecule was unsatisfactory, since C(6L) was found to have the geometry of a sp^3 carbon. O(2L) does not lie in a plane with C(1L), C(6L) and C(5L), and had a fractional site occupancy factor of only 0.306(8). This disorder model was, therefore, abandoned.

An extinction coefficient of 0.00928 was applied, and the structure refined to a final R_1 = 0.0638.

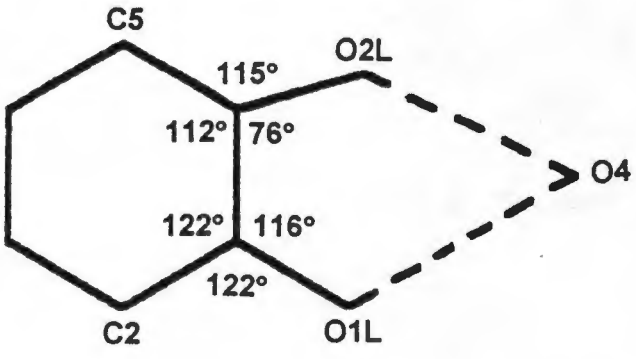

C(1L) - C(2L) : 1.48Å
C(1L) - O(1L) : 1.23Å
C(1L) - C(6L) : 1.48Å
C(6L) - O(2L) : 1.52Å
C(6L) - C(5L) : 1.50Å
O(1L)...O(4) : 2.733Å
O(2L)...O(4) : 2.978Å

Figure 6.5 : A schematic representation of the disorder model attempted for guest L.

Molecular Structure :

The molecular structure of ETHCHO is shown in figure 6.6. Each guest molecule is hydrogen bonded to one of the host hydroxyl groups. The hydrogen bonding details are given in table 6.2. Figure 6.7 shows the crystal packing found in ETHCHO. The host molecules pack in layers, with guests located within a series of intersecting channels. Guest G is located within a constricted channel parallel to [110] and centred at *z*=0.5, guest J is located within a channel parallel to [100], also centred at *z*=0.5, while guests K and L are located within a zig-zag channel parallel to [100], centred at *z*=0 (figure 6.8).

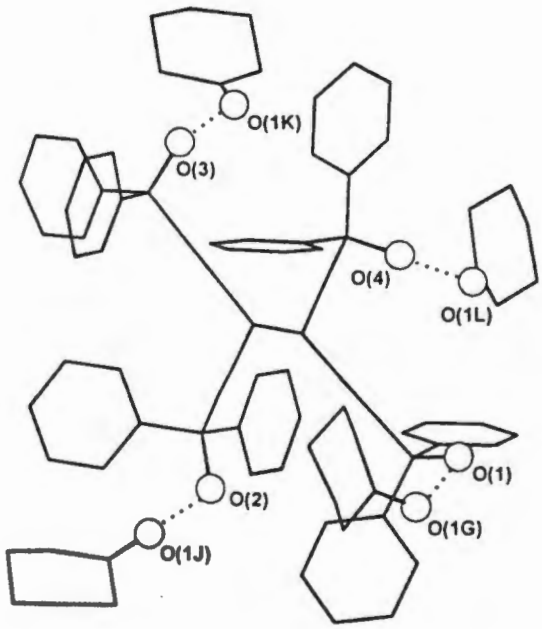

Figure 6.6 : Molecular structure of ETHCHO (the hydrogen atoms are omitted and the hydrogen bonds are indicated as dotted lines).

Table 6.2 : Hydrogen bond data for ETHCHO.

(D)onor	(A)cceptor	D-H (Å)	D...A (Å)	D-H...A (°)
O(1)	O(1G)	0.89(4)	2.789(4)	170(4)
O(2)	O(1J)	0.91(4)	2.841(4)	162(4)
O(3)	O(1K)	0.85(4)	2.847(4)	160(4)
O(4)	O(1L)	0.77(4)	2.759(6)	151(5)

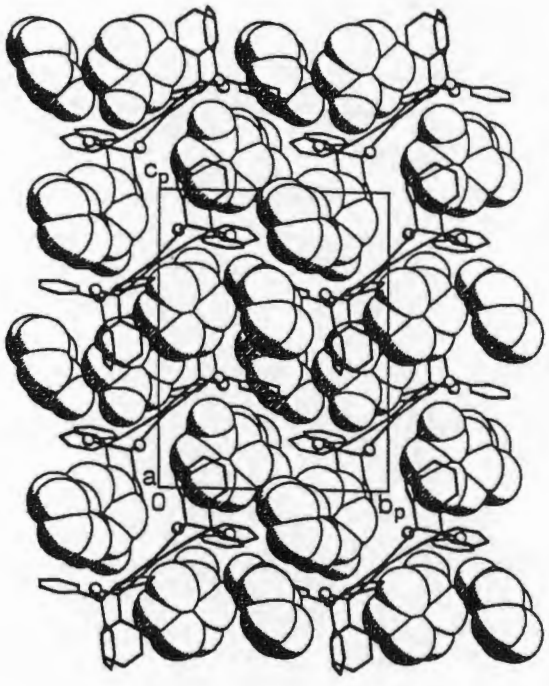

Figure 6.7a : Crystal packing in ETHCHO, viewed down [100]. The host is represented by stick figures, while the guests are shown as space-filled models.

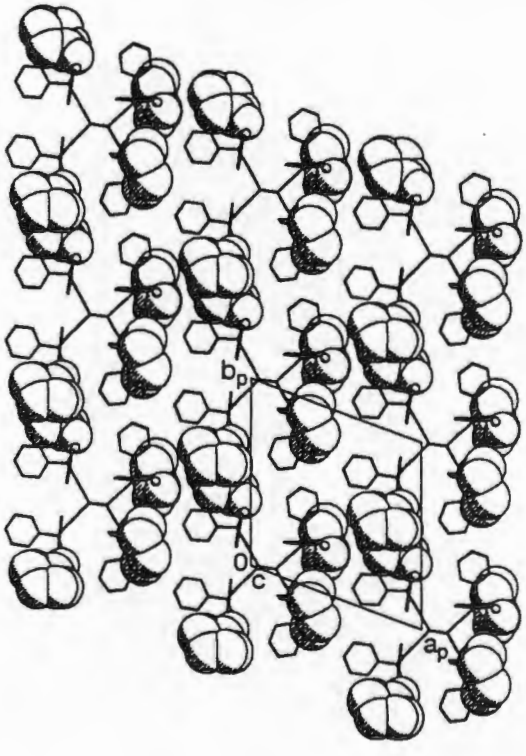

Figure 6.7b : Crystal packing in ETHCHO, viewed down [001]. The host is represented by stick figures, while the guests are shown as space-filled models.

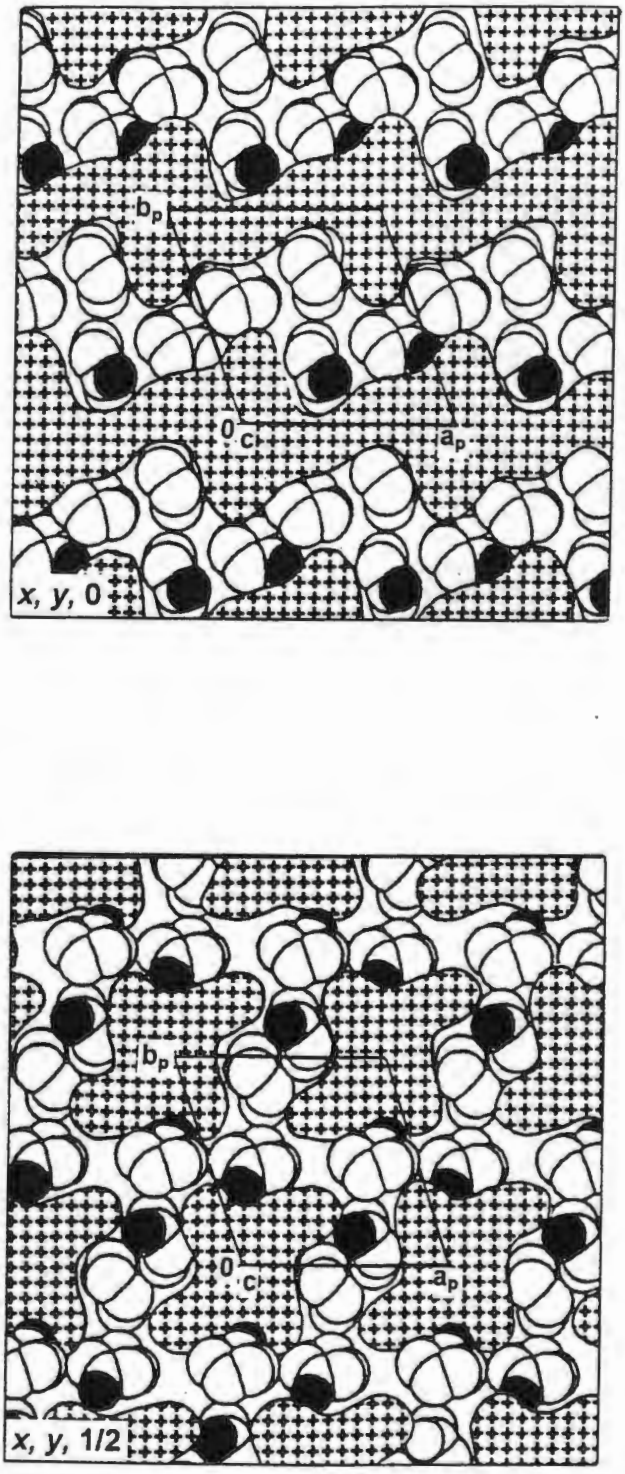

Figure 6.8 : Cross section of ETHCHO viewed along [001] : a) guests K and L, b) guests G and J. The hatched region is that occupied by the host molecules. The guest molecules (with the oxygens shaded) are shown in the channels.

Thermal Analysis :

The TG and DSC traces can be seen in figure 6.9. The TG curve shows a single step guest loss, which confirms the 1:4 host to guest ratio modelled in the crystal structure (expected mass loss : 31.5%, observed mass loss 31.6%). The DSC curve shows a single guest loss endotherm at *ca* 70°C, followed by a second endotherm at 192°C corresponding to melting of the host, which rapidly decomposes.

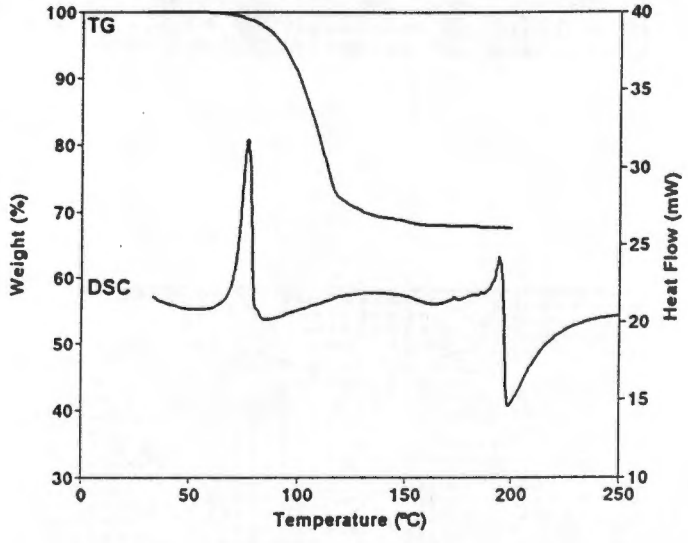

Figure 6.9 : TG and DSC traces for ETHCHO.

ETHDMA

$C_{62}H_{44}O_4.2C_4H_9NO$
Guest : dimethyl acetamide
Space Group : P $\bar{1}$

a = 8.474(2)Å	α = 67.16(2)°
b = 13.103(2)Å	β = 83.20(2)°
c = 13.821(3)Å	γ = 87.82(2)°

Volume = 1404.8(5)Å^3
Z = 1

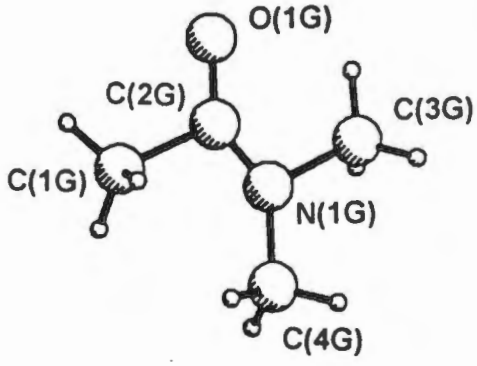

Crystal Structure :

Like ETHBN, the structure of ETHDMA has the host molecules located on a centre of inversion.

Refinement :

All the non-hydrogen atoms were refined anisotropically. The hydroxyl hydrogens were located in the difference electron density map and refined isotropically. All the remaining hydrogens were placed in geometrically calculated positions, with a temperature factor linking similar groups (U (CH) : 0.073(2)Å^2; U (C-CH_3) : 0.19(1)Å^2; U (N-CH_3) : 0.173(9)Å^2). The structure refined successfully to a final R_1 = 0.0519.

Molecular Structure :

The molecular structure of ETHDMA is shown in figure 6.10. The guest molecules are located on either side of the central ethylene bond, and are held in position by two hydrogen bonds between the carbonyl guest oxygen and both the hydroxyl groups on the same side of the ethylene bond. The hydrogen bonding details are tabulated in table 6.3. Crystal packing in ETHDMA can be seen in figure 6.11. The central ethylene bond is parallel to [001]. The host molecules pack in layers parallel to [100], creating cavities between adjacent host molecules within which the guest molecules are situated (figure 6.12). These cavities are interconnected, and have dimensions of 15 x 7 x 4Å.

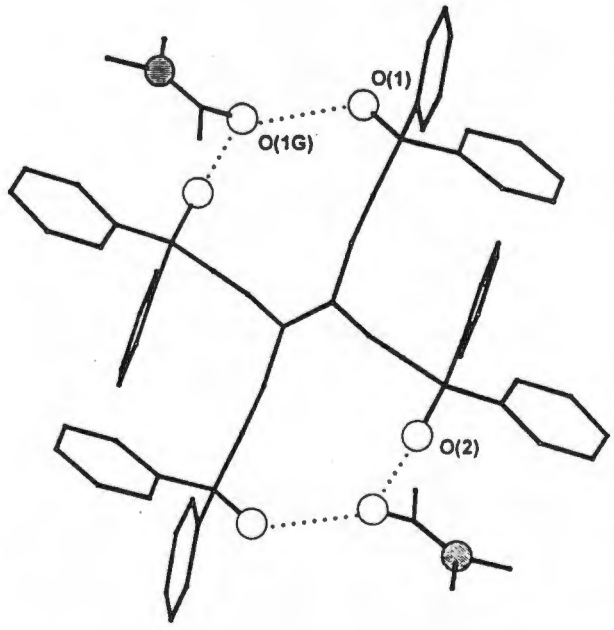

Figure 6.10 : Molecular structure of ETHDMA. (hydrogen atoms are omitted and the nitrogen atoms are shaded)

Table 6.3 : Hydrogen bonding details of ETHDMA.

(D)onor	(A)cceptor	D-H (Å)	D...A (Å)	D-H...A (°)
O(1)	O(1G)	0.83(4)	2.757(3)	158(4)
O(2)	O(1G)[a]	0.90(4)	2.837(3)	179(3)

a : *-x, -y, 2-z*

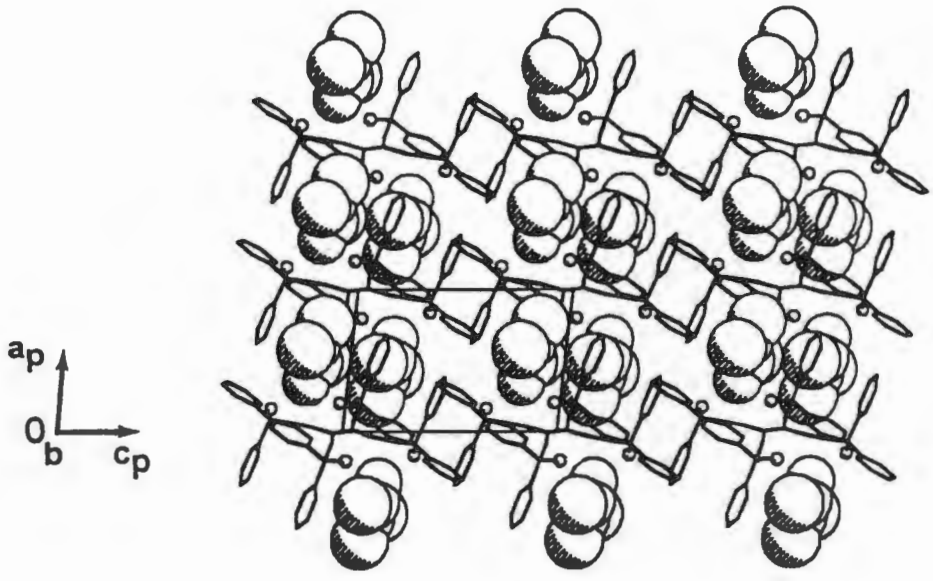

Figure 6.11 : Crystal packing in ETHDMA, viewed down [010]. The host is represented by stick figures, while the guests are shown as space-filled models.

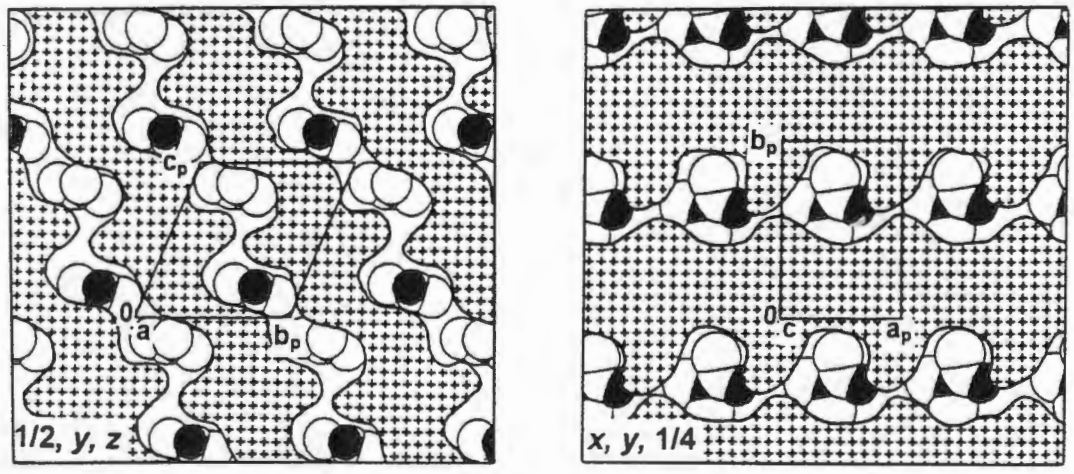

Figure 6.12 : Projected cross-section of the host molecules (hatched area) of ETHDMA viewed along a) [100], and b) [001], showing the interconnected cavities in which the guest molecules are located. The guest molecules are shown in van der Waals representation with the oxygen atoms shaded.

Thermal Analysis :

The thermograms of ETHDMA are shown in figure 6.13. The TG curve shows a single step guest loss corresponding to a host to guest ratio of 1:2 (expected mass loss : 17.0%, observed mass loss : 16.7%). The DSC trace shows a single endotherm at *ca* 174°C corresponding to the guest loss, and dissolution of the host material in the guest. Dimethyl acetamide is not a very volatile solvent (b.p. = 163-165°C) and may not be driven off by the DSC purge gas, resulting in the host material dissolving in the hot released guest liquid. TG is performed in an open pan, and as a result the dimethyl acetamide is more likely to be removed by the purge gas, so host dissolution is not a complicating step in the desolvation process.

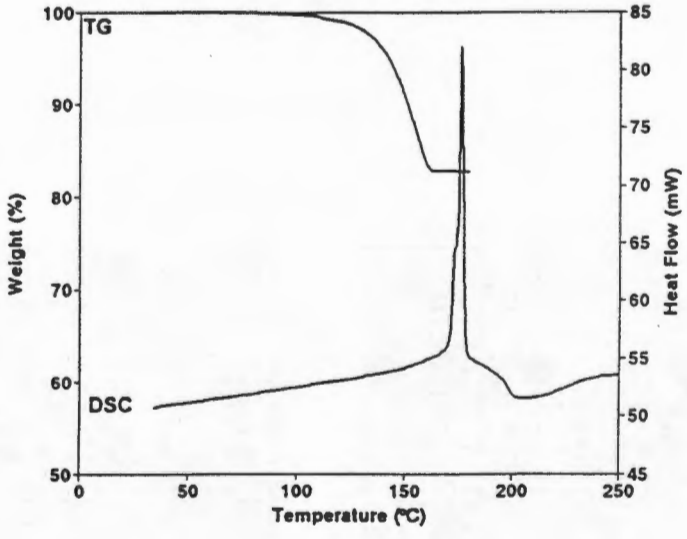

Figure 6.13 : TG and DSC traces of ETHDMA.

Kinetics of Desolvation :

The kinetics of desolvation of ETHDMA were determined by a series of isothermal TG experiments over the temperature range 80 - 115°C. A deceleratory α-time curve was obtained, and an example is shown in figure 6.14. The best-fit reaction mechanism was found to be the geometrical model for contracting volume (R3). An activation energy of 117(2)kJ.mol^{-1} was obtained for this reaction over the α-range 0.05 - 0.95. The semilogarithmic plot of ln k vs 1/T is shown in figure 6.15.

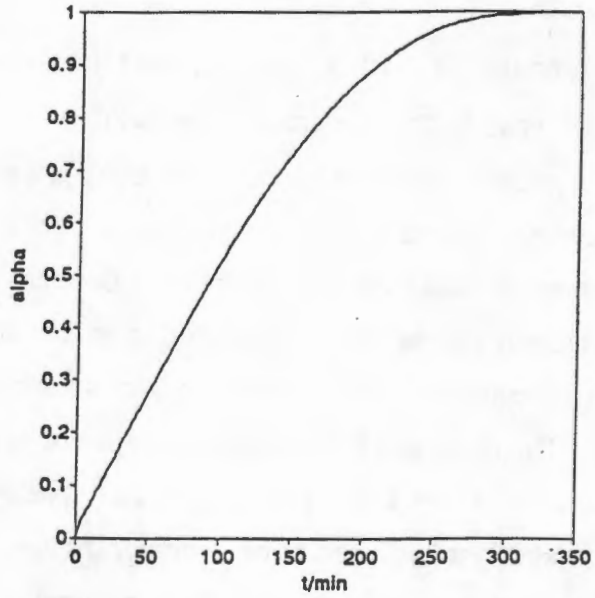

Figure 6.14 : An example of an α-time curve obtained for ETHDMA.

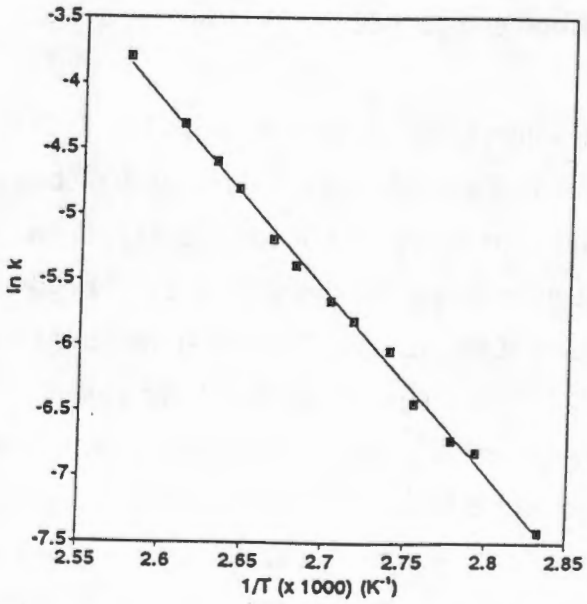

Figure 6.15 : Arrhenius plot for the desolvation of ETHDMA.

DISCUSSION

Although host **3** is significantly smaller than hosts **1** and **2**, is was decided that the data collections for its inclusion compounds should still be done at low temperature. The X-ray diffraction data for both ETHCHO and ETHDMA were collected at 223K. A low temperature data collection for ETHBN was not necessary, and the data was collected at room temperature. All three of the structures refined well, with only a small amount of disorder observed in ETHCHO.

The non-porous α-phase of host **3** was obtained from benzene and 2-hexanone. Unlike host **1**, the non-porous α-phase of host **3**, ETHBN, is stabilised by intermolecular hydrogen bonds. The bulky phenyl groups, which cause steric crowding around the hydroxyl groups, do not prevent the establishment of host to host hydrogen bonding. Despite these stabilising intermolecular hydrogen bonds, host **3** was found to be an efficient host, forming inclusion compounds with small organic solvents with suitable functional groups. The hydrogen bonds between adjacent host molecules are relatively weak, and as a result can presumably be replaced by alternative hydrogen bonds to stronger hydrogen bond acceptor groups. Unfortunately, as previously discussed in chapter 3, host **3** was found to have decayed during the duration of this project, thereby preventing any further investigation of other host **3** inclusion compounds.

The two inclusion compounds studied, ETHCHO and ETHDMA, are very different. The ETHCHO crystals are not particularly stable, cracking shortly after being removed from the mother liquor. ETHCHO has a host to guest ratio of 1:4, with each host hydroxyl group involved in a hydrogen bond to the carbonyl group of one of the guests. The guest molecules are located within channels, suggesting that they can be lost fairly easily. The crystals of ETHDMA are, however, more stable. ETHDMA has a host to guest ratio of 1:2. The guest molecules are located in cavities, and are held in position by two hydrogen bonds from the host hydroxyl groups, located on either side of the ethylene bond. Therefore, the increased stability of ETHDMA relative to ETHCHO can be accounted for by the fact that the dimethyl acetamide guest

molecules are located in cavities within the host framework, rather than in channels, and are held in position more strongly by a second hydrogen bond. An activation energy of 117(2) $kJ.mol^{-1}$ was obtained for the desolvation of ETHDMA.

HOST CONFORMATION

Host **3** is smaller than both hosts **1** and **2**, however, the large number of possible host conformations is not reduced. As in hosts **1** and **2**, the bulky end phenyl groups rotate freely around the rigid 'leg', and relative to each other. In all three structures, the host molecules crystallise in very different conformations (figure 6.16), clearly showing the rotational flexibility of this host.

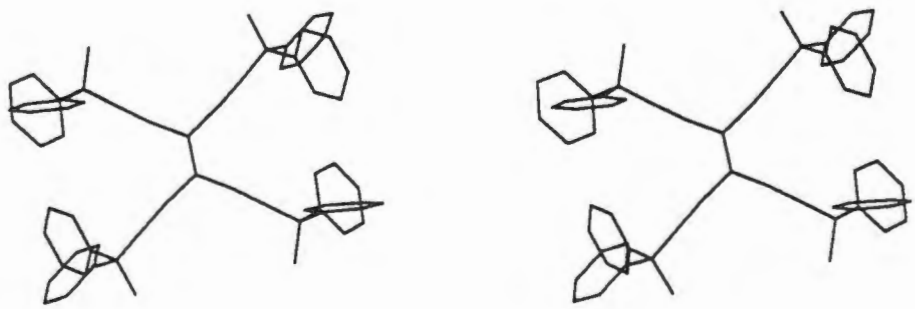

Figure 6.16a : Host conformation in ETHBN, viewed perpendicular to the plane through C(2) and the ethylene bond (hydrogen atoms are omitted for clarity).

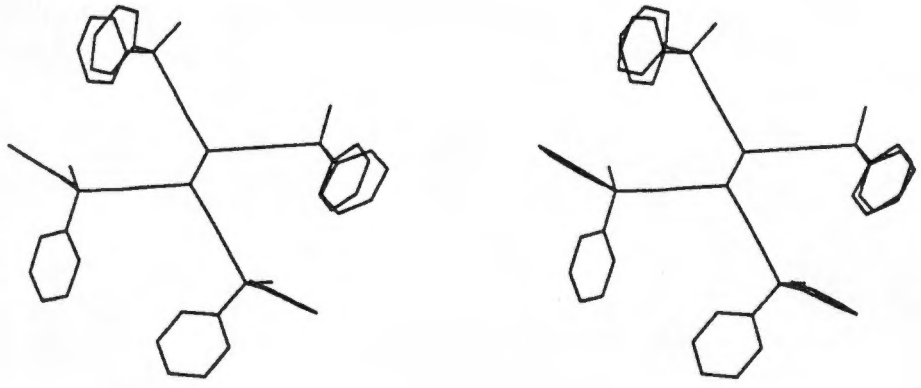

Figure 6.16b : Host conformation in ETHCHO, viewed perpendicular to the plane through C(2) and the ethylene bond (hydrogen atoms are omitted for clarity).

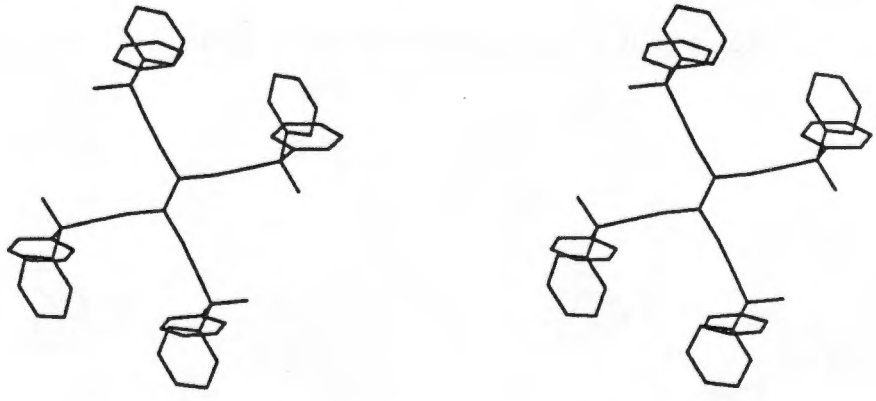

Figure 6.16c : Host conformation in ETHDMA viewed perpendicular to the plane through C(2) and the ethylene bond (hydrogen atoms are omitted for clarity).

Aspects of the conformation of the host which need to be considered involve the orientation of the phenyl and hydroxyl groups on each 'leg' in relation to the central ethylene bond. As was stated for both hosts **1** and **2**, the numbering of the host molecule, although carried out uniformly, was arbitrarily done. Thus a direct comparison of the torsion angles defining the position of the phenyl rings on each 'leg' in relation to the central ethylene bond is not possible. The torsion angles under consideration are indicated in the scheme below. For each 'leg', τ_1 will define the smallest torsion angle, and τ_3 will define the smaller of the two angles defining the position of the second phenyl ring. Table 6.4 reports the torsion angles obtained for each of the structures. The torsion angles for each 'leg' in ETHDMA are comparable, as are three out of the four in ETHCHO. The fourth torsion angle is reversed relative to the others, thereby destroying the centre of inversion observed in both ETHBN and ETHDMA.

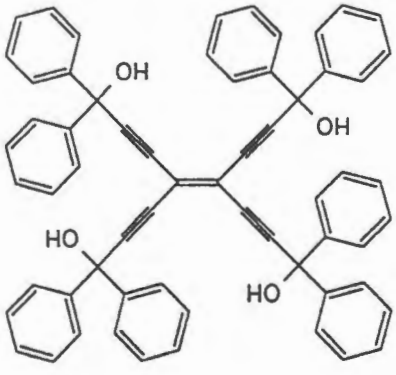

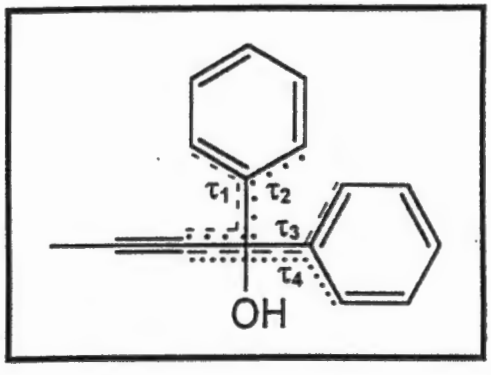

Table 6.4 : Torsion angles defining the conformation of host **3** structures.

Compound	τ1 (°)	τ2 (°)	τ3 (°)	τ4 (°)
ETHBN	32.9(3)	-150.3(2)	37.5(2)	-147.4(2)
	0.1(3)	179.7(2)	-55.1(2)	126.3(2)
ETHDMA	19.9(3)	-162.8(2)	-56.8(3)	123.1(3)
	18.4(3)	-164.5(2)	-51.0(3)	130.1(3)
ETHCHO	21.2(5)	-159.6(3)	-50.5(4)	130.7(3)
	-36.6(4)	146.6(3)	44.9(4)	-136.6(3)
	27.2(4)	-155.2(3)	-41.9(4)	142.6(3)
	33.6(4)	-147.5(3)	-46.8(4)	135.8(3)

In all three structures the phenyl rings can be considered to be planar, with maximum deviations from their least squares planes less than 0.02Å. The angles between the planes of the phenyl rings, on each 'leg' are tabulated in table 6.5. The angle between the planes in ETHDMA are very similar, as are the angles observed in ETHCHO. However, in ETHCHO, these angles are noticeably smaller, than in ETHDMA, presumably in order to accommodate the guest molecules within the host framework.

Table 6.5 : Angle between the planes of the phenyl rings on each 'leg'.

Angle between	ETHBN (°)	ETHDMA (°)
C(5)-C(10)/C(11)-C(16)	76.29(9)	78.67(8)
C(20)-C(25)/C(26)-C(31)	86.10(9)	80.92(8)

Angle between	ETHCHO (°)
C(5)-C(10)/C(11)-C(16)	76.7(1)
C(21)-C(26)/C(27)-C(32)	74.0(1)
C(36)-C(41)/C(42)-C(47)	74.5(1)
C(51)-C(56)/C(57)-C(62)	72.7(2)

The hydroxyl groups of ETHBN are directed away from the central ethylene bond, while in ETHDMA, they are directed in towards it. In ETHCHO, the two hydroxyl groups on the one side of the ethylene bond are directed away from it, while on the other side, the hydroxyl groups are directed in towards it. The torsion angle defining the position of each hydroxyl group relative to the central ethylene bond is shown in the scheme below. These torsion angles are tabulated in table 6.6.

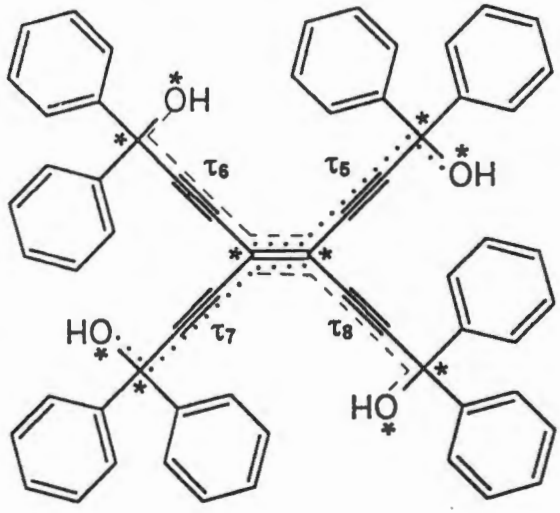

Table 6.6 : Torsion angles of the hydroxyl groups relative to the central ethylene bond.

Torsion angle (°)	ETHBN	ETHDMA	ETHCHO
τ_5	176.8(2)	8.7(3)	-176.9(3)
τ_6	-166..4(2)	20.3(3)	45.1(3)
τ_7	-176.8(2)	-8.7(3)	50.5(3)
τ_8	166.4(2)	-20.3(3)	179.7(3)

The different bond types in host **3** are indicated in the scheme below, and the bond length ranges observed for each of the structures are summarised in table 6.7. All the bond lengths and angles are comparable with known values[1].

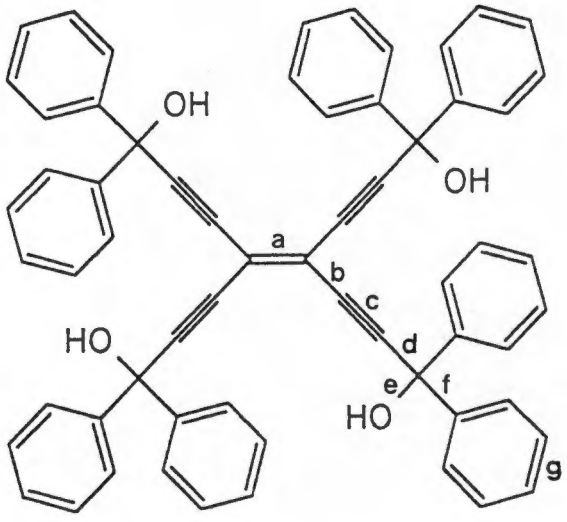

Table 6.7 : Bond length ranges observed for host **3**.

Bond		ETHBN (Å)	ETHCHO (Å)	ETHDMA (Å)	Ref 1 (median)
a = C = C		1.362(3)	1.370(4)	1.347(4)	1.35(1)
b = C_{sp}^2 - C_{sp}	min	1.428(2)	1.424(4)	1.436(3)	1.43(1)
	max	1.430(2)	1.435(4)	1.438(3)	
c = C ≡ C	min	1.192(2)	1.188(4)	1.190(3)	1.19(1)
	max	1.195(2)	1.196(4)	1.193(3)	
d = C_{sp} - C_{sp}^3	min	1.479(2)	1.483(4)	1.472(3)	1.47(1)
	max	1.481(3)	1.489(4)	1.473(3)	
e = C_{sp}^3 - O	min	1.424(4)	1.419(4)	1.418(3)	1.43(1)
	max	1.447(2)	1.425(4)	1.421(3)	
f = C_{sp}^3 - C_{ar}	min	1.522(3)	1.528(5)	1.536(3)	1.53(2)
	max	1.534(3)	1.539(5)	1.541(3)	
g = C_{ar} ≃ C_{ar}	min	1.355(4)	1.354(7)	1.361(5)	1.38(1)
	max	1.389(3)	1.399(5)	1.400(4)	

REFERENCES

1. F. H. Allen, O. Kennard, D. G. Watson, L. Brammer, A. G. Orpen, R. Taylor, *J. Chem. Soc., Perkin Trans. 2*, 1987, S1.

CHAPTER 7

CONCLUSION

Hexakis(3-hydroxy-3,3-diphenyl-2-propynyl)benzene (host **1**), 1,2,3,5,6,7-hexakis(3-hydroxy-3,3-diphenyl-2-propynyl)naphthalene (host **2**) and tetra(3-hydroxy-3,3-diphenyl-2-propynyl)ethylene (host **3**) are very interesting host compounds forming a number of inclusion compounds with a wide variety of organic solvents, which differ in size, shape and volatility.

These host molecules are bulky, and awkward, but not as rigid as was initially expected. The phenyl rings are free to rotate in relation to the central electron rich region and each other, resulting in a large number of possible conformations. This conformational flexibility enables the hosts to adjust in order to include the different guest molecules within its framework.

The crystals of the inclusion compounds studied were all found to be unstable in air. In order to prevent desolvation of the inclusion compounds during the X-ray diffraction data collection, the crystals had to be mounted in Lindemann capillary tubes, which were then flame sealed. Also, due to the size of these host compounds, the X-ray diffraction data of the inclusion compounds was collected at low temperature in order to minimise the expected high thermal motion of the molecules. All the structures refined well, and, where observed, the dominating components of host (NAP2H), or guest disorder were modelled. However, a residual electron density in the region of the guests could often not be sensibly modelled.

A large number of different host to guest ratios, hydrogen bonding patterns, and packing motifs were observed for each of the hosts. The host to guest ratios for host **1** were found to be very variable ranging from 1:2 to 1:6, while those for host **2** were either 1:4 or 1:6, which is considerably richer in guest than is usually observed for organic host compounds. The slightly larger central aromatic region of host **2** compared with that of host **1**, possibly facilitates the inclusion of a greater number of guest molecules, and the uniformity of the host to guest ratios. The host to guest ratios observed for host **3** were 1:2 and 1:4.

The variability of the host to guest ratios results in a number of different hydrogen bonding patterns being observed between the host and guest molecules. In all of the inclusion compounds studied, no hydrogen bonding was observed between the host molecules. The bulky phenyl groups cause steric crowding around the hydroxyl groups thereby reducing the possibility of the formation of a hydrogen bond between two adjacent host molecules. All the guest molecules were involved in hydrogen bonding with a host molecule, except in SPAB, SPDIOX, SPCHO and NAPCHO where one of the guest molecules is not involved in hydrogen bonding and is held in position by van der Waals forces. This reinforces the idea that every crystal structure is the result of an intricate balance between a range of intermolecular forces.

Hosts **1** and **2** have six hydroxyl groups, thus the optimum host to guest ratio would be 1:6, with each of the hydroxyl groups involved in a hydrogen bond with the functional group of one of the guest molecules. This pattern was only observed for host **2** in NAPDMA and NAPDMF. Similarly, host **3** has four hydroxyl groups, suggesting that the optimum host to guest ratio would be 1:4, with each hydroxyl group involved in a hydrogen bond with one of the guests. This pattern was observed in ETHCHO.

A number of different packing motifs for each of the host compounds were observed for the various guest molecules included by the hosts. The different packing motifs of the host compounds confirms the flexibility of these hosts to adapt in order to include the respective guest solvent. The differences observed in the packing of the host molecules results in different modes of inclusion of the guest molecules, namely channels, constricted channels, cavities, or a combination of these. Interestingly, of all of the inclusion compounds investigated only two pairs were isostructural, namely NAPDMA and NAPDMF, SPDEK and SPETH. This again reiterates the conformational freedom and packing flexibility of these host compounds.

The large number of phenyl rings and the electron rich central region of the hosts, lead to the investigation of possible π-π interactions with π-intercalators, such as benzene. However, for all three hosts, on crystallisation from benzene, the α-phase obtained. Suitable crystals for X-ray diffraction were obtained for hosts **1** and **3**, but unfortunately, suitable crystals of the host **2**

α-phase were not obtained during the course of this study. The α-phase of host **3**, ETHBN, was characterised by intermolecular hydrogen bonding between the host molecules, but this was the only case where this was observed. In the α-phase of host **1**, SPBN, only intramolecular hydrogen bonding between the hydroxyl groups was observed.

The presence of a slight acetonitrile impurity within a host **1** benzene crystallisation, led to an interesting result. On crystallisation a mixed guest inclusion compound, SPAB, resulted. No π-π interactions were observed and the benzene guest molecules were found to be held in position by van der Waals forces. However, the inclusion of benzene by host **1** appears to depend on the presence of acetonitrile.

Host **1** was also found to selectively include compounds containing a carbonyl functional group over those containing only ether oxygens. This result was obtained accidentally by the surprise inclusion of a 1,3-dioxolan-2-one impurity in 1,3-dioxolane (SPDIOXO), but was confirmed by the selective inclusion of cyclohexanone from a mixture of cyclohexanone and 1,4-dioxane (SPDICHO).

The kinetics of desolvation were determined for some of the inclusion compounds investigated, and the results are reported in table 7.1. In previous kinetic studies (Chapter 1, p 15), the activation energies for the desolvation of organic inclusion compounds with the same host appear to be related to the mode of inclusion of the guest molecules within the host framework. Channel type guest inclusion was found to have a lower activation energy than guest inclusion within cavities. This is clearly observed for both hosts **1** and **2**. For the host **1** inclusion compounds where the mode of inclusion is the same, the stability of the compound may explain the differences in activation energies. A crude measure of the stability can be obtained from DSC results, using T_{on}-T_b.[1] E_a increases as the stability of the inclusion compound increases, with the exception of SP2H. 2-Hexanone is a much larger guest molecule than dimethyl acetamide, diethyl ketone or diethyl ether, which are all similar in size, suggesting that possibly the size of the guest molecules may also influence the activation energy required for desolvation of an inclusion compound.

Table 7.1 : Kinetics of desolvation for selected inclusion compounds.

Compound	Inclusion mode	T_{on} (°C)	T_b (°C)	T_{on}-T_b (°C)	T-range (°C)	E_a (kJ.mol^{-1})	Reaction mechanism
SPDIOX	constricted channels	115	101.1	13.9	56-75	148(2)	F1
SPMEK	channels/ cavities	75	79.6	-4.6	62-72	156(9)	B1
SPDMA	cavities	135	164	-29	75-105	154(3)	A2
SPDEK	cavities	86	101.5	-15.5	55-80	163(5)	A2
SPETH	cavities	77	34.6	42.4	55-75	190(6)	A2
SP2H	cavities	99	128	-29	80-100	264(3)	A2
NAPDMA	channels/ cavities	123	164	-41	65-80	148(5)	D3
NAP2H	cavities	74	128	-54	55-75	256(4)	F1
ETHDMA	cavities	174	164	10	80-115	117(2)	R3

A comparison of the activation energies obtained in previous studies for the desolvation of inclusion compounds of similar hosts (size and shape) with the same guest also indicates that the E_a of desolvation is related to the mode of inclusion of the guest within the host framework; where the mode of inclusion is the same, the thermal stability of the inclusion compound, roughly indicated by T_{on}-T_b, may explain the differences observed. Hosts **1** and **2** are similar in size and a comparison of the modes of inclusion of the dimethyl acetamide guests in SPDMA and NAPDMA suggests that SPDMA should have the slightly higher E_a, which is observed. A similar comparison between SPDMA and ETHDMA, or NAPDMA and ETHDMA is not possible since host **1** and **3**, and hosts **2** and **3** are significantly different in size.

For SP2H and NAP2H the mode of inclusion of the 2-hexanone guest molecules is the same (cavities). However, SP2H appears to be more stable that NAP2H, suggesting a higher E_a for SP2H. Experimentally, the E_a for SP2H was found to be slightly higher than the E_a obtained for NAP2H.

Host **3** did not include 2-hexanone, presumably this host is too small to create a stable inclusion compound with this solvent, and the α-phase was obtained on crystallisation from 2-hexanone. This reconfirms the idea that because host **3** is significantly smaller than hosts **1** and **2**, its inclusion behaviour is different.

A much larger data set of the activation energies of desolvation of organic inclusion compounds is required before conclusive results can be drawn between them all.

REFERENCES

1. S. A. Bourne, L. R. Nassimbeni, *J. Org. Chem.*, 1992, **57**, 2438.

APPENDICES

APPENDIX A

The thermal analysis results obtained for the inclusion compounds formed by hosts **1-3** are shown here. From the TG curves the host to guest ratios were determined. The observed and calculated mass losses are reported in tables A1-A3. The difference between the observed and calculated mass losses was rarely greater than 1%.

Table A1 : Thermogravimetric results for the inclusion compounds formed by host **1**.

Guest	Observed mass loss (%)	Expected mass loss (%)	Difference (%)	Host:Guest
acetone	20.0	20.9	-0.9	1:6
acetonitrile	16.2	15.8	0.4	1:6
acetonitrile/benzene	14.8	15.3	-0.5	1:2:2
acetophenone	21.9	21.5	0.4	1:3
cyclohexanone	26.5	27.2	-0.7	1:5
cyclopentanone	11.9	11.0	0.9	1:2
diethyl ketone	11.1	11.6	-0.5	1:2
dimethyl acetamide	20.3	20.1	0.2	1:4
dimethyl sulphoxide	19.4	19.2	0.2	1:4
1,4-dioxane	24.3	25.1	-0.8	1:5
1,3-dioxolan-2-one	11.8	11.8	0	1:2
ether	9.1	10.1	1	1:2
2-hexanone	12.7	13.2	-0.5	1:2
methyl acetate	22.0	22.0	0	1:5
methyl ethyl ketone	13.3	14.1	-0.8	1:3
2-picoline	22.0	22.0	0	1:4
3-picoline	17.6	17.5	0.1	1:3
4-picoline	23.2	22.0	1.2	1:4
propyl acetate	12.4	13.4	1	1:2
pyridine	19.1	19.4	-0.3	1:4

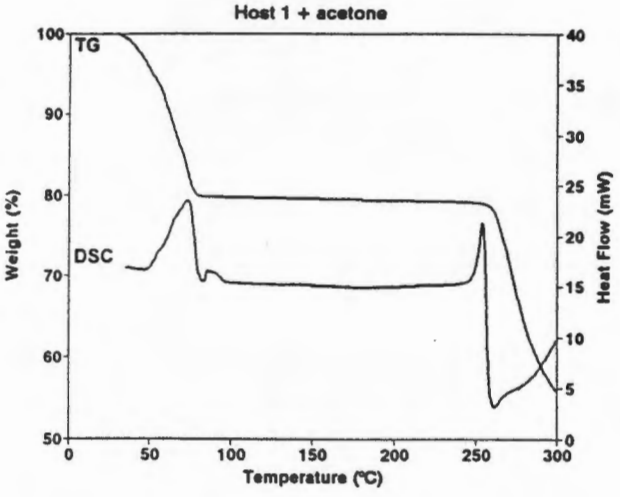
Host 1 + acetone
TG
DSC
Weight (%)
Heat Flow (mW)
Temperature (°C)

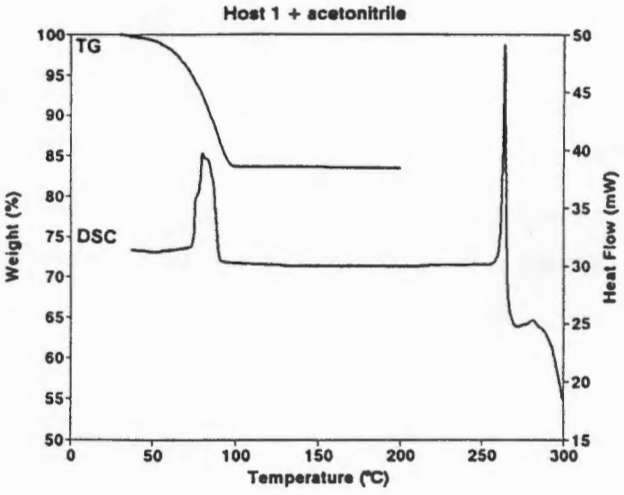
Host 1 + acetonitrile
TG
DSC
Weight (%)
Heat Flow (mW)
Temperature (°C)

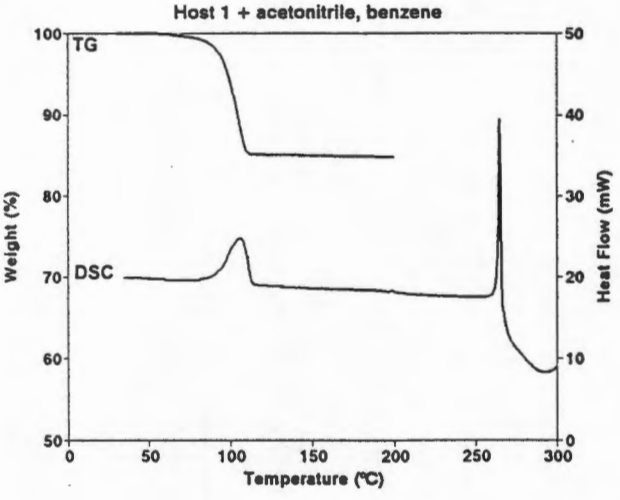
Host 1 + acetonitrile, benzene
TG
DSC
Weight (%)
Heat Flow (mW)
Temperature (°C)

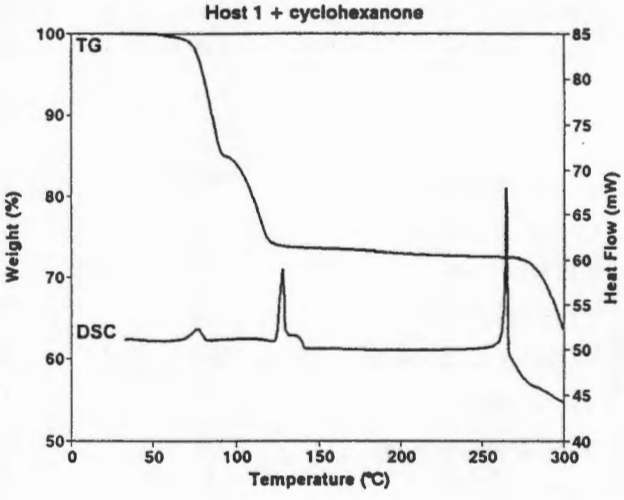
Host 1 + cyclohexanone
TG
DSC
Weight (%)
Heat Flow (mW)
Temperature (°C)

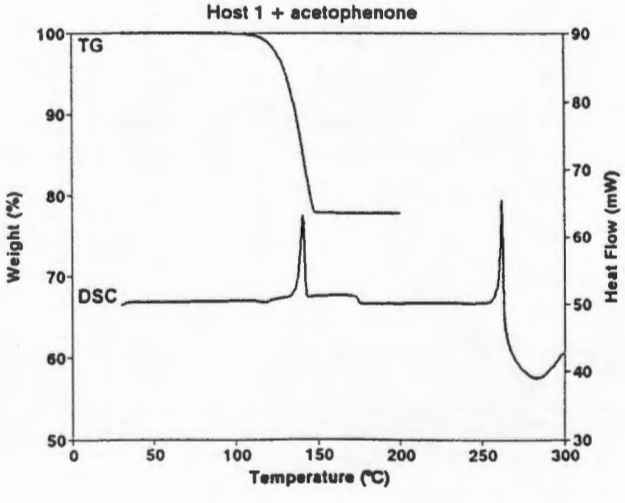
Host 1 + acetophenone
TG
DSC
Weight (%)
Heat Flow (mW)
Temperature (°C)

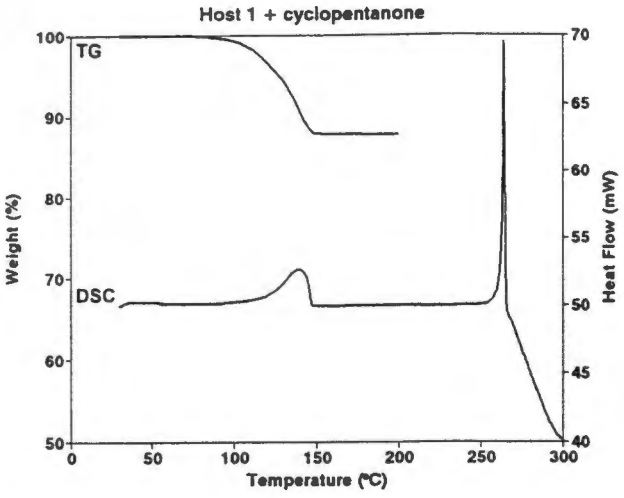
Host 1 + cyclopentanone
TG
DSC
Weight (%)
Heat Flow (mW)
Temperature (°C)

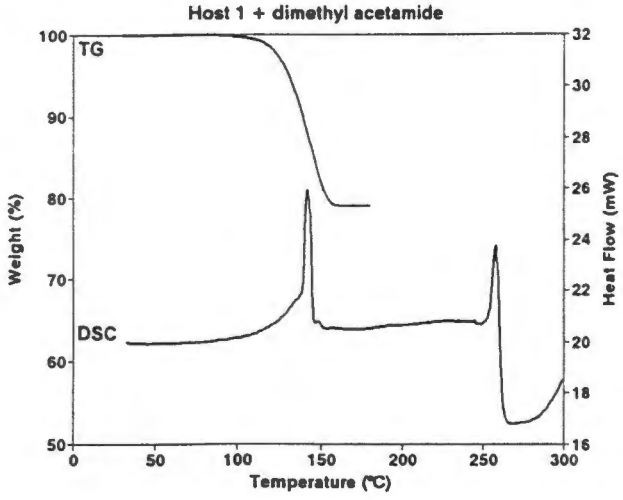
Host 1 + dimethyl acetamide
TG
DSC
Weight (%)
Heat Flow (mW)
Temperature (°C)

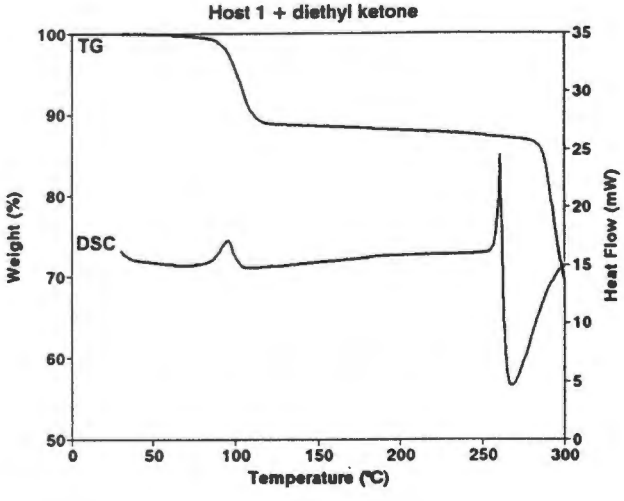
Host 1 + diethyl ketone
TG
DSC
Weight (%)
Heat Flow (mW)
Temperature (°C)

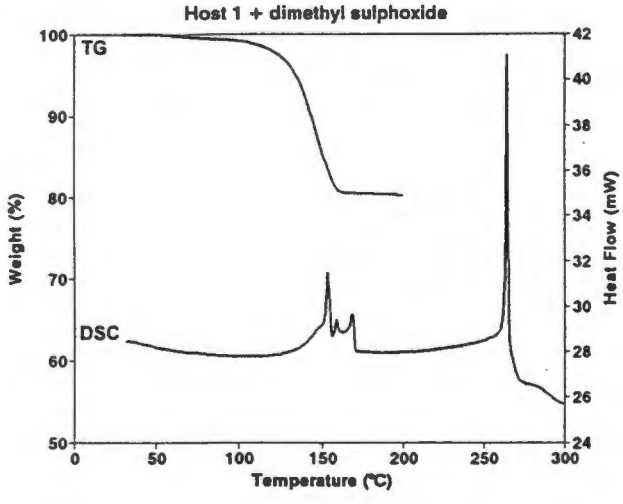
Host 1 + dimethyl sulphoxide
TG
DSC
Weight (%)
Heat Flow (mW)
Temperature (°C)

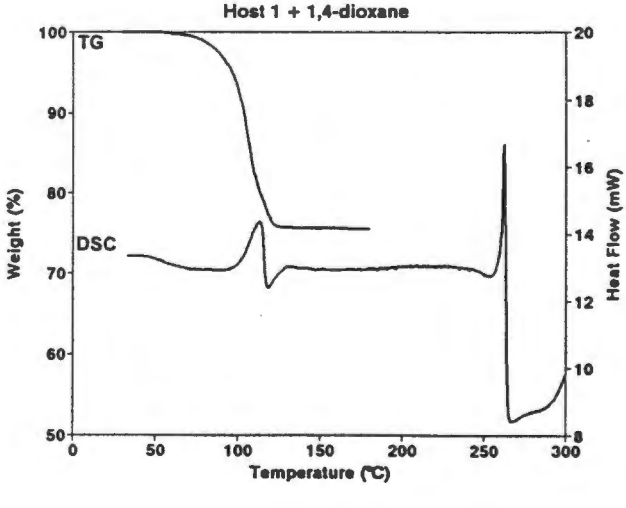
Host 1 + 1,4-dioxane
TG
DSC
Weight (%)
Heat Flow (mW)
Temperature (°C)

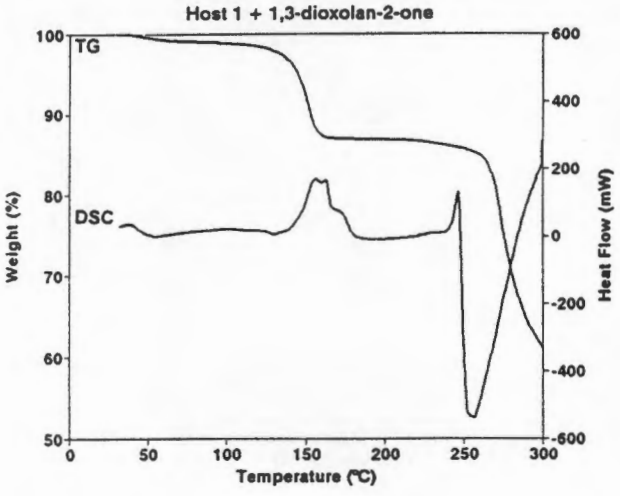
Host 1 + 1,3-dioxolan-2-one
TG
DSC
Weight (%)
Heat Flow (mW)
Temperature (°C)

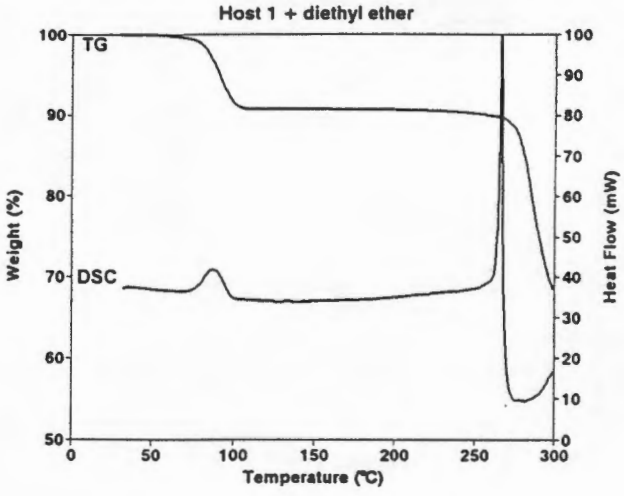
Host 1 + diethyl ether
TG
DSC
Weight (%)
Heat Flow (mW)
Temperature (°C)

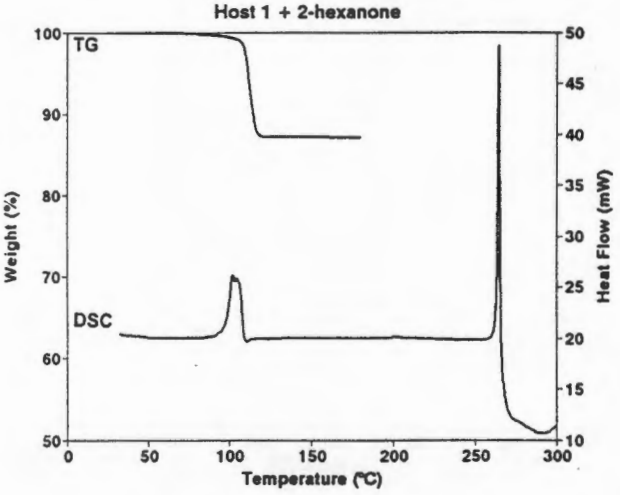
Host 1 + 2-hexanone
TG
DSC
Weight (%)
Heat Flow (mW)
Temperature (°C)

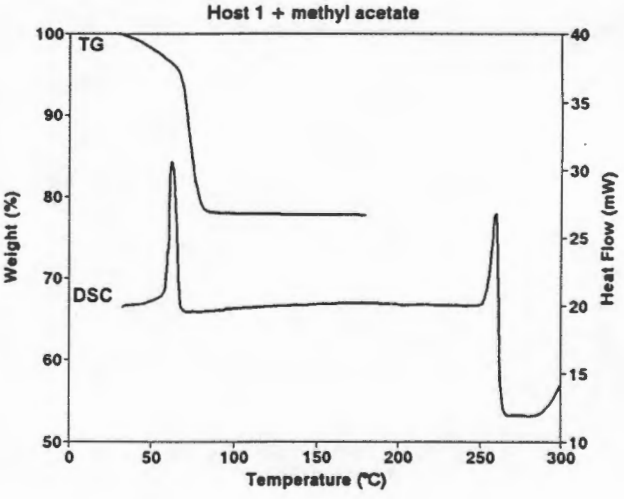
Host 1 + methyl acetate
TG
DSC
Weight (%)
Heat Flow (mW)
Temperature (°C)

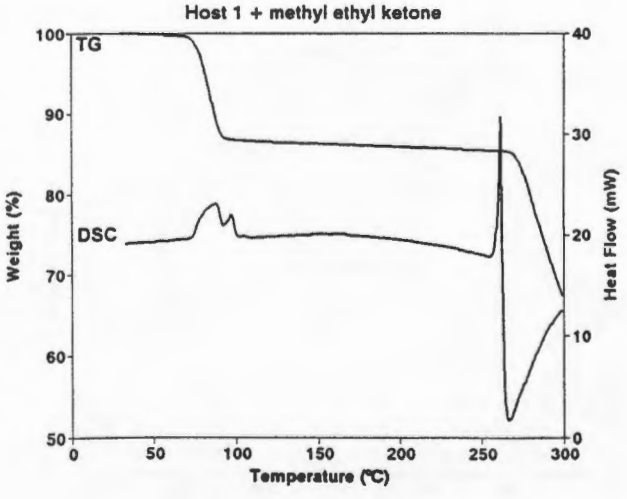
Host 1 + methyl ethyl ketone
TG
DSC
Weight (%)
Heat Flow (mW)
Temperature (°C)

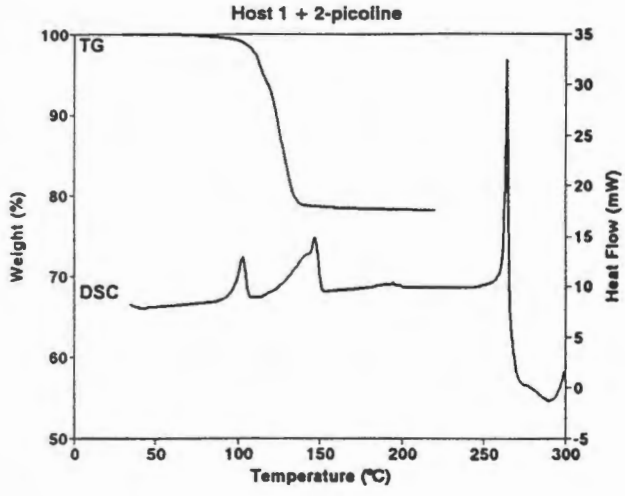
Host 1 + 2-picoline
TG
DSC
Weight (%)
Heat Flow (mW)
Temperature (°C)

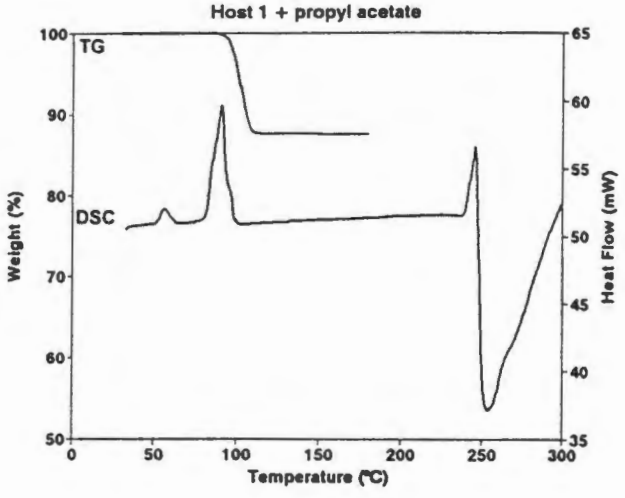
Host 1 + propyl acetate
TG
DSC
Weight (%)
Heat Flow (mW)
Temperature (°C)

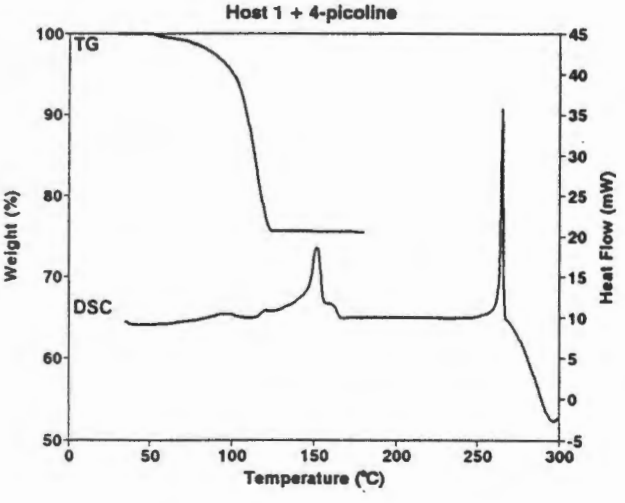
Host 1 + 4-picoline
TG
DSC
Weight (%)
Heat Flow (mW)
Temperature (°C)

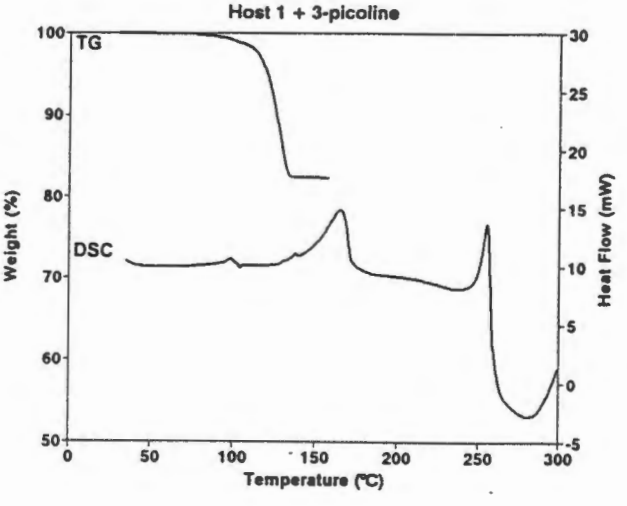
Host 1 + 3-picoline
TG
DSC
Weight (%)
Heat Flow (mW)
Temperature (°C)

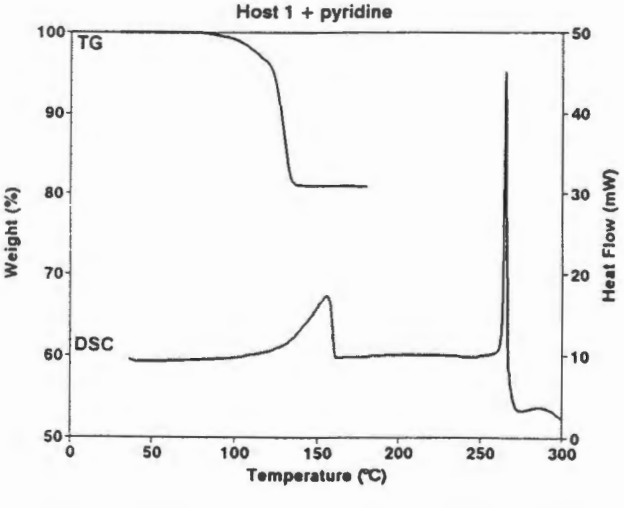
Host 1 + pyridine
TG
DSC
Weight (%)
Heat Flow (mW)
Temperature (°C)

Table A2 : Thermogravimetric results for the inclusion comopunds formed by host **2.**

Guest	Observed mass loss (%)	Expected mass loss (%)	Difference (%)	Host:Guest
acetone	14.2	14.5	-0.3	1:4
cyclohexanone	29.9	30.1	-0.2	1:6
dimethyl acetamide	26.9	27.7	-0.8	1:6
dimethyl formamide[a]	24.8	24.3	1.5	1:6
dimethyl formamide[b]	17.7	17.7	0	1:4
2-hexanone	21.8	22.7	-0.8	1:4
2,4-lutidine	31.2	32.0	-0.8	1:6
2,6-lutidiine	24.7	23.9	0.8	1:4
3,5-lutidine	31.2	32.0	-0.8	1:6
2-picoline	28.8	29.0	-0.2	1:6
3-picoline	29.5	29.0	0.5	1:6
4-picoline	30.2	29.0	1.2	1:6
pyridine	25.7	25.8	-0.1	1:6

a) prismatic crystals, b) needles.

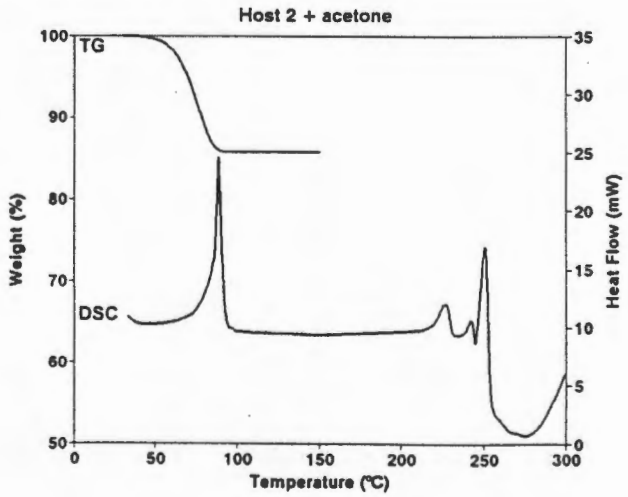

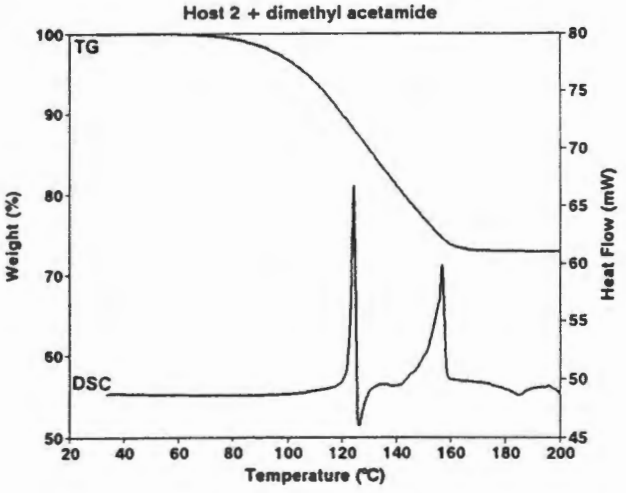
Host 2 + dimethyl acetamide
TG
DSC
Weight (%)
Heat Flow (mW)
Temperature (°C)

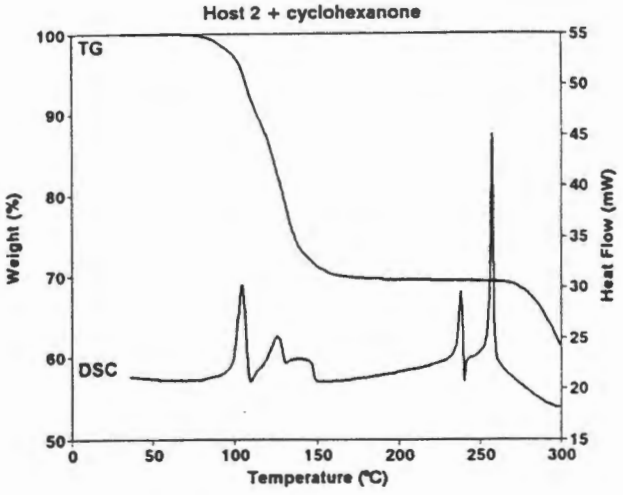
Host 2 + cyclohexanone
TG
DSC
Weight (%)
Heat Flow (mW)
Temperature (°C)

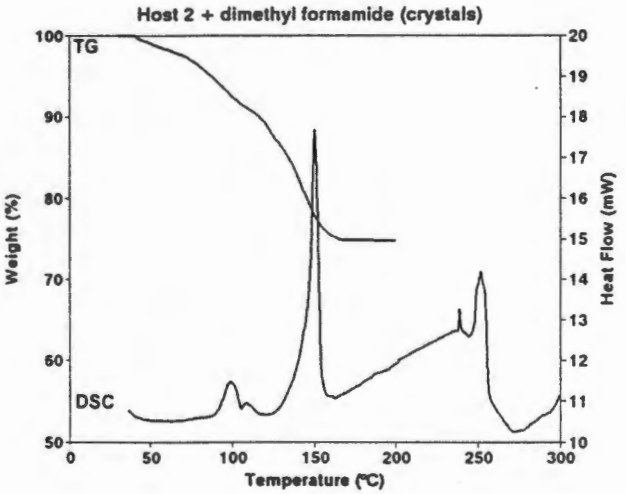
Host 2 + dimethyl formamide (crystals)
TG
DSC
Weight (%)
Heat Flow (mW)
Temperature (°C)

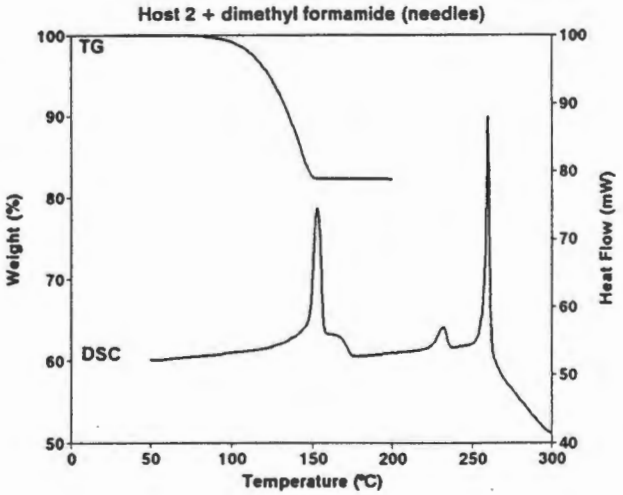
Host 2 + dimethyl formamide (needles)
TG
DSC
Weight (%)
Heat Flow (mW)
Temperature (°C)

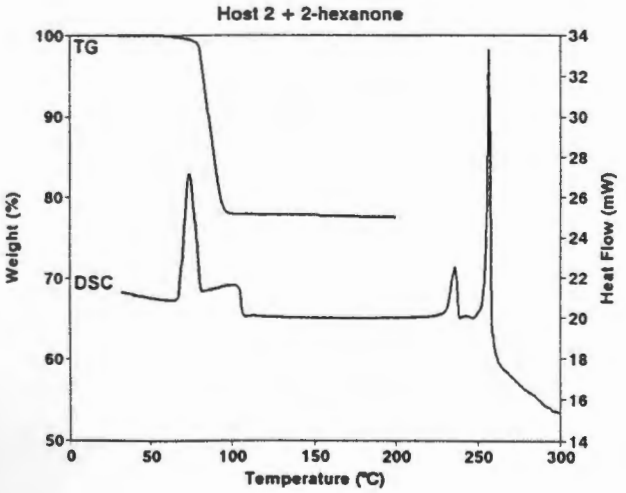
Host 2 + 2-hexanone
TG
DSC
Weight (%)
Heat Flow (mW)
Temperature (°C)

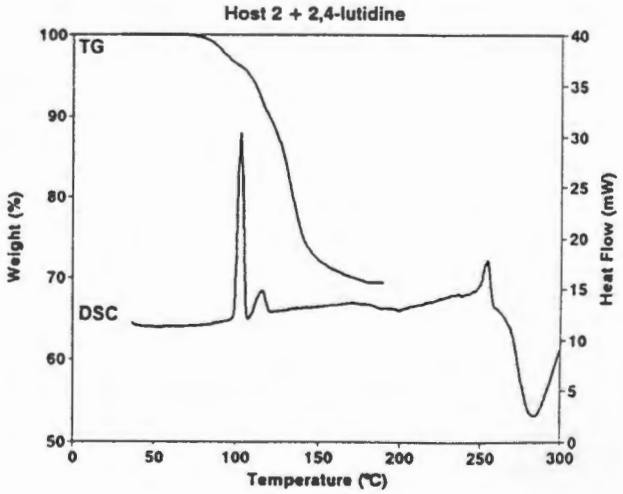
Host 2 + 2,4-lutidine
TG
DSC
Weight (%)
Heat Flow (mW)
Temperature (°C)

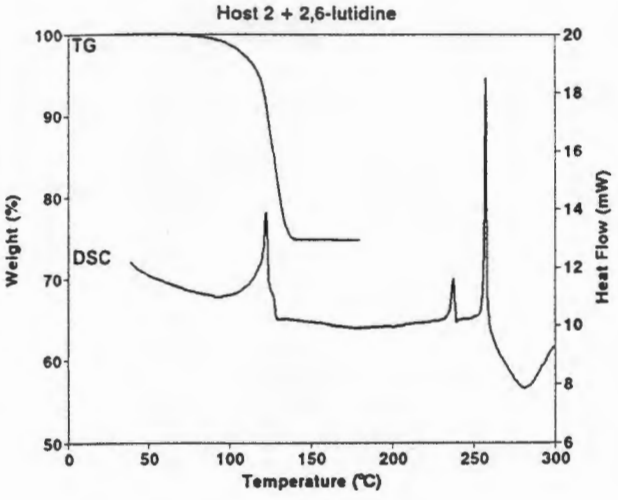
Host 2 + 2,6-lutidine
TG
DSC
Weight (%)
Heat Flow (mW)
Temperature (°C)

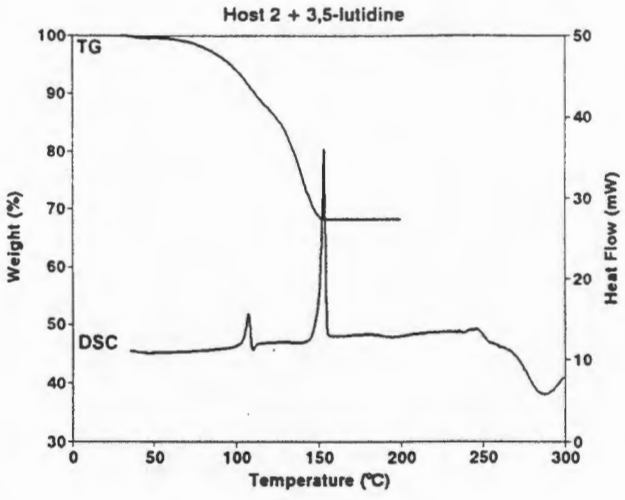
Host 2 + 3,5-lutidine
TG
DSC
Weight (%)
Heat Flow (mW)
Temperature (°C)

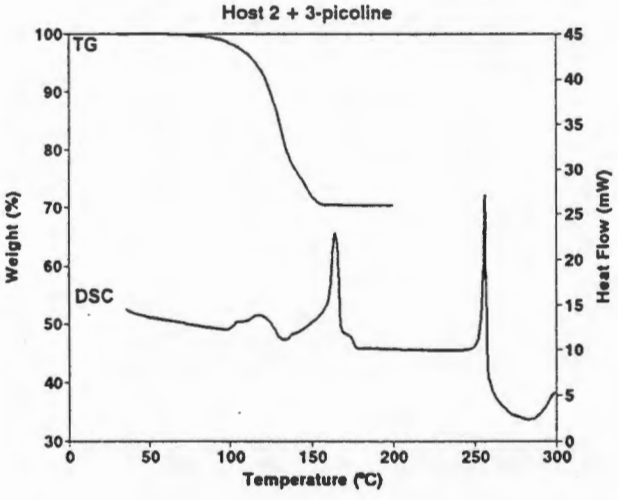
Host 2 + 3-picoline
TG
DSC
Weight (%)
Heat Flow (mW)
Temperature (°C)

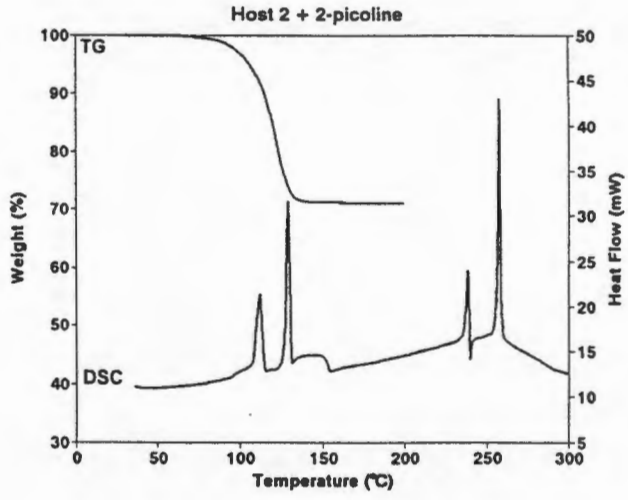
Host 2 + 2-picoline
TG
DSC
Weight (%)
Heat Flow (mW)
Temperature (°C)

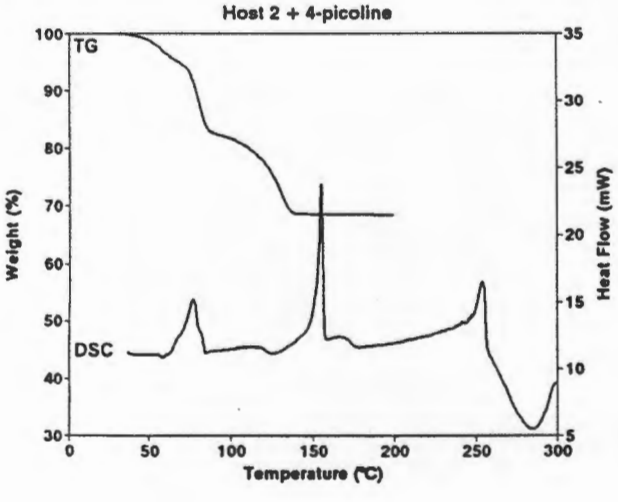
Host 2 + 4-picoline
TG
DSC
Weight (%)
Heat Flow (mW)
Temperature (°C)

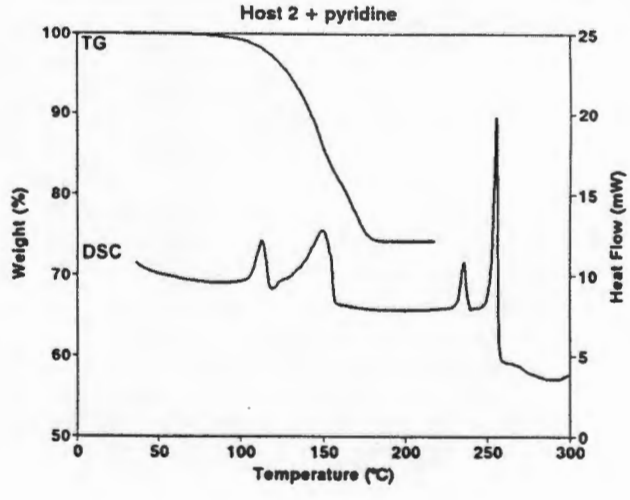
Host 2 + pyridine
TG
DSC
Weight (%)
Heat Flow (mW)
Temperature (°C)

Table A3 : Thermogravimetric results for the inclusion compounds formed by host **3**.

Guest	Observed mass loss (%)	Expected mass loss (%)	Difference (%)	Host:Guest
cyclohexanone	31.6	31.5	0.1	1:4
dimethyl acetamide	16.7	17.0	-0.3	1:2

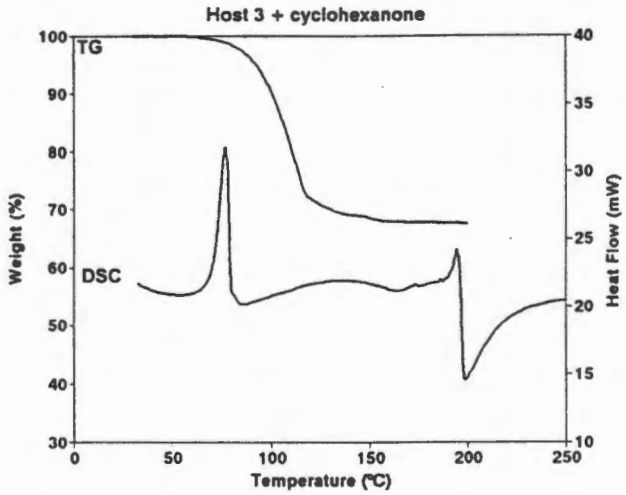

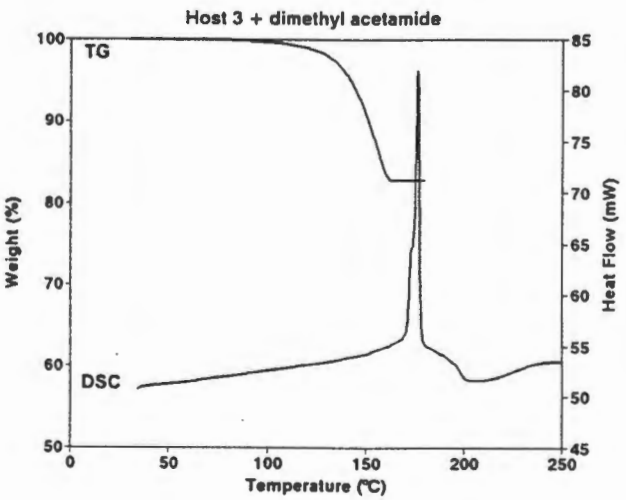

APPENDIX B

The kinetics of desolvation of some of the inclusion compounds studied were determined using powdered samples grown by continuous stirring. The experimental X-ray powder diffraction patterns obtained for the powdered samples, and the powder patterns calculated from the crystal structures for the inclusion compounds are shown. There is good agreement between the two patterns, suggesting that, although different methods of preparation were used, the powdered samples and crystals, grown by slow evaporation, have the same structure. The calculated powder pattern of SPMEK could not be determined using LAZYPULVERIX[1] due to the size of the structure. In all cases, on desolvation of the inclusion compounds, there is a phase change to the non-porous α-phase of the relevant host.

Single crystals of host **2**, suitable for X-ray diffraction, were not obtained during the course of this study. The experimental XRD trace for host **2** is reported. The XRD traces obtained for the desolvated products of NAPDMA and NAP2H have a hump-like shape, suggesting that part of the sample may be amorphous. This can be explained by sample fragmentation, which may occur on desolvation, due to the difference in solid reactant and product volumes, causing a loss of long range order resulting in products which are amorphous[2].

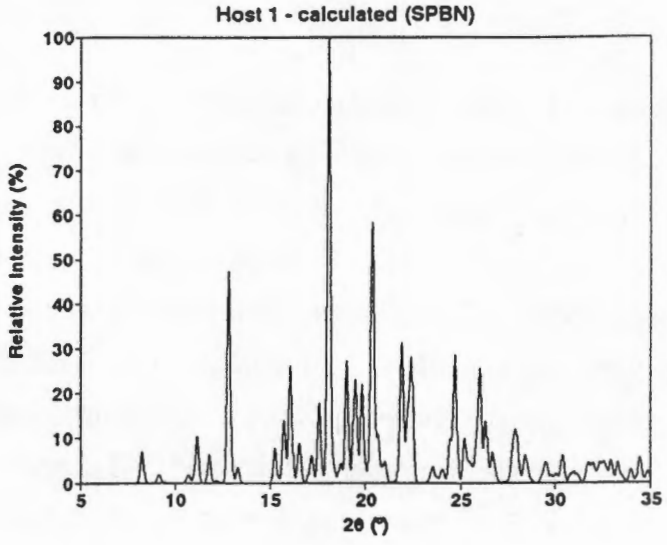
Host 1 - calculated (SPBN)
Relative Intensity (%)
2θ (°)

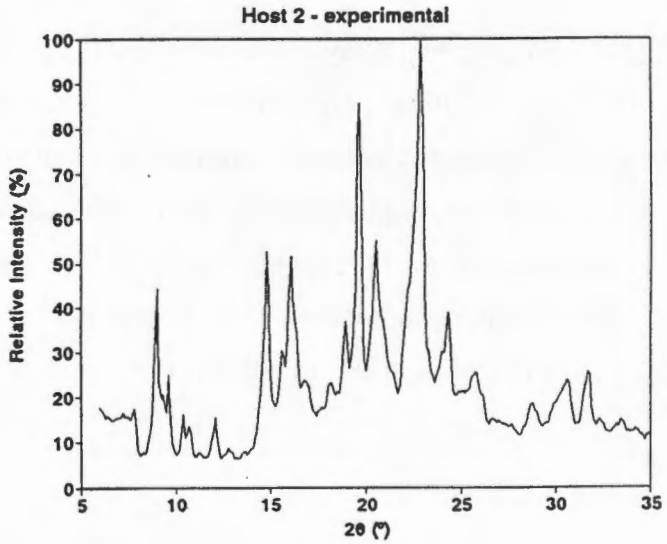
Host 2 - experimental
Relative Intensity (%)
2θ (°)

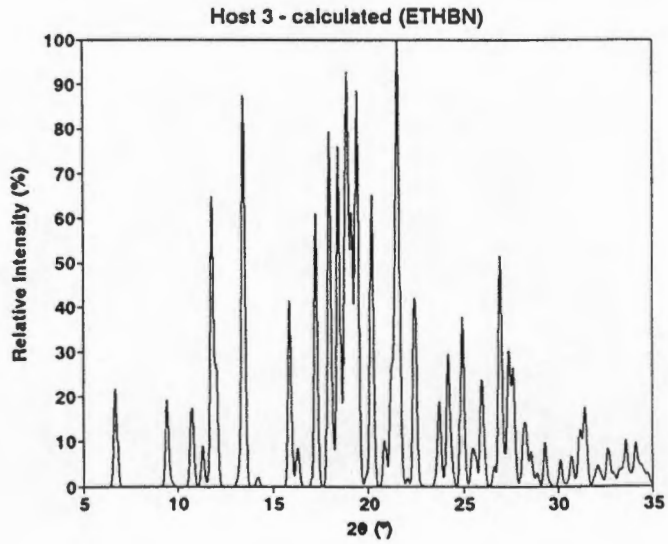
Host 3 - calculated (ETHBN)
Relative Intensity (%)
2θ (°)

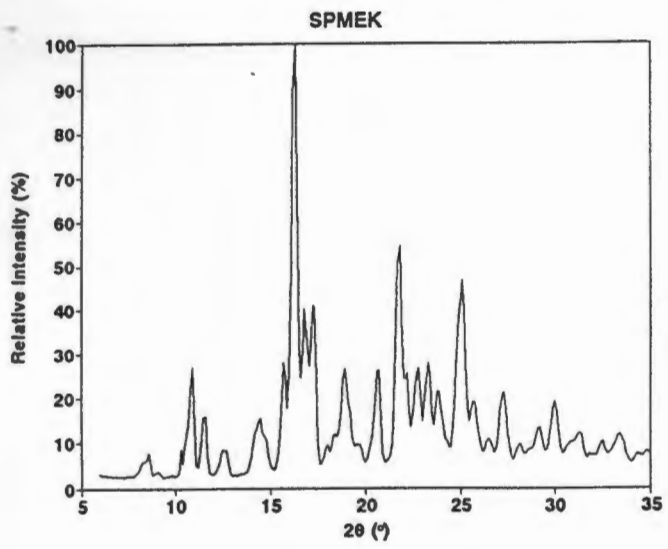
SPMEK
Relative Intensity (%)
2θ (°)

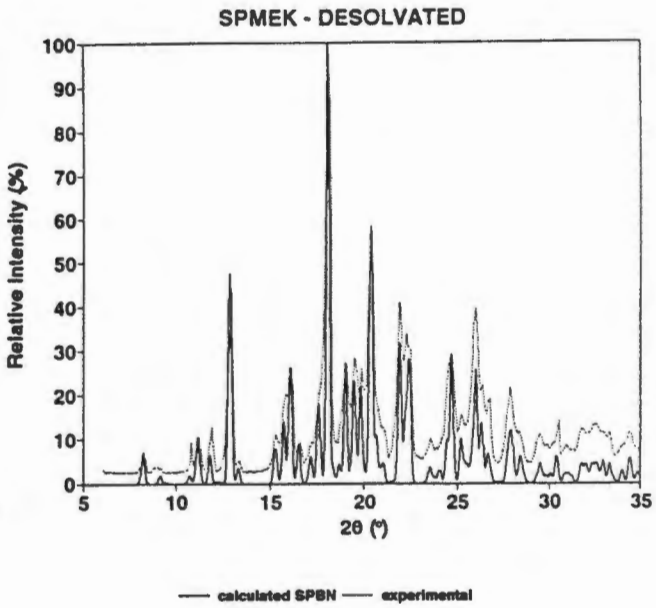
SPMEK - DESOLVATED
Relative Intensity (%)
2θ (°)
calculated SPBN
experimental

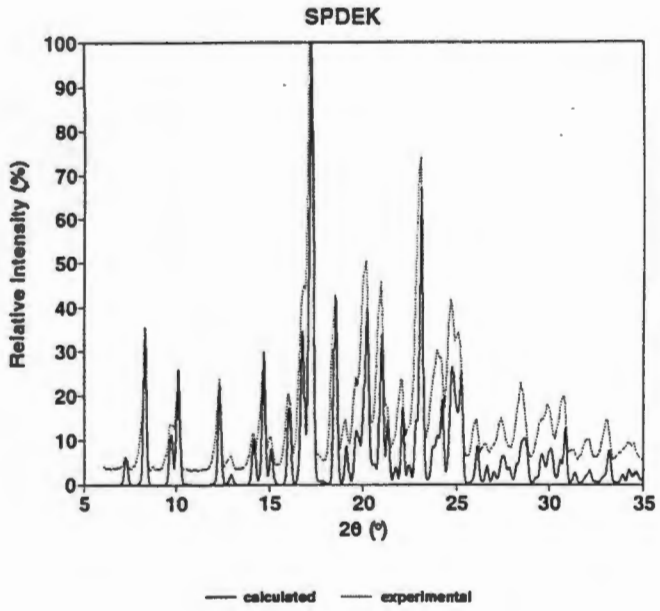
SPDEK
Relative Intensity (%)
2θ (°)
calculated
experimental

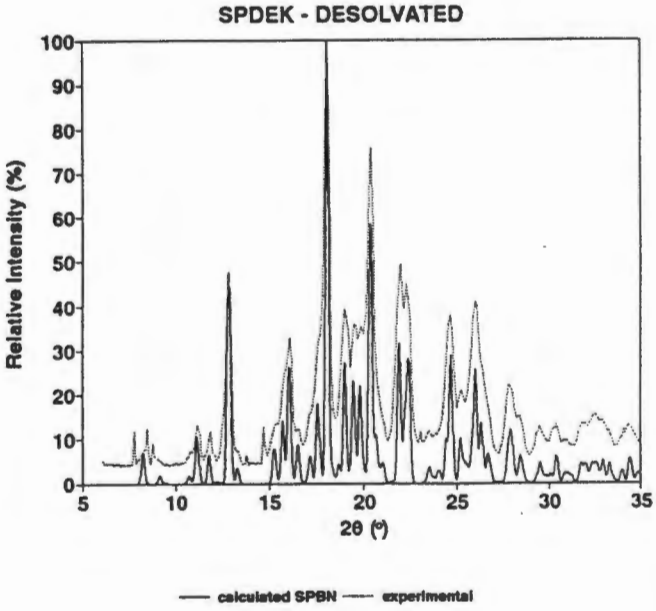
SPDEK - DESOLVATED
Relative Intensity (%)
2θ (°)
calculated SPBN
experimental

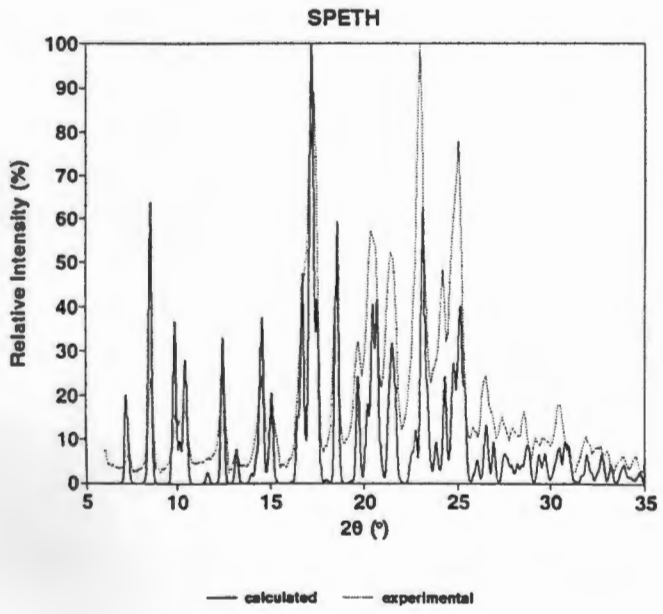
SPETH
Relative Intensity (%)
2θ (°)
calculated
experimental

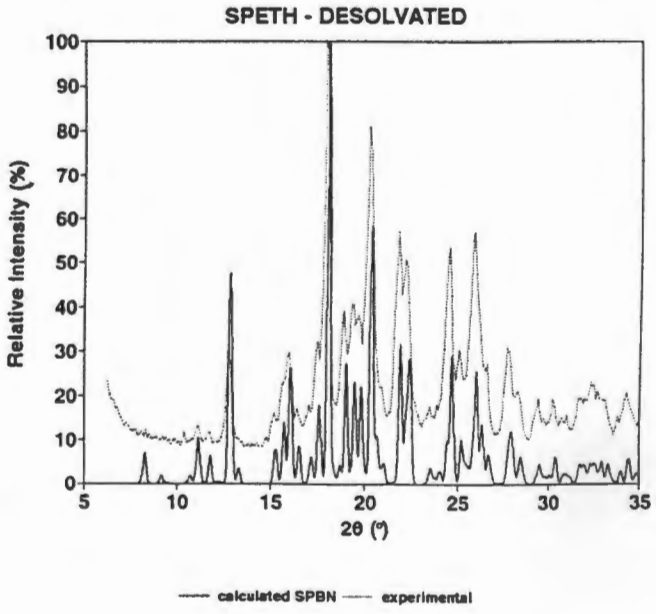
SPETH - DESOLVATED
Relative Intensity (%)
2θ (°)
calculated SPBN
experimental

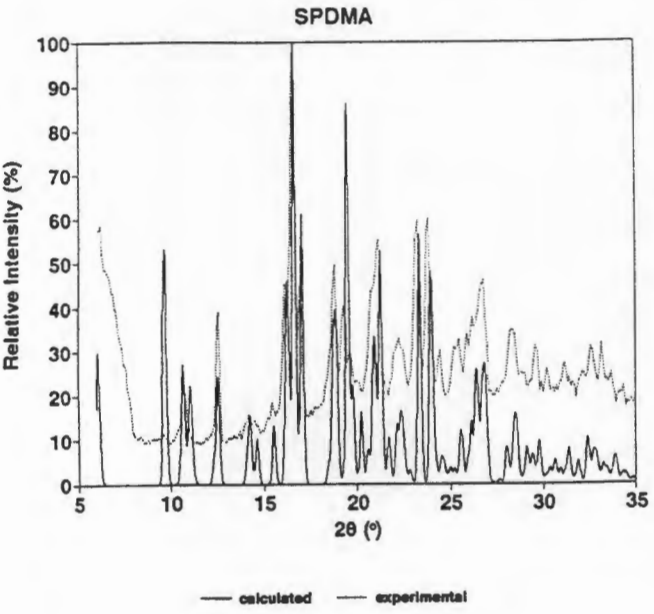
SPDMA
Relative Intensity (%)
2θ (°)
calculated
experimental

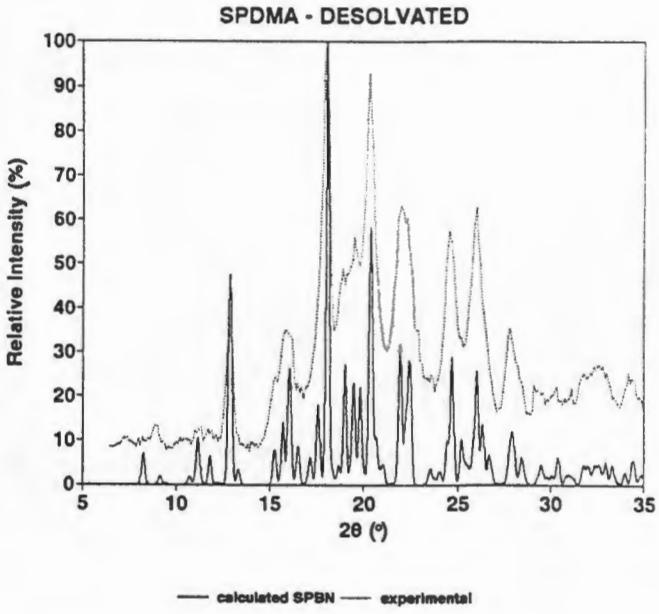
SPDMA - DESOLVATED
Relative Intensity (%)
2θ (°)
calculated SPBN
experimental

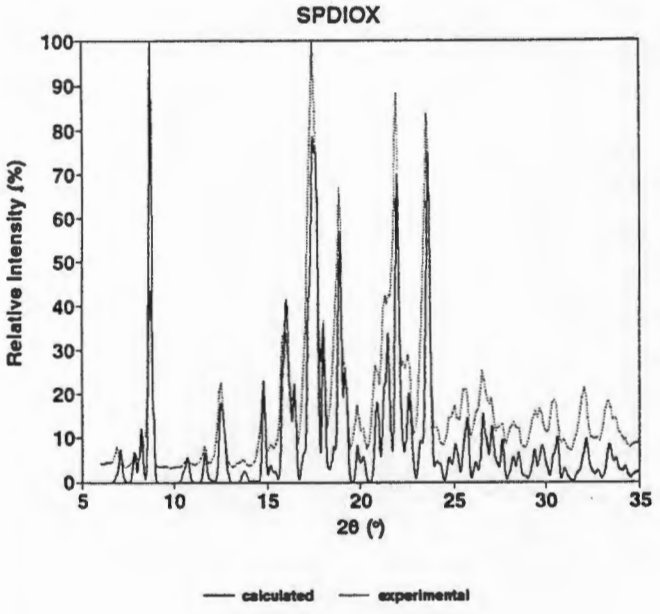
SPDIOX
Relative Intensity (%)
2θ (°)
calculated
experimental

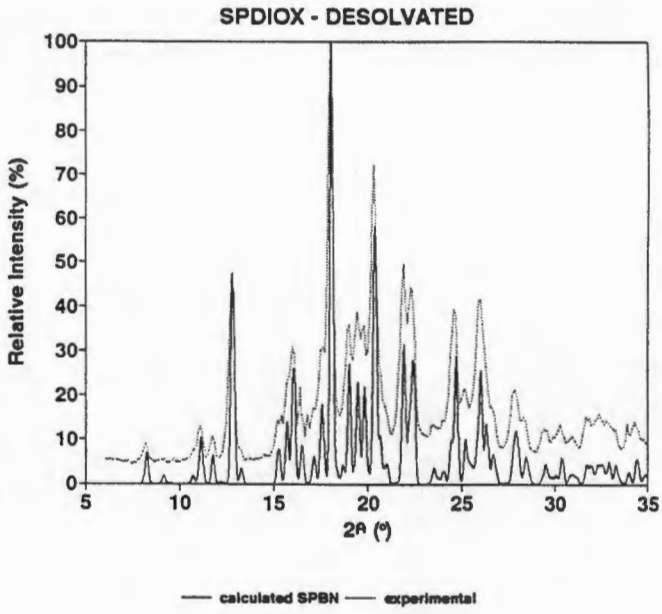
SPDIOX - DESOLVATED
Relative Intensity (%)
2θ (°)
calculated SPBN
experimental

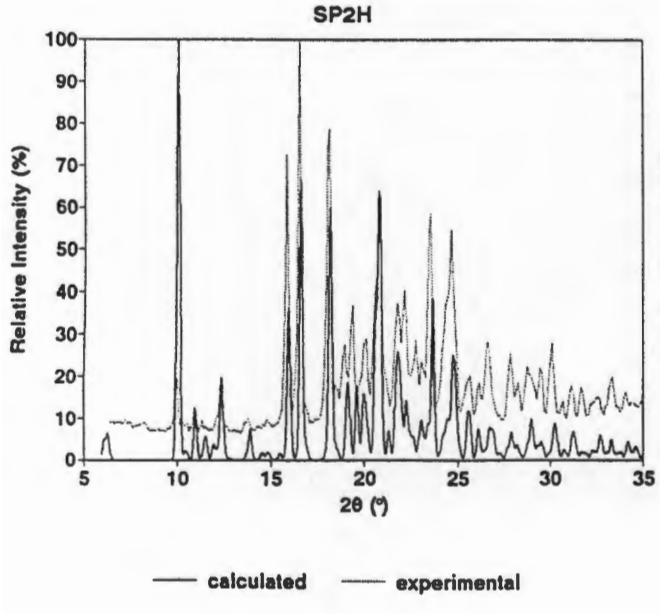
SP2H
Relative Intensity (%)
2θ (°)
calculated
experimental

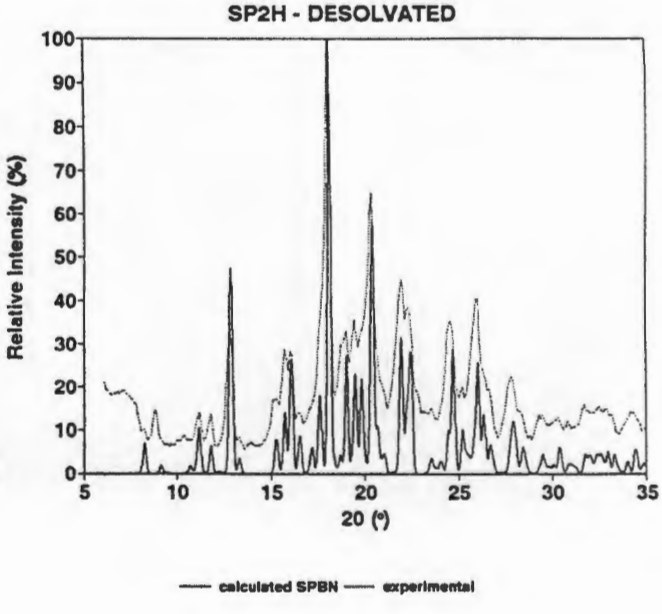
SP2H - DESOLVATED
Relative Intensity (%)
2θ (°)
calculated SPBN
experimental

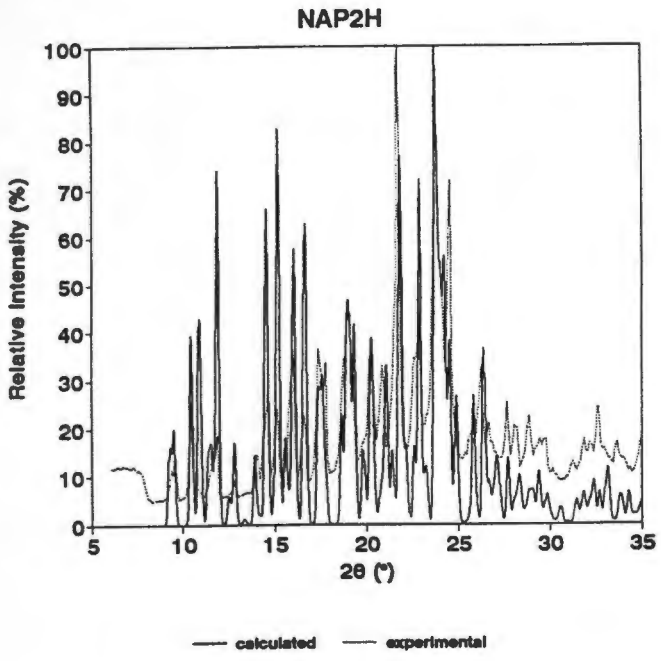
NAP2H
Relative Intensity (%)
2θ (°)
calculated
experimental

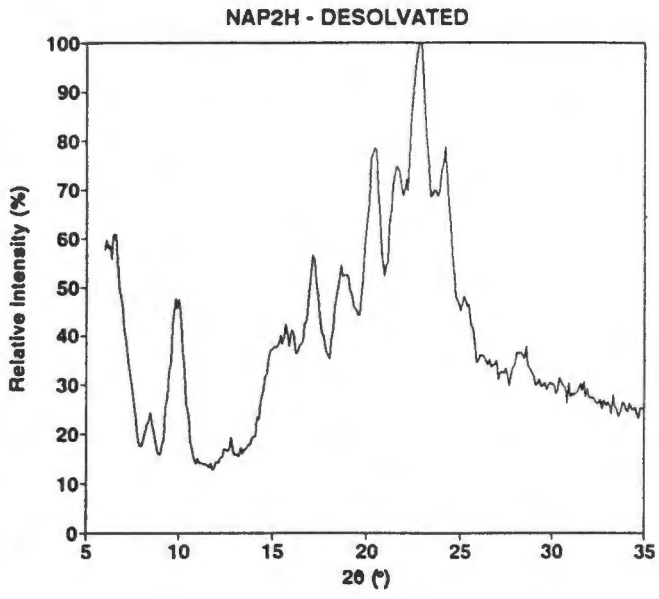
NAP2H - DESOLVATED
Relative Intensity (%)
2θ (°)

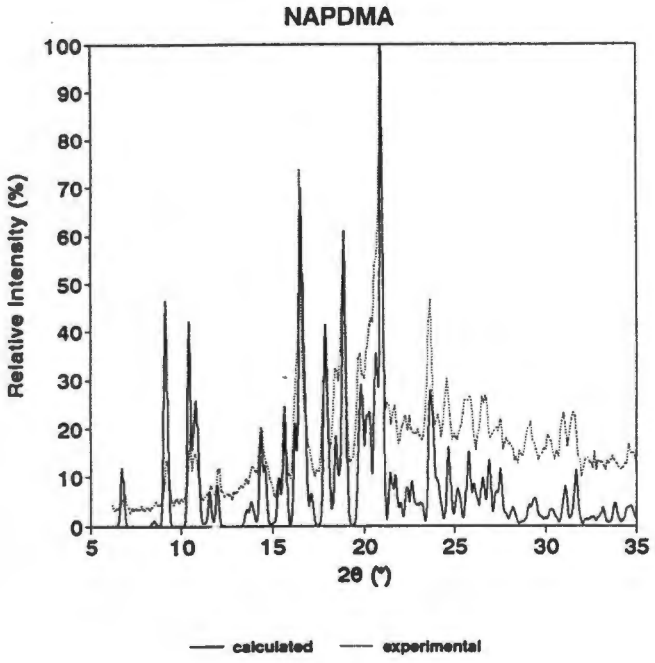
NAPDMA
Relative Intensity (%)
2θ (°)
calculated
experimental

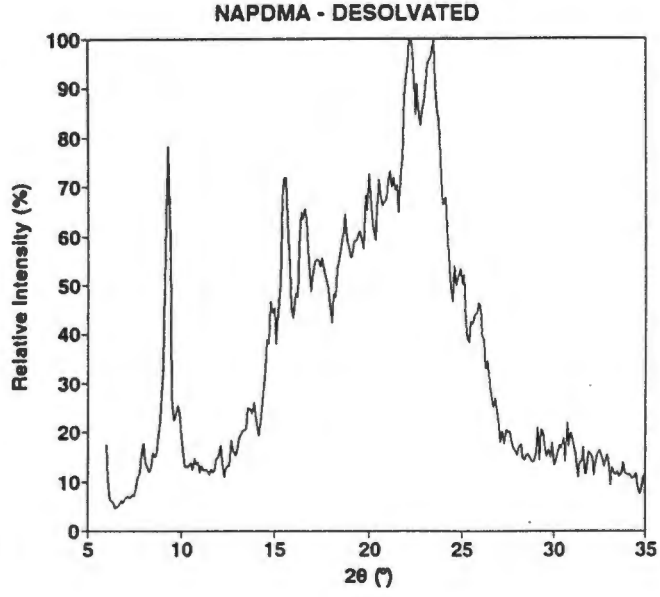
NAPDMA - DESOLVATED
Relative Intensity (%)
2θ (°)

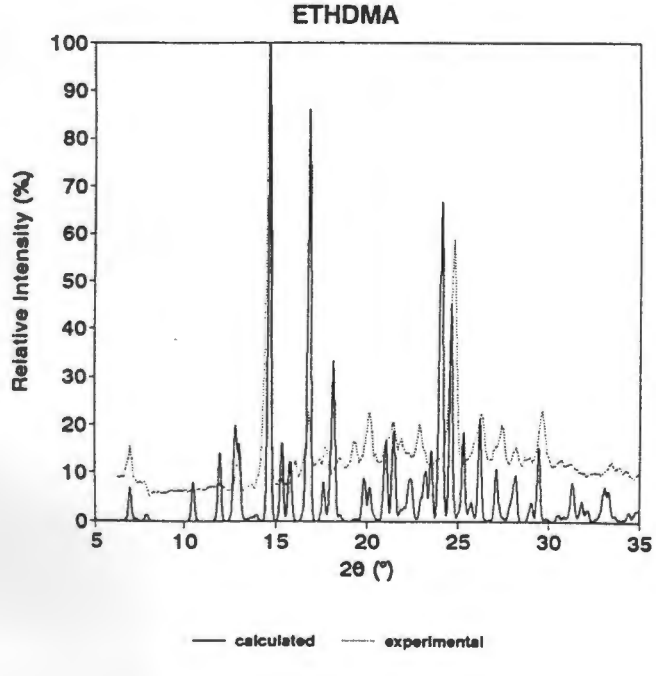
ETHDMA
Relative Intensity (%)
2θ (°)
calculated
experimental

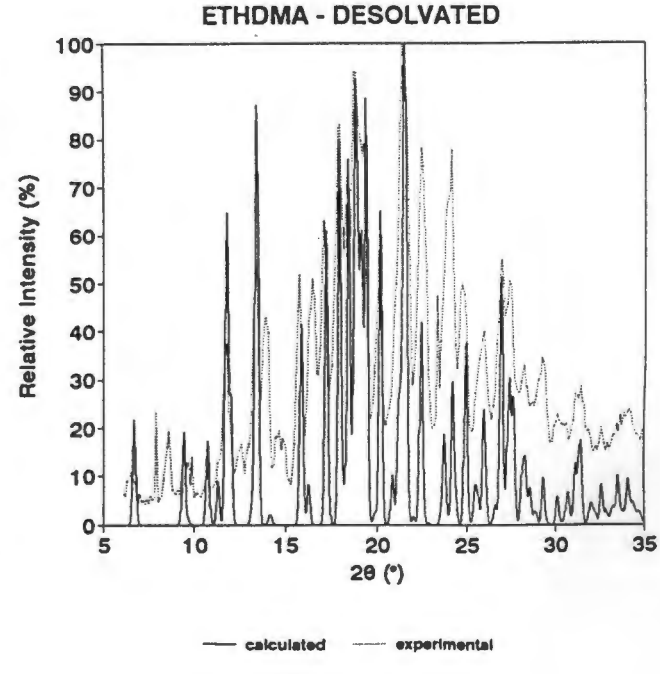
ETHDMA - DESOLVATED
Relative Intensity (%)
2θ (°)
calculated
experimental

REFERENCES :

1. K. Yvon, W Jeitschko, E. Parthe, *J. Appl. Cryst.*, 1977, **10**, 73
2. D. Dollimore, *Thermochimica Acta.*, 1992, **203**, 7.

APPENDIX C (diskette)

For each of the structures solved, there is a text file (ASCII format) containing :

- atomic coordinates and isotropic displacement parameters,
- bond lengths and angles,
- anisotropic displacement parameters,
- hydrogen coordinates and isotropic displacement parameters.

APPENDIX D (diskettes)

There is a text file (ASCII format) for each of the structures solved containing the observed and calculated structure factors as F_o^2 and F_c^2 with standard deviations for observed structure factors ($\sigma(F_o^2)$).

Disk 1 : SPBN, SPAB, SPDMA, SPMEK, SPDEK, SPETH
Disk 2 : SP2H, SPCHO, SPDIOX, SPDIOXO, SPDICHO, NAP2H
Disk 3 : NAPCHO, NAPDMA, NAPDMF, ETHBN, ETHCHO, ETHDMA